

Nonlinear Ultrasound Spectroscopy for Chemical Quantification

Jonathan R. Dion

Department of Chemistry
McGill University, Montreal
Quebec, Canada

August 2011

*A thesis submitted to McGill University in partial fulfillment of the requirements of the
degree of Doctor of Philosophy*

© Jonathan R. Dion, 2011

Abstract

Analyte quantification is an area of great practical interest for biomedical and commercial applications. Measurement in highly scattering media such as tissue, blood, and other biological fluids is challenging using conventional spectroscopic methods. Likewise, measurement of compounds on-line or in opaque containers can be extremely challenging. This thesis presents general approaches for analyte quantification in liquids by the frequency analysis of ultrasound waves.

Initially, this research focused on the quantification of analytes using dispersive hydrogel sensors. These sub-micron hydrogels vibrate at characteristic resonance frequencies when exposed to ultrasound. The resonance frequencies of the sensors could be modulated by generating molecularly imprinted pockets that would recognize and bind to molecules. Changes in the measured ultrasound frequency spectrum upon binding could then be detected. Using this approach, quantification of theophylline between 10 μM and 6.1 mM was shown.

Improvements in analyte quantification using ultrasound were made by designing hydrogel sensors coupled to antibodies. The high affinity of antibodies for a specific antigen allowed the quantification of acetaminophen between 3.5 nM and 20.8 nM. The highly selective antibodies were also demonstrated to allow acetaminophen determination in a variety of biological media. Though the ultrasound frequency profiles change in the different media, frequencies used for multilinear determination of the analyte were

clustered in certain regions of the spectrum. This indicated that the resonance frequencies were minimally affected by the media.

Antibody-linked sensors were also used to determine concentrations of tumor necrosis factor- α . The larger mass of this analyte compared to the acetaminophen was accompanied by an increase in sensitivity; concentrations between 115 pM and 592 pM could be determined. Based on this connection between analyte mass and the detection limit, dendrimer-based antibody sensors were then designed to further explore the mass dependence. Although the dendrimer sensor had a different vibration mechanism than the first antibody sensor, it was shown that the mass could be related to shifts in the resonance frequency components.

During propagation, ultrasound undergoes distortion processes that are characteristic of the chemicals present in the solution. This non-linear distortion of the waveform can be measured in the ultrasound frequency profile. In the second portion of this research, it was shown that characteristic changes in the ultrasound frequencies could be measured and correlated with variations in mixture composition. Volume fractions in three-component mixtures of water, methanol, and ethanol could be estimated simultaneously with errors between 2.9% and 3.8% using a hierarchical calibration approach.

The nonlinear distortion was likewise used to determine the composition of commercial beverages. The two major components, ethanol and carbohydrates, were determined simultaneously. Though a wide range of other constituents at various levels are present in beverages, the major components could be estimated with errors of 0.81% for ethanol and 17 mg/mL for carbohydrates.

Overall, the methods presented in this thesis show improvements over conventional approaches for analyte quantification. For point-of-care diagnostics, these methods are attractive due to the short measurement time and the minimal sample treatment required. Likewise, simple methodology and ability to examine optically opaque samples makes this technique highly applicable to on-line measurement in a variety of commercial manufacturing processes. Further applications and possible refinements are discussed in the conclusions chapter.

Résumé

La quantification de substances chimiques sous analyse (dit « analytes ») est un champ d'importance capitale ayant des applications biomédicales et commerciales. La précision des mesures dans les milieux à grande variation tels les tissus, le sang, et autres liquides biologiques est difficile utilisant les méthodes de spectroscopie conventionnelles. La mesure de corps composés en ligne, ou dans de contenants opaques est aussi un défi considérable. Cette thèse présente des approches générales pour quantifier les substances chimiques par l'analyse des fréquences de vagues d'ultrasons.

La cible initiale de cette recherche fut la quantification des analytes utilisant des capteurs d'hydrogel dispersants. Ces hydrogels aux particules submicroniques vibrent à une fréquence de résonance distinctive lorsque soumis aux ultrasons. La fréquence de résonance des capteurs peut être modulée en générant des pochettes moléculaires empreintes pouvant reconnaître et se lier aux molécules. Le changement au spectre de fréquence d'ultrason suite à cette liaison peut être détecté. Avec cette approche, la quantification de la théophylline fut établie entre 10 μM et 6.1 mM.

La quantification des analytes par ultrasons fut améliorée en créant des capteurs d'hydrogel liés avec des anticorps. L'affinité accrue des anticorps à un antigène particulier a permis la quantification d'acétaminophène entre 3.5 nM et 20.8 nM. Ces anticorps très sélectifs permettent aussi de déterminer l'acétaminophène dans des milieux biologiques variés. Quoique le profil de la fréquence des ultrasons change dans différents milieux, les fréquences pour la détermination multilinéaire des analytes étaient

regroupées dans certaines régions du spectre. Ceci indique que le milieu affecte peu la fréquence des résonances.

Des capteurs liés à des anticorps ont aussi été utilisés pour déterminer les concentrations de facteur de nécrose tumorale alpha. Cette analyte, à masse plus grande que l'acétaminophène, a entraîné une sensibilité accrue; des concentrations entre 115 pM et 592 pM ayant été établies. Basé sur le lien entre la masse de l'analyte et la limite de détection, des capteurs anticorps à base de dendrimère ont été créés afin d'explorer la dépendance sur la masse. Quoique le capteur dendrimère avait un mécanisme de vibration différent du premier capteur anticorps, il fut établi que la masse pouvait être reliée à des décalages dans les composants de la fréquence de résonance.

Durant la propagation, les ultrasons subissent un processus de distorsion typique aux produits chimiques dans la solution. Cette distorsion non linéaire de la forme d'onde peut être mesurée dans le profil de la fréquence de l'ultrason. La seconde partie de la recherche a montré que les changements typiques aux fréquences des ultrasons pouvaient être mesurés et reliés aux variations des composants du mélange. Le volume des parts d'un mélange à trois composants (soit eau, méthanol et éthanol) pouvait être estimé simultanément avec une moyenne d'erreur entre 2.9 % et 3.8 % en utilisant une approche de calibration hiérarchique.

La distorsion non linéaire fut utilisée comme ceci afin d'établir la composition de breuvages. Les deux composants majeurs, l'éthanol et les glucides ont été déterminés simultanément. Quoiqu'une variété importante de composants, à des niveaux variés, étaient présents, les composants majeurs peuvent être estimés avec une moyenne d'erreur de 0.81 % pour l'éthanol et 17 mg/mL pour les glucides.

Dans l'ensemble, ces méthodes démontrent des améliorations vis-à-vis les méthodes de quantification conventionnelles. Pour les soins de santé primaires, l'échantillonnage minime à traiter et l'analyse plus rapide rends ces méthodes de diagnostics désirables. Au niveau commercial, les procédés simples et la capacité de traiter des échantillons opaques rendent ces techniques très employables pour faire des mesures en ligne.

Table of Contents

List of Tables	xiii
List of Figures.....	xiv
List Symbols and Abbreviations.....	xvi
Original Contribution to Knowledge	xviii
Contribution of Authors.....	xix
Acknowledgements.....	xxii
Chapter 1: Introduction and Background	1
1.1 Project Overview	1
1.2 History of Acoustics and Ultrasonics	2
1.2 Fundamentals of Ultrasound.....	4
1.2.1 Ultrasound Instrumentation	11
1.2.2 Advantages of Ultrasound.....	14
1.3 Ultrasound in Analytical Chemistry	15
1.3.1 Fixed Acoustic Oscillators.....	15
1.3.2 Ultrasound Velocity Measurements.....	17
1.4 Ultrasound in Biomedical Applications.....	19
1.4.1 Ultrasound Imaging	20
1.4.2 Ultrasound Contrast Agents.....	22
1.4.2.1 Targeted Ultrasound Contrast Agents.....	25
1.5 Nonlinear Ultrasound Propagation	26
1.5.1 Nonlinear Ultrasound in Analytical Chemistry	30
1.5.2 Nonlinear Ultrasound in Biomedical Applications.....	33
1.5.2.1 Nonlinearity in Contrast Agents	34
1.6 Conclusions and Research Objectives	36
1.7 References.....	38
Chapter 2: Quantification of Theophylline using Ultrasonically-Active Molecularly Imprinted Hydrogel Sensors	59

2.1	Foreward	59
2.2	Manuscript	65
2.3	Abstract	65
2.4	Introduction	66
2.4.1	Background	66
2.4.2	Principle	68
2.5	Materials and Methods	71
2.5.1	Polymer Preparation	71
2.5.2	Measurement Apparatus	72
2.5.3	Data Analysis	74
2.6	Results and Discussion	77
2.7	Conclusions	82
2.8	Acknowledgements	83
2.9	References	83

Chapter 3: Ultrasonic Frequency Analysis of Antibody-Linked Hydrogel

	Biosensors for Rapid Point of Care Testing	88
3.1	Foreward	88
3.2	Manuscript	90
3.3	Abstract	90
3.4	Introduction	91
3.4.1	Principle	95
3.5	Materials and Methods	97
3.5.2	Materials	99
3.5.3	Samples	101
3.5.4	Methods of Analysis	102
3.6	Results and Discussion	104
3.7	Conclusions	115
3.8	Acknowledgements	116
3.9	References	116

Chapter 4: Quantification of Tumor Necrosis Factor-α Protein using	
Antibody-Linked Dendrimeric Hydrogel Sensors	122
4.1 Foreward	122
4.2 Manuscript	128
4.3 Abstract	128
4.4 Introduction.....	129
4.4.1 Background	129
4.4.2 Principle	131
4.5 Materials and Methods.....	134
4.5.1 Reagents	134
4.5.2 Ultrasound Apparatus	135
4.5.3 Methods of Analysis	139
4.6 Results and Discussion	140
4.7 Conclusions.....	147
4.8 Acknowledgements.....	149
4.9 References.....	149
Chapter 5: Determination of Volume Fractions in Multi-Component Mixtures	
using Ultrasound Frequency Analysis	154
5.1 Foreward	154
5.2 Manuscript	156
5.3 Abstract	156
5.4 Introduction.....	157
5.5 Materials and Methods.....	161
5.5.1 Reagents	161
5.5.2 Ultrasound Apparatus	161
5.5.3 Methods of Analysis.....	164
5.6 Results and Discussion	166
5.6.1 Measurement of Binary Mixtures	166
5.6.2 Measurement of 3-Component Mixtures.....	176
5.8 Acknowledgements.....	186

5.9	References.....	186
Chapter 6: Simultaneous Determination of Alcohol and Carbohydrate Content in Commercial Beveragesby Ultrasound Frequency Analysis 190		
6.1	Foreward	190
6.2	Manuscript	192
6.3	Abstract.....	192
6.5	Materials and Methods.....	196
6.5.1	Reagents.....	196
6.5.3	Methods of Analysis	200
6.6	Results and Discussion	202
6.6.1	Ultrasound Measurements of Two-Component Mixtures	202
6.6.2	Ultrasound Measurement of Three-Component Mixtures.....	210
6.6.3	Ultrasound Measurement of Commercial Beverages	215
6.7	Conclusions.....	223
6.8	Acknowledgements.....	225
6.9	References.....	225
Chapter 7: Conclusions and Future Work..... 230		
7.1	Conclusions.....	230
7.2	Future Work	234
7.2.1	Instrumentation	234
7.2.2	Resonance Frequency Sensors.....	235
7.2.3	Nonlinear Distortion in Bulk Media	238
7.3	References.....	242
Appendix A: Ultrasonic Quantification using Smart Hydrogel Sensors 243		
A.1	Abstract	243
A.2	Introduction.....	244
A.2.1	Background.....	244
A.3	Materials and Methods.....	250
A.3.1	Synthesis of Theophylline Imprinted HPC Polymer.....	250

A.3.2	Synthesis of Theophylline Imprinted NIPA Polymer	250
A.3.3	Hydrogel Solutions	251
A.3.4	Instrumentation	253
A.3.5	Data Processing.....	253
A.4	Results and Discussion.....	255
A.5	Conclusions.....	259
A.6	Acknowledgements.....	260
A.7	References.....	261

List of Tables

Table 1.1.	Acoustic properties of relevant materials.	10
Table 1.2.	A selection of current ultrasound contrast agents.	24
Table 1.3.	Acoustic properties of selected materials.	29
Table 3.1.	Acetaminophen concentration estimation based on ultrasonic measurements in selected biological fluids.	113
Table 4.2.	Molecular weight and size of PAMAM dendrimers.	136
Table 4.3.	Figures of merit for the determination of fractional components in binary mixtures.	143
Table 5.1.	Figures of merit for the determination of fractional components in binary mixtures.	174
Table 5.2.	Hydrogen bond lengths (Å) in molecular dimers.	180
Table 5.3.	Figures of merit for the determination of fractional volumes in 3-component mixtures.	182
Table 6.1.	Ethanol and carbohydrate content of commercial beverages studied.	197
Table 6.2.	Figures of merit for the determination of fractional components in three- component mixtures.	214
Table 6.3.	Figures of merit for the determination of fractional components in beverages.	217
Table 6.4.	Figures of merit for the determination of fractional components in beverages over targeted ranges.	221

List of Figures

Figure 1.1.	Visualizing a longitudinal acoustic wave.	7
Figure 1.2.	Block diagram of basic ultrasound spectrometer operation.....	13
Figure 1.3.	Distortion of an ultrasound waveform.	27
Figure 2.1.	Theophylline quantification in the presence of caffeine interferent.	63
Figure 2.2.	Ultrasonic configuration used for the experiments.....	73
Figure 2.3.	Image of the cellulose hydrogel polymer.....	76
Figure 2.4.	Measurement of hydrogel phase transition.	78
Figure 2.5.	Theophylline quantification using the matched frequency response transducers and T1 Development Board pulser	81
Figure 3.1.	Schematic diagram of the ultrasound frequency analyzer.	98
Figure 3.2.	Frequency profiles of antibody-linked sensor.....	106
Figure 3.3.	Quantification of acetaminophen in a dilute whole blood.	108
Figure 3.4.	Quantification of acetaminophen in a series of biological fluids.	111
Figure 4.1.	Quantification of TNF in buffered solutions using cellulose hydrogel sensor	124
Figure 4.2.	Antibody-linked hydrogel sensor diagram.....	132
Figure 4.3.	Instrumental configuration.....	137
Figure 4.4.	Ultrasound frequency changes with increasing dendrimer size.....	141
Figure 4.5.	Correlation between estimated and known TNF concentrations using dendrimer hydrogel sensor.....	144
Figure 4.6.	Dendrimer sensor performance in albumin.....	146
Figure 5.1.	Schematic diagram of the ultrasound frequency analyzer.	162
Figure 5.2.	Ultrasonic frequency spectra of individual components.....	167
Figure 5.3.	Relationship between ultrasound propagation velocity and the volume fraction of water.	169
Figure 5.4.	Frequency profiles of binary liquid mixtures where the mean spectral profile has been subtracted.	171

Figure 5.5.	Determination of the volume fraction of components in binary liquid mixtures.....	175
Figure 5.6.	Determination of the volume fraction of components in three-component mixtures.....	178
Figure 5.7.	Determination of the volume fraction of components in three-component mixtures over a narrow range of volume fractions.	183
Figure 6.1.	Schematic diagram of the instrumentation used for multi-frequency ultrasound measurements.....	199
Figure 6.2.	Change in ultrasound velocity in water with increasing component levels.	203
Figure 6.3.	Frequency profiles of binary liquid mixtures where the mean spectral profile has been subtracted.	206
Figure 6.4.	Determination of components in binary liquid mixtures.	208
Figure 6.5.	Determination of components in three-component mixtures of water/ethanol/sucrose.....	212
Figure 6.6.	Determination of components in commercial beverages.....	216
Figure 6.7.	Determination of components in commercial beverages over narrow concentration ranges.	220
Figure 7.1.	Determination of vitamin D3 using a binding protein-linked sensor.	237
Figure 7.2.	Determination of water contaminants.....	240
Figure 7.3.	Effect of increasing concentrations of water contaminants.	241
Figure A.1.	Frequency profiles of NIPA and HPC hydrogels undergoing phase transition as a result of increasing temperature.....	246
Figure A.2.	Schematic for ultrasound data acquisition.	252
Figure A.3.	Theophylline quantification results in presence of caffeine.	256

List Symbols and Abbreviations

Ab	Antibody
CMC	Carboxymethyl Cellulose
DLS	Dynamic Light Scattering
DVS	Divinyl Sulfone
EDC	1-Ethyl-3-[3-dimethylaminopropyl]carbodiimide hydrochloride
G5/G6/G7	Dendrimer generation (size)
HPC	Hydroxypropyl Cellulose
MIP	Molecularly Imprinted Polymer
MLR	Multilinear regression
NIPA	N-isopropyl Acrylamide
PAMAM	Poly-amidoamine
POC	Point-of-Care
PDI	Polydispersity Index
QCM	Quartz Crystal Microbalance
SMLR	Stagewise Multilinear Regression
TNF	Tumor Necrosis Factor- α
A	Area
a_e	Equilibrium radius
AI	Arbitrary Intensity
c	Velocity
d	Thickness

f	Frequency
G	Shear modulus
I	Intensity
K	Bulk modulus
m	Mass
p	Pressure
s	Entropy
Z	Acoustic Impedance
η	Viscosity
κ	Compressibility
λ	Wavelength
μ	Reduced mass
ρ	Density

Original Contribution to Knowledge

1. Demonstrated a novel, ultrasound-sensitive biosensor using resonance frequency changes in molecularly imprinted cellulose hydrogels induced by analyte binding. The resonance frequency changes could be measured ultrasonically and used for quantification of the analyte concentration.
2. Developed antibody-linked cellulose hydrogel sensors for small molecules and for proteins. Changes in the resonance frequencies were induced by antigen recognition and binding, and could be measured ultrasonically and used for rapid quantification.
3. Showed that the characteristic antibody-linked hydrogel resonance frequencies could be measured in diverse biological matrices with minimal sample preparation and provided similar analyte sensitivity as compared to matrix-free solutions.
4. Developed antibody-linked, dendrimer-based hydrogel sensors that showed ultrasound resonance frequency characteristics dependent on the sensor mass and that could be used for analyte quantification.
5. Developed the concept and demonstrated the utility of analyzing nonlinear ultrasound frequency distortions to construct multi-variate regression models for the quantification of solvent/solute mixtures.

Contribution of Authors

Articles included as part of this dissertation are listed below, along with an outline of the responsibility of each author. Overall, Professor Burns served as both thesis supervisor and critical reviewer to Mr. Dion.

Chapter 2

- J. R. Dion, S. Cassin, and D. H. Burns, “Quantification of Theophylline using Ultrasonically-Active Molecularly Imprinted Hydrogel Sensors”.

Mr. Dion designed the procedure and set up the experimental equipment. Experimental data were collected by Mr. Cassin under the supervision of Mr. Dion. The procedure for the molecularly imprinted sensor synthesis was designed by Mr. Dion. Data analysis was done by Mr. Dion. Prof. Burns suggested approaches for interpreting the data. The manuscript was written and prepared by Mr. Dion and edited with Prof. Burns.

Chapter 3

- J. R. Dion and D. H. Burns, “Ultrasonic Frequency Analysis of Antibody-Linked Hydrogel Biosensors for Rapid Point of Care Testing”, *Talanta* 85, 1364 (2010).
Reprinted with permission.

The instrumentation and antibody-linked sensor were developed by Mr. Dion. Likewise, data were collected and analyzed by Mr. Dion with advice from Prof. Burns. Manuscripts were written and prepared by Mr. Dion and edited with Prof. Burns.

Chapter 4

- J. R. Dion, M. A. Tycon, D. H. Burns, “Determination of Tumor Necrosis Factor- α using Ultrasound-Sensitive Dendrimeric Hydrogel Sensors”.

Mr. Dion developed the antibody-dendrimer coupling protocol and set up the instrumentation. Experimental data were collected by Mr. Tycon as part of his undergraduate honours research project under the supervision of Mr. Dion. Data analysis was done by Mr. Dion. Prof. Burns suggested approaches for interpreting the data. The manuscript was written and prepared by Mr. Dion and edited with Prof. Burns.

Chapters 5 and 6

- J. R. Dion and D. H. Burns, “Determination of Volume Fractions in Multicomponent Mixtures Using Ultrasound Frequency Analysis”, *Applied Spectroscopy* 65(6), 98 (2011). *Reprinted with permission.*
- J. R. Dion and D. H. Burns, “Simultaneous Determination of Alcohol and Carbohydrate Content in Commercial Beverages by Ultrasound Frequency Analysis”, *Talanta*, in press. *Reprinted with permission.*

As the work in these two chapters is closely associated, the following description is valid for both articles. Mr. Dion designed the procedure, set up the instrumentation, and acquired the experimental data. Data analysis was carried out by Mr. Dion with advice from Prof. Burns. Manuscripts were written and prepared by Mr. Dion and edited with Prof. Burns.

Appendix A

- D. Troiāni, J. R. Dion, D. H. Burns, “Ultrasonic Quantification using Smart Hydrogel Sensors”, *Talanta* 85, 1371 (2010). *Reprinted with permission.*

Both Mr. Troiāni and Mr. Dion were considered primary authors and had equal contributions to the publication. The instrument configuration, polymer synthesis, data acquisition, and analysis of results, were carried out independently by each graduate student for separate hydrogel sensors. All work related to N-isopropyl acrylamide was carried out by Mr. Troiāni, and all work related to hydroxypropyl cellulose was done by Mr. Dion. Prof. Burns suggested approaches for interpreting the data. The manuscript was written and prepared by both Mr. Troiāni and Mr. Dion and edited with Prof. Burns.

Acknowledgements

I wish that I could thank every person that has played a part in helping me complete this thesis... As luck would have it, I can do just that!

I would like to start by thanking my supervisor Professor David Burns for his guidance, enthusiasm, and generally being a great mentor. He gave me opportunities not only to do some cool research, but also to travel to many conferences, supervise students, and learn about academia. He also put up with a lot of my eccentricities, and he always asked how I was doing, which I've always appreciated. I was indeed having fun. Thanks Dave!

I'd want to thank professors Eric Salin and Cameron Skinner for their interesting courses and valuable input throughout the years. I'm sure they're relieved that they won't have to tell me to graduate for the third year running. Likewise, I would like to thank the thesis committee for agreeing to review my dissertation; sorry for using the heavy paper!

To the National Sciences and Engineering Research Council (NSERC), Fonds québécois de la recherche sur la nature et les technologies (FQRNT), and McGill University, I extended my thanks for all the years of financial support. Their support not only made this research possible, but also paid for all my favorite vices.

I'm also very thankful to Chantal Marotte for friendly support, guidance, and gentle reminders about administrative things that I occasionally forgot (every year).

I'd like to thank various members of the Burns lab throughout the years for their advice, encouragement, or just generally helping me do things (*i.e.* listening to me complain): Lucy Botros, Steven Cassin, Andrew Dafoe, Francis Esmonde-White, Shing Kwok, Fabiano Pandozzi, Kristin Power, Andrien Rackov, Pieter Roos, and David Troïani.

Although a member of the lab, Fabiano Pandozzi also gets his very own paragraph for spending countless hours discussing research, reading abstracts and papers, listening to practice presentations, grilling meats, and generally being a very good friend.

I also want to give my sincerest thanks to all of the undergraduate students that I've supervised over the years: Subir Sudtrahar, Michael Tycon, Steven Cassin, Andrew Dafoe, James Duffy, and Joshua Potel. Somehow they all managed to teach me something new and different. Often the lessons were related to patience, but I won't hold it against them. Also, they allowed our group to win a disproportionate amount of Honours competitions and prizes. Good for us!

The past 6 years would have passed much more slowly without my friends. I want to thank John for being the best friend that I could have asked for, with just the right amount of judgment when I deserve it. We also couldn't have done it without David, Bryan, and Alissa, since we needed a tank and two dps. And, for better or for worse, my time also wouldn't have been the same without Joe.

I want to thank Kim for restoring my faith in juggling as a method for attracting girls. I knew it would work! I love you!

Finally, I want to thank my parents Ginette and Eric, Grandparents Fernand and Mariette, aunt Diane and uncles Robert and Daniel, along with their many spouses and children, for their neverending support and encouragement. I love you all!

Actually, I lied, that wasn't the last acknowledgement. I want to thank my one mom one more time for a lifetime of love and support, without which I could never have been who I am today. Thank you, Mummy!

Chapter 1

Introduction and Background

1.1 Project Overview

Analytical measurements are made every day in commercial, research, and biomedical fields. Whether it be the ratio of components in a mixture or the presence of certain metabolites in a medical patient, determining the precise concentration of chemicals in samples is critical in today's world. An important factor for valuable measurements is the speed at which the elements can be quantified. It is often impractical to stop a process, whether it is a product assembly line or a diagnostic exam, in order to determine the constituents of a sample. For this reason, there is always a need for more efficient methods of chemical quantification.

The goal of the research presented in this thesis is the development of minimally-invasive analyte quantification methodologies using ultrasound. Rapid, on-site measurements improve diagnostic decision-making, optimization of processes, and reduce costs. Towards this end, point-of-care technologies in two general research themes were developed: 1) analyte quantification using target-specific vibrating sensors, and 2) mixture composition determination by ultrasonic frequency analysis.

For the first section of the research, hydrogel sensors were developed for multiple different analytes. Sensors require the coupling of a molecular recognition element with a transducer that produces a recognizable signal. The molecular receptors used in this work consisted of molecularly imprinted polymers and antibodies. These were coupled with hydrogel networks that can be probed by an ultrasound wave. This procedure allowed for quantitative estimates of analyte concentrations in samples of unknown composition.

In the second portion of this research, quantification of mixture composition was done. Instead of a reporter label, this section measured the change in the ultrasound frequency spectrum that was caused by nonlinear distortion in the media. This approach provided a simple means to simultaneously determine multiple components in unknown samples.

1.2 History of Acoustics and Ultrasonics

The field of acoustics is dedicated to the study of mechanical waves or vibrations. These types of waves can be generally divided into three categories. The first, and most familiar, is the audible range of sounds for humans. These sounds have frequencies between 20 Hz and 20 KHz. This includes all the sounds found in every day life, from a conversation to the sounds on a construction site. Sounds at lower frequencies (<20 Hz) are called “infrasonic,” and include the vibrations produced by seismic events and some animals such as whales. Finally, the third category consists of sounds with frequencies above 20 KHz. These sounds are known as “ultrasonic,” and are used by animals such as bats for echolocation. Ultrasound has found applications in the past century in a wide

variety of applications including medicine, industrial quality control, and scientific research.

The earliest work in the field of acoustics was in the study of musical sounds and notes.^{1,1,1,2} Early, Pythagoras (c. 570–495 BCE) recognized that vibrating strings on the lyre would produce harmonious notes when the ratios between them were integer values. Modern acoustical theory started to emerge with the scientific revolution of the 16th century. Marin Mersenne (1588–1648) and Galileo Galilei (1564–1642) independently discovered that pitch (or frequency) of musical tones is related to the number of vibrations in a moment of time. Later, Isaac Newton (1642–1727) would begin to derive acoustical relationships for sound velocity in his *Principia*. However, music continued to play a key role in acoustical theory, with the discovery of combination tones by Giuseppe Tartini in the 18th century.

The discovery of piezoelectric materials was critical in the advancement of acoustic research. The piezoelectric effect was first observed in the late 19th century by the Curie brothers, Jacques and Pierre, in 1880.^{1,3} Piezoelectric materials generate an electric potential when they undergo compression. The inverse effect was also shown the following year; materials could be made to oscillate by applying alternating electric potentials. These materials permitted acoustic and ultrasonic waves to be easily generated. While earlier work had roots in musical instruments, acoustic waves at specific frequencies and intensities could now be generated, allowing scientific study and the development of new, practical applications.

Great scientific interest in acoustics, and particularly ultrasonics, grew out of the two world wars at the start of the 20th century. Sound Navigation and Ranging (SONAR)

was developed using ultrasonic pulses as a countermeasure to the emerging submarine threat in the north Atlantic. From this application for submarine detection, as well as signalling and depth-finding, ultrasound grew extensively following the wars.

The extension of ultrasound from water into opaque media demonstrated the real potential of acoustical analysis. Sergei Sokolov developed ultrasound systems for flaw testing in bulk materials using first continuous wave and then more practical pulse-echo ultrasound systems.^{1.4} This pulse-echo methodology would later be extensively employed in numerous applications such as medical imaging with arrays of ultrasound transducers.^{1.5} Today, ultrasound is used not only in materials testing and medical imaging, but also in a wide variety of other applications such as cleaning, quality control, electrochemistry, and chemical synthesis catalysis.^{1.6-1.8} With the leaps in computer technology and digital processing, applications using ultrasound are now diverse and advancing rapidly.

1.2 Fundamentals of Ultrasound

Ultrasound, like other acoustic waves, is a mechanical disturbance that propagates through elastic media. These mechanical disturbances can take different forms depending on the type of medium through which propagation occurs. These modes indicate the direction of particle displacement in the medium relative to the direction of wave propagation. The two primary modes are transverse and longitudinal waves.^{1.9} Transverse ultrasound waves cause particles in the medium to oscillate perpendicular to the direction of propagation. These waves are only possible in solids and highly viscous fluids. In

longitudinal waves, the particles in the medium instead oscillate parallel to the direction of propagation. Longitudinal waves are the most common form of ultrasound propagation in solids and liquids. Different modes of propagation are also present at phase interfaces. For example, at solid/liquid boundaries, surface waves (also known as Lamb, Rayleigh, or Rayleigh-Lamb waves) can propagate along the interface.^{1,9} Here, the oscillation of the particles is a combination of longitudinal and shear behavior.

Longitudinal waves are the more commonly examined form of propagation in analytical and biomedical applications. When pressure is generated at a source, for example an ultrasound transducer, the medium on which this force is applied will be compressed. This will increase the local particle density in the layer adjacent to the source. Because the pressure in this layer (L1) is higher than in the subsequent, undisturbed layer (L2), a pressure gradient will develop. The pressure gradient will result in the compression of L2, and in the process, will decompress or rarefy L1. Further, as the particles in a medium are displaced from a resting state, the elastic forces of the medium will act as a restoring force. The process will then be repeated as the compressive force is transmitted to subsequent layers (L3+). This alternating compression and rarefaction is the acoustic wave. In ultrasound, these pressure gradients oscillate at a frequency greater than 20 KHz.

The longitudinal pressure gradients can be considered a planar wave made up of a series of compression and rarefaction phases that oscillate harmonically. These pressure phases can repeat at a single frequency, or as the sum of multiple frequencies. In a simple, undamped system, a single frequency pressure waveform can be described by

$$y(t) = A \sin(2\pi ft + \phi) \quad (1.1)$$

where A is the amplitude of the wave, f is the frequency, and φ is the phase offset. The response function, $y(t)$, can be interpreted as the molecular displacement of a particle, or as the deviation in pressure (p/p_0), density (ρ/ρ_0), or particle velocity (c/c_0) at a given location and time caused by the ultrasound wave. Figure 1.1 illustrates a sinusoidal wave (top) along with the particle distribution caused by an ultrasound wave (bottom). When the pressure is positive, particles in the medium are closer together due to the compression. In contrast, when the pressure is negative, the particle density is lowered. The wavelength (λ) of an ultrasound wave is related to the velocity (c) and frequency of the by

$$\lambda = \frac{c}{f} \quad (1.2)$$

and measures the length of a full compression and rarefaction cycle. As the ultrasound wave is solely made up of these pressure fluctuations, a medium is required through which to propagate. The physical properties of this medium, in turn, dictate the velocity of the ultrasound wave. In liquids, the velocity is dependent on the compressibility (κ) and density (ρ) of the medium such that

$$c = \sqrt{\frac{1}{\rho\kappa}} \quad (1.3)$$

where the compressibility of the medium is the inverse of the compression modulus.^{1.10} In general, ultrasound waves will travel more quickly through solids than through liquids due to the lower compressibility of solids. Likewise, propagation through liquids is quicker than through gasses. For example, the velocity of ultrasound in water ice is 3900 m/s, as compared to 1496 m/s in liquid water (25°C), and just 494 m/s in water

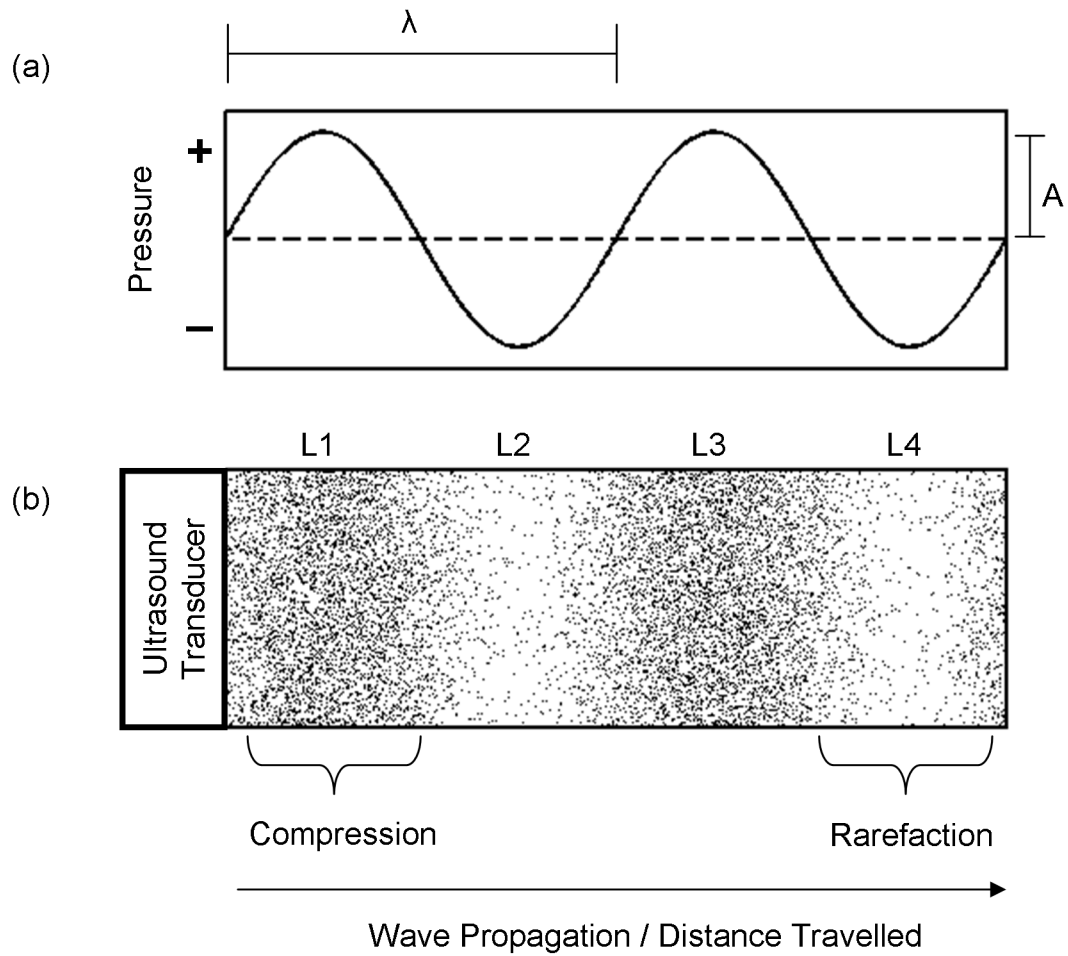


Figure 1.1: Visualizing a longitudinal acoustic wave. (a) Pressure waveform varying sinusoidally at a given wavelength (λ) and amplitude (A), (b) Particle distribution caused by an ultrasound wave illustrating successive compression (L1, L3) and rarefaction (L2, L4) layers.

vapour.^{1.9,1.11} Heterogeneous mixtures such as colloids, and suspensions are a combination of these.

Propagation of ultrasound through a medium is not lossless. Significant ultrasound attenuation results from absorption of the wave. Absorption losses occur due to the movement of particles during compression and rarefaction. This includes shearing between the particles oscillating in the acoustic field and the medium, as well as heat conduction caused by the pressure.^{1.12} The result is an exponential decrease in intensity of the ultrasound wave:

$$I_x = I_0 e^{-\alpha x} \quad (1.4)$$

where I_x is the intensity at a given propagation distance x , I_0 is the initial intensity, and α is the attenuation coefficient. The attenuation coefficient, which is frequency-dependent, can be approximated by

$$\alpha = af^b \quad (1.5)$$

where a and b are medium-specific constants.^{1.13} In general, penetration into a sample will decrease as the ultrasound frequency increases. The penetration depth, which is the distance into a sample at which 50% of the ultrasound energy has been attenuated, is an important measurement consideration for non-destructive testing, where large sample vessels can result in poor signal-to-noise ratios. Likewise, for biomedical measurements, the increased resolution using higher frequencies must be balanced with the depth of the studied tissue. For example, the penetration depth in soft tissue of a 1 MHz ultrasound wave is 7 cm, while for 10 MHz is less than 1 cm.^{1.14} Likewise, the penetration depth is dependent on the specific tissue. For example, the penetration depth of the 1 MHz ultrasound wave is 5 cm in fatty tissue, but less than 1 cm in a tendon or bone.^{1.15}

Ultrasound is also highly affected by propagation through interfaces. Both reflection and refraction can occur, depending on the specific instrument configuration. These effects must be taken into account when designing an ultrasound spectrometer, as is discussed further in Section 1.2.1. Both reflection and refraction are dependent on the acoustic impedance of the two media at the interface. This parameter measures the resistance of the medium to the transmission of ultrasound and is described by the velocity and density of the medium as:

$$Z = \rho c \quad (1.6)$$

Some examples of the impedance in relevant materials can be found in Table 1.1. When an ultrasonic wave impinges on a particle or interface at normal incidence, the fraction of the reflected power, R , is given by

$$R = \left(\frac{Z_2 - Z_1}{Z_2 + Z_1} \right)^2 \quad (1.7)$$

and the transmitted intensity is $T = 1 - R$.^{1,9,1.1} Thus, with a large difference between two media, a greater amount of the ultrasound intensity will be reflected. When Z_1 and Z_2 converge, the transmitted fraction approaches 100%, making impedance matching between interfaces an important consideration. To decrease the fraction of ultrasound reflected between two substances, a third layer with an acoustic impedance

$$Z_{match} = \sqrt{Z_1 Z_2} \quad (1.8)$$

can be placed between the two media.^{1.1} As will be discussed in later chapters, this plays an important role for instrument development and data analysis, where maximizing the signal intensity and improving temporal resolution is critical.

Table 1.1: Acoustic properties of relevant materials.^{1.9,1.11,1.163,1.164}

Medium	Density (g/cm ³)	Speed (m/s)	Acoustic Impedance (10 ⁶ Kg/m ² s)
Air	1.2 x 10 ⁻³	333	4 x 10 ⁻⁴
Water	1.00	1496	1.48
Ethanol	0.79	1159	0.92
Blood	1.06	1560	1.66
Bone (Skull)	1.34	3198	4.61
Bone (Femur)	1.80	3880	6.10
Fat	0.92	1446	1.33
Muscle	1.07	1542-1626	1.65-1.74

The refraction of ultrasound waves can also play an important role in the attenuation process when the angle of incidence is not perpendicular. As in optical phenomena, refraction of ultrasound waves propagating in media with different properties obeys Snell's law,^{1,11} where the incident (θ_1) and refracted angles (θ_2) are related by:

$$\frac{\sin \theta_1}{\sin \theta_2} = \frac{c_1}{c_2} \quad (1.9)$$

Though ultrasound is typically applied to a sample at a normal incidence, internal structures or layered media may result in significant refraction,^{1,16} making this effect an important consideration.

1.2.1 Ultrasound Instrumentation

Measurements of the magnitudes of ultrasound frequencies can be made using an ultrasonic spectrometer. Similar to traditional optical measurements, both a source and a detector are required. Several types of transducers are capable of generating ultrasound waves, including magnetostrictive, pneumatic, and mechanical sources.^{1,2} However, limitations such as high heat production or low maximum frequencies limit these forms in analytical and biomedical applications. Laser sources have also been used to generate ultrasound waves, though this requires more complex optics.^{1,17,1.18} In current analytical and biomedical applications, piezoelectric transducers are typically used as both the ultrasound source and detector. Although quartz crystals were used in early ultrasound applications, they are rarely used in current transducers due to their brittleness. Instead, lead zirconium titanate ceramic elements are commonly used. By heating these ceramics

above their Curie temperatures, the electric dipoles can then be aligned in an external electric field, and result in elements showing a high piezoelectric effect for both generation and measurement of ultrasound waves.

The general schemes of two common ultrasound spectrometer configurations are depicted in Figure 1.2. In the first, a single transducer is used to both emit and measure ultrasound. This “pulse-echo” configuration is common in biomedical, industrial, and research settings. Reflections at interfaces in a sample will result in echoes that can be detected. The delay time and intensity of these reflected ultrasound echoes are then used for a variety of applications such as flaw detection or imaging reconstruction. In the second configuration, separate transducers are used to emit and then measure the ultrasound wave that propagates through a sample. Here the intensity of the ultrasound that has passed through any objects following any reflective losses is determined.

A generator is used to produce high voltage electrical pulses with short durations. These electrical pulses drive the source ultrasound transducer which produces mechanical vibrations. The ceramic element in the transducer will vibrate at a specific frequency that is dependent on the chemical composition and size of the piezoelectric material. The frequencies produced by the transducer depend on the pulse duration. A shorter pulse will result in a wider bandwidth, or, more frequencies being generated. In contrast, as a pulse increases in length, bandwidth decreases, and frequencies generated are more narrowly distributed around resonance frequency.

When a liquid sample is placed between the source and detector, the mechanical vibration propagates through this sample. Properties such as temperature, density, and viscosity will alter the intensity and frequency distribution of the ultrasound.

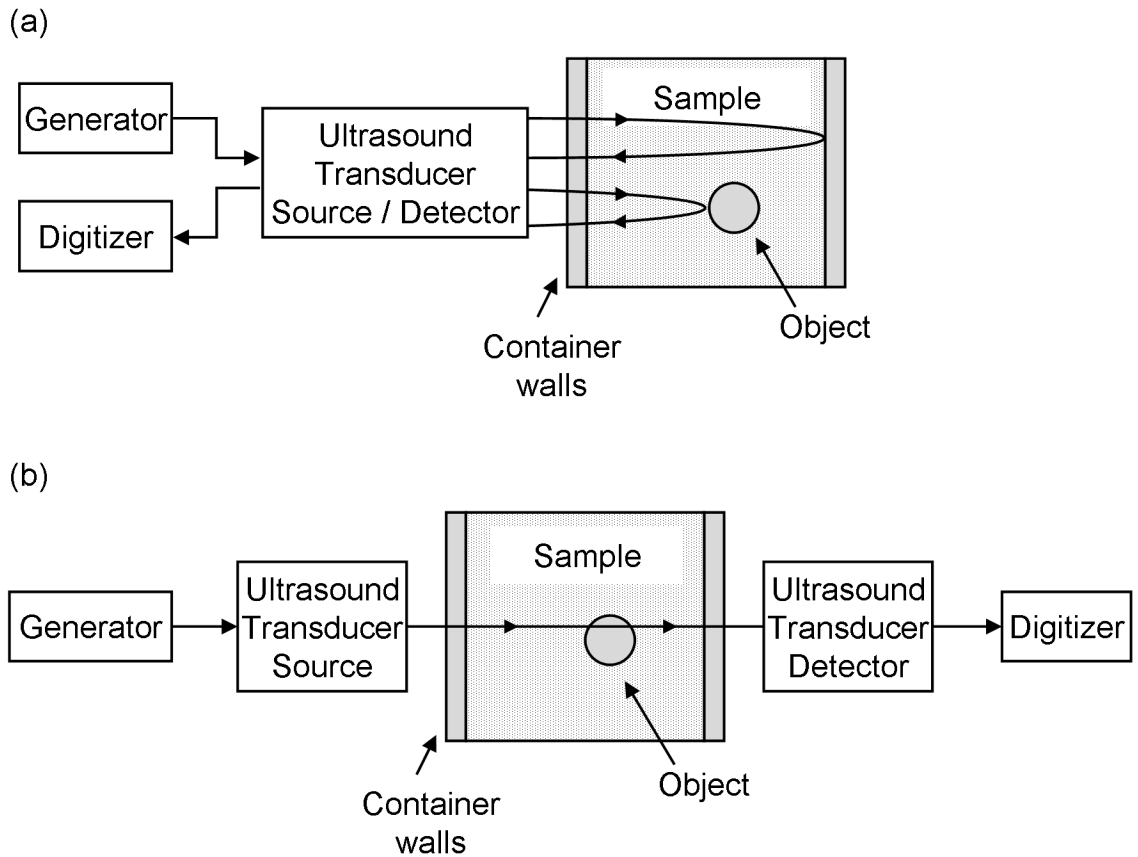


Figure 1.2: Block diagram of basic ultrasound spectrometer operation. (a) Single-transducer pulse-echo configuration; reflections from surfaces and objects in the samples are measured, (b) Two-transducer configuration; ultrasound propagating through the sample is measured.

Additional frequency components can also arise due to resonance frequency vibrations of components in the sample. The ultrasound wave containing these components then impinges on the detector, which is positioned opposite to the source. The detector is a second piezoelectric transducer. This transducer will convert the mechanical vibrations that have propagated through the sample into an electrical signal. These electrical signals are digitized by an analog-to-digital converter, and analytical signals can then be extracted from the readout data using computer-assisted processing.

1.2.2 Advantages of Ultrasound

Several advantageous factors make ultrasound an attractive tool for industrial, analytical, and biomedical measurements. As a mechanical wave, ultrasound can be used to probe the contents of sealed containers such as pipelines, reactors, and bottled products. Likewise, ultrasonic waves can propagate freely through optically opaque and scattering samples such as tissues, biological fluids, foods and beverages, and plastics.

Ultrasound waves are non-destructive and non-ionizing, ensuring the safety of a subject or sample being examined, while offering similar sensitivities as other techniques such as MRI or CT.^{1,19} Likewise, this increases the safety for a technician as there is no radiation exposure. Measurements are also made quickly, allowing real time monitoring instead of static imaging.

Analysis of samples using ultrasound also offers financial advantages. Instrument costs are relatively low compared to many other measurement techniques. The capability of the ultrasound examination without extensive sample handling or treatment also

reduces operating costs. Likewise, the simplicity of the method decreases the expertise and training needed for a technician, as well as removing the need for dedicated laboratory facilities. The low cost, short time, and minimal sample preparation can therefore allow increased throughput using ultrasonic techniques, which is attractive for routine monitoring and point-of-care type measurements.

There are also disadvantages to the use of ultrasound. The relationship between penetration depth and resolution can be limiting due to the greater attenuation at high frequencies. Frequencies above 10 MHz will penetrate only a few millimeters in tissues,^{1,14} so lower frequencies must be used for deep tissue imaging, reducing resolution. The inability to differentiate between similar materials can also be limiting. For example, similar tissue properties can reduce contrast in medical imaging.^{1,20} However, a wide variety of methods have been developed to address this limitation, such as contrast agents and frequency measurements. These methods are further described in subsequent sections.

1.3 Ultrasound in Analytical Chemistry

1.3.1 Fixed Acoustic Oscillators

One of the early applications of piezoelectric devices for ultrasound-based sample analysis was the development of the quartz crystal microbalances (QCM). Thin piezoelectric quartz crystals making up the QCM surface oscillate at characteristic frequencies. Typical oscillators used in these measurements will vibrate between

1-10 MHz. When mass is added to a QCM surface, there is a fractional change to the resonating frequency that can be measured. In 1959, Sauerbrey derived the basic relationship between the mass loading on a surface of a vibrating crystal and the measured changes in the resonance frequency.^{1,21} The frequency of the resonating crystal could be related linearly to the mass deposited on the surface,^{1,22} where the change in frequency,

$$\Delta f_m = -\frac{f_0}{d_q \rho_q} \frac{\Delta m_s}{A} \quad (1.10)$$

where f_0 is the natural resonance frequency of the quartz crystal, d_q the thickness of the quartz crystal, ρ_q the density of the quartz crystal, A the area of the quartz sensor, and Δm_s the change in mass on the sensor.

The first demonstrated use of a vibrating microbalance for chemical quantification was by King in 1964, who determined hydrocarbons and other small molecules.^{1,23} Early work was limited to measurements in the gas phase, examining analytes such as organic vapours.^{1,24} Early applications also extended to immunoassays, allowing coupling in the liquid phase and subsequent drying before measurement in the gas phase.^{1,25} Measurements in the liquid phase remained limited, as the linear relationship between the mass and resonance frequency did not hold.

More recent advancements in QCM have extended the method to the analysis of liquids. The presence of the liquid adds another frequency shift, defined by

$$\Delta f_l = \sqrt{f_0^3 \frac{\eta_l \rho_l}{\pi \mu_q \rho_q}} \quad (1.11)$$

where η_l and ρ_l are the viscosity and density of the liquid, and μ_q is the shear modulus of the quartz crystal.^{1,22,1,26} The overall change in resonance frequency in these systems

when mass is loaded on the QCM can then be determined by summing the two components,^{1,22,1.27} such that:

$$\Delta f_{total} = \Delta f_m + \Delta f_1. \quad (1.12)$$

This has been used to determine analyte concentrations in liquids by measuring shifts in the resonance frequency of these sensors.^{1.22}

Surface coatings have also been applied to crystal surfaces to facilitate specific analyte capture and immobilization. This has included coating based on molecular imprinting,^{1.28} antibodies,^{1.29} and molecular affinities such as carbohydrate adhesion.^{1.22} These targeted microbalances have been used for the determination of a wide variety of proteins, biomarkers, and antibiotics.^{1.22} Sensor fouling in these applications remains problematic, due to the sensitivity of the devices to interfacial effects such as molecular motion, surface irregularities, and adsorption of unwanted analytes.^{1.30} Despite these effects, QCMs represent a powerful and growing platform for analyte detection and quantification.

1.3.2 Ultrasound Velocity Measurements

Measurements of ultrasound velocity and attenuation can also easily be done. Since these parameters are dependent on the viscoelastic properties and density of the media, they have characteristic values. Early applications examining the velocity and attenuation values were in the analysis of liquids. An ultrasonic pulse would be emitted from a transducer, propagate through a sample, and be reflected back to the transducer to be measured. Using this pulse-echo configuration, the characteristic sound velocity and

attenuation in liquids can be measured.^{1.31,1.32} These parameters are dependent on the viscoelastic properties of the medium.^{1.32,1.33} As a result, characteristic values for a medium can be attributed to the chemical structure.

Measuring ultrasound velocity has also been used to determine concentrations in binary mixtures.^{1.34-1.36} However, a major problem in velocity-based ultrasound measurements is that the relationship between sound velocity and chemical composition is not always monotonic over a broad range. These nonlinearities can reduce the range of concentrations over which the analysis is possible.^{1.37} Estimating concentrations in multi-component mixtures is likewise limited.^{1.38,1.39} Different ratios of the components can give rise to similar velocities. As a result, estimates of the composition of these mixtures can have non-unique solutions. By measuring at multiple temperatures, unique solutions can be found.^{1.33} However, the need for multiple measurements increases the complexity and time required for the determination.

The attenuation coefficients and velocities have also been shown to be frequency-dependent.^{1.40-1.42} Attenuation and velocity at multiple frequencies can be measured independently to create a spectral profile that is characteristic of sample composition. This has been used in a wide variety of applications, from following a chemical reaction^{1.43} to measuring the concentrations in heterogeneous mixtures such as surfactant emulsions^{1.44} and suspensions.^{1.40} Polymer characteristics have also been studied, including the formation of polymer networks during crosslinking,^{1.45} conformational changes by phase transitions,^{1.46} and particle size distributions.^{1.12, 1.40} The ability to non-destructively and non-invasively measure constituents is also of great interest in the food and drink industry. Ultrasonic velocity spectroscopy has been used to

measure important food characteristics such as gelling,^{1.47,1.48} coagulation,^{1.49} and fermentation,^{1.8} as well as beverage constituent concentrations.^{1.39} These measurements also demonstrate the capability of ultrasound to propagate through a variety of media with high optical scattering and absorption.

In general, limitations in these velocity-based ultrasonic measurements arise from physical constraints. Due to the temperature dependence of the viscoelastic properties, any variability will quickly degrade sensitivity. Though it is possible to compensate for temperature changes, this is generally limited to narrow ranges of application.^{1.50} Likewise, variability in the path length will result in estimation errors. Simultaneous changes in multiple components or physical parameters is also limiting due to nonlinear behavior.

1.4 Ultrasound in Biomedical Applications

As with analytical uses discussed above, measurements of ultrasound velocity have been used extensively in biomedical applications. Using velocity measurements, ultrasound has found application in the biomedical field as one of the most widespread imaging techniques. The pulse-echo technique is used to obtain both static pictures and for real-time imaging of a wide variety of tissues and organs. Typical applications consist of measuring the time elapsed between the transmission of an ultrasound pulse and the detection of backscattered waves. The intensity of this reflected ultrasound pulse can also be measured to provide more detailed imaging. Reflection of ultrasound waves occurs most strongly at interfaces between materials with different acoustic impedances. The

large contrast between tissue and growths or inclusions has also made the methodology useful for the diagnostic examination of tissue.

At higher intensities, absorption of the ultrasound energy by the medium can also be used to heat tissues. Therapeutic heating of tissues was suggested by Freundlich *et al.* in 1932, who demonstrated the effect at 300 KHz.^{1.51} Today, ultrasound is a common non-pharmacological treatment for pain used by physical therapists using frequencies below 3 MHz.^{1.52,1.53} This has also been shown as an effective method to assist wound healing.^{1.54} At normal diagnostic ultrasound powers, however, this heating is not a concern.^{1.55}

1.4.1 Ultrasound Imaging

When propagating through tissue layers, a fraction of the ultrasound power will be reflected at interfaces. By measuring the delay time between emission and detection of the reflected wave, an image of internal structure can be constructed. Further, the magnitude of reflection will depend on the impedance of the media. A large mismatch, for example between muscle and bone, results in a larger fraction of the wave being reflected (see Equation 1.7). Likewise, the attenuation caused by different tissues varies.^{1.15} As a result, the attenuation of the ultrasound wave is also an important imaging characteristic.

The main advantage when using ultrasound for biomedical measurements is the inherent non-invasiveness and safety of the method.^{1.55} Further, the high scattering and optical opacity of tissues and biological fluids are limiting to most spectroscopic

techniques. These factors do not limit the penetration of ultrasound, allowing imaging of tissues within a patient. Other imaging techniques used in medicine such as magnetic resonance imaging can sometimes require potentially hazardous contrast agents.^{1.56,1.57} Likewise, the cost of ultrasound imaging is significantly less and the imaging apparatus is portable, making it suitable for measurements in the field.^{1.58} Though differentiation between tissues is generally possible, lower contrast is seen between tissues with similar acoustic properties.^{1.20} However, despite this minor limitation, ultrasound imaging is one of the most used imaging techniques.

The majority of ultrasound imaging applications use an array of 1–20 MHz ultrasound transducers to create 2 dimensional images. Biomedical ultrasound is often associated with fetal imaging during pregnancy. Obstetric sonography can be used for a variety of applications including determining fetal sex, screening for abnormalities, and monitoring growth.^{1.59} Similar analyses are also used to monitor heart physical condition,^{1.60, 1.61} kidney and liver function,^{1.62} and to look for and identify brain injuries.^{1.63} Studies in these diverse tissues demonstrate the broad applicability of ultrasound for biomedical imaging.

Real-time measurements using ultrasound also allow for the detection of a Doppler shift in a signal. A sample moving towards the transducer will result in a slightly higher frequency, while one moving away from the transducer will show a decrease in frequency. This has allowed ultrasound imaging of blood flow, expanding ultrasound imaging to measure cardiac output, which is an important monitor of cardiovascular function.^{1.64} Doppler measurements in kidneys have also been used to assess the hepatic arterial flow, which is a diagnostic marker for conditions such as renal cirrhosis, portal

hypertension, and arteriosclerosis.^{1.65,1.66} Measuring blood flow in the brain has also recently been used to examine brain function.^{1.67} This real-time measurement capability provides significant advantages over other imaging modalities.

1.4.2 Ultrasound Contrast Agents

One of the fundamental aspects of ultrasound that have been developed recently are dispersive contrast agents. Development of ultrasound contrast enhancing agents began in 1968, when Gramiak and Shah injected saline into subjects to improve aortic imaging.^{1.68} Finding that the saline improved imaging, they suggested that this was caused by bubbles in the solution. Bove *et al.* (1969) would subsequently show that these bubbles could be generated by rapid injection through a catheter.^{1.69} The increase in the ultrasonic backscattering allowed imaging of structures that were otherwise hard to distinguish, making the development of safe contrast materials appealing for the growing ultrasonic imaging field.

Most early work focused on the improvement of cardiac imaging.^{1.70} The signal enhancement provided by contrast agents is also useful for monitoring ischemia and reperfusion.^{1.71} Contrast enhancement has also found use in a variety of other applications such as tumor visualization,^{1.72} evaluation of brain perfusion,^{1.73} and identification of lesions in the liver.^{1.74} Perfusion of the contrast agents through tissues can also be used to enhance visualization when the surrounding tissues have similar properties.^{1.20} These applications demonstrate the usefulness of selectively altering the ultrasound response in a targeted location.

A wide variety of contrast agents were developed through the 1980s using a variety of materials such as polygelin colloids,^{1.75} collagen microspheres,^{1.76} albumin solutions,^{1.77} and nongaseous perfluorocarbon emulsions.^{1.78} Hydrogen peroxide (0.2% in water) was also used to generate microbubbles by chemical reaction *in situ*.^{1.79} Several different microbubbles were also designed, including gelatin-encapsulated nitrogen bubbles,^{1.72} saccharide microspheres,^{1.80} carbon dioxide bubbles,^{1.81} and albumin-encapsulated air microbubbles.^{1.82} Though providing tissue contrast, early agents often had poor durability or variable contrast enhancement.

The current generation of commercially available ultrasound contrast agents consists primarily of stable, well-defined encapsulated bubbles. Examples of current commercial agents are listed in Table 1.2. The high scattering cross-section in gas-filled bubbles generally make these appealing to maximize the contrast enhancement.^{1.83} Though allergic reactions to the chemicals and surfactants are possible,^{1.84} no pattern of specific brain, liver, or kidney toxicity has been shown.^{1.85} As a result, contrast agents are also generally considered safe and routinely used to improve imaging.

Quantitative measurements using contrast agents can also be made. The ultrasound backscatter intensity, I_s , is related to the incident intensity and the scattering cross-section of the contrast agent. When there are multiple scatterers present,

$$I_s = I_i(\sigma N), \quad (1.13)$$

where I_i is the initial intensity, σ is the scattering cross section of the contrast agent, and N is the number of contrast molecules in solution.^{1.86} Though complex, the relationship between the measured intensity and the contrast agent content in a sample or tissue could be modeled.^{1.87} This relationship has proved useful for determining quantitative values of

Table 1.2: A selection of current ultrasound contrast agents.^{1.73,1.84}

Trade Name	Solid Material	Gas	Mean Diameter (μm)
Albunex	Albumin	Air	3.8
Definity	Phospholipid bilayer	C ₃ F ₈	1.1 – 3.3
EchoGen	Dodecafluoropentane emulsion	–	2.0 – 5.0
Echovist	Galactose	Air	2.0
Levovist	Galatose + Palmitic acid	Air	2.0
Optison	Albumin	C ₃ F ₈	2.0 – 4.5
SonoVue	Phospholipid, PEG, Palmitic acid	SF ₆	2.5

perfusion in organs^{1.88} and tumors.^{1.89} Further, with repeat ultrasound measurements, the rate of perfusion can be determined.^{1.90} This kinetic information can aid in the diagnostic process, and likewise demonstrates the value of real-time measurement.

1.4.2.1 Targeted Ultrasound Contrast Agents

Interest has also grown in the development of contrast agents with molecular recognition elements. This would allow contrast agents to recognize and bind to specific epitopes, allowing identification of the target. Lanza *et al.* (1996) first reported the use of biotinylated C₃F₈ emulsion contrast agents for targeting arterial blood clots which had been flushed with avidin.^{1.91} The high binding constants between biotin and avidin promoted fast molecular association, overcoming earlier limitations caused by rapid biological clearance.^{1.78} Although high-flow conditions can pose a challenge to efficient binding, targeting molecular sites with high surface density can promote fast recognition.^{1.92} Though this allows fast imaging of clots, it was suggested that modifying the surface chemistry would allow for a wide range of tissues to be targeted.

The targeting mechanism of these contrast agents have since been expanded to other recognition mechanisms including antibodies,^{1.93,1.94} shorter oligopeptides,^{1.95} and polysaccharides.^{1.96} Targeted contrast agents have found application in imaging of a variety of pathological tissues, such as tumor sites.^{1.97} Other targets have also included blood clots,^{1.98} arteriogenesis,^{1.99} scanning for cardiac transplant rejection,^{1.93} and monitoring kidney damage and inflammation.^{1.94} The localized contrast enhancement can aid in assessment of tissue, as well as aiding in biopsy targeting for diagnostics.

1.5 Nonlinear Ultrasound Propagation

Ultrasound propagation has both linear and nonlinear mechanisms. Distortions in the ultrasound propagation resulting from nonlinear mechanisms are important in a wide variety of applications. This distortion arises due to inequalities in the waveform velocity. The ultrasound wave consists of alternating compression and rarefaction phases. Due to particle motion induced by the propagating wave, positive particle velocity (caused by compression) is slightly higher than negative velocity (resulting from rarefaction). As a result, the portion of the waveform at positive pressures steepens, while the negative pressure regions flatten. Figure 1.3(a) shows a sinusoidal waveform and the sawtooth profile resulting from nonlinear distortion can be seen in Figure 1.3(b). When the ultrasound wave is examined in the frequency domain, this distortion can be quantified by the generation and increase in magnitude of harmonic frequencies.^{1.100,1.101} These differences in the frequency domain are shown in Figures 1.3(c and d). Although the particle velocity is generally smaller than the propagation speed, the nonlinear distortion effect is cumulative.^{1.100,1.102} As a result, larger distortions are seen over longer propagation path lengths and at higher ultrasound intensities.

The magnitude of the nonlinear distortion in a medium can be described according to the nonlinearity ratio B/A . This value is derived from the state equation of acoustic propagation through a liquid,

$$p = p(\rho, s) \quad (1.14)$$

which p is the pressure, ρ is the density, and s is the entropy.^{1.103} This equation can be expressed by a Taylor series expansion as

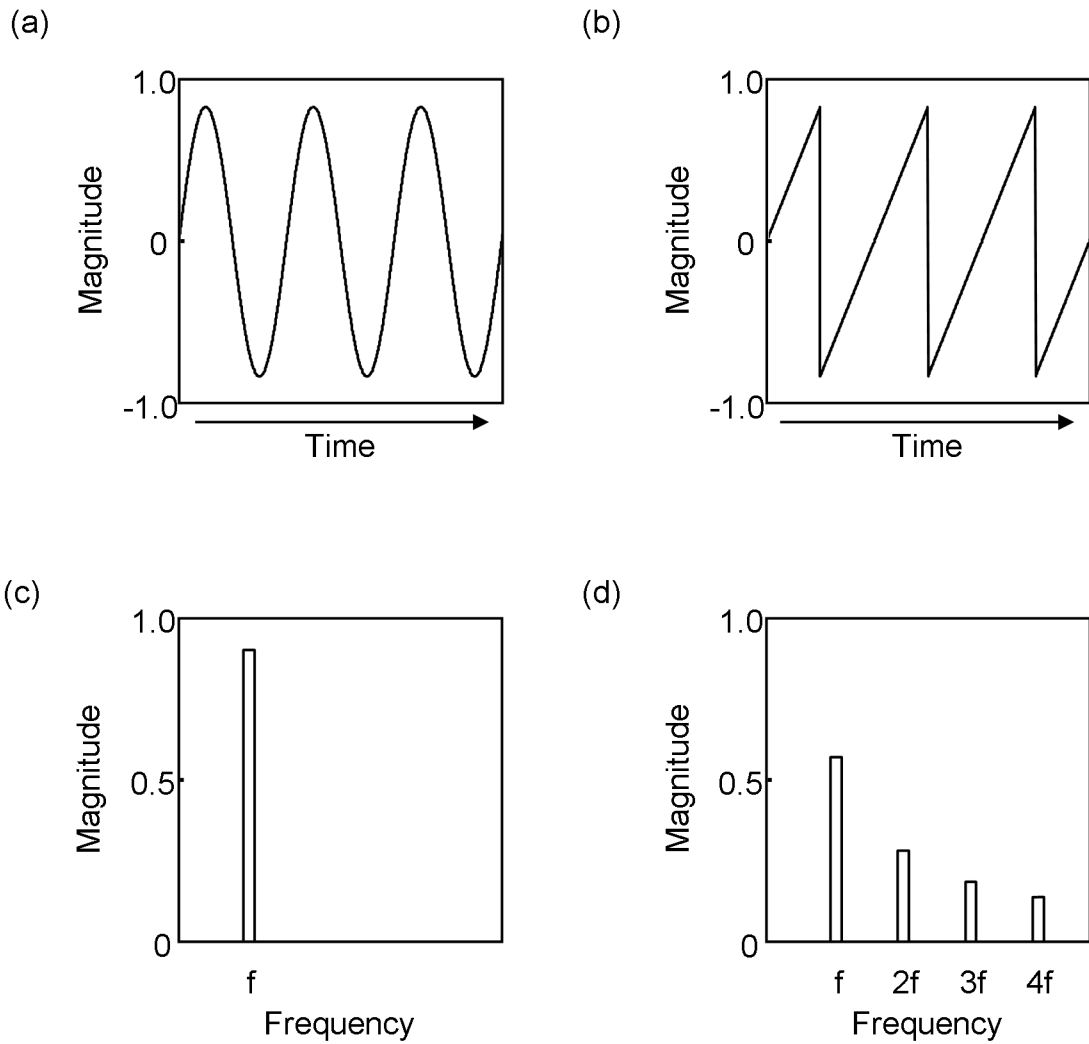


Figure 1.3: Distortion of an ultrasound waveform. (a) undistorted sinusoidal waveform, (b) Sawtooth distortion due to nonlinear propagation, (c) Frequency profile of un-distorted waveform showing prominent single frequency (f), (d) Frequency profile of nonlinearly distorted wave showing harmonic frequency components ($2f$, $3f$, $4f$...). All units are arbitrary.

$$p = p_0 + \left(\frac{\partial p}{\partial \rho} \right)_{\rho=0,s} (\rho - \rho_0) + \left(\frac{\partial^2 p}{\partial \rho^2} \right)_{\rho=0,s} \frac{(\rho - \rho_0)^2}{2!} + \dots \quad (1.15)$$

where p_0 and ρ_0 are the equilibrium pressures and mass densities of the medium.^{1.104} Changes in the entropy are small and can be neglected.^{1.105} With the derivatives taken at $\rho = \rho_0$ and s held constant, this equation can be rewritten as

$$p = p_0 + A \left(\frac{\rho - \rho_0}{\rho_0} \right) + \frac{B}{2!} \left(\frac{\rho - \rho_0}{\rho_0} \right)^2 + \dots \quad (1.16)$$

in which the linear coefficient $A = \rho_0 (\partial p / \partial \rho)_{\rho=0,s} = \rho_0 c_0^2$, where c_0 is the velocity of the ultrasonic wave, and the second order $B = \rho_0^2 (\partial^2 p / \partial \rho^2)_{\rho=0,s}$.^{1.104,1.105} Though the nonlinear propagation is also reflected in higher order terms in the Taylor expansion, these are generally neglected due to their smaller contributions.^{1.103,1.104} Likewise, cross terms that arise due to heterogeneities in mixtures are not well characterized and are not included. When these higher order and cross-terms are ignored, the dimensionless second order elastic ratio

$$\frac{B}{A} = \frac{\rho}{c_0^2} \left(\frac{\partial^2 p}{\partial \rho^2} \right)_{\rho=0,s} = 2\rho_0 c_0 \left(\frac{\partial c}{\partial p} \right)_s \quad (1.17)$$

can be written, which describes the amount of nonlinear waveform distortion caused by the medium through which the acoustic wave propagates.^{1.104} The nonlinear parameter is characteristic of a given medium, relating the distortion processes of a propagating ultrasound wave to the molecular structure of the media. Examples of the nonlinear parameter in notable media are shown in Table 1.3. The B/A parameter accounts for nonlinearity up to the second order. However, higher order terms can also be used to

Table 1.3: Acoustic properties of selected materials.^{1,9,1.165}

Medium	Velocity (m/s)	Nonlinearity ratio (B/A)
Distilled water	1480	5.0
Sea water	1531	5.25
Methanol	1103	9.42
Ethanol	1159	10.52
Whole blood (human)	1570	6.1
Fat	1450	10
Muscle	1590	7.4

describe the distortion processes in systems.^{1.106} The evaluation of the distortions in the ultrasound wave due to these nonlinear effects will be evaluated in this thesis.

1.5.1 Nonlinear Ultrasound in Analytical Chemistry

Frequency distortions due to the nonlinear propagation of ultrasound are useful for analytical applications. The generation of harmonics is dependent on the medium through which the ultrasound propagates. Although many high order harmonics are generated, ultrasound attenuation increases with higher frequencies. As a consequence, nonlinear changes in the lower harmonic orders are of higher intensity.^{1.103} Measuring the intensity of these frequencies can provide a method to probe the physical properties of the medium, which depend on the molecular composition.

Measurement of the B/A parameter has been used to derive information about the structural properties and compositions of sample media. It has been shown that the nonlinearity parameter is dependent on the concentrations of constituents in, for example, in low molecular weight alcohols^{1.107} and amino acids.^{1.108} Estimates of the ratio of free to bound water molecules in protein solutions have also been demonstrated, showing potential applications in biomedical tissue measurement.^{1.109} The nonlinearity parameter in mixtures has also been examined, showing that mixtures of two different liquids have B/A values that are not linear combinations of the two pure liquids.^{1.110,1.111} This is attributed to the solvent-solute interactions resulting in the formation of clathrates.^{1.36} Recently, nonlinear ultrasound propagation has also been shown useful for the analysis of bulk materials such as concrete and metal alloys. The generation of harmonic frequencies

has been used to identify microstructure damage and fatigue.^{1.112–1.115} The non-destructive assessment is particularly appealing in these applications as it allows routine measurement without degradation of the structure.

Acoustic emissions generated *in situ* have also been used for non-invasive analytical measurement of material properties. Ultrasound vibro-acoustography was first proposed by Fatemi and Greenleaf (1998) using two focused ultrasound sources.^{1.116} One source generates a frequency f_0 , while the second is operated at $f_0 + \Delta f$. The offset, Δf , can range from a few Hz to hundreds of KHz. At the focal point of these two beams, interference will result in an oscillating acoustic force, which will induce vibrations in the material at the Δf frequency. This amplitude of this emission is then measured using a separate transducer. This measurement of the acoustic emission is analogous to medical palpitation used in tissue examination. The intensity of the acoustic emission is dependent on the size, shape, and viscoelastic properties^{1.117,1.118} by the relation

$$P_{\Delta f} = 4\rho c^2 H_{\Delta f}(l) Q_{\Delta f} F_{\Delta f} . \quad (1.18)$$

The medium transfer function, $H_{\Delta f}$, represents the effect of the medium on the ultrasound emission. This parameter is dependent on the distance travelled, l . The acoustic outflow, $Q_{\Delta f}$, describes the volume of the medium displaced by the mechanical response of the object to the difference frequency. Finally, $F_{\Delta f}$, is the force applied on the object. Together, these parameters demonstrate the dependence of the acoustic signal measured on the mechanical properties of the system.

Due to the dependence of the intensity of the acoustic emission on the viscoelastic properties, vibro-acoustic techniques are useful for detection and imaging of hard materials surrounded by a softer medium such as determining the tensile modulus of

solids immersed in liquids,^{1.119} and the identification of flaws in ceramics and electronic chips.^{1.120} The technique has also been used to image tissue inclusions, such as calcification in breast^{1.121,1.122} and arterial tissues,^{1.123} as well as for locating metallic implants.^{1.124,1.125} These applications demonstrate the applicability of vibro-acoustography for both material evaluation and biomedical imaging.

Vibro-acoustic measurements can also be made simultaneously at multiple values of the offset frequency Δf . This is accomplished by increasing the number of transducers, or by using frequency-modulated ultrasound beams.^{1.120,1.126,1.127} Multi-frequency approaches have been used to improve imaging and material testing.^{1.120,1.127} The advantage of multiple frequency measurements is an improvement in the signal-to-noise ratio and contrast by selecting the best frequency offset in samples in which the response is unknown.

Nonlinear distortions of ultrasound by a medium are also used in Acoustic Resonance Spectrometry (ARS). In this technique, two ultrasound transducers are connected by a quartz rod. The rod, which is bent, can then be placed in contact with a sample. A fraction of the ultrasound will propagate through the sample, which creates an interference pattern with the rest of the wave. Although this technique was first used to examine linear effects,^{1.128} nonlinear effects have more recently been considered.^{1.129} Measurements using this system have been demonstrated for process monitoring in solid tablets^{1.129, 1.130} and in colloidal lotions.^{1.131} Due to the distortion of the ultrasound wave in the interrogated medium, new frequency components are generated that correspond to the sample composition.

1.5.2 Nonlinear Ultrasound in Biomedical Applications

Though ultrasound had been used in medical applications for decades, it was suggested in a pair of companion papers in 1980 that nonlinear effects were appreciable at biomedical frequencies and intensities.^{1.100,1.132} By 1985, this effect had been demonstrated in muscle tissue *in vivo*.^{1.133} Since then, much interest and development has taken place in biomedical applications of ultrasound distortion, including improvements in imaging, lithotripsy, and surgery.

Improvements in biomedical imaging were achieved by measuring the harmonics that arise due to nonlinear distortion.^{1.134} The intensity of harmonic frequencies can be measured rather than the fundamental, resulting in several advantages. Part of the image degradation arises due to the surface layers which are of little interest. As the harmonic frequencies are generated *in situ*, these bypass the surface layers and can improve the contrast ratio between tissues.^{1.135} A similar improvement in the contrast to noise ratio arises due to the lower intensity of the harmonic frequencies. The imaging properties are related to the width of the ultrasound beam. The ultrasound power of the harmonic frequencies is proportional to the square of the fundamental frequency.^{1.136} As a result, the magnitude of the center of the beam will increase relative to the sidelobes, and noise due to scattering and reverberation will decrease. Further, the shorter wavelength, narrower beam, and reduced sidelobe of the harmonic frequencies improves both the axial and the lateral resolution.^{1.137, 1.138} This has been used to improve imaging, including cardiac muscle structure,^{1.139} abdominal imaging,^{1.135,1.137} and for detecting tissue

abnormalities such as breast lesions.^{1.136} Overall, the improved contrast and structural visualization due to this nonlinear effect are advantageous for imaging.

The nonlinear distortion of the ultrasound beam has also been used in therapeutic and surgical applications. The large shear differential that arises from the sawtooth-like nonlinear distortion can be used to generate shock waves at high powers. By focusing the ultrasound beams, these shocks can be created at specific sites. This has been shown to allow the breakup of gallbladder^{1.140} and kidney^{1.141} stones *in situ*. However, care must be taken to minimize tissue morbidity. When focused on tissue sites, the nonlinear ultrasound waves can increase the temperature by over 20°C in fractions of a second, which is typically sufficient to destroy cells in less than 10 seconds.^{1.142,1.143} Targeted temperature increases induced by focusing ultrasound have been shown useful for ablating tumors^{1.144–1.146} and blood vessel occlusions.^{1.147} However, heating leading to tissue ablation is not a concern at normal diagnostic ultrasound powers.^{1.55}

1.5.2.1 Nonlinearity in Contrast Agents

The nonlinear response of contrast agents has also been used to enhance visualization in medical imaging. In contrast agents, the B/A parameter may be orders of magnitude larger than for bulk media.^{1.148} With ultrasonic compression and rarefaction, contrast agents oscillate isotropically at specific resonance frequencies.^{1.149–1.151} The resonance frequency for thin-shelled microspheres in solution can be approximated as

$$f_0 = \frac{1}{2\pi a_e} \sqrt{\frac{3K_p}{\rho_L}}, \quad (1.19)$$

where a_e is the equilibrium radius of the microbubble, K_p is bulk modulus of the polymeric microbubble capsule, and ρ_L is the density of the surrounding liquid, which resembles the Minnaert equation for microbubbles.^{1.149} The resonance frequency for most commercial microbubbles, which have diameters between 1–5 μm , are typically between 1–10 MHz.^{1.84} This is advantageous as many commercial ultrasound instruments are sensitive in this range.

Similar to the distortion seen in liquids, compression of the contrast agents occurs more rapidly than expansion, resulting in a nonlinear distortion of the resonance frequency and generating new frequency components. These include harmonic frequencies ($2f_0$, $3f_0$, ...), ultraharmonics ($1.5f_0$, $2.5f_0$, ...), and subharmonics ($0.5f_0$, $0.25f_0$, ...).^{1.152,1.153} Even at low intensities in common ultrasound instruments, significant nonlinear distortion can occur in contrast agents.^{1.154} In some cases, this is seen simply as a large increase in contrast, however, the generation of other harmonic frequency components provides the opportunity for further analysis.

Harmonic frequencies, rather than the fundamental, are used for second harmonic imaging (SHI). By first injecting a contrast material and then filtering the signal to a resonance harmonic, it is possible to compensate for inadequate signal-to-noise ratios when measuring capillary blood flow and perfusion.^{1.155,1.156} This form of imaging continues to be used today to improve imaging of low signal-to-noise tissues such as the brain,^{1.157,1.158} offering significant potential for monitoring of difficult to image tumors and infarctions.

More recently, interest has grown in the use of subharmonic frequencies to further suppress the signal from tissues. Results have shown that imaging shows improvement

in vitro.^{1.152} The relatively lower generation of subharmonics in tissue has also been shown useful to improve the identification of breast cancers^{1.159} and in imaging of hepatic veins.^{1.160} The intensity of subharmonic frequencies has also been correlated with pressure,^{1.161,1.162} showing potential for localized blood pressure measurements.

1.6 Conclusions and Research Objectives

Overall, ultrasound is an important tool in many disciplines involving rapid analysis. The non-invasive and non-destructive properties of ultrasound make this platform appealing for point-of-care measurements. Biomedical and industrial imaging applications are well established and routinely used. However, applications making use of ultrasound for analyte quantification remain in the development phase. Traditional measurements of velocity and attenuation are limited to the analysis of simple systems due to nonlinear responses in more complex media. Frequency domain analysis of the ultrasound signal offers the possibility of determining quantitative information about the system under investigation. Single-frequency analyses have shown promising results for both sample characterization and biomedical imaging. Second harmonic imaging of contrast agents, for example, can increase the signal to noise ratio of the measurement. However, the non-linearities that occur during ultrasound propagation result in broadband frequency changes that are linked with the viscoelastic properties of a sample. Despite this, multi-frequency measurements remain minimally explored. This provides the opportunity to develop point-of-care technologies to address the need for analyte quantification in complex system such as mixtures and biological fluids.

This dissertation is presented in seven chapters, which discuss the research programs touching on the ultrasound methods presented in the background. In Chapter 2, the quantification of theophylline using molecularly imprinted cellulose hydrogels and an inexpensive detection system is presented. This work is a supplement to a co-principal-authored manuscript published in the journal *Talanta*, which is attached in Appendix A. Chapter 3 demonstrates the clinically-relevant quantification of acetaminophen in a series of biological fluids using an immunoglobulin-linked cellulose hydrogel. This chapter demonstrates the strengths of the ultrasound methodology as a point-of-care technique, allowing measurements to be made rapidly without the need for an extensive laboratory analysis. Chapter 4 presents the development of a dendrimeric polymer sensor with a new vibrational mechanism. Quantification of a larger molecule, the protein Tumor Necrosis Factor- α , is presented to demonstrate the mass-dependence of the ultrasound sensor measurements. Together, these three chapters represent novel extensions of nonlinear ultrasound contrast agent behavior and analysis.

The nonlinear distortion of ultrasound caused by the medium is then used for volume fraction estimation in water, methanol, and ethanol mixtures in Chapter 5. These distortions are related to the molecular structures in these mixtures. This is followed, in Chapter 6, by fractional composition determination of ethanol and carbohydrate content in commercial beverages using the nonlinear distortion. Finally, Chapter 7 presents a summary of the overall thesis and discusses future directions for ultrasound frequency analysis techniques.

1.7 References

- 1.1. Thomas D. Rossing, *Springer handbook of acoustics* (Springer, New York, 2007).
- 1.2. Daniel R. Raichel, *The Science and Applications of Acoustics*, (Springer-Verlag, New York, 2000).
- 1.3. J. Curie and P. Curie, “Développement par compression de l’électricité polaire dans les cristaux hémihédres à faces inclinées”, *B. Soc. Fr. Mineral.* **3**, 90–93 (1880).
- 1.4. I. Woloshyn, “Industrial ultrasonics in the U.S.S.R.”, *Ultrasonics* **1**, 14–26 (1963).
- 1.5. J.W. Hunt, M. Arditi, and F.S. Foster, “Ultrasound transducers for pulse-echo medical imaging”, *IEEE T. Bio-med. Eng.* **30**, 453–481 (1983).
- 1.6. J. Capelo-Martínez, “Ultrasound in Chemistry”, WILEY-VCH Verlag GmbH & Co. Weinheim, 209
- 1.7. K. Vilku, R. Mawson, L. Simons, D. Bates, “Applications and opportunities for ultrasound assisted extraction in the food industry – A review”, *Innov. Food Sci. Emerg.* **9**, 161–169 (2008).
- 1.8. F.P. Capote and L. de Castro, “Ultrasound in analytical chemistry”, *Anal. Bioanal. Chem.* **387**, 249–257 (2007).
- 1.9. Heinrich Kuttruff, *Acoustics: An introduction*, (Taylor and Francis, New York, 2004).
- 1.10. P. Resa, T. Bolumar, L. Elvira, G. Pérez, and F. Montero de Espinosa, “Monitoring of lactic acid fermentation in culture broth using ultrasonic velocity”, *J. Food Eng.* **78**, 1083–1091 (2007).

- 1.11. R.C. Weast, *CRC Handbook of Chemistry and Physics*, 58th edition, (CRC Press, Inc., Ohio, 1977). pp E47-E48.
- 1.12. A.S. Dukhin and P.J. Goetz, “Acoustic spectroscopy for concentrated polydisperse colloids with high density contrast”, *Langmuir* **12**, 4987–4997 (1996).
- 1.13. G. ter Haar and C. Coussios, “High intensity focused ultrasound: Physical principles and devices”, *Int. J. Hyperthermia* **23**(2), 89–104 (2007).
- 1.14. C.J. Diederich and K. Hynynen, “Ultrasound technology for hyperthermia”, *Ultrasound Med. Biol.* **25**, 871–887 (1999).
- 1.15. A. Marin, H. Sun, G.A. Hussein, W.G. Pitt, D.A. Christensen, and N.Y. Rapoport, “Drug delivery in pluronic micelles: effect of high-frequency ultrasound on drug release from micelles and intracellular uptake”, *J. Control. Release* **84**, 39–47 (2002).
- 1.16. X. Fan and K. Hynynen, “The effect of wave reflection and refraction at soft tissue interfaces during ultrasound hyperthermia treatments”, *J. Acoust. Soc. Am.* **91**, 1727–1736 (1992).
- 1.17. H. Wang, S. Fleming, and Y. Lee, “A remote, non-destructive laser ultrasonic material evaluation system with simplified optical fibre interferometer detection”, *J. Nondestruct. Eval.* **28**(2), 75–83 (2009).
- 1.18. X. Chen, T. Stratoudaki, S.D. Sharples, and M. Clark, “A laser-activated MEMS transducer for efficient generation of narrowband longitudinal ultrasonic waves”, *IEEE T. Ultrason. Ferr.* **58**, 470–476 (2011).

- 1.19. M. Lulow, X. Yu, A. Li, T. Jiang, M. Chen, B. Zhao, X. Zhou, and J. Wang, “Comparison of Contrast Enhanced Ultrasound and Contrast Enhanced CT or MRI in Monitoring Percutaneous Thermal Ablation Procedure in Patients with Hepatocellular Carcinoma: A Multi-Center Study in China”, *Ultrasound Med. Biol.* **33**, 1736–1749 (2007).
- 1.20. M.A. Wheatley, F. Forsberg, K. Oum, R. Ro, and D. El-Sherif, “Comparison of in vitro and in vivo acoustic response of a novel 50:50 PLGA contrast agent”, *Ultrasonics* **44**, 360–367 (2006).
- 1.21. G. Sauerbrey, “Use of quartz oscillators for weighing thin layers and for Microweighing”, *Z. Phys.* **155**, 206–222 (1959).
- 1.22. M.A. Cooper and V.T. Singleton, “A survey of the 2001 to 2005 quartz crystal microbalance biosensor literature: applications of acoustic physics to the analysis of biomolecular interactions”, *J. Mol. Recognit.* **20**, 154–184 (2007).
- 1.23. W.H. King, “Piezoelectric sorption detector”, *Anal. Chem.* **36**, 1735–1739 (1964).
- 1.24. C.K. O’Sullivan and G.G. Guilbault, “Commercial quartz crystal microbalances – theory and applications”, *Biosens. Bioelectron.* **14**, 663–670 (1999).
- 1.25. J. Ngeh-Ngwainbia, A.A. Suleiman, and G.G. Guilbault, “Piezoelectric crystal biosensors”, *Biosens. Bioelectron.* **5**, 13–26 (1990).
- 1.26. G.C. Dunham, N.H. Benson, D. Petelenqt, and J. Janata, “Dual Quartz Crystal Microbalance”, *Anal. Chem.* **67**, 267–272 (1996).
- 1.27. K.K. Kanazawa, “Mechanical behaviour of films on the quartz microbalance”, *Faraday Discuss.* **107**, 77–90 (1997).

- 1.28. C.J. Percival, S. Stanley, M. Galle, A. Braithwaite, M.I. Newton, G. McHale, and W. Hayes, “Molecular-Imprinted, Polymer-Coated Quartz Crystal Microbalances for the Detection of Terpenes”, *Anal. Chem.* **73**, 4225–4228 (2001).
- 1.29. J. Rickert, T. Weiss, W. Kraas, G. Jung, and W. Göpel, “A new affinity biosensor: self-assembled thiols as selective monolayer coatings of quartz crystal microbalances”, *Biosens. Bioelectron.* **11**, 591–598 (1996).
- 1.30. M. Thompson, A.L. Kipling, W.C. Duncan-Hewitt, L.V. Rajaković, and B.A. Čavić-Vlasak, “Thickness-shear-mode acoustic wave sensors in the liquid phase. A review”, *Analyst* **116**, 881–890 (1991).
- 1.31. J.R. Pellam and J.K. Galt, “Ultrasonic propagation in liquids: application of pulse technique to velocity and absorption measurement at 15 megacycles”, *J. Chem. Phys.* **14**, 608–613 (1946).
- 1.32. Andreae and P.L. Joyce, “30 to 230 megacycle pulse technique for ultrasonic sorption measurements in liquids”, *Brit. J. Appl. Phys.* **13**, 462–467 (1962).
- 1.33. A. Warsinke, “Point-of-care testing of proteins”, *Anal. Bioanal. Chem.* **393**, 1393–1405 (2009).
- 1.34. M. Van Sint Jan, M. Guarini, A. Guesalaga, J. Ricardo Pérez-Correa, and Y. Vargas, “Ultrasound based measurements of sugar and ethanol concentrations in hydroalcoholic solutions”, *Food Control* **19**(1), 31–35 (2008).
- 1.35. N.I. Contreras, P. Fairley, D.J. McClements, and M.J.W. Povey, “Analysis of the sugar content of fruit juices and drinks using ultrasonic velocity measurements”, *Int. J. Food Sci. Tech.* **21**, 515–529 (1992).

- 1.36. E.K. Baumgartner and G. Atkinson, “Ultrasonic velocity in nonelectrolyte-water mixtures”, *J. Phys. Chem.* **76**, 2336–2340 (1971).
- 1.37. G.W. Villard, “Temperature Coefficient of Ultrasonic Velocity in Solutions”, *J. Acoust. Soc. Am.* **19**, 235–241 (1947).
- 1.38. M. Vatandas, A.B. Koc, and C. Koc, “Ultrasonic velocity measurements in ethanol-water and methanol-water mixtures”, *Eur. Food. Res. Technol.* **225**, 525–532 (2007).
- 1.39. P. Resa, L. Elvira, F. Montero de Espinosa, and Y. Gómez-Ullate, “Ultrasonic velocity in water–ethanol–sucrose mixtures during alcoholic fermentation”, *Ultrasonics* **43**, 247–252 (2005).
- 1.40. A.K. Holmes, R.E. Challis, and D.J. Wedlock, “A wide-bandwidth ultrasonic study of suspensions: the variation of velocity and attenuation with particle size”, *J. Colloid Interf. Sci.* **168**, 339–348 (1994).
- 1.41. A.S. Dukhin and P.J. Goetz, “Characterization of aggregation phenomena by means of acoustic and electroacoustic spectroscopy”, *Colloid. Surface. A.* **144**, 49–58 (1998).
- 1.42. B. Park, A.D. Whittaker, R.K. Miller, and D.E. Bray, “Measuring intramuscular fat in beef with ultrasonic frequency analysis”, *J. Anim. Sci.* **72**, 117–125 (1994).
- 1.43. W. Ko and V. Buckin, “Ultrasonic monitoring of reaction of Fullerene [C60] with 3-Chloroperoxy Benzoic Acid”, *Elastomer* **41**(1), 57–62 (2006).
- 1.44. J. Hsu and A. Nacu, “Behavior of soybean oil-in-water emulsion stabilized by nonionic surfactant”, *J. Colloid Interf. Sci.* **259**, 374–381 (2003).

- 1.45. F. Lionetto, A. Sannino, and A. Maffezzoli, “Ultrasonic monitoring of the network formation in superabsorbent cellulose based hydrogels”, *Polymer* **46**, 1796–1803 (2005).
- 1.46. K. Van Durme, L. Delellio, E. Kudryashov, V. Buckin, and B. Van Mele, “Exploration of high-resolution ultrasonic spectroscopy as an analytical tool to study demixing and remixing in poly(N-isopropyl acrylamide)/water solutions”, *J. Polym. Sci. Pol. Phys.* **43**, 1283–1295 (2005).
- 1.47. F. Lionetto, A. Maffezzoli, M. Ottenhof, I.A. Farhat, and J.R. Mitchell, “Ultrasonic investigation of wheat starch retrogradation”, *J. Food Eng.* **75**, 258–266 (2006).
- 1.48. L. Lehmann, E. Kudryashov, and V. Buckin, “Ultrasonic monitoring of the gelatinization of starch”, *Prog. Coll. Poly. Sci.* **123**, 136–140 (2004).
- 1.49. L. Lehmann and V. Buckin, “Determination of the heat stability profiles of concentrated milk and milk ingredients using high resolution ultrasonic spectroscopy”, *J. Dairy Sci.* **88**, 3121–3129 (2005).
- 1.50. K. Ikeda, “Ultrasonic liquid-concentration sensor with temperature compensation”, *P. IEEE Int. Freq. Cont.* 652–659 (1998).
- 1.51. H. Freundlich, K. Söllner, and F. Rogowski, “Einige Biologische Wirkungen von Ultraschallwellen”, *J. Mol. Med.* **11**, 1512-1513 (1932).
- 1.52. T.J. Mason, “Therapeutic ultrasound an overview”, *Ultrason. Sonochem.* **18**, 847–852 (2011).
- 1.53. S. Mitragotri, “Healing sound: the use of ultrasound in drug delivery and other therapeutic applications”, *Nat. Rev. Drug Discov.* **4**, 255–260 (2005).

- 1.54. L.B. Feril, K. Tachibana, K. Ogawa, K. Yamaguchi, I.G. Solano, and Y. Irie, “Therapeutic potential of low-intensity ultrasound (part 1): thermal and sonomechanical effects”, *J. Med. Ultrason.* **35**, 153–160 (2008).
- 1.55. G. ter Haar, “Ultrasound bioeffects and safety”, *Proc. Inst. Mech. Eng. H* **224**, 363–373 (2010).
- 1.56. K.J. Murphy, J.A. Brunberg, and R.H. Cohan, “Adverse reactions to gadolinium contrast media: A review of 36 cases”, *Am. J. Roentgenol.* **167**, 847–9 (1996).
- 1.57. H. Ersoy, F. Rybicki, and M. Prince, “Contrast Agents for Cardiovascular MRI”, in *Cardiovascular Magnetic Resonance Imaging*, R.Y. Kwong, ed. (Humana Press Inc., New Jersey, 2008), pp 237–254.
- 1.58. B.P. Nelson and K. Chason, “Use of ultrasound by emergency medical services: a review”, *Int. J. Emerg. Med.* **1**(4), 253–259 (2008).
- 1.59. P. Owen, M.L. Donnet, S.A. Ogston, A.D. Christie, P.W. Howie, and N.B. Pate, “Standards for ultrasound fetal growth velocity”, *Brit. J. Obstet. Gynaec.* **103**, 60–69 (1996).
- 1.60. J. D'hooge¹, A. Heimdal, F. Jamal, T. Kukulski, B. Bijmens, F. Rademakers, L. Hatle, P. Suetens, and G.R. Sutherland, “Regional strain and strain rate measurements by cardiac ultrasound: principles, implementation and limitations”, *Eur. J. Echocardiogr.* **1**(3), 154–170 (2000).
- 1.61. , “Assessment of left ventricular function by cardiac ultrasound”, *J. Am. Coll. Cardiol.* **48**, 2012–2025 (2006)

- 1.62. A. Kurjak, P. Kirkinen, V. Latin, and D. Ivankovic, "Ultrasonic assessment of fetal kidney function in normal and complicated pregnancies", *Am. J. Obstet. Gynecol.* **141**, 266–270 (1981).
- 1.63. T.M. O'Shea, S.J. Counsell, D.B. Bartels, and O. Dammann, "Magnetic resonance and ultrasound brain imaging in preterm infants", *Early Hum. Dev.* **81**(3), 263–271 (2005).
- 1.64. S. Meyer, D. Todd, I. Wright, L. Gortner, and G. Reynolds, "Review article: Non-invasive assessment of cardiac output with portable continuous-wave Doppler ultrasound", *Emerg. Med. Australas.* **20**, 201–208 (2008).
- 1.65. T. Iwao, A. Toyonaga, K. Oho, C. Tayama, H. Masumoto, T. Sakai, M. Sato, and K. Tanikawa, "Value of doppler ultrasound parameters of portal vein and hepatic artery in the diagnosis of cirrhosis and portal hypertension", *Am. J. Gastroenterol.* **92**, 1012–1017 (1997).
- 1.66. R. Ikee, S. Kobayashi, N. Hemmi, T. Imakiire, Y. Kikuchi, H. Moriya, S. Suzuki, and S. Miura, "Correlation between the resistive index by doppler ultrasound and kidney function and histology", *Am. J. Kidney Dis.* **46**, 603–609 (2005).
- 1.67. N. Hatanaka, H. Tokuno, A. Nambu, and M. Takada, "Transdural doppler ultrasonography monitors cerebral blood flow changes in relation to motor tasks", *Cereb. Cortex* **19**, 820–831 (2009).
- 1.68. R. Gramiak and P.M. Shah, "Echocardiography of the Aortic Root", *Invest. Radiol.* **3**, 356–366 (1968).

- 1.69. A.A. Bove, M.C. Ziskin, and W.L. Mulchin, “Ultrasonic detection of in-vivo cavitation and pressure effects of high-speed injections through catheters”, *Invest. Radiol.* **4**, 236–240 (1969).
- 1.70. B.B. Goldberg, J. Liu, and F. Forsberg, “Ultrasound contrast agents: a review”, *Ultrasound Med. Biol.* **20**, 319–333 (1994).
- 1.71. T.R. Porter, F. Xie, A. Kricsfeld, and K. Kilzer, “Noninvasive identification of acute myocardial ischemia and reperfusion with contrast ultrasound using intravenous perfluoropropane-exposed sonicated dextrose albumin”, *J. Am. Coll. Cardiol.* **26**, 33–40 (1995).
- 1.72. B. Carroll, R. Turner, E. Tickner, D. Boyle, and S. Young, “Gelatin encapsulated nitrogen microbubbles as ultrasonic contrast agents”, *Invest. Radiol.* **15**, 260–266 (1980).
- 1.73. A.D. Martina, K. Meyer-Wiethe, E. Allémann, and G. Seidel “Ultrasound Contrast Agents for Brain Perfusion Imaging and Ischemic Stroke Therapy”, *J. Neuroimaging* **15**, 217–232 (2005).
- 1.74. H. Ernst, E.G. Hahn, T. Balzer, R. Schlieff, and N. Heyder, “Color doppler ultrasound of liver lesions: signal enhancement after intravenous injection of the ultrasound contrast agent Levovist®”, *J. Clin. Ultrasound* **24**, 31–35, (1996).
- 1.75. T. Santoso, J. Roelandt, H. Mansyoer, N. Abdurahman, R.S. Meltzer, and P.G. Hugenholtz, “Myocardial perfusion imaging in humans by contrast echocardiography using polygelin colloid solution”, *J. Am. Coll. Cardiol.* **6**, 612–620 (1985).

- 1.76. J. Ophir, A. Gobuty, R.E. McWhirt, and T.F. Makland, “Ultrasonic backscatter from contrast producing collagen microspheres”, *Ultrasonic Imaging* **2**, 67–77 (1980).
- 1.77. S.L. Lin, J.H. Lo, C.Y. Mou, S.J. Ho, R.H. Liu, J.Y. Chan, M.S. Chang, H.T. Chiang, and C.Y. Chen, “Left ventricular opacification after peripheral venous injection of a modified albumin solution”, *Int. J. Card. Imaging* **8**, 53–61 (1992).
- 1.78. G.M. Lanza, R.L. Trousil, K.W. Wallace, J.H. Rose, C.S. Hall, M.J. Scott, J.G. Miller, P.R. Eisenberg, P.J. Gaffney, and S.A. Wickline, “In vitro characterization of a novel, tissue-targeted ultrasonic contrast system with acoustic microscopy”, *J. Acoust. Soc. Am.* **104**, 3665–3672 (1998).
- 1.79. F. Gaffney, J. Lin, R. Peshock, L. Bush, and L. Buja, “Hydrogen peroxide contrast echocardiography”, *Am. J. Cardiol.* **52**, 607–609 (1983).
- 1.80. M.D. Smith, J.L. Elion, R.R. McClure, O.L. Kwan, A.N. Demaria, J. Evans, and T.H. Fritsch, “Left heart opacification with peripheral venous injection of a new saccharide echo contrast agent in dogs”, *J. Am. Coll. Cardiol.* **13**, 1622–1628 (1989).
- 1.81. R.S. Meltzer, P.W. Serruys, P.G. Hugenholtz, and J. Roelandt, “Intravenous carbon dioxide as an echocardiographic contrast agent”, *J. Clin. Ultrasound* **9**, 127–131 (1981).
- 1.82. H.J. Bleeker, K.K. Shung, J.L. Barnhart, “Ultrasonic characterization of Albunex, a new contrast agent”, *J. Acoust. Soc. Am.* **87**, 1792–1797 (1990).

- 1.83. E.G. Schutt, D.H. Klein, R.M. Mattrey, and J.G. Riess, “Injectable microbubbles as contrast agents for diagnostic ultrasound imaging: the key role of perfluorochemicals”, *Angew. Chem. Int. Ed.* **42**, 3218–3235 (2003).
- 1.84. J. M. Correas, L. Bridal, A. Lesavre, A. Méjean, M. Claudon, and O. Hélénon, “Ultrasound contrast agents: properties, principles of action, tolerance, and artifacts”, *Eur. Radiol.* **11**, 1316–1328 (2001).
- 1.85. E. Quaia, “Microbubble ultrasound contrast agents: an update”, *Eur. Radiol.* **17**, 1995–2008 (2007).
- 1.86. K.Q. Schwarz, G.P. Bezante, X. Chen, and R. Schlieff, “Quantitative echo contrast concentration measurement by doppler sonography”, *Ultrasound Med. Biol.* **19**, 289–297 (1993).
- 1.87. S.L. Bridal, O. Lucidarme, J. Correas, P.N. Bums, J. Moreau, and G. Berger, “Quantification of Ultrasound Contrast Agent in an In Vitro Perfusion Phantom”, *IEEE Ultrasonics Symposium* **2**, 1759-1762 (1999).
- 1.88. N.G. Rognin, P. Frinking, M. Costa, and M. Arditi, “In-vivo perfusion quantification by contrast ultrasound: validation of the use of linearized video data vs. raw RF data”, *IEEE Ultrasonics Symposium*, 1690–1693 (2008).
- 1.89. N. Lassau, L. Chami, B. Benatsou, P. Peronneau, and A. Roche, “Dynamic contrast-enhanced ultrasonography (DCE-US) with quantification of tumor perfusion: a new diagnostic tool to evaluate the early effects of antiangiogenic treatment”, *Eur. Radiol. Suppl.* **17**(6), F89–F98 (2007).
- 1.90. M. Krix, F. Kiessling, N. Farhan, K. Schmidt, J. Hoffend, and S. Delorme, “A multivessel model describing replenishment kinetics of ultrasound contrast agent

- for quantification of tissue perfusion”, *Ultrasound Med. Biol.* **29**, 1421–1430 (2003).
- 1.91. G. Lanza, K.D. Wallace, M.J. Scott, W.P. Cacheris, D.R. Abendschein, D.H. Christy, A.M. Sharkey, J.G. Miller, G. James, P.J. Gaffney, and S.A. Wickline, “Thrombi/arteries: a novel site-targeted ultrasonic contrast agent with broad biomedical application”, *Circulation* **94**, 3334–3340 (1996).
- 1.92. A.M. Takalkar, A.L. Klibanov, J.J. Rychak, J.R. Lindner, and K. Ley, “Binding and detachment dynamics of microbubbles targeted to P-selectin under controlled shear flow”, *J. Control. Release* **96** (2004) 473– 482
- 1.93. G.E.R. Weller, E. Lu, M.M. Csikari, A.L. Klibanov, D. Fischer, W.R. Wagner, and F.S. Villanueva, “Ultrasound Imaging of acute cardiac transplant rejection with microbubbles targeted to intercellular adhesion molecule-1”, *Circulation* **108**, 218–224 (2003).
- 1.94. J.R. Lindner, J. Song, J. Christiansen, A.L. Klibanov, F. Xu, and K. Ley, “Ultrasound assessment of inflammation and renal tissue injury with microbubbles targeted to P-selectin”, *Circulation* **104**, 2107–2112 (2001).
- 1.95. E.C. Unger, T.P. McCreery, R.H. Sweitzer, D. Shen, and G. Wu, “In vitro studies of a new thrombus-specific ultrasound contrast agent”, *Am. J. Cardiol.* **81** (12, Suppl 1), 58G–61G (1998).
- 1.96. A.L. Klibanov, J.J. Rychak, W.C. Yang, S. Alikhani, B. Li, S. Acton, J.R. Lindner, K. Ley, and S. Kaul, “Targeted ultrasound contrast agent for molecular imaging of inflammation in high-shear flow”, *Contrast Media Mol. I.* **1**, 259–266 (2006).

- 1.97. D.B. Ellegala, H. Leong-Poi, J.E. Carpenter, A.L. Klibanov, S. Kaul, M.E. Shaffrey, J. Sklenar, and J.R. Lindner, “Imaging Tumor Angiogenesis With Contrast Ultrasound and Microbubbles Targeted to $\alpha v\beta 3$ ”, *Circulation* **108**, 336–341 (2003).
- 1.98. E. Unger, P. Metzger, E. Krupinski, M. Baker, R. Hulett, D. Gabaeff, J. Mills, D. Ihnat, and T. McCreery, “The use of a thrombus-specific ultrasound contrast agent to detect thrombus in arteriovenous fistulae”, *Invest. Radiol.* **35**, 86–89 (2000).
- 1.99. H. Leong-Poi, J. Christiansen, P. Heppner, C.W. Lewis, A.L. Klibanov, S. Kaul, and J.R. Lindner, “Assessment of endogenous and therapeutic arteriogenesis by contrast ultrasound molecular imaging of integrin expression”, *Circulation* **111**, 3248–3254 (2005).
- 1.100. T.G. Muir and E.L. Carstensen, “Prediction of nonlinear acoustic effects at biomedical frequencies and intensities”, *Ultrasound Med. Biol.* **6**, 345–357 (1980).
- 1.101. T. Walsh and M. Torres, “Finite element methods for nonlinear acoustics in fluids”, *J. Comput. Acoust.* **15**, 353–375 (2007).
- 1.102. G. Pinton, F. Coulouvrat, J.L. Gennisson, and M. Tanter, “Nonlinear reflection of shock shear waves in soft elastic media”, *J. Acoust. Soc. Am.* **127**, 683–691 (2010).
- 1.103. H. Khelladi, F. Plantier, J.L. Daridon, and H. Djelouah, “Measurement under high pressure of the nonlinearity parameter B/A in glycerol at various temperatures”, *Ultrasonics* **49**, 668–675 (2009).

- 1.104. R.T. Beyer, "Parameter of Nonlinearity in Fluids", *J. Acoust. Soc. Am.* **32**, 719–721 (1960).
- 1.105. A.B. Coppens, R.T. Beyer, M.B. Seiden, J. Donohue, F. Guepin, R.H. Hodson, and C. Townsend, "Parameter of Nonlinearity in Fluids. II", *J. Acoust. Soc. Am.* **38**, 797–804 (1965).
- 1.106. K.A. Jayalatha, J. Amoros, and S. Ravi, "Estimation of second-, third- and fourth-order nonlinearity parameters for specific fluorocarbon drug delivering nanosystems", *Phys. Chem. Liq.* **49**, 309–317 (2011).
- 1.107. C.M. Sehgal, B.R. Porter, and J.F. Greenleaf, "Ultrasonic nonlinear parameters and sound speed of alcohol–water mixtures", *J. Acoust. Soc. Am.* **79**, 566–570 (1986).
- 1.108. A.P. Sarvazyan, T.V. Chalikian, and F. Dunn, "Acoustic nonlinearity parameter B/A of aqueous solutions of some amine acids and proteins", *J. Acoust. Soc. Am.* **88**, 1555–1561 (1990).
- 1.109. Y. Yang and F. Dunn, "Acoustic non-linearity method for estimating the ratio of bound to free water of biological media", *Ultrasonics* **31**, 35–38 (1993).
- 1.110. K.D. Wallace, C.W. Lloyd, M.R. Holland, and J.G. Miller, "Finite amplitude measurements of the nonlinear parameter B/A for liquid mixtures spanning a range relevant to tissue harmonic mode", *Ultrasound in Med. Biol.* **33**, 620–629 (2007).
- 1.111. K.D. Wallace, C.W. Lloyd, M.R. Holland, and J.G. Miller, "Finite amplitude measurements of the nonlinear parameter B/A for liquid mixtures spanning a

- range relevant to tissue harmonic mode”, *Ultrasound Med. Biol.* **33**, 620–629 (2007).
- 1.112. J.H. Cantrella, “Ultrasonic harmonic generation from fatigue-induced dislocation substructures in planar slip metals and assessment of remaining fatigue life”, *J. Appl. Phys.* **106**, 093516 (2009).
- 1.113. J.H. Cantrella and W.T. Yost, “Determination of precipitate nucleation and growth rates from ultrasonic harmonic generation”, *Appl. Phys. Lett.* **77**, 1952–1954 (2000).
- 1.114. J. Kim, L.J. Jacobs, J. Qu, and J.W. Littles, “Experimental characterization of fatigue damage in a nickel-base superalloy using nonlinear ultrasonic waves”, *J. Acoust. Soc. Am.* **120**, 1266–1273 (2006).
- 1.115. A.A. Shah and Y. Ribakov, “Non-linear ultrasonic evaluation of damaged concrete based on higher order harmonic generation”, *Mater. Des.* **30**, 4095–4102 (2009).
- 1.116. M. Fatemi and J.F. Greenleaf, “Ultrasound-stimulated vibro-acoustic spectrography”, *Science* **280**, 82–85 (1998).
- 1.117. M. Fatemi and J.F. Greenleaf, “Vibro-acoustography: An imaging modality based on ultrasound-stimulated acoustic emission”, *Proc. Natl. Acad. Sci. USA* **96**, 6603–6608 (1999).
- 1.118. P.Z. He, R.M. Xia, S.M. Duan, W.D. Shou, and D.C. Qian, “The affection on the tissue lesions of difference frequency in dual-frequency high-intensity focused ultrasound (HIFU)”, *Ultrason. Sonochem.* **13**, 339–345 (2006).

- 1.119. J.C. Brigham, W. Aquinoa, F.G. Mitri, J.F. Greenleaf, and M. Fatemi, “Inverse estimation of viscoelastic material properties for solids immersed in fluids using vibroacoustic techniques”, *J. Appl. Phys.* **101**, 023509 (2007).
- 1.120. F.G. Mitria and M. Fatemi, “Improved vibroacoustography imaging for nondestructive inspection of materials”, *J. Appl. Phys.* **98**, 114901 (2005).
- 1.121. M. Fatemi, L.E. Wold, A. Alizad, and J.F. Greenleaf, “Vibro-acoustic tissue mammography”, *IEEE T. Med. Imaging* **21**, 1–8 (2002).
- 1.122. A. Alizad, M. Fatemi, L.E. Wold, and J.F. Greenleaf, “Performance of vibroacoustography in detecting microcalcifications in excised human breast tissue: a study of 74 tissue samples”, *IEEE T. Med. Imaging* **23**, 307–312 (2004).
- 1.123. C. Pislaru, B. Kantor, R.R. Kinnick, J.L. Anderson, M.C. Aubry, M.W. Urban, M. Fatemi, and J.F. Greenleaf, “In vivo vibroacoustography of large peripheral arteries”, *Invest. Radiol.* **43**, 243–252 (2008).
- 1.124. F.G. Mitri, P. Trompette, and J. Chapelon, “Using vibro-acoustography to detect brachytherapy metal seeds”, *IEEE Ultrasonics Symposium* **2**, 1528–1531 (2003).
- 1.125. F.G. Mitri, B.J. Davis, J.F. Greenleaf, and M. Fatemi, “In vitro comparative study of vibro-acoustography versus pulse-echo ultrasound in imaging permanent prostate brachytherapy seeds”, *Ultrasonics* **49**, 31–38 (2009).
- 1.126. M.W. Urban, G.T. Silva, M. Fatemi, and J.F. Greenleaf, “Multifrequency vibroacoustography”, *IEEE T. Med. Imaging* **25**, 1284–1295 (2006).
- 1.127. M.W. Urban, M. Fatemi, and J.F. Greenleaf, “Modulation of ultrasound to produce multifrequency radiation force”, *J. Acoust. Soc. Am.* **127**, 1228–1238 (2010).

- 1.128. T.P. Mills, A. Jones, and R.A. Lodder, "Identification of wood species by acoustic-resonance spectrometry using multivariate subpopulation analysis", *Appl. Spectrosc.* **47**, 1880–1886 (1993).
- 1.129. J. Medendorp and R.A. Lodder, "Acoustic-resonance spectrometry as a process analytical technology for rapid and accurate tablet identification", *AAPS PharmSciTech* 2006 **7**(1), 25 (2006).
- 1.130. R.G. Buice, P. Pinkston, and R.A. Lodder, "Optimization of acoustic-resonance spectrometry for analysis of intact tablets and prediction of dissolution rate", *Appl. Spectrosc.* **48**, 517–524 (1994).
- 1.131. J. Medendorp, R.G. Buice, and R.A. Lodder, "Acoustic-resonance spectrometry as a process analytical technology for the quantification of active pharmaceutical ingredient in semi-solids", *AAPS PharmSciTech* **7**(3), 59 (2006).
- 1.132. E.L. Carstensen, W.K. Law, and N.D. McKay, "Demonstration of nonlinear acoustical effects at biomedical frequencies and intensities", *Ultrasound Med. Biol.* **6**, 359–368 (1980).
- 1.133. H.C. Starritt, M.A. Perkins, F.A. Duck, and V.F. Humphrey, "Evidence for ultrasonic finite-amplitude distortion in muscle using medical equipment," *J. Acoust. Soc. Am.* **77**, 302–306 (1985).
- 1.134. B. Ward, A.C. Baker, and V.F. Humphrey, "Nonlinear propagation applied to the improvement of resolution in diagnostic medical ultrasound", *J. Acoust. Soc. Am.* **101**, 143–154 (1997).

- 1.135. T.S. Dresser, R.B. Jeffrey, M.J. Lane, and P.W. Ralls, "Tissue harmonic imaging: utility in abdominal and pelvic sonography", *J. Clin. Ultrasound* **27**, 135–142 (1999).
- 1.136. E.L. Rosen and M.S. Soo, "Tissue harmonic imaging next term sonography of breast lesions: Improved margin analysis, conspicuity, and image quality compared to conventional ultrasound", *Clin. Imag.* **25**, 379–384 (2001).
- 1.137. S. Choudhry, B. Gorman, J.W. Charboneau, D.J. Tradup, R.J. Beck, J.M. Kofler, and D.S. Groth, "Comparison of Tissue Harmonic Imaging with Conventional US in Abdominal Disease", *Radiographics* **20**, 1127–1135 (2000).
- 1.138. M.A. Averkiou, D.N. Roundhill, and J.E. Powers, "A new imaging technique based on the nonlinear properties of tissues" *IEEE Ultrasonics Symposium* **2**, 1561–1566 (1997).
- 1.139. M. Kornbluth, D.H. Liang, and A. Paloma, "Native tissue harmonic imaging improves endocardial border definition and visualization of cardiac structures", *J. Am. Soc. Echocardiog.* **11**, 693–701 (1998).
- 1.140. M. Sackmann, M. Delius, T. Sauerbruch, J. Holl, W. Weber, E. Ippisch, U. Hagelauer, O. Wess, W. Hepp, W. Brendel, and G. Paumgartner, "Shock-Wave Lithotripsy of Gallbladder Stones", *New Engl. J. Med.* **318**, 393–397 (1988).
- 1.141. C. Chaussy and E. Schmiedt, "Extracorporeal shock wave lithotripsy (ESWL) for kidney stones. An alternative to surgery?", *Urol. Radiol.* **6**, 80–87 (1984).
- 1.142. G. ter Haar, "Intervention and therapy", *Ultrasound Med. Biol.* **26** (Suppl 1), S51–S54 (2000).

- 1.143. L. Chen, G. ter Haar, and C.R. Hill, “Influence of ablated tissue on the formation of high-intensity focused ultrasound lesions”, *Ultrasound Med. Biol.* **23**, 921–931 (1997).
- 1.144. S. Thüroff, C. Chaussy, G. Vallancien, W. Wieland, H.J. Kiel, A. Le Duc, F. Desgrandchamps, J.J. De La Rosette, and A. Gelet, “High-Intensive Focused Ultrasound in Localized Prostate Cancer : efficacy results from the European multicentric study”, *J. Endourol.* **14**, 293–299 (2000).
- 1.145. A. Sibille, F. Prat, J. Chapelon, F.A.E. Fadil, L. Henry, Y. Theilliere, T. Ponchon, and D. Cathignol, “Characterization of extracorporeal ablation of normal and tumor-bearing liver tissue by high intensity focused ultrasound”, *Ultrasound Med. Biol.* **19**, 803–813 (1993).
- 1.146. J.B. Adams, R.G. Moore, J.H. Anderson, J.D. Strandberg, F.F. Marshall, and L.R. Davoussi, “High-Intensity Focused Ultrasound Ablation of Rabbit Kidney Tumors”, *J. Endourol.* **10**, 71–75 (1996).
- 1.147. S. Vaezy, R. Martin, B. Goldman, E. Chi, W. Chandler, P. Kaczkowski, and L. Crum, “Biological mechanisms of acoustically-induced hemostasis”, *IEEE Ultrasonics Symposium* **2**, 1401–1404 (1999).
- 1.148. J. Wu and J. Tong, “Measurements of the nonlinearity parameter B/A of contrast agents”, *Ultrasound Med. Biol.* **24**, 153–159 (1998).
- 1.149. L. Hoff, P. C. Sontum, J.M. Hovem, “Oscillations of polymeric microbubbles: effect of the encapsulating shell”, *J. Acoust. Soc. Am.* **107**, 2272–2280 (2000).

- 1.150. S. Qin and K.W. Ferrara, “The Natural Frequency of Nonlinear Oscillation of Ultrasound Contrast Agents in Microvessels”, *Ultrasound Med. Biol.* **33**, 1140–1148 (2007).
- 1.151. J.A. Ketterling and J. Mamou, “Subharmonic Response from Polymer-Shelled Contrast Agents”, *IEEE Ultrasonics Symposium* **3**, 1077–1080 (2007).
- 1.152. F. Forsberg, W.T. Shi, and B.B. Goldberg, “Subharmonic imaging of contrast agents”, *Ultrasonics* **38**, 93–98 (2000).
- 1.153. W.T. Shi and F. Forsberg, “Ultrasonic characterization of the nonlinear properties of contrast microbubbles”, *Ultrasound Med. Biol.* **26**, 93–104 (2000).
- 1.154. M. Tang, N. Kamiyama, and R.J. Eckersley, “Effects of nonlinear propagation in ultrasound contrast agent imaging”, *Ultrasound Med. Biol.* **36**, 459–466 (2010).
- 1.155. B.A Schrope, V.L. Newhouse, and V. Uhlendorf, “Simulated capillary blood flow measurement using a nonlinear ultrasonic contrast agent”, *Ultrasonic Imaging* **14**, 134–158 (1992).
- 1.156. B.A Schrope and V.L. Newhouse, “Second harmonic ultrasound blood perfusion measurement”, *Ultrasound Med Biol* **19**, 567–579 (1993).
- 1.157. J.U. Harrer, L. Mayfrank, M. Mull, and C. Klötzsch, “Second harmonic imaging: a new ultrasound technique to assess human brain tumour perfusion”, *J. Neurol. Neurosur. Ps.* **74**, 333–338 (2003).
- 1.158. G. Seidel, C. Algermissen, A. Christoph, L. Claassen, M. Vidal-Langwasser, and T. Katzer, “Harmonic imaging of the human brain visualization of brain perfusion with ultrasound”, *Stroke* **31**, 151–154 (2000).

- 1.159. F. Forsberg, C.W. Piccoli, D.A. Merton, J.J. Palazzo, and A.L. Hall, “Breast Lesions: Imaging with Contrast-enhanced Subharmonic US - Initial Experience”, *Radiology* **244**, 718–726 (2007).
- 1.160. J.R. Eisenbrey, J.K. Dave, V.G. Halldorsdottir, D.A. Merton, P. Machado, J.B. Liu, C. Miller, J.M. Gonzalez, S. Park, S. Dianis, C.L. Chalek, K.E. Thomenius, D.B. Brown, V. Navarro, and F. Forsberg, “Simultaneous grayscale and subharmonic ultrasound imaging on a modified commercial scanner”, *Ultrasonics* **51**, 890–897 (2011).
- 1.161. F. Forsberg, J. Liu, W.T. Shi, J. Furuse, M. Shimizu, and B.B. Goldberg, “In vivo pressure estimation using subharmonic contrast microbubble signals: proof of concept”, *IEEE T. Ultrason. Ferr.* **52**, 581–583 (2005).
- 1.162. K.S. Andersen and J.A. Jensen, “Non-invasive estimation of blood pressure using ultrasound contrast agents”, *Phys. Procedia* **3**, 245–253 (2010).
- 1.163. S.A. Goss, R.L. Johnston, and F. Dunn, “Compilation of empirical ultrasonic properties of mammalian tissues”, *J. Acoust. Soc. Am.* **64**, 423–457 (1978).
- 1.164. S.A. Goss, R.L. Johnston, and F. Dunn, “Compilation of empirical ultrasonic properties of mammalian tissues, II”, *J. Acoust. Soc. Am.* **68**, 93–108, (1980).
- 1.165. L. Bjørnø, “Forty Years of Nonlinear Ultrasound”, *Ultrasonics* **40**, 11–17 (2002).

Chapter 2

Quantification of Theophylline using Ultrasonically-Active Molecularly Imprinted Hydrogel Sensors

2.1 Foreward

Quantitative analysis in many biomedical applications is currently done using a variety of optical, electrochemical, and spectrometric methods. While many analytes can be determined over broad concentration ranges, these analyses are often slow, costly, and require skilled personnel. In this chapter, a new approach is presented to overcome these limitations. Ultrasound, an acoustic wave, is extensively used for imaging through opaque materials ranging from tissues to construction materials.^{2.1,2.2} It is also recognized that the frequency content of an ultrasound waveform can carry information about the material properties through which the wave propagates. The use of ultrasound to determine analyte concentration would allow rapid measurements without the need for extensive sample preparation or chromatographic separation.

The goal of the current chapter is twofold. First, the utility of ultrasound for monitoring changes in mechanical properties of hydrogels is demonstrated. Due to large volume phase transitions that occur in hydrogel polymers, mechanical properties such as size and stiffness can be easily changed. The large change in physical properties can then

be related to the measured ultrasound signal. The second goal is to develop a sensor that can be probed by an ultrasonic wave. This was accomplished using a molecularly imprinted hydroxylpropyl cellulose polymer, which showed a high affinity for a target molecule, and undergoes mechanical changes upon binding that can be monitored ultrasonically.

The molecularly imprinted sensor was used to quantify theophylline, a pharmaceutical chemical that is used in the treatment of respiratory conditions such as asthma and chronic obstructive pulmonary disease. For medical diagnostics, theophylline is typically quantified with a blood test that is sent to a laboratory for HPLC or immunological analysis.^{2,3} However, the lead time for laboratory measurements can be extensive, often requiring from several hours to several days.^{2,4} For theophylline, or any number of other xenobiotics that are routinely determined, a measurement technique that could be performed on-site would improve patient outcomes.

The design of a hydrogel sensor for theophylline estimation was included as part of a joint publication titled “Ultrasonic Quantification using Smart Hydrogel Sensors.” Both graduate student authors were considered primary authors and had equal contributions to the publication. However, according to the current thesis guidelines (accessed 2011-06-01), if both students write manuscript-based theses, only one author may use the article as a chapter. As a result, this publication could not be included as a research chapter in my manuscript-based thesis. An overview of my contributions from this article is given below, and more details can be found in the article, which is attached as Appendix A.

The co-authored publication presented hydrogel sensors based on two different polymers: N-isopropyl acrylamide and hydroxypropyl cellulose (“cellulose”). My work dealt with the development of cellulose sensors, which are attractive for biomedical and point-of-care diagnostics due to their biocompatibility. Cellulose molecularly imprinted polymers (MIP) were made using theophylline as a template molecule. The mean diameter of these MIP sensors was determined to be 105 nm (0.39 PDI) by dynamic light scattering using a Brookhaven Instruments ZetaPALS particle size analyzer. In the presence of theophylline, the mean particle size of the hydrogel increased by 14%. Binding between the hydrogel and the analyte was also found to cause changes in the ultrasound frequency profile.

An experiment was designed to determine if characteristic changes in the frequency domain could be used to estimate theophylline concentration. A series of samples with theophylline ranging between 100 μ M and 6.1 mM were prepared and examined with the ultrasound instrument. Using a multivariate regression approach, a correlation was found between the target concentration and a subset of ultrasound frequencies. With three ultrasound frequencies, theophylline concentration could be estimated with an r^2 greater than 0.99 and a standard error of 0.1 mM.

The selectivity of the MIP sensor for analyte quantification was also tested with the use of a structurally-similar molecule that might compete for the analyte binding sites. Caffeine is commonly coupled with theophylline to test for selective binding.^{2,5,2,6} Also a xanthine derivative, the presence of an additional N-methyl group on the imidazole ring results in steric strain and a lower binding constant in the molecularly imprinted pocket. Mixtures containing both theophylline and caffeine were prepared. Theophylline was

varied between 0.2 and 6.1 mM and caffeine concentrations ranged from 0 to 9.1 mM. Despite the high concentration of the interfering species, a correlation was found between the concentration of theophylline and 6 ultrasonic frequencies. The frequencies used for this estimation are shown in Figure 2.1(a) and include 1.1 and 1.2 MHz, which were in the region used for theophylline estimation with no interferent molecules present. This suggests that the resonance frequency of the hydrogel sensor when bound to the target analyte is constant, and that other frequencies used by the model may be the result of cross-reactivity with the caffeine interferent. The particle size of cellulose sensor incubated with caffeine was found to increase by 23%, which supports the cross-reactivity. Using these frequencies, the theophylline in the mixtures could be estimated with an r^2 of 0.95 and a standard error of 0.6 mM. Figure 2.1(b) shows the estimate values plotted against the known concentrations, illustrating a linear trend over the range examined. Although the molecules were chemically similar, the caffeine concentration could only be estimated with an r^2 less than 0.6, demonstrating the selectivity of this ultrasound method.

In this chapter, an extension of the cellulose MIP sensor work is presented. Methods were developed to improve both the analyte sensitivity and to reduce the cost of the instrument. These two considerations are critical for developing a point-of-care platform. Likewise, the work centers on the molecular imprinting of cellulose due to the biocompatibility of these hydrogels. To decrease the analysis cost, measurements are presented using an inexpensive development board to generate ultrasonic pulses. This replacement of the commercial ultrasound pulser reduces the cost of the overall system by over 60%. To increase the sensitivity of the measurement, the signal intensity was

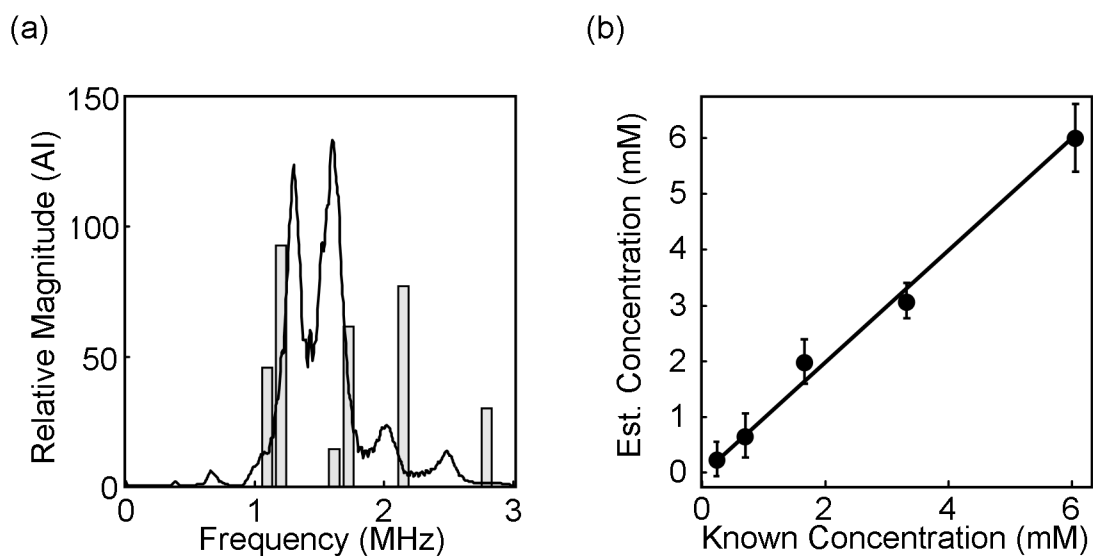


Figure 2.1: Theophylline quantification in the presence of caffeine interferent. (a) Ultrasonic frequencies selected to construct theophylline SMLR model, (b) Known theophylline concentrations correlated with the estimated values by the multilinear model.

improved by using ultrasound transducers with greater frequency overlap. Further, a lower concentration of the cellulose sensor was used, improving the signal to noise ratio. Data were acquired, under my supervision, by undergraduate summer research student Steven Cassin. The fundamental changes in the sensor were correlated to an optical measurement, which suggests that the hydrogel sensor synthesis could also be tuned to increase sensitivity.

2.2 Manuscript

Quantification of Theophylline using Ultrasonically-Active Molecularly Imprinted Hydrogel Sensors

Authors:

Jonathan R. Dion, Steven Cassin, and David H. Burns

2.3 Abstract

Analyte quantification is of importance in a variety of medical, industrial, and research applications. Many samples are opaque to spectroscopies used for routine analysis, require sample pretreatment or separation before measurement. However, these steps increase the complexity of the measurement. Ultrasound has been shown to easily penetrate opaque samples, presenting an opportunity to minimize sample handling. We have developed a general approach for creating smart sensors based on molecularly imprinted hydrogel polymers with characteristic ultrasound frequency profiles. Analyte recognition and binding induces changes in the physical properties of the sensor, causing a change in the measured ultrasound signal that is dependent on analyte concentration. Multilinear analyte calibration in hydrogel solutions provided quantification of the chosen analyte, theophylline, from 10 to 50 μM with an r^2 of 0.95 and a standard error of 1.5 μM . This ultrasound methodology demonstrates promising analytical performance for the estimation of theophylline at therapeutically relevant levels. Cost and time savings

using this technique make it appealing for on-site, point-of-care diagnostic measurements.

2.4 Introduction

2.4.1 Background

Analyte detection in many biomedical and industrial industries is currently done using a variety of optical, electrochemical, and spectrometric methods. However, samples typically contain multiple analytes with chemical signatures that can overlap.^{2.7-2.9} Coupling these methods with techniques such as chromatography or chemical pretreatment can improve the sensitivity of an analysis. However, the disadvantage of additional procedural steps is an increased cost, length of analysis, and complexity. As a result, there is a need for faster, single-method analyses to improve analytical detection and quantification in these fields.

Interest in ultrasound analysis for analytical measurements has increased in recent years. As acoustic waves are mechanical in nature, transmission is not restricted in optically opaque materials such as tissues or concrete.^{2.1,2.2} Further, due to the relatively simplicity of the technology, the cost is minimal and the throughput potentially high. However, there is a need to impart analyte sensitivity and specificity to the platform.

Contrast agents have been developed to improve imaging using ultrasound. Typically gas-filled microbubbles, these agents act to attenuate or enhance ultrasound to improve resolution in imaging applications.^{2.10} Although the velocity of propagating

ultrasound waves has typically been measured, it is also possible to monitor the frequency distribution. In acoustic fields, contrast microbubbles are known to resonate at specific frequencies that can be measured with high precision.^{2.11} Development of a contrast agent with a resonance frequency that can be altered by contact with an analyte should allow quantitative measurement using ultrasound.

Many hydrogel polymers are known to undergo volume phase transitions in aqueous solutions between two distinct states.^{2.12,2.13} In an expanded state, the hydrogels are swollen, due to the hydrogen bonding with the media being favored. These polymer-solvent interactions allow water to permeate through the polymer network. A second state occurs when the physical conditions, such as temperature, destabilize the polymer-solvent hydrogen bonding. The decrease in hydrogen bonding causes water to be expelled from the polymer network. In this collapsed state, the hydrogel shrinks and becomes stiffer. The transition between swollen and collapsed states is reversible, and can be triggered by a variety of physical changes such as fluctuations in ionic strength, electric fields, temperature, and hydrostatic pressure.^{2.14-2.16} Volume phase transition in hydrogel polymers induce changes the physical properties of the solution, including changes to the turbidity and polymer stiffness. These physical changes should also induce changes to the resonance frequency of the polymer that could be measured ultrasonically.

Although hydrogel polymers undergo large physical changes as a result of various stimuli, there is a need to impart analyte specificity to the physical changes that are measured ultrasonically. Molecular imprinting of polymers has been used to create target-specific recognition sites by allowing self-assembly of the monomer around a template molecule.^{2.17} Following polymerization, the molecular pockets show a high

sensitivity for the template molecule due to steric interactions and forces such as hydrogen bonding. As with volume phase transition, binding of the template molecule into a molecularly imprinted polymer (MIP) induces changes to the physical properties of the gel.^{2,5}

We have developed a colloidal sensor based on hydroxypropyl cellulose (HPC), a modified polymer that undergoes large phase transition and that has a unique ultrasound frequency signature. The physical properties of the polymer, including the size and stiffness, change with analyte binding. As a result, changes are also seen in the ultrasound frequency profile, and can then be measured. We have applied this method using a HPC hydrogel that was molecularly imprinted with theophylline, a xanthine molecule that is used for treatment of respiratory diseases with concentrations in the 50 to 100 μM range.^{2,18} Quantification of theophylline is typically done using a blood test that is sent to a laboratory for HPLC or immunological analysis.^{2,3} However, this is not ideal due to the high lead times and costs of operating a laboratory.^{2,4} Quantification of theophylline using the rapid and simple ultrasound methodology is shown over a range of concentrations by the analysis of the ultrasound frequencies associated with MIP sensors.

2.4.2 Principle

Considerable work has been done to model the response of deformable microspheres in acoustic fields.^{2,19,2,20} Although not an exact solution, non-microbubble polymers show similar resonance effects in ultrasonic fields.^{2,21} By comparing hydrogel MIPs to be similar to gas-filled microspheres, a conceptual model can be developed to

illustrate the impact of changing polymer properties on the ultrasound frequency spectrum. With compression and rarefaction, these deformable microbubbles have been shown to resonate isotropically at characteristic frequencies. Harmonic and subharmonic frequencies are also commonly generated by the resonating spheres.

The resonance frequency of microspheres has been shown to vary as a function of their physical properties, specifically, the modulus (or stiffness) and the size. A change to either parameter induces a predictable resonance frequency modulation. These changes are analogous to behavior seen in molecularly imprinted hydrogels presented in this work. When impinged on by ultrasound waves, polymer beads oscillate isotropically at specific resonance frequencies dependent on these physical properties.^{2,21} The physical properties of molecularly imprinted hydrogels can be altered, and have been shown to both increase in stiffness and decrease in size with target recognition and binding.^{2,22,23}

The resonance frequency (f_0) for these types of oscillators can be derived from the linear shell-encapsulated bubble equation,

$$f_0 = \frac{1}{2\pi a_e} \sqrt{\frac{1}{\rho_L} \left(3kp_0 + 12G_s \frac{d_{se}}{a_e} \right)}, \quad (2.1)$$

where a_e is the equilibrium oscillator radius, ρ_L is the density of the surrounding medium, k is the polytropic exponent of the gas, p_0 is atmospheric pressure, G_s is the shell shear modulus, and d_{se} is the shell thickness.^{2,19} While the bulk modulus of an adiabatic gas, K_g , can be written as, $K_g = kp_0$, the bulk modulus of a polymeric bubble

$$K_p = K_g + 4G_s \frac{d_{se}}{a_e} \quad (2.2)$$

includes contributions from the shear modulus of the polymer. Thus, for a deformable hydrogel microbubble, the bulk modulus contribution from adiabatic gas can be negated ($K_g = 0$), and using Equation 2.2, Equation 2.1 can be written as,

$$f_0 = \frac{1}{2\pi a_e} \sqrt{\frac{3K_p}{\rho_L}}, \quad (2.3)$$

which resembles the Minnaert equation for microbubble resonance.^{2,19,2.20} As the stiffness of the polymer increases, the resonance frequency would increase. In contrast, with an increase in hydrogel size, the resonance frequency would be expected to decrease.

The physical properties of a molecularly imprinted hydrogel are also dependent on binding to a target molecule.^{2.5} As a result, the resonance frequency will also be related to these properties as shown above. However, as both stiffness and size are expected to change simultaneously, an interrelationship between the two parameters should give rise to characteristic changes ultrasound frequency spectrum. In a MIP with multiple binding sites, the interrelationship between the size and stiffness as multiple sites are filled successively should result in specific frequency profiles for hydrogels dependent on the target molecule concentration. As the magnitude of vibrations in the propagating ultrasound wave is related to the volume fraction of a molecular species,^{2.24} simultaneous analysis of multiple resonating polymers should be possible using a multivariate approach.

2.5 Materials and Methods

2.5.1 Polymer Preparation

Molecularly imprinted HPC was prepared by dissolving 0.5 g of HPC powder (10^5 MW) and 0.1 g of theophylline (template) in 49.4 g of dH₂O and stirring for 3 days to form a homogeneous 1 wt% solution of HPC. To this solution, 3 mg of sodium chloride and 40 μ L of divinylsulfone (DVS) were then added and stirred for 3 hours.^{2,25} To initiate crosslinking within the HPC hydrogel, 5 drops of 1 M sodium hydroxide were added to the solution to raise the pH to 12. The cross-linking reaction was allowed to continue for 5 hours. Following this, the pH was neutralized to stop any further reaction.

The cross-linked HPC was dialyzed against distilled water for 24 hours to remove the template molecule and any free DVS. The removal of theophylline was confirmed spectroscopically at 271 nm using a HP 8453 UV–visible diode array spectrophotometer. The MIP was then diluted 1/10 with distilled water to form a 0.1 wt% solution. Although the magnitude of the change with sensor binding is decreased at lower sensor concentration, the relative change with analyte recognition is higher, improving the signal to noise ratio. The 0.1 wt% sensor was used for subsequent experiments. Samples with theophylline at 7 concentrations between 10 and 50 μ M were prepared in triplicate.

The mean diameter of the HPC hydrogel was determined to be 105 nm (0.39 PDI) by dynamic light scattering using a Brookhaven Instruments ZetaPALS particle size analyzer.^{2,26} With binding to theophylline, a 14% increase in size could be measured. All

chemicals were purchased from Sigma-Aldrich (Oakville, CA) and used without any further purification.

2.5.2 Measurement Apparatus

The general configuration of the ultrasound instrument used in this work is shown in Figure 2.2. The sample reservoir consisted of a 5 mL Plexiglas cuvette with a 1.8 cm path length. Ultrasound transducers were attached to opposing faces of this cell. A T1 Development Board (Airmar Technology Corporation, Milford, US) was used to generate a $<0.05 \mu\text{s}$, 400 V tone burst at a repetition rate of 25 Hz. These electrical pulses were used to drive a 1.9 MHz narrow-band transducer (Advanced Technology Labs Inc., Pennsylvania, US). The transducer emitted ultrasound pulses, which were transmitted through the sample cell, and detected on the opposite side using a 2.25 MHz wideband transducer (Technisonic, Fairfield, US). To reduce the loss between the transducer faces and the sample reservoir, a thin layer of petroleum jelly was used to as a coupling medium. The ultrasound waveforms were digitized by a Handyscope HS3 (TiePie Engineering, Sneek, NL) computer-controlled oscilloscope. Data were sampled at 50 MHz using 12 bit A/D conversion. Total acquisition time for each sample was 2 minutes, during which 4000 ultrasound waveforms were collected. For measurement of theophylline concentration, the ambient temperature during the experiment varied between 22.3 and 22.9°C. For the optical and ultrasound analysis of the MIP undergoing phase transition, the temperature was varied between 44.0 and 52.0°C as described below.

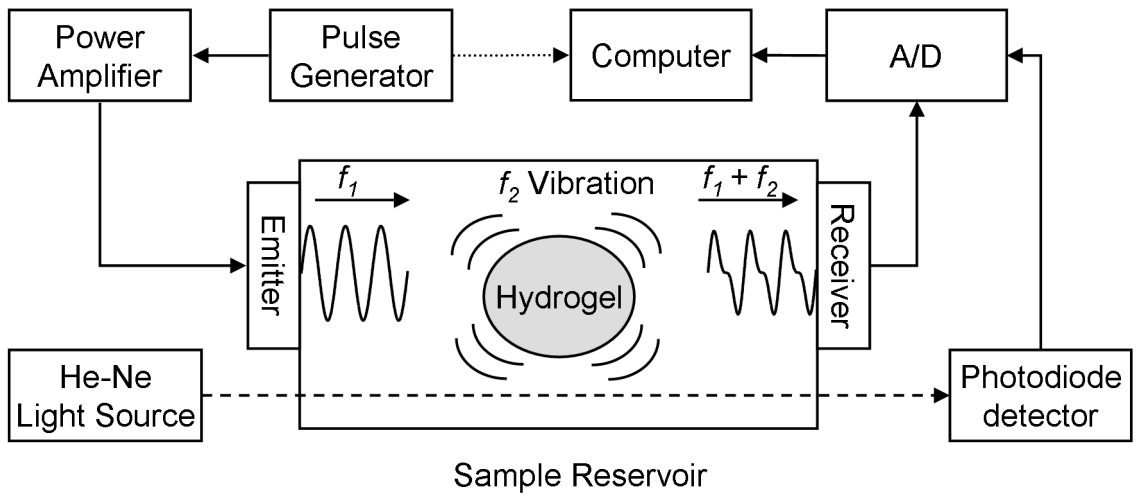


Figure 2.2: Ultrasonic configuration used for the experiments.

2.5.2.1 Measurement of Hydrogel Phase Transition

To examine the effect of the temperature-induced phase transition, measurements of the hydrogel were made in a temperature-controlled system. A sample of the hydrogel was held in a 12 mL, 4 cm long cylindrical chamber. To control the temperature of the sample, the chamber was surrounded by a circulating water jacket. Water was circulated through the jacket chamber by a RTE-111 water bath (Neslab Instruments, Portsmouth, US), allowing the temperature in the bath to be regulated to within 0.1°C. To prevent pressure changes due to changing temperature, an opening was left in the sample chamber window, allowing expansion of the hydrogel sample.

To measure the state of the hydrogel, transmission of visible light through the sample was measured. A Melles Griot (Albuquerque, US) Helium–Neon laser ($\lambda = 632.8$ nm, 5 mW) was used as the light source. An Electro-Optics Technology (Traverse City, US) ET-2000 photodiode detector was positioned on the opposite side of the sample chamber to measure the intensity of the light passing through the sample.

2.5.3 Data Analysis

All hydrogel samples were prepared in triplicate and measured in a randomized order to avoid correlation with instrumental response or external conditions. To compensate for potential phase offsets caused by variable temperature, signals were aligned to the highest positive signal intensity in the ultrasonic waveform. For each sample, the 4000 recorded ultrasound waveforms were averaged to improve the signal to

noise ratio. A fast Fourier transform was used to compute the frequency power spectrum of each sample. Some variability in the frequency spectrum is caused by changes in ambient conditions and instrumental response. To minimize this effect, the frequency spectra were normalized to the total area and smoothed by a 0.1 MHz moving average to further minimize noise.

Stagewise multilinear regression (SMLR) was used to estimate the concentration of theophylline in a series of solutions. The ultrasound frequency spectra were first divided into independent calibration and test sets. Using the calibration subset of the data, a multilinear regression model was determined to estimate the concentration of the theophylline based on the magnitude of ultrasound frequencies. The algorithm first determined the frequency showing the highest correlation with the concentration values. The residual values were then calculated and the process was repeated iteratively with the frequencies not yet included in the model. The data were described in the form

$$Y = b_0 + b_1X_1 + b_2X_2 + \dots + b_nX_n \quad (2.4)$$

where Y is the dependent variable (theophylline concentration in a sample), $\{X\}$ are independent variables (magnitude of ultrasound frequencies), and $\{b\}$ are weighting coefficients. Using the regression equation determined by this model, the concentration of theophylline in the independent test data set were then estimated. To avoid overfitting the multilinear model, a parsimonious model was determined by an F-test ($\alpha = 0.05$) between regression models so that any additional parameters would not significantly change the model.^{2,27} All data analysis was done in Matlab (The MathWorks Inc., 2008a, Massachusetts, U.S.).

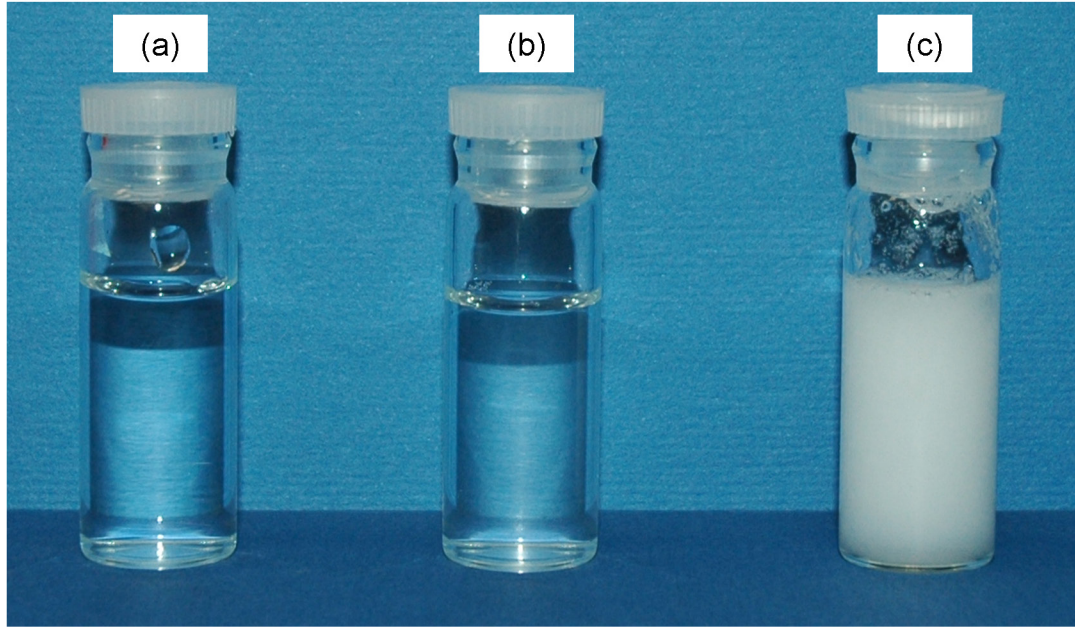


Figure 2.3: Image of the cellulose hydrogel polymer (a) Water, (b) Swollen hydrogel at 44 degrees, (c) Collapsed hydrogel at 52 degrees.

2.6 Results and Discussion

Hydrogels undergo a large volume phase transition when the temperature of a solution increases. As shown in Figure 2.3, the increase in optical scattering caused by the change in mechanical properties of the hydrogel causes the solution to become opaque. To illustrate the effect of changing mechanical properties on ultrasound waves, frequency profiles of the MIP cellulose hydrogels were measured over a series of temperatures. The phase transition temperature for the polymer is approximately 48°C. Above this critical temperature, the polymer networks constrict, expelling water in favor of non-polar interactions. Ultrasound frequency spectra were measured between 44 and 52°C to encompass both states of the hydrogel. The turbidity of the hydrogel sample was simultaneously verified using an optical measurement.

Below the critical phase transition temperature, the hydrogel solution was optically transparent to the wavelength of the light source. However, as shown in Figure 2.4(a), light intensity decreased sharply at 48°C. At temperatures above 48°C, no light was transmitted through the sample due to the hydrogel contracting and subsequently scattering light. This optical measurement verified that the phase transition occurred at this temperature. Although the transition from expanded to swollen states was rapid, it is not instantaneous, as evidenced by curvature in the light intensity plot. This behavior is expected as the phase transition process has been shown to be continuous in both linear and spherical polymer gels.^{2,28} Crosslinking in the hydrogel network is also known to broaden the phase transition due to the larger distribution of polymer conformations.^{2,29} As a result, the temperature at which large changes in the hydrogel

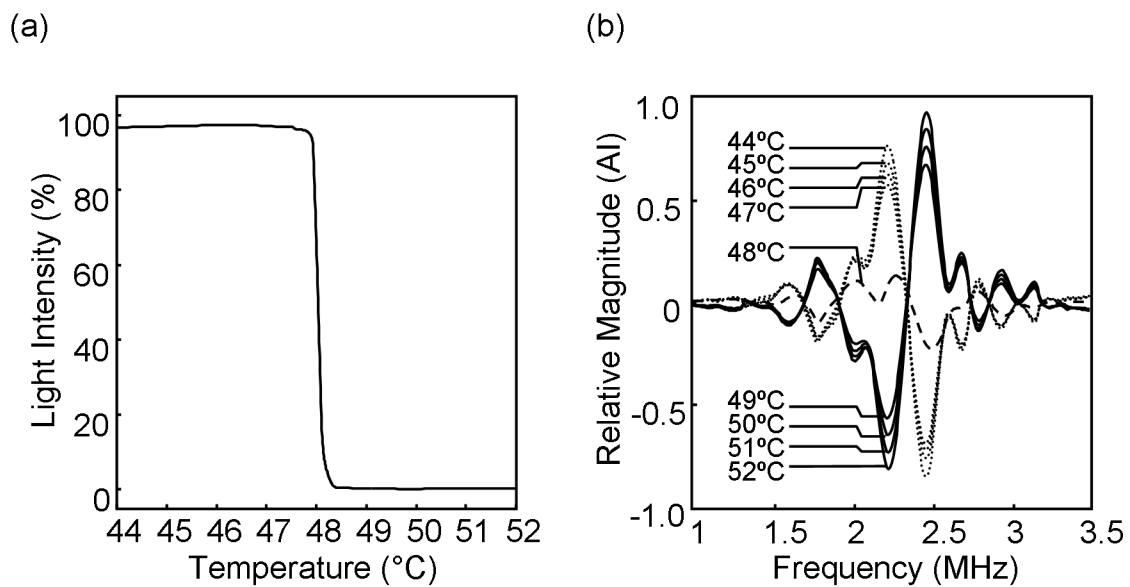


Figure 2.4: Measurement of hydrogel phase transition. (a) Optical transmission measurement showing the gel becomes opaque at the critical temperature, (b) Ultrasound frequency measurements showing a continuous exchange between the 1.92 – 2.34 MHz and the 2.34 – 2.75 MHz regions.

physical characteristics occur could be tuned during synthesis.

The ultrasound frequency spectrum of the MIP sample was measured simultaneously over the same temperature range. To facilitate the comparison of the ultrasound frequencies, the mean of the spectra was subtracted from the individual profiles. The resulting mean-centered ultrasound frequency profiles are shown in Figure 2.4(b). As with the optical measurement, a rapid change in the ultrasound frequency spectrum was measured at the critical temperature. The largest change in the profile is an exchange between the frequencies in the 1.92–2.34 MHz region and those in the 2.34–2.75 MHz region. This is caused by the peak maximum shifting from 2.33 MHz to 2.36 MHz. This may be the result of the resonance frequency of the MIP changing due to the phase transition. Smaller frequency exchanges are also seen at both lower and higher frequencies. As the MIP hydrogels are not monodisperse, the small frequency exchanges may be caused by the resonance frequency of polymer microspheres of slightly different sizes that are less abundant in the sample. Unlike the optical measurement, smaller changes in the ultrasound frequency profiles also occur outside of the phase transition. The capability to examine mechanical changes beyond the critical temperature also demonstrates the usefulness of the ultrasound measure, which can easily propagate through opaque media.

Changes in the physical properties of the MIP sensor are also induced when theophylline binds to the molecularly imprinted pockets.^{2,26} The balance between increasing sensor size and the mechanical stresses induced on the network result in a characteristic change to the resonance frequency of the MIP that can be measured. Changes in design methodology were examined to improve the results reported using the

MIP sensor for theophylline estimation. A lower concentration of hydrogel sensor than previously reported was used (0.1 wt%) for the analyses. Though the lower concentration reduces the magnitude of the hydrogel frequency components, the relative change with theophylline is greater. Further, this decreases the cost of the sensor, which is an important consideration for routine point-of-care measurements. Transducers with similar center frequencies (1.9 and 2.25 MHz) were also used for the analyses. The greater overlap in bandwidth increased the signal intensity of the measured ultrasound waveforms. When combined, these changes should allow a more sensitive detection of the target analyte using the MIP sensor.

The ultrasound frequency spectrum of the HPC hydrogel was measured with the addition of a series of theophylline concentrations. Using the characteristic changes in the magnitudes of several frequencies, a multilinear regression model was developed to estimate the theophylline concentrations. Using the SMLR algorithm, it was determined that theophylline concentrations between 10 and 50 μM could be determined with an r^2 of 0.95 and a standard error of 1.5 μM , as shown in Figure 2.5(a). This represents an improvement of two orders of magnitude in general sensitivity. Figure 2.5(b) shows the frequency components that were used for the quantification. Though identical frequency components were not expected due to the different transducer configuration, there is some overlap in the frequency regions, such as 1.6 MHz and 2.2 MHz. It is likely that these frequencies are related to the intrinsic resonance frequency of the MIPs being probed by the ultrasound waves. This would potentially allow rapid determination of concentrations in samples with varying matrices.

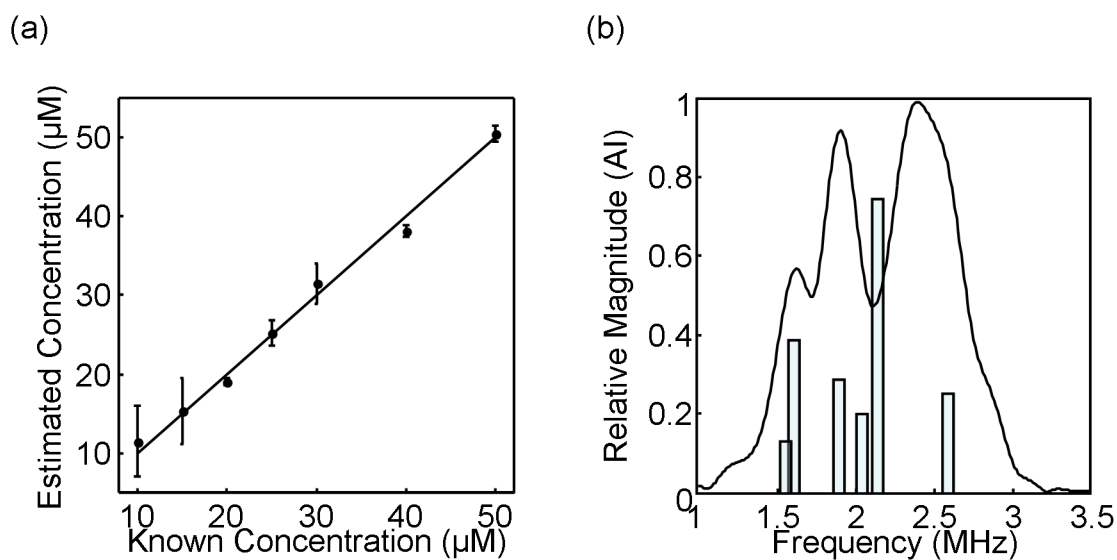


Figure 2.5: Theophylline quantification using the matched frequency response transducers and T1 Development Board pulser (a) Known theophylline concentrations correlated with the estimated values by the multilinear model, (b) ultrasonic frequencies selected to construct theophylline SMLR model.

As outlined, this methodology allows inexpensive measurements of a variety of analytes at low cost in point-of-care type analyses. Sensitivity using the MIP sensor could be further improved by targeting analytes with more specific binding sites using a variety of non-covalent binding mechanisms such as ionic interactions or π stacking. The use of the inexpensive development board and low concentration of the sensor also represent substantial cost savings, making the ultrasound platform highly desirable for routine measurements.

2.7 Conclusions

Ultrasound frequency analysis of hydrogel polymers molecularly imprinted for theophylline was presented. Measurements of temperature-induced hydrogel phase transition were shown. Changes in the physical properties of the hydrogel sensor caused by phase transition could be visualized as rapid, continuous changes in the ultrasound frequency profile. Changes in the sensor physical properties can also be induced by binding between the polymer and an analyte. The resonance frequency of small polymer particles can be approximated by the Minneart equation, and can be related to the stiffness and size. Certain frequency ranges were found to be consistently related to theophylline concentration, indicating that the molecular recognition between the imprinted cellulose and theophylline induced significant and characteristic changes in these physical parameters. A multilinear analysis revealed close correlations between a subset of frequencies and theophylline concentrations between 10 and 50 μM . This range is important for physiological monitoring of theophylline.^{2,18} It may be possible to

optimize the sensitivity of theophylline measurements by tuning the hydrogel synthesis to produce a steep change in the physical characteristics with binding, similar to the changes induced by phase transition.

Though only the determination of theophylline is presented, a variety of analytes could be investigated adjusting the target recognition chemistry in the MIPs. Likewise, increasing the binding constant for the analyte, for example by using an aptamer or antibody recognition site could also lead to increased sensitivity and selectivity. Overall, the presented method of ultrasound frequency analysis appears promising for the detection of small molecules in a variety of environmental, industrial, and clinical applications.

2.8 Acknowledgements

This work was supported in part by the National Science and Engineering Research Council of Canada and by the Fonds Québécois de la Recherche sur la Nature et les Technologies.

2.9 References

- 2.1. H. Ernst, E.G. Hahn, T. Balzer, R. Schlieff, and N. Heyder, “Color Doppler Ultrasound of Liver Lesions: Signal Enhancement After Intravenous Injection of the Ultrasound Contrast Agent Levovist®”, *J. Clin. Ultrasound* **24**, 31–35, (1996).

- 2.2. A.A. Shah and Y. Ribakov, “Non-linear ultrasonic evaluation of damaged concrete based on higher order harmonic generation”, *Mater. Des.* **30**, 4095–4102 (2009).
- 2.3. A.J. Pesce, M. Rashkin, and U. Kotagal, “Standards of laboratory practice: theophylline and caffeine monitoring” *Clin. Chem.* **44**, 1124–1128 (1998).
- 2.4. C.P. Price, A. St John, and J.M. Hicks, “Point-of-Care Testing: What, Why, When, and Where?”, AACC Press, Washington, 2004.
- 2.5. W. Fan and W.R. Seitz, “Swellable theophylline selective microparticles for sensing applications”, *Analyst* **132**, 1103–1106 (2007).
- 2.6. S.R. Carter and S. Rimmer, “Molecular Recognition of Caffeine by Shell Molecular Imprinted Core–Shell Polymer Particles in Aqueous Media”, *Adv. Mater.* **14**, 667–670 (2002).
- 2.7. A. Ojha and A. Pargal, “Determination of nicorandil concentrations in human plasma using liquid chromatography”, *J. Pharm. Biomed. Anal.* **21**, 175–178 (1999).
- 2.8. R. Panchagnula, A. Sood, N. Sharda, K. Kaur, and C.L. Kaul, “Determination of rifampicin and its main metabolite in plasma and urine in presence of pyrazinamide and isoniazid by HPLC method”, *J. Pharm. Biomed. Anal.* **18**, 1013–1020 (1999).
- 2.9. I. Calleja, M.J. Blanco-Príeto, N. Ruz, M.J. Renedo, and M.C. Dios-Viéitez, “High-performance liquid-chromatographic determination of rifampicin in plasma and tissues”, *J. Chromatogr. A.* **1031**, 289–294 (2004).

- 2.10. E. Quaia, “Microbubble ultrasound contrast agents: an update”, *Eur. Radiol.* **17**, 1995–2008 (2007).
- 2.11. J.M. Correas, L. Bridal, A. Lesavre, A. Méjean, M. Claudon, and O. Hélénon, “Ultrasound contrast agents: properties, principles of action, tolerance, and artifacts”, *Eur. Radiol.* **11**, 1316–1328 (2001).
- 2.12. X. Xia, S. Tang, X. Lu, and Z. Hu, “Formation and Volume Phase Transition of Hydroxypropyl Cellulose Microgels in Salt Solution”, *Macromolecules* **36**, 3695–3698 (2003).
- 2.13. X. Zhang, D. Wu, and C. Chu, “Effect of the Crosslinking Level on the Properties of Temperature-Sensitive Poly(N-isopropylacrylamide) Hydrogels”, *J. Polym. Sci. Part B Polym. Phys.* **41**, 582–593 (2003).
- 2.14. E. Kato, “Volume-phase transition of N-isopropylacrylamide gels induced by hydrostatic pressure”, *J. Chem. Phys.* **106**, 3792–3797 (1997).
- 2.15. T. Oya, T. Enoki, A.Y. Grosberg, S. Masamune, T. Sakiyama, T. Takeoka, K. Tanaka, G. Wang, T. Yilmaz, M.S. Feld, R. Dasari, and T. Tanaka, “Reversible molecular adsorption based on multiple-point interaction by shrinkable gels”, *Science* **286**, 1543–1545 (1999).
- 2.16. Y. Osada, H. Okuzaki, and H. Hori, “A polymer gel with electrically driven motility”, *Nature* **355**, 242–244 (1992).
- 2.17. K. Mosbach and O. Ramström, “The Emerging Technique of Molecular Imprinting and Its Future Impact on Biotechnology”, *Nat. Biotechnol.* **14**, 163–170 (1996).

- 2.18. P.J. Barnes, “Theophylline: new perspectives on an old drug”, *Amer. Jour. Respir. Crit. Care Med.* **167**, 813–818 (2003).
- 2.19. L. Hoff, P. C. Sontum, and J.M. Hovem, “Oscillations of polymeric microbubbles: effect of the encapsulating shell”, *J. Acoust. Soc. Am.* **107**, 2272–2280 (2000).
- 2.20. A. Kvikliene, R. Jurkonis, M. Ressner, L. Hoff, T. Jansson, B. Janerot-Sjöberge, A. Lukoševičius, and P. Ask, “Modelling of nonlinear effects and the response of ultrasound contrast micro bubbles: simulation and experiment”, *Ultrasonics* **42**, 301–307 (2004).
- 2.21. A. Strybulevych, V. Leroy, M.G. Scanlon, and J.H. Page, “Characterizing a model food gel containing bubbles and solid inclusions using ultrasound”, *Soft Matter* **3**, 1388–1394 (2007).
- 2.22. R. Nossal, “A Novel Dynamic Light-Scattering Method to Determine the Modulus of Gels”, *Rubber Chem. Technol.* **16**, 255–260 (1988).
- 2.23. W.R. Seitz, M.T.V. Rooney, E.W. Miele, H. Wang, N. Kaval, L. Zhang, S. Doherty, S. Milde, and J. Lenda, “Derivatized, swellable polymer microspheres for chemical transduction”, *Anal. Chim. Acta* **400**, 55–64 (1999).
- 2.24. B. Avvaru and A.B. Pandit, “Oscillating bubble concentration and its size distribution using acoustic emission spectra”, *Ultrason. Sonochem.* **16**, 105–115 (2009).
- 2.25. U. Anbergen and W. Oppermann, “Elasticity and swelling behaviour of chemically crosslinked cellulose ethers in aqueous systems”, *Polymer* **31**, 1854–1858 (1990).

- 2.26. D. Troïani, J. R. Dion, and D. H. Burns, “Ultrasonic quantification using smart hydrogel sensors”, *Talanta* **85**, 1371–1375 (2011).
- 2.27. N. R. Draper and H. Smith, *Applied Regression Analysis* (John Wiley and Sons, New York, 1981) 2nd ed., pp 294–352.
- 2.28. C. Wu and S. Zhou, “Volume Phase Transition of Swollen Gels: Discontinuous or Continuous?”, *Macromolecules* **30**, 574–576 (1997).
- 2.29. M. Shibayama, M. Morimoto, and S. Nomura, “Phase Separation Induced Mechanical Transition of Poly(N-isopropylacrylamide)/Water Isochore Gels”, *Macromolecules* **27**, 5060–5066 (1994).

Chapter 3

Ultrasonic Frequency Analysis of Antibody-Linked Hydrogel Biosensors for Rapid Point of Care Testing

3.1 Foreward

In this chapter, studies are presented that demonstrate the feasibility of an ultrasound-responsive hydrogel sensor for point-of-care measurements. For these types of rapid measurements, determination of an analyte is preferably done without any sample pretreatment. However, biological fluids contain a wide variety of proteins, salts, hormones, and small molecules. These constituents could potentially act as interferents, reducing the sensitivity of the method. To increase the specificity of the sensor, the molecular imprinting recognition was replaced with antibodies imbedded in the hydrogel network. Due to the high selectivity of these proteins for specific antigens, this should allow the sensor to recognize the analyte without interference from other constituents in the biological fluids.

The antibody-linked hydrogel sensor was used to estimate analyte concentrations in blood, blood plasma, saliva, and urine. All of these biological fluids represent different matrices with changing viscosity and composition. Measurements of acetaminophen concentration are presented in this chapter. Acetaminophen (also known as Paracetamol)

is one of the most commonly used analgesics. However, when the concentration exceeds the micromolar range, there is a high probability of organ damage, which can lead to death. The combination of non-specific symptoms accompanying overdose and limited time window for treatment make rapid, inexpensive point-of-care measurement of acetaminophen critical.

The goal of the work presented in this chapter is three-fold. First, the ultrasound frequency measurement is tested with an antibody-linked cellulose hydrogel. The increased binding constant and selectivity of this recognition scheme provide a novel extension to the previous chapter. Further, the selective binding should reduce non-specific binding. Second, the determination of an analyte in a complex biological matrix is tested. Analyses directly in the biological fluids are an important step towards the development of a point-of-care technology, demonstrating that the wide variety of other molecules do not degrade the sensitivity. Likewise, this demonstrates potential savings in both time and cost, as the samples do not need to be handled or processed extensively prior to ultrasound analysis. Finally, clinically-relevant concentrations of acetaminophen are determined, and demonstrate that the ultrasound method is an improvement to current measurement techniques.

3.2 Manuscript

Ultrasonic Frequency Analysis of Antibody-Linked Hydrogel Biosensors for Rapid Point of Care Testing

Authors:

Jonathan R. Dion and David H. Burns

3.3 Abstract

Analyte quantification in highly scattering media such as tissue, blood, and other biological fluids is challenging using conventional spectroscopic methods. Ultrasound easily penetrates these opaque samples, yet currently provides little chemical information. We have developed a general approach for creating hydrogel biosensors based on antibody-linked cellulose polymers. Target recognition induces changes to the sensor stiffness and size, which is accompanied by characteristic changes to a measured ultrasonic frequency profile. Using this technique, nM sensitivity for acetaminophen is demonstrated in a series of biofluids including whole blood, blood plasma, saliva, and urine. Likewise, this methodology is attractive for point of care diagnostics due to the short measurement time, simple methodology which excludes pretreatment of samples, and has minimal chemical or buffer requirements.

3.4 Introduction

Subtle biochemical changes can have far-reaching physiological impacts on the human body. Changes in metabolite concentrations or the introduction of xenobiotics can lead to responses ranging from minor allergic reactions to complete organ failure and death in a matter of minutes. Biochemical changes are also strong prognosticators of patient health. For instance, measurement of lactate concentrations in blood can provide information about tissue perfusion and oxygenation, which in turn leads to more efficient patient diagnosis.^{3.1} A greater understanding of both the mechanisms of action and the biochemistry of medical conditions has led to a wide growth of specialized diagnostic medicine and treatment in recent years.

Laboratory test results play a key role in diagnostic decisions. In general, fast quantification of medicines and drugs of abuse leads to better patient health outcomes.^{3.2,3.3} Biomedical analyte quantification is typically done spectrophotometrically. However, due to the highly scattering nature of tissue and biological fluids, optical measurements are often difficult to perform and involve sample pretreatment such as centrifugation. Although current methodologies are well established, a lead time of several hours for results is common due to testing protocols and administrative overhead.^{3.4} Likewise, operation of a full-scale laboratory to test for a broad range of analytes is often cost-prohibitive outside of primary care facilities. The resulting financial burden is therefore a large impetus to routine patient care and diagnostics.

Point of care (POC) diagnostic techniques have experienced substantial growth as an answer to remote diagnostics. Technologies have been developed using a wide variety of platforms such as lateral flow immunoassays and microfluidic devices,^{3,5} all with the aim of providing quick results on-site and minimizing operating costs. These devices have been used in the analysis of a wide variety of analytes including proteins, biomarkers, and viral infections.^{3,5,3.6} Due to the financial and time savings, the development of POC technologies for small molecules in time-critical environments such as emergency rooms would be highly advantageous.

Acetaminophen (paracetamol) is a widespread medicine used for management of pain and inflammation. This analgesic is available without prescription and under a wide range of trade-names and dosages. However, acetaminophen is also one of the leading causes of liver failure as a result of accidental and deliberate overdose.^{3,7,3.8} Fortunately, if acetaminophen overdose is detected within the first 12 hours, an antidote, N-acetylcysteine, can be administered to a patient and provides nearly 100% protection of liver function. Determination of acetaminophen levels can be done in blood, urine, and saliva, using immunological and chromatographic assays.^{3,9-3.11} Unfortunately, acetaminophen overdose is accompanied by non-specific diagnostic symptoms such as abdominal pain, nausea, sweating, and diarrhea. Specific indicators of hepatic failure such as jaundice and pruritus are typically delayed. As a result, diagnosing an acetaminophen overdose can be challenging without a blood test, often leading to liver damage before a diagnosis can be made. Metabolic processing of acetaminophen also creates a diagnostic challenge. Due to excretion, metabolism, and sequestering processes, the threshold of hazardous acetaminophen levels in blood lowers over time.

Acetaminophen concentrations in blood above 1.3 mM represent a health hazard one hour following ingestion. The threshold for hazardous concentrations decreases exponentially with time, reaching 20 μ M after 24 hours. As a result, there is a need for a technology capable of making sensitive measurements over a wide dynamic range. A quick and inexpensive technology for routine determination of acetaminophen concentrations in blood, or other biofluids, would therefore be extremely valuable. The design of this technology is the driving force of the work presented here.

Fixed acoustic oscillators for specific analyte determination have seen great interest with the advent of quartz crystal microbalances (QCM). These sensors are based on the linear relationship between the resonance frequency of a vibrating crystal and the mass deposition on the QCM sensor.^{3.12} Mass loading on the QCM surface results in a fractional change to the resonance frequency of the crystal that can be measured. Surface coatings have been applied to crystal surfaces to facilitate specific analyte capture and immobilization. These targeted microbalances have been used for the determination of a wide variety of proteins, biomarkers, and antibiotics.^{3.13} Arrays of microbalances have also been used to develop an "electronic nose," with the aim of simultaneous multi-analyte recognition.^{3.14,3.15} However, sensor fouling in these applications remains problematic.^{3.16} Device responsivities are dependent on interfacial effects such as molecular motion, surface irregularities, and adsorption of unwanted analytes.

Techniques have been developed to overcome interfacial effects that can limit QCM devices. Ultrasonic frequency analysis examines the attenuation of acoustic waves propagating through a medium. The contribution of molecular vibrations to the change in the ultrasonic intensity is related to the volume fraction of a molecular species.^{3.17} This

form of ultrasonic analysis has been employed for numerous rheological studies in colloids and for nano-particle sizing.^{3.18,3.19} The colloids in these applications can also be designed to resonate at specific ultrasonic frequencies. Specifically tailored colloids have been developed into an image enhancement tool known as contrast agents. Typically used to improve visibility, the application of contrast agent is largely limited to qualitative information.^{3.20} The ultrasonic frequencies and intensities required to make these measurements are non-destructive to biological samples. Likewise, the ultrasonic frequencies easily traverse media that are difficult to probe optically. Quantitative measurements using contrast agents or other acoustic resonators are therefore highly applicable to biofluid analysis.

In this work, we present dispersed, ultrasound-responsive resonators that are sensitive to acetaminophen. The sensors, which are analogous to contrast agents, consist of antibodies embedded in a polymer matrix. Antibody capture of target molecules is advantageous due to both the high selectivity and binding constants of antibodies towards an antigen. We propose that the conformational changes in the antibody that accompany antigen docking will alter the network stiffness of the polymer. The physical change in the polymer network will shift the resonating frequency of the sensor. The application of this sensor technique was investigated using acetaminophen. A simultaneous analysis of several frequencies allowed for the development of multivariate calibration models, which were validated on independent test data sets. Although the sensor could potentially be injected into tissue, there are a wide variety of *in vitro* applications for biological fluid analysis. Analyte assays in biological fluids are routinely performed in biomedical

settings. The robustness of the system was examined by performing the analyses in samples of acetaminophen-doped blood, blood plasma, saliva, and urine.

3.4.1 Principle

Ultrasound-responsive polymer networks have been the focus of extensive treatment and characterization for ultrasonic contrast agent development and characterization. Contrast agents typically consist of a polymeric shell encapsulating an inert gas. Previous work has also shown that with ultrasonic compression and rarefaction, these contrast materials oscillate isotropically at specific resonant and subharmonic frequencies based on the physical properties of the polymer.^{3.21-3.23} The proposed sensor platform relies on sub-micron hydrogels composed of crosslinked cellulose polymer chains. A number of cellulose hydrogel polymers are known to undergo large volume phase transitions between swollen and condensed states. Phase transition can be induced by changes in environmental forces such as temperature, ionic strength, and hydrostatic pressure.^{3.24,3.25} The major step towards developing the ultrasonic sensor platform is to create a recognition site in these hydrogel polymers. Antibodies (IgG) were added to the polymer network in order to provide specific analyte targeting. When antigen binding occurs, conformational changes are induced in the antibody structure.^{3.26,3.27} With the antibody crosslinked into the hydrogel network as described in the methodology, antigen-induced structural changes will also affect the cellulose network. Increased network strain, as well as mass loading from the antigen, results in stiffening of the overall polymer network. This, in turn, changes the fundamental resonance frequency of

the polymer when an acoustic field is applied. Likewise, the change in mass loading and conformational change will also alter the effective size of the sensor, further modulating the resonance frequency of the polymer in the ultrasonic field. The result is a change to the ultrasonic frequency response of the solution that is induced by a specific external input (presence of the antigen).

There are many different models that can be generated to describe the resonance effect due to ultrasound. Although hydrogel microspheres have different physical characteristics than gas filled contrast agents, solid polymer particles are known to show a similar resonance effect.^{3,28} The relationship between resonance frequency of hydrogels and the properties of the oscillating polymer can be illustrated using a conceptual model based on the work by Hoff *et al.*^{3,21} The resonance frequency (f_0) of the polymer sensors with respect to the network properties network can be approximated as

$$f_0 \propto \frac{1}{2\pi a_e} \sqrt{\frac{3K_p}{\rho_L}} \quad (3.1)$$

where a_e is the radius of the polymer gel at equilibrium, K_p is the bulk modulus of the polymer gel, and ρ_L is the density of the surrounding medium. Increasing the bulk modulus (stiffness of the polymer) increases the oscillation frequency in an asymptotic manner. In contrast, as the size of the polymer increases, an exponential decrease in the resonance frequency is expected. With analyte binding to the sensor, the resonance frequency is expected to shift to a new value dependent on both size and stiffness. The interrelationship between the two nonlinear parameters would lead to specific resonance frequency shifts based on the concentration of the target analyte. Though the specific frequency change may not be linear, multilinear analysis of the results should allow analytical quantification.

3.5 Materials and Methods

3.5.1 Apparatus

Measurements of acetaminophen concentration were made using the transmission-mode ultrasound configuration depicted in Figure 3.1. An ultrasonic Transmitter/Receiver (500PR Panametrics Inc.) was used to generate a <20 ns, 250 V negative impulse with a 0.002% duty cycle. This electrical impulse drove a 5.0 MHz Standard Contact ultrasonic transducer made by Technisonic (Fairfield, CT), which generated an ultrasonic wave train. Reflection of ultrasound waves at interfaces is significant. The wave train resulting from a single impulse reverberated back and forth within the sample cell. The result was an increased background signal and potentially overlapping signals. It was therefore important to allow sufficient time for the attenuation of the ultrasonic reverberations to baseline noise levels. A repetition rate of 1 KHz was used to ensure that any reflections were completely attenuated by the media before the subsequent impulse was generated.

The ultrasonic wave train was transmitted across a 0.9 mL Plexiglas cell with a 1.4 cm path length. Ultrasonic waves travel freely through both the liquid sample and the walls of the sample cell. Matching the cell width to the transducer diameter ensures that the measured ultrasound signal interacted only with the fluid media. In order to minimize interfacial ultrasound losses, the ultrasonic transducers were coupled to the sample across two layers. First, the Plexiglas cell wall was removed and replaced with a 60 μm acetate window. Acetate was used due to the lower damping of the acoustic waves compared

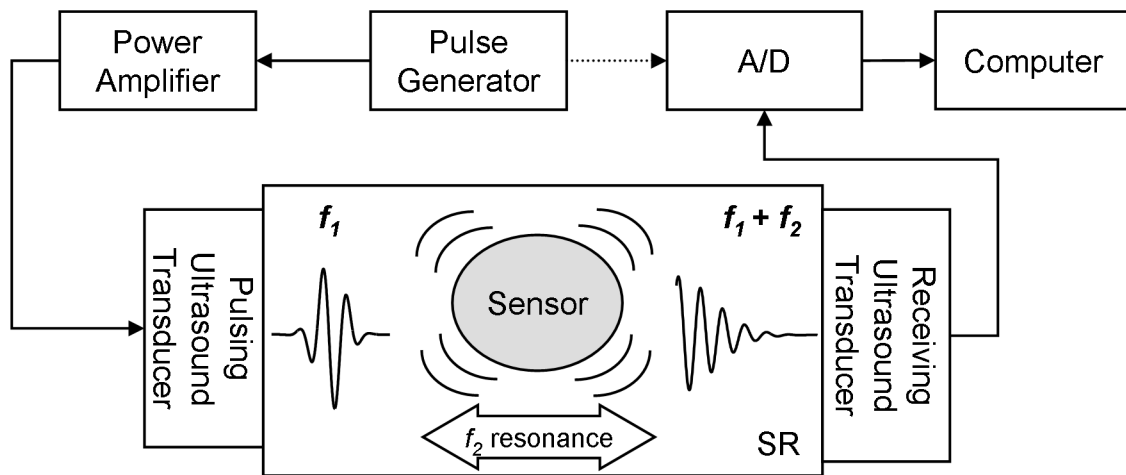


Figure 3.1: Schematic diagram of the ultrasound frequency analyzer. Sample reservoir (SR) holds the biofluid sample and the antibody sensor. An ultrasound transducer generates a pulse waveform (f_1), which interacts with the media and sensor. A receiving ultrasound transducer records the waveform that has propagated through the SR and includes the resonance frequency of the sensor (f_2).

to the Plexiglas. The high acoustic impedance of air is a strong attenuator. To reduce the loss between the transducer face and the acetate window, a thin layer of petroleum jelly was used as a coupling medium. Coupled together, the acetate window material and petroleum jelly layers did not significantly attenuate the ultrasound transmission. The transducer used to measure the transmitted acoustic waves was a second Technisonic 5.0 MHz probe. Overlapping bandwidth allows better frequency coverage and an increased sensitivity. The receiver was also coupled using an acetate window and petroleum jelly. Waveforms were digitized using a computer controlled oscilloscope (Handyscope HS3, TiePie Engineering) sampling at 50 MHz with a 12 bit dynamic range.

3.5.2 Materials

Deionized water was purified using a Millipore (Billerica, US) Milli-Q OM-154 water purification system, which was used for all experiments. Chemicals were obtained from Sigma-Aldrich (Oakville, CA) unless otherwise noted. Peptide conjugation to the hydrogel network was accomplished using carbodiimide chemistry.^{3,29} Carboxymethylcellulose (cellulose, 150000 MW) was dissolved completely into 10 ml of buffer (0.1 M MES, 0.3 M NaCl, pH 6.5) to form a 0.01% solution. The coupling agent, 1-Ethyl-3-[3-dimethylaminopropyl]carbodiimide hydrochloride (EDC, 51 µg) was added to the cellulose solution. A protecting agent, N-hydroxysuccinimide (NHS, 15 µg) was added simultaneously to avoid hydrolysis of the EDC activated carboxylic acids, and to prevent the rearrangement of the o-acylisourea to the stable n-acylisourea product. The

mixture was stirred for 15 minutes to allow complete dissolution. Polyclonal anti-acetaminophen (2.66 nmol, American Research Products, Waltham, US) was then added and stirred for 4 hours to allow the carbodiimide coupling reaction. Divinylsulfone (30 μL) was added in 10 μL aliquots every hour to generate crosslinking within the cellulose chains. The ratio of carbodiimide to antibody in the solution should allow multiple conjugations with the cellulose. Likewise, divinylsulfone may also generate crosslinking with nucleophilic amino acid functional groups, in addition to cellulose crosslinking. The conjugated antibody-polymer hydrogels were dialyzed for 24 hours using Spectra/Por regenerated cellulose membrane tubing (3500 MWCO) from Spectrum Laboratories (Rancho Dominguez, US) to remove any unreacted crosslinking agents. Phosphate buffered saline (0.10 M, 137 mM NaCl, pH 7.4) was used during the dialysis to exchange the reaction buffer to physiological conditions for better antibody binding.

To characterize the hydrogel sensor, two preparations of the cellulose polymer were made using the above procedure. The first batch was prepared with no antibody present. The resulting hydrogel is a crosslinked cellulose network with no analyte-specific binding sites. The second batch was made with the antibody present. Analyte recognition sites were present in this second batch, which represents the sensor used in subsequent experiments. Particle diameter and polydispersity index (PDI) measurements were made by dynamic light scattering using a ZetaPALS system (Brookhaven Instruments Corporation, Holtsville, US). The mean particle diameter when no antibody was present in the hydrogel was determined to be 0.39 μm (0.53 PDI). Introduction of the antibody to the hydrogel network resulted in 20% growth of the hydrogel networks, with a mean particle diameter of 0.47 μm (0.45 PDI). The batch-to-

batch reproducibility of the particle diameter was determined to be 10%, with a variation in the polydispersity index of 19%. Typical IgG antibody size is less than 20 nm, therefore simple surface coating of the cellulose gels to achieve this size increase is not likely. The increase in size suggests that antibodies may act as bridging sites between cellulose chains during the network formation. As a result, partial to complete embedding of the antibodies into the polymer network is expected. The impact of analyte binding to the sensor was also measured by the addition of acetaminophen to fill 100% of the antibody recognition sites present in a sample. A growth of 4% in the mean diameter (0.49 μm) was measured. An increase in size with the analyte present suggests that binding to the sensor is occurring, and further, that this is inducing strain on the network. As shown in the theory section, an increase in size should decrease the resonance frequency of the hydrogel sensor. Though other mechanisms of analyte adsorption may also be present, multilinear analysis of several ultrasonic frequencies should allow for acetaminophen quantification based on acetaminophen-antibody binding.

3.5.3 Samples

Whole bovine blood and rat blood plasma were obtained from the Comparative Medicine & Animal Resources Centre at McGill University. Human urine and saliva were collected approximately 2 hours before analysis. Trials consisted of 21 independent samples. Aliquots of the antibody sensor were mixed with the acetaminophen-doped biofluids and were incubated for approximately 5 minutes to allow coupling between the antibody sensor and acetaminophen present in the sample. Hydrogel sensor concentration

in these samples was 0.01% by mass. Following incubation, biofluids containing the antibody sensor were injected into the sample reservoir for ultrasonic frequency measurement. The order of sample analysis was randomized to avoid sampling bias. Ultrasonic frequency spectra were collected after incubation at room temperature ranging between 21 and 24°C.

3.5.4 Methods of Analysis

Total data acquisition time for each sample was 1 minute, during which 1500 waveforms were measured and saved. All data processing and analysis was done in Matlab (The MathWorks Inc., 2008a, Natick, US). Analysis consisted of three primary steps: waveform alignment, frequency transform, and multilinear modeling. The velocity of ultrasound, and therefore the phase of the ultrasonic waveform, is related to temperature. To reduce temperature effects in the power spectrum, phase matching of the recorded waveforms was made. Each waveform was aligned relative to the highest amplitude in the first peak. Following this alignment, the 1500 waveforms were averaged to increase the signal to noise ratio in each sample.

Reverberations are present in the data due to reflections at the cell interfaces. Since the impulse wave train is short relative to the path length of the cell, the reverberations are well separated temporally. Only the first transient waveform was retained for further analysis in order to decrease high-frequency ringing and baseline noise. The fast Fourier transform algorithm was then applied to the averaged waveform data to give frequency domain ultrasonic spectra. The frequency data were used for

subsequent model generation. The frequency spectrum of each waveform was normalized to the total area. Likewise, water was measured between acetaminophen samples, and the normalized frequency distribution was subtracted to correct for any instrumental drift. Frequency data between 1 and 10 MHz were retained for further processing.

Triplicate samples were prepared for each measured concentration of acetaminophen. Frequency spectra of the samples were divided into independent calibration and test sets. The calibration set consisted of two replicates of each concentration, representing two thirds of the total data. The test set was made up of the remaining samples not included in the calibration set. The calibration data were used to develop a model for acetaminophen concentration.

A stagewise multilinear regression (MLR) algorithm was used to correlate the intensity of ultrasonic frequencies with the acetaminophen concentration in samples. The algorithm determined the regression of the analyte concentrations with the intensity at each individual frequency. The residual values were then calculated and the process is repeated iteratively with the subset of frequencies that were not yet been incorporated into the model. The linear combination of frequencies with the highest correlation to analyte concentration described the data in the form

$$Y = b_0 + b_1X_1 + b_2X_2 + \dots + b_nX_n \quad (3.2)$$

where Y is the dependent variable (here the acetaminophen concentration), $\{X\}$ are independent variables (the intensity at a given ultrasound frequency), and $\{b\}$ are the weighting coefficients determined. This multilinear regression model was then used to estimate and assign a numerical value for acetaminophen concentration in the independent test data set. To reduce overfitting of the regression, the standard error of the

model was computed at the addition of each independent variable and weighting coefficient. The most parsimonious model was selected using an F-test ($\alpha = 0.05$) between calibrations so that the addition of any additional parameters would not significantly change the model. Details of the MLR model selection are provided in Draper and Smith^{3.30} and the routine is presented in Arakaki and Burns.^{3.31} Effectiveness of each model is tested by calculating the correlation coefficient and standard error of the estimate for the independent test samples.

3.6 Results and Discussion

In order to determine the sensitivity of the method, a trial was designed to investigate acetaminophen quantification in whole blood, which is the most common biofluid analyzed. However, blood is composed of a wide array of proteins, metabolites, nutrients, and other chemicals that could potentially interfere with the ultrasonic detection. Sensitivity determination in this matrix therefore represents realistic conditions in which POC measurements using the antibody sensors would be made.

The relationship between the ultrasonic signal and antigen binding was investigated by varying the concentration of acetaminophen in whole bovine blood. Minimizing the volume of blood required for the measurement is important to lower the burden on a patient. To mirror what would be measured *in vivo*, acetaminophen was added directly to whole blood at concentrations ranging from 0.35 to 1.8 mM. These concentrations correspond to real toxic threshold levels in humans over 12 hours following an overdose. The concentration of antibody sensor used was significantly

lower, which necessitated dilution of the acetaminophen-doped blood samples. At each acetaminophen concentration, a 50 μ L blood aliquot was taken, mimicking a single drop. The acetaminophen-doped blood was then diluted into phosphate buffered saline using serial dilutions. Final acetaminophen concentrations in the diluted samples ranged between 3.5 and 18.0 nM, representing a final dilution of $1/10^5$. The antibody sensor was then added to individual samples 5 minutes before the spectra were collected to allow time for antibody-antigen conjugation.

The interrelationship between the size and stiffness of the sensor polymer results in specific ultrasonic frequency profiles dependent on the analyte concentration. Figure 3.2 shows the frequency profiles of the antibody sensor with low (solid line) and high (dashed line) acetaminophen concentrations. The mean of the two profiles has been subtracted, which more clearly illustrates the characteristic differences in the frequency profiles. The principal effect is an exchange from low (<4 MHz) to high (>4 MHz) frequencies, whereby some frequencies increase and others decrease with concentration changes. Likewise, some changes occur in quadrature, where transient frequencies appear only at intermediate concentrations of acetaminophen. The exchange in frequencies is consistent with the model shown in Equation 3.1. As acetaminophen becomes bound to the sensor, the stiffness will increase due to conformational changes induced during antibody-antigen binding, and the resonance frequency will increase.

Based on changes in the frequency spectra, a multilinear calibration model was developed for the estimation of acetaminophen concentration in the whole blood samples. A subset of the data (33% of the total samples) was used as an independent evaluation set. The multilinear model revealed a close correlation between known and estimated

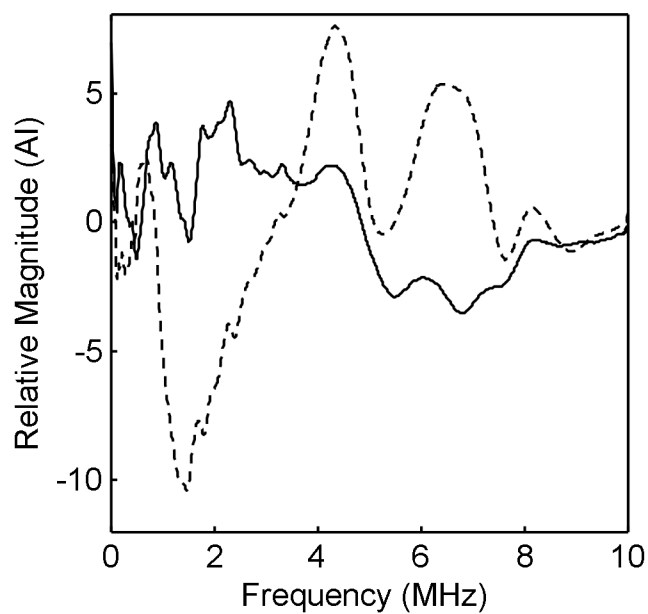


Figure 3.2: Frequency profiles of antibody-linked sensor. Low concentration (solid line) and high concentration (dashed line) of acetaminophen where the mean spectral profile has been subtracted.

acetaminophen concentrations in both the calibration and the test data sets ($r^2 = 0.97$, $SEE = 0.6$ nM) using 5 best fit frequencies. Estimates of analyte concentrations using the multilinear model were plotted against the known values and are shown in Figure 3.3(a). This plot demonstrates good linearity over the range of 3.5–18 nM with minimal bias.

The frequency response of the ultrasound system for the hydrogel polymer can be estimated by comparison to an existing ultrasound contrast agent. Albunex is a commercial contrast material that consists of air-filled albumin microspheres with a bulk modulus of 5.3 MPa (at radius of 1 μm).^{3,32} Using Equation 3.1, a contrast agent with these properties is expected to resonate at approximately 20 MHz. Whereas the hydrogel sensors are not identical to this type of model, they should be in a similar range, therefore subharmonic frequencies would be measured using the 5 MHz ultrasound transducers. Figure 3.3(b) illustrates the frequencies selected for the estimation of acetaminophen concentration using the cellulose sensor. The frequencies used in the multilinear model are clustered above 4 MHz. this range of frequencies would likely be associated with the third subharmonic of the fundamental resonance frequency. The absence of frequencies below 4 MHz in the multilinear model would then be expected because the fourth subharmonics in this range are of a lower magnitude. Ultrasonic analysis nearer to the fundamental harmonic frequency of the polymer sensor should further increase the sensitivity of the technique.

Concentrations of acetaminophen that represent a health concern are high, typically several millimolar. Therefore, monitoring the resonance frequency of the polymer as outlined above is several orders of magnitude more sensitive than needed for measurements in blood. When accounting for the dilution, the concentration range

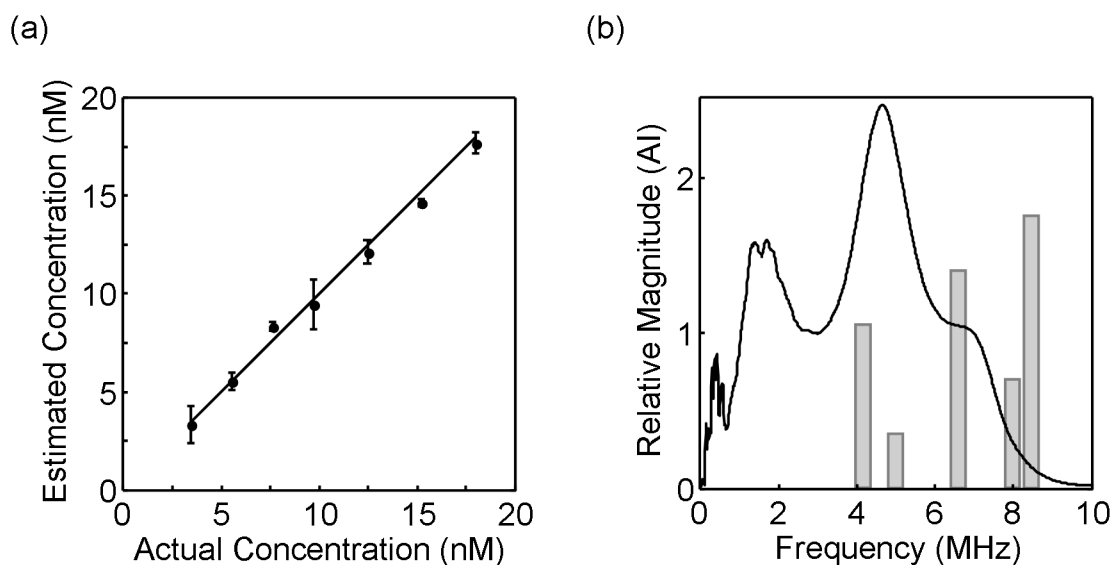


Figure 3.3: Quantification of acetaminophen in a dilute whole blood. (a) Known acetaminophen concentration correlated with the concentration of acetaminophen as estimated by the multilinear model. (b) Typical ultrasonic power spectrum for the antibody sensor in the buffered albumin matrix. Shaded bars illustrate the frequencies selected through MLR for the quantification of acetaminophen, height represents order of selection.

examined corresponds to 0.35–1.8 mM of acetaminophen in the undiluted blood sample. This range is crucial for POC diagnostic purposes as these acetaminophen concentrations correspond to dangerous levels of acetaminophen found in blood up to 8 hours following an overdose. Although concentrations of acetaminophen below the detection limit presented would not be detectable, the dilution factor is easily adjusted. The hazardous threshold after 24 hours is approximately 20 μM . Reducing the dilution factor to 1/100 would allow for the quantification of acetaminophen in a blood sample with no other modifications to the procedure.

To determine if ultrasonic frequency analysis is possible in this less dilute range, a trial was designed where whole blood was diluted 1/6. Biofouling and nonspecific adsorption is a common concern in these types of sensors. Reducing the dilution factor for the blood analysis increases the concentrations of a large number of molecules. As a result, any adsorption of the analyte, or other molecules, into the polymer network would be increased. Additionally, lower dilution will also increase the viscosity of the biofluid analysis sample, which could result in a greater attenuation of the ultrasound signal and shifts in the resonance frequency. For comparison with the highly dilute samples prepared above, the acetaminophen concentrations were in the same range (8.3–20.8 nM) after 1/6 dilution. Due to the lower dilution factor, these concentrations of acetaminophen in blood prior to dilution (50–125 nM) represent hazardous biological levels over 24 hours after an overdose. Although changes in the frequency baseline profile are apparent with the increased concentration of blood, the addition of a sixth frequency in the multilinear model allows quantification. Multilinear estimation of acetaminophen concentrations showed a close correlation between known and estimated values for both

the calibration and the test data sets ($r^2 = 0.95$, $SEE = 1.1$ nM) using 6 frequencies. Results demonstrate that the dilution factor plays a minimal effect on the quantification of acetaminophen. Despite a 1000 fold increase in whole blood concentration, similar detection limits are observed, with an increase in error from 0.6 nM to 1.1 nM. This similarity suggest that the resonance frequency of the polymer sensor is minimally affected by the matrix. Likewise, although nonspecific binding to the hydrogel network may increase, multilinear correlation between the sensor resonance frequency and acetaminophen loading is still possible.

A trial using blood plasma was designed to determine if quantification of acetaminophen was more accurate with the removal of blood cells (including red, white, and thrombocytes). Plasma is composed largely of water, and contains a wide array of proteins, dissolved nutrients, and other metabolites. Due to the absence of blood cells, plasma is less viscous than whole blood. The trial was designed to match acetaminophen concentrations with those in the 1/6 dilution whole blood, 8.3 nM to 20.8 nM. Similarly, the plasma samples were diluted 1/10. Multilinear analysis revealed a high correlation between estimated and known concentrations of acetaminophen ($r^2 = 0.97$, $SEE = 0.8$ nM). The concentrations of acetaminophen estimated by the multilinear model were plotted against the known values in Figure 3.4(A). As with the 1/6 dilution blood, the concentration of acetaminophen in the plasma prior to dilution (83 nM to 208 nM) represents toxic levels over 24 hours after an overdose. The error of the acetaminophen quantification in plasma is similar to that in the $1/10^5$ dilute blood (0.6 nM). The multilinear fit of the determination in 1/6 dilution whole blood was lower ($r^2 = 0.95$),

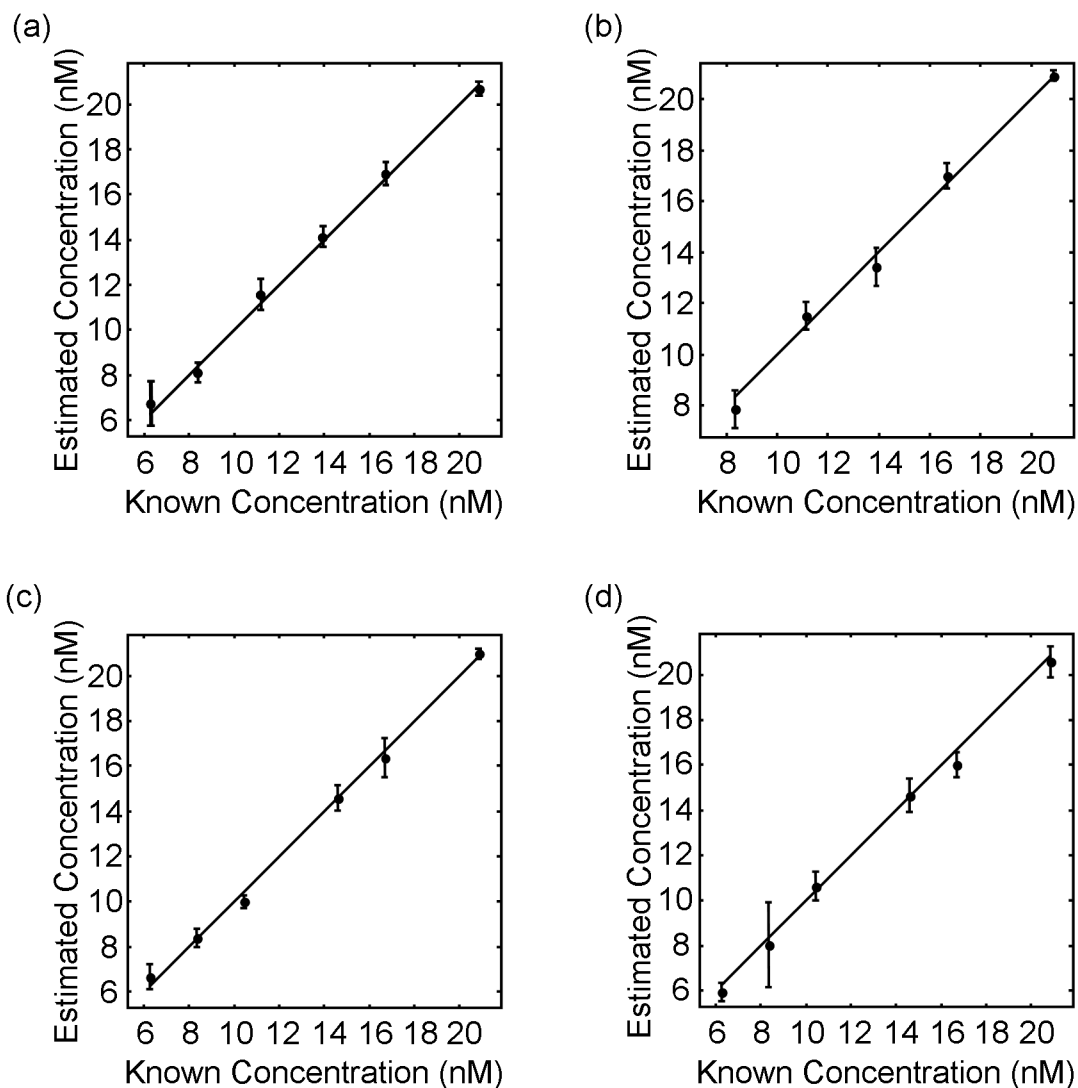


Figure 3.4: Quantification of acetaminophen in a series of biological fluids. Known acetaminophen concentration correlated with the concentration of acetaminophen as estimated by the multilinear model in (a) Blood plasma, (b) Saliva, (c) Undiluted urine, and (d) Dilute urine.

which would be expected because the samples were significantly more viscous than plasma or dilute blood.

To examine if the ultrasonic sensor platform was applicable for other matrices commonly used for acetaminophen measurements, quantification in saliva was also investigated. The trial was designed to compare the same concentrations of acetaminophen as in the blood samples, since both biofluids have similar levels.^{3,33} As outlined in Table 3.1, good quantification of acetaminophen was shown over the same range as 1/6 dilution whole blood. Prior to a 1/3 dilution, concentrations of acetaminophen in saliva from 25 nM to 62 nM would also be expected over 24 hours after an overdose. Figure 3.4(B) illustrates the correlation between the estimated and known concentrations of acetaminophen in saliva. Saliva demonstrated the second lowest sensitivity in the biofluids examined, with nearly twice the error of the 1/10⁵ dilution whole blood. This is probably due, in part, to the large number of human and bacterial cells, as well as dissolved gas bubbles, which are present in saliva. Likewise, saliva also contains a glycosylated mucous, which is highly viscous, and attenuates ultrasound propagation similar to results seen for whole blood. Despite the sensitivity limitations, saliva can be collected quickly and non-invasively, making measurement of acetaminophen in this biofluid appealing for point of care applications.

In order to determine the effect of diluting the biofluid matrix while keeping the viscosity relatively constant, acetaminophen quantification was determined in urine. The viscosity of urine is low relative to whole blood and saliva due to the higher water content. Although primarily made up of water, urine also contains a wide variety of small molecules, and can be excreted over a relatively wide pH range. Due to metabolic

Table 3.1: Acetaminophen concentration estimation based on ultrasonic measurements in selected biological fluids.

Biofluid	Dilution Factor	Acetaminophen Concentration Range (nM)	Fit (r^2)	Error (nM)
Whole Blood (Bovine)	1/10 ⁵	3.5 – 18.0	0.97	0.6
Whole Blood (Bovine)	1/6	8.3 – 20.8	0.95	1.1
Saliva (Human)	1/3	8.3 – 20.8	0.96	1.1
Blood Plasma (Rat)	1/10	6.2 – 20.8	0.97	0.8
Urine (Human)	0	6.2 – 20.8	0.97	0.9
Urine (Human)	1/10 ⁴	6.2 – 20.8	0.97	0.6

processing, less than 5% of the acetaminophen dose is excreted in urine without conjugation, though this can increase up to 10% in patients with toxic doses.^{3,34} In clinical practice, the low concentration of biomarkers (including acetaminophen) often necessitates collecting the first urine of the day to take advantage of overnight bio-concentration. To simulate these conditions, acetaminophen quantification was examined in both a morning sample of urine and in a dilute urine sample ($1/10^4$).

The analysis of both undiluted and dilute urine revealed a close correlation between the ultrasonic frequency intensities and acetaminophen concentrations between 6.2 and 20.8 nM (see Table 3.1). Figures 3.4(c and d) show the concentration estimates plotted against the known values, demonstrating that minimal bias in the calibration is present. For the dilute urine with approximately 5% excretion in urine, these concentrations of acetaminophen in urine prior to dilution would indicate blood concentrations of 62 μ M to 208 μ M. This represents hazardous biological levels between 5 to 10 hours following an overdose. For the completely undiluted urine, the nM concentrations would be expected in toxic cases over 24 hours following the overdose. The acetaminophen concentration was estimated with a high correlation ($r^2 = 0.97$) in both cases, and with only a 0.3 nM difference in the standard error between concentrations. Results suggest that the low concentration of other constituents in the urine matrix had a minor impact on the sensor resonance frequency when the viscosity is not changed significantly.

As with whole blood, the detection limits of acetaminophen in blood plasma, saliva, and urine are several orders of magnitude better than the diagnostic requirements for the detection of an overdose. Further, the dynamic range of the measurement can be

increased by adjusting the biofluid dilution factor. This provides an advantage over current POC systems such as the TOX Drug Screen (Triage, San Diego, CA) which provide qualitative assessment of toxicity based on a fixed acetaminophen concentration. Ultrasonic measurements of the antibody sensor could indicate whether a patient would have a low or high risk of serious health problems due to acetaminophen consumption over wider time window following overdose.

3.7 Conclusions

Ultrasonic frequency analysis is a promising technique for the determination of specific analytes using antibody-based sensors. The dispersed, sub-micron antibody sensor has a high ratio of surface area to volume, which can improve the sensitivity of the sensor.^{3,35} The sensor platform was shown to be sensitive in blood, blood plasma, saliva, and urine, each of which contains a wide variety of proteins, metabolites, and other small molecules. While biofouling of the hydrogels through nonspecific absorption can be a serious problem for these types of sensors, multilinear analysis revealed systematic variations in frequency response which can be used to correct for these effects. Frequency variations were measured and used to create multilinear models to quantify acetaminophen between 3.5 nM and 20.8 nM. Conventional biomedical blood tests are currently costly and time consuming. The key advantage of the technique outline in this work is that all steps from sample collection to measurement and diagnostic results can be carried out in less than 10 minutes. With an appropriate sample dilution method, this is comparable in size, analysis time, and complexity with other commercial POC systems

on the market. The use of ultrasound allows for direct analysis without significant sample treatment, which is important for fast medical response in a relatively narrow treatment window for acetaminophen overdose. Minimizing procedural steps is important not only for acetaminophen analysis, but also for other analytes which could potentially be measured using this methodology. Additionally, the instrumentation costs are low relative to operating a fulltime laboratory. Likewise, the cellulose-based sensor is non-toxic, reducing the environmental footprint of the device. Because laboratory tests play a key role in the majority of diagnostic decisions, using this technique for analyte determination would decrease time and cost burdens on the health care system and result in better patient outcomes.

3.8 Acknowledgements

This work was supported in part by the National Science and Engineering Research Council of Canada, the Canadian Institutes of Health Research, and the Fonds québécois de la recherche sur la nature et les technologies.

3.9 References

- 3.1. T.C. Jansen, J.V. Bommel, P.G. Mulder, A.P. Lima, B.V.D. Hoven, J.H. Rommes, F.T.F. Snellen, and J. Bakker, “Prognostic Value of Blood Lactate Levels: Does the Clinical Diagnosis at Admission Matter?”, *J. Trauma* **66**, 377–385 (2009).

- 3.2. F.S. Apple, R. Ler, A.Y. Chung, M.J. Berger, and M.M. Murakami, “Point-of-Care i-STAT Cardiac Troponin I for Assessment of Patients with Symptoms Suggestive of Acute Coronary Syndrome”, *Clin. Chem.* **52**, 322–325 (2006).
- 3.3. E.A. Trevino, and A.S. Weissfeld, “The Case for Point-of-Care Testing in Infectious-Disease Diagnosis”, *Clin. Microbiol. News.* **29**, 177–179 (2007).
- 3.4. C.P. Price, and A. St John, J.M. Hicks, “Point-of-Care Testing: What, Why, When, and Where?”, AACCC Press, Washington, 2004.
- 3.5. P. Yager, G.J. Domingo, and J. Gerdes, “Point-of-care diagnostics for global health”, *Annu. Rev. Biomed. Eng.* **10**, 107–144 (2008).
- 3.6. A. Warsinke, “Point-of-care testing of proteins”, *Anal. Bioanal. Chem.* **393**, 1393–1405 (2009).
- 3.7. W.M. Lee, “Acute liver failure”, *N. Engl. J. Med.* **329**, 1862–1872 (1993).
- 3.8. F.V. Schiødt, F.A. Rochling, D.L. Casey, and W.M. Lee, “Acetaminophen Toxicity in an Urban County Hospital”, *N. Engl. J. Med.* **337**, 1112–1118 (1997).
- 3.9. J. MacDaniel, V.S. Bebarta, H.A. Schwertner, and J.F. Martin, “Comparison of urine and serum testing for early detection of acetaminophen ingestion”, *Mil. Med.* **172**, 399–401 (2007).
- 3.10. I.V. Kovachevich, S.N. Kondratenko, A.K. Starodubtsev, and L.G. Repenkova, “Pharmacokinetics of acetaminophen administered in tablets and capsules under long-term space flight conditions”, *Pharmacol. Chem. J.* **43**, 130–133 (2009).
- 3.11. E. Pufal, M. Sykutera, G. Rochholz, H.W. Schütz, K. Sliwka, and H.J. Kaatsch Fresenius. “Determination of paracetamol (acetaminophen) in different body

- fluids and organ samples after solid-phase extraction using HPLC and an immunological method”, *J. Anal. Chem.* **367**, 596–599 (2000).
- 3.12. H. Muramatsu, J.M. Kim, and S.M. Chang, “Quartz-crystal sensors for biosensing and chemical analysis”, *Anal. Bioanal. Chem.* **372**, 314–321 (2002).
- 3.13. M.A. Cooper and V.T. Singleton, “A survey of the 2001 to 2005 quartz crystal microbalance biosensor literature: applications of acoustic physics to the analysis of biomolecular interactions”, *J. Mol. Recognit.* **20**, 154–184 (2007).
- 3.14. D. James, S.M. Scott, Z. Ali, and W.T. O’Hare, “Chemical sensors for electronic nose systems”, *Microchim. Acta.* **149**, 1–17 (2005).
- 3.15. C.D. Natale, R. Paolesse, A. Macagnano, A. Mantini, A. D’Amico, A. Legind, L. Lvova, A. Rudnitskaya, and Y. Vlasov, “Electronic nose and electronic tongue integration for improved classification of clinical and food samples”, *Sens. Actuators, B.* **64**, 15–21 (2000).
- 3.16. M. Thompson, A.L. Kipling, W.C. Duncan-Hewitt, L.V. Rajaković, and B.A. Čavić-Vlasak, “Thickness-shear-mode acoustic wave sensors in the liquid phase. A review”, *Analyst* **116**, 881–890 (1991).
- 3.17. B. Avvaru and A.B. Pandit, “Oscillating bubble concentration and its size distribution using acoustic emission spectra”, *Ultrason. Sonochem.* **16**, 105–115 (2009).
- 3.18. H.P. Pendse and A. Sharma, “Particle Size Distribution Analysis of Industrial Colloidal Slurries using ultrasonic spectroscopy”, *Part. Part. Syst. Char.* **10**, 229–233 (1993).

- 3.19. L. Liu, “Application of ultrasound spectroscopy for nanoparticle sizing in high concentration suspensions: A factor analysis on the effects of concentration and frequency”, *Chem. Eng. Sci.* **64**, 5036–5042 (2009).
- 3.20. A.L. Klibanov, “Targeted delivery of gas-filled microspheres, contrast agents for ultrasound imaging”, *Adv. Drug Deliver Rev.* **37**, 139-157 (1999).
- 3.21. L. Hoff, P. C. Sontum, J.M. Hovem, “Oscillations of polymeric microbubbles: effect of the encapsulating shell”, *J. Acoust. Soc. Am.* **107**, 2272–2280 (2000).
- 3.22. S. Qin and K.W. Ferrara, “The Natural Frequency of Nonlinear Oscillation of Ultrasound Contrast Agents in Microvessels”, *Ultrasound Med. Biol.* **33**, 1140–1148 (2007).
- 3.23. J.A. Ketterling and J. Mamou, “Subharmonic Response from Polymer-Shelled Contrast Agents”, *IEEE Ultrasonics Symposium* **3**, 1077–1080 (2007).
- 3.24. E. Kato, “Volume-phase transition of N-isopropylacrylamide gels induced by hydrostatic pressure”, *J. Chem. Phys.* **106**, 3792–3797 (1997).
- 3.25. T. Oya, T. Enoki, A.Y. Grosberg, S. Masamune, T. Sakiyama, T. Takeoka, K. Tanaka, G. Wang, T. Yilmaz, M.S. Feld, R. Dasari, and T. Tanaka, “Reversible molecular adsorption based on multiple-point interaction by shrinkable gels”, *Science* **286**, 1543–1545 (1999).
- 3.26. O. Keskin, “Binding induced experimental conformational changes of proteins correlate with their intrinsic fluctuations: A case study of antibodies”, *BMC Struct. Biol.* **7**, 31 (2007).

- 3.27. M. Oda, H. Kozono, H. Morii, and T. Azuma, “Evidence of allosteric conformational changes in the antibody constant region upon antigen binding”, *Int. Immunol.* **15**, 417-426 (2003).
- 3.28. A. Strybulevych, V. Leroy, M.G. Scanlon, and J.H. Page, “Characterizing a model food gel containing bubbles and solid inclusions using ultrasound”, *Soft Matter* **3**, 1388–1394 (2007).
- 3.29. J.D. Lathia, L. Leodore, M.A. Wheatley, “Polymeric Contrast Agent with Targeting Potential”, *J. Ultrasonics* **42**, 763–768 (2004).
- 3.30. N. R. Draper and H. Smith, *Applied Regression Analysis* (John Wiley and Sons, New York, 1981) 2nd ed., pp 294–352.
- 3.31. L.S.L. Arakaki and D.H. Burns, “Multispectral analysis for quantitative measurements of myoglobin oxygen fractional saturation in the presence of hemoglobin interference”, *Appl. Spectrosc.* **46**, 1919–1927 (1992).
- 3.32. L. Hoff, P.C. Sontum, and B. Hoff, “Acoustic properties of shell-encapsulated, gas-filled ultrasound contrast agents”, *IEEE Ultrasonics Symposium* **2**, 1441-1444 (1996).
- 3.33. T.W. Hahn, S.W. Henneberg, R.J. Holm-Knudsen, K. Eriksen, S.N. Rasmussen, and M. Rasmussen, “Pharmacokinetics of rectal paracetamol after repeated dosing in children”, *Br. J. Anaesth.* **85**, 512–519 (2000).
- 3.34. L.F. Prescott and N. Wright, “The effects of hepatic and renal damage on paracetamol metabolism and excretion following overdose: A pharmacokinetic study”, *Br. J. Pharmacol.* **49**, 602–613 (1973).

- 3.35. N. Levit, D. Pestov, and G. Tepper, “High surface area polymer coatings for SAW-based chemical sensor applications” *Sensor. Actuat. B-Chem.* **82**, 241–249 (2002).

Chapter 4

Quantification of Tumor Necrosis Factor- α Protein using Antibody-Linked Dendrimeric Hydrogel Sensors

4.1 Foreward

In Chapter 3, acetaminophen concentrations in biological samples were determined using antibody-linked cellulose sensors. It was shown that characteristic changes in the ultrasound frequency profile were induced by binding between the hydrogel sensor and the target molecule. These frequency changes could be correlated to nanomolar concentrations of acetaminophen, providing an attractive method for the determination of this analyte.

For point-of-care applications, many other pharmaceutical agents are monitored. Likewise, a wide variety of metabolites arising from biochemical changes can be used as diagnostic markers. There is a need for rapid quantification of many such molecules, including numerous cytokine proteins, which are involved in metabolic response. Certain cytokines can be present at low pM concentrations. To address the need for rapid point-of-care determination of these low concentration analytes, an effort to increase the sensitivity of the ultrasound sensor methodology is presented in this chapter.

Using the same synthesis methodology as in the previous chapter, an antibody-linked cellulose sensor was created for the protein Tumor Necrosis Factor- α (TNF). This protein is a cytokine that has a role in numerous biological responses, including acetaminophen-induced organ damage.^{4.1} While the analytes measured in Chapters 2 and 3 have molecular weights below 200 g/mol, the molecular weight of TNF is 17 kDa. The larger mass of this analyte represents an increase in size of two orders of magnitude. A trial was designed to investigate whether the large mass of this analyte would produce a greater change in resonance frequency, allowing a more sensitive determination of analyte concentration.

Frequency profiles of the TNF sensor were then measured and analyzed using a similar methodology as in the previous chapters. Multilinear analysis found that using the 6 frequencies shown in Figure 4.1(a), the concentration of TNF in the prepared samples could be estimated with an r^2 of 0.95 and a standard error of 38 pM. As shown in Figure 4.1(b), the estimation shows little bias over the examined range of 115–592 pM. Results show a significant increase in the sensitivity of the ultrasound determination relative to the determination of acetaminophen. The increased sensitivity indicates that the mass of the analyte examined plays a key role in the ultrasound frequency profile analysis

Rapid quantification of proteins is often challenging due to the large variety of species in tissues and biofluids. One of the major components in some biological fluids is the protein albumin. To determine if high concentrations of interferent proteins would limit the sensitivity of the TNF quantification, a series of solutions were prepared containing a range of TNF concentrations and 30 g/L of bovine serum albumin (“BSA”),

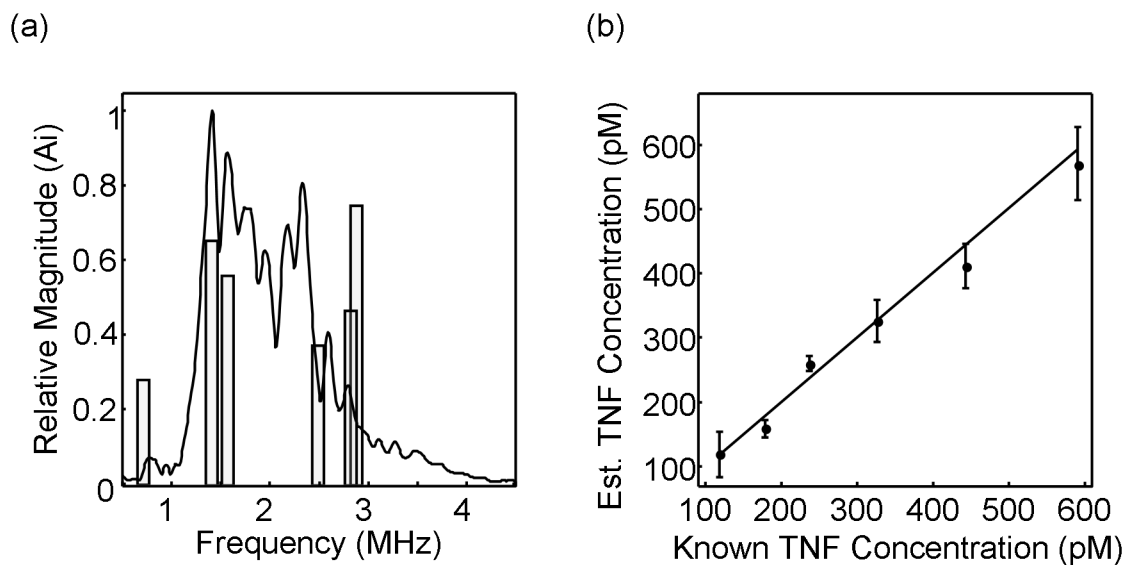


Figure 4.1: Quantification of TNF in buffered solutions using cellulose hydrogel sensor
 (a) Frequencies used in the multilinear model (b) Correlation between estimated and known TNF concentrations.

a physiologically-relevant level. Using the multilinear regression analysis approach, TNF concentrations could be estimated with an r^2 of 0.95 and a standard error of 60 pM. The frequencies used for the estimation of TNF in BSA were different than those used in the buffer solution, as shown in Table 4.1. In looking at the frequencies, there is a shift to slightly lower frequencies. This may be a result of damping caused by the viscous BSA. However, the capability for picomolar protein determination in the presence of other species is nonetheless advantageous due to the simplicity and speed of the method.

Dynamic light scattering measurements have shown that the above cellulose sensors are polydisperse. The goal of the work presented in this chapter is to develop a monodisperse sensor that can be used to further explore the relationship between the sensor mass and the frequency changes. A dendrimeric hydrogel was used for this purpose, as the chemical synthesis allows these polymers to be generated at discrete sizes with high monodispersity. Under these new conditions, the specific size and mass of dendrimers enables the investigation of sensors that are chemically-similar, but have different molecular weights.

As would be expected for these types of sensors, the antibody is no longer encapsulated within the hydrogel. Instead, the antibody-dendrimer system would resemble a 2-body oscillator. Mass changes in oscillating bodies are known to be linked to variations in the resonance frequency. This mass dependence of the resonance frequency is well established in the operation of crystal microbalances.^{4.2} Though the sensors presented in this thesis are dispersive rather than fixed, we propose that the shift in the frequency profile of the ultrasound-sensitive hydrogel sensors will show a similar

Table 4.1: Figures of merit for TNF estimation using cellulose sensors

BSA (g/L)	r^2	SE (pM)	Range (pM)	Frequencies (MHz)
0	0.95	38	115 – 592	2.87, 1.27, 1.47, 2.81, 2.59, 0.68
30	0.95	60	115 – 592	0.67, 4.46, 0.92, 0.51, 2.59

mass-dependence. Three dendrimer sizes were used to create antibody-linked sensors. These sensors were then used to estimate concentrations of TNF. Data in this chapter were acquired, under my supervision, by undergraduate summer research student Michael A. Tycon as part of his honours research project.

4.2 Manuscript

Quantification of Tumor Necrosis Factor- α Protein using Antibody-Linked Dendrimeric Hydrogel Sensors

Authors:

Jonathan R. Dion, Michael A. Tycon, and David H. Burns

4.3 Abstract

Quantification of proteins, pharmaceuticals, and metabolites plays a key role in biomedical diagnostics. Although rapid measurements can lead to better patient outcomes, the concentration of these species is often very low, resulting in the need for extensive sample handling, expensive equipment, and skilled personnel. To provide an alternative methodology for these critical measurements, an antibody-linked dendrimer sensor is presented. A series of ultrasound frequency measurements were acquired from samples containing known concentrations of Tumor Necrosis Factor- α (77–565 pM). Results showed that the concentration of the analyte could be estimated using a subset of ultrasound frequencies with an r^2 greater than 0.93 and a standard error of 55 pM. The resonance frequencies of these sensors were also shown to be dependent on the size of the dendrimer used. Similar TNF estimation was shown using three different sizes of dendrimers, offering the possibility of simultaneous multi-analyte measurement. The dendrimer sensor was also tested in a matrix containing physiological levels of albumin,

an abundant protein in blood. Although the increased viscosity of the albumin results in a damping of the ultrasound frequencies, quantification was possible at higher concentrations (263–922 pM) with similar errors, demonstrating the applicability of the method to biological measurements. Overall, these findings suggest that dendrimer-based ultrasound biosensors show promise for quantification of low-concentration proteins in point-of-care situations.

4.4 Introduction

4.4.1 Background

Accurate chemical quantification is essential in understanding biological systems. Small changes in the concentration of proteins and other metabolites can have far reaching impacts on health and can be indicative of medical situations ranging from immune response to heart failure. Rapid and accurate measurement of biochemical concentrations therefore has a strong importance as a diagnostic tool.

Quantification of bioanalytes has traditionally been done using immunological, spectroscopic, or electrochemical techniques. However, these measurements are often difficult to analyze due to the complexity of biological matrices, which can contain hundreds or thousands of other chemicals, metabolites, and proteins. Likewise, the high opacity and scattering in biological fluids is often limiting for optical techniques. Analyses in biological systems have therefore often required extensive pretreatment of samples such as chromatographic separation, centrifugation, and precipitation.^{4.3–4.5}

Although these techniques are well established, a lead time of up to several hours can be expected.^{4,6} Likewise, the high cost of operating a laboratory is limiting for small clinical centers, further increasing the analysis time. Due to the time-critical nature of medical diagnostics, a simple and more rapid methodology would be advantageous.

Tumor Necrosis Factor- α (TNF) is a cytokine, or small signaling protein, which is important in human metabolic responses. This protein is responsible for a wide variety of biological responses such as inflammation, immuno-regulation, and cytotoxicity.^{4,7} It has also been reported as an important biological marker for many medical conditions including heart disease^{4,8}, Alzheimers^{4,9}, and multiple sclerosis.^{4,10} Measurement of TNF concentrations in a patient can provide a means to monitor the severity and progression of these conditions. Though TNF concentration in biological fluids are often measured by enzyme-linked immunosorbent assay (ELISA), this technique is time consuming.^{4,10,4,11} Development of a fast and inexpensive methodology for the measurement of the TNF would be advantageous for medical diagnostics.

To address the need for rapid and inexpensive biomedical diagnostics, we have developed a sensor platform based on ultrasound frequency analysis. Ultrasound waves consist of oscillating compressive and rarefying pressure phases that travel through elastic media. As these waves are mechanical in nature, ultrasound can easily penetrate samples such as tissues and biological fluids that have a high optical absorbance and scattering. When an ultrasonic wave encounters a region of different impedance or density, reflection occurs. Measurement of this backscattered wave is used extensively for medical imaging in fields such as obstetrics and cardiology due to the ease of ultrasound penetration into tissues.

In this work, we present a general approach to create a dispersive, dendrimer sensor that is sensitive to TNF. Analyte-sensitivity is imparted by linking antibodies to the hydrogel polymers. The high binding constants and selectivity of antibodies make them appealing for identification and quantification of target molecules in biological fluids. The high mass of the TNF should result in a large change in the sensor resonance frequency when binding occurs. By monitoring a wide range of ultrasound frequencies, it should be possible to quantify the TNF concentration in a sample based on the resonance characteristic of the hydrogel sensor.

4.4.2 Principle

In previously reported dispersive hydrogel sensors, the ultrasound molecular probes have consisted of antibodies encapsulated by a polymeric cellulose network.^{4.12} This encapsulation is represented in Figure 4.2(a), where the polymer network surrounds part of the antibody. In the current work, dendrimeric hydrogels were coupled to the antibody without any further crosslinking. As a result, the antibody should be tethered to the surface of the dendrimer, as illustrated in Figure 4.2(b). With this difference in structure, the mechanism of the ultrasound change may be more analogous to molecular vibration. The resonance frequency in this type of system can be written as

$$f_0 = \frac{1}{2\pi} \sqrt{\frac{S}{\mu}} \quad (4.1)$$

where S is the restoring force and μ is the reduced mass^{4.13,4.14}, which is given by

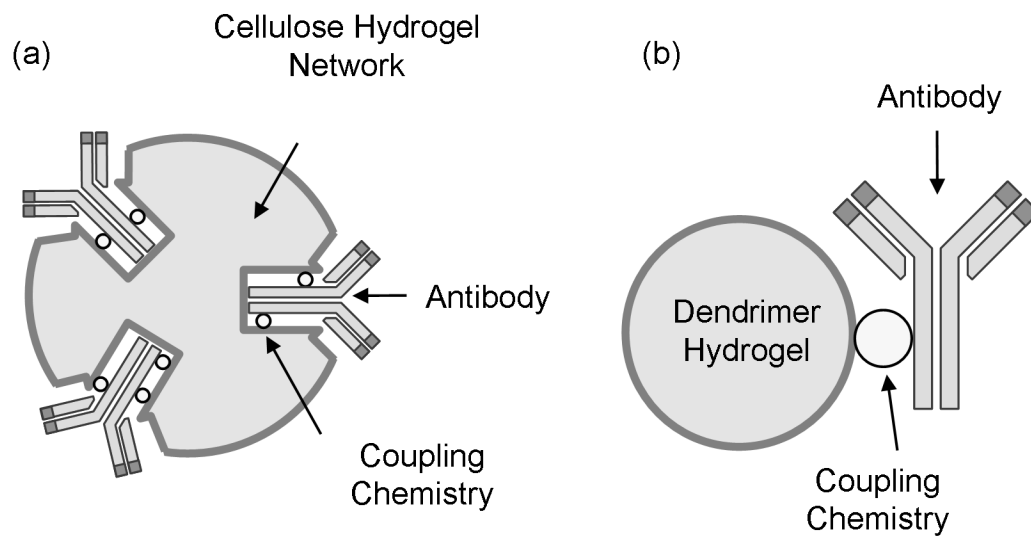


Figure 4.2: Antibody-linked hydrogel sensor diagram. (a) Cellulose-based sensor encapsulating antibody, (b) Dendrimer-based sensor with antibody tethered to the hydrogel network.

$$\mu = \frac{(m_1 m_2)}{(m_1 + m_2)} \quad (4.2)$$

where m_1 and m_2 are the masses of the dendrimer and the antibody. In this sensor application, the resonance frequency would therefore be altered by a change in the reduced mass due to analyte binding to the antibody.

This mass dependence of the resonance frequency is well established in the operation of crystal microbalances. These sensors are based on the linear relationship between the resonance frequency of a vibrating crystal and the mass deposition on the QCM sensor.^{4,2} Thin quartz crystals making up the QCM surface oscillate at characteristic frequencies. When mass is added to a QCM surface, there is a fractional change to the resonating frequency that can be measured. The dispersed, oscillating finite masses making up the dendrimer sensor would behave like localized microbalances. The oscillation of finite masses has been used to describe other systems such as resonating contrast bubbles^{4,13,4.15} and molecular vibrations.^{4,14} The change in the resonance frequency (Δf_m) can be related linearly to the change in mass (Δm) by

$$\Delta f_m = -\frac{f_0^2}{f_0 d_q \rho_q} \frac{\Delta m_s}{A} = -\frac{f_0^2}{N_q \rho_q} \frac{\Delta m_s}{A} = -f_0 \frac{\Delta m}{m_0} \quad (4.3)$$

where f_0 is the natural resonance frequency of the oscillator, m_0 initial mass of the unperturbed resonator, and d_q , ρ_q , and A describe the thickness, density, and area of the sensor.^{4,16} The variable N_q is the resonance frequency constant for a specific resonator. However, in viscous media such as biological fluids, oscillation requires a displacement of the surrounding liquid. The result is a frequency shift, which has been described as

$$\Delta f_1 = \sqrt{f_0^3 \frac{\eta_1 \rho_1}{\pi N_q^2}} \quad (4.4)$$

where η_l and ρ_l are the viscosity and density of the media.^{4.2,4.17,4.18} The viscosity of this layer also results in a damping of the resonance frequency.^{4.15,4.17} The total frequency change when a mass binds to the surface can be found by summing these contributions, so that:

$$\Delta f_{total} = \Delta f_m + \Delta f_1 \quad (4.5)$$

The linear dependence of the resonance frequency shift on the change in mass suggests that a larger mass would have a greater impact on the frequency profile. Changes in the resonance frequency could therefore provide a means to measure mechanical changes occurring in a resonating sensor when mass is added by analyte binding. With multiple, dispersed resonators, the ratio of bound to unbound sensors could therefore be used to determine the analyte concentration.

4.5 Materials and Methods

4.5.1 Reagents

Unless otherwise noted, chemicals were purchased from Sigma-Aldrich (Oakville, CA). All water used in this work was purified by a Millipore (Billerica, US) Milli-Q OM-154 water purification system. Monoclonal anti-tumor necrosis factor- α (TNF) was generously donated by Professor C. D. Skinner, Concordia University, Canada. Bovine serum albumin (“BSA”) was purchased from BioFX Laboratories (Owings Mills, US).

Poly-amidoamine dendrimers were purchased from Dendritech (Midland, US). Due to the controllable synthesis, PAMAM dendrimers are highly monodisperse, have a

spherical shape, and can be created at different sizes. Three sizes, or generations, of dendrimers were used in this work. The weight and size of these are shown in Table 4.2. Antibody linking onto each dendrimer generation was performed separately.

PAMAM dendrimers were coupled to antibodies using carbodiimide chemistry.^{4,18} The Anti-TNF (2.66 nmol) was dissolved into 10 mL of buffer (0.1 M MES, 0.3 M NaCl, pH 6.5). A carbodiimide coupling agent, 1-Ethyl-3-[3-dimethylaminopropyl] carbodiimide hydrochloride (EDC, 51 μ g) was then added, along with a protecting agent, N-hydroxysuccinimide (NHS, 15 μ g). This protecting agent was to prevent hydrolysis of the EDC-activated carboxylic acids and to prevent the rearrangement of the o-acylisourea to the stable n-acylisourea product. The solution was then stirred for 10 minutes to allow complete mixing. Dendrimer (26 nmol) was then added and stirred for 4 hours to allow the coupling reaction.

Conjugated antibody-hydrogel sensors were finally dialyzed for 24 hours using Spectra/Por regenerated cellulose membrane tubing (3500 MWCO) from Spectrum Laboratories (Rancho Dominguez, CA) to remove any unreacted crosslinking agents. A phosphate buffer (0.1 M, 137 mM NaCl, pH 7.4) was used during the dialysis to exchange the reaction buffer. This buffer was a better mimic of physiological conditions, improving antibody recognition and binding.

4.5.2 Ultrasound Apparatus

The configuration of the instrument used to measurement TNF concentration is shown in Figure 4.3. Two ultrasonic transducers were used to allow transmission-mode

Table 4.2: Molecular weight and size of PAMAM dendrimers.^{4,31}

Generation	MW (10 ³ g/mol)	Diameter (nm)
5	28	4.3
6	58	6.9
7	116	8.0

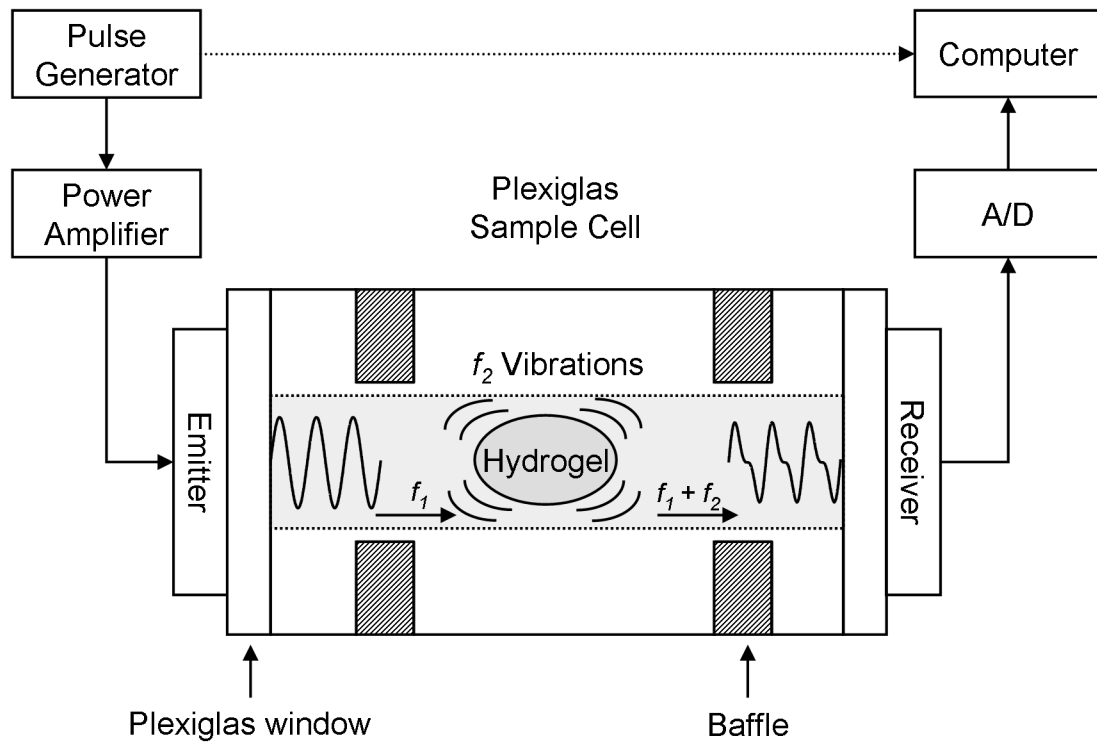


Figure 4.3: Instrumental configuration.

measurements through a sample cell. A 1.9 MHz narrow-band transducer (Advanced Technology Labs Inc., Pennsylvania, U.S.) was used to generate ultrasound pulses. This transducer was driven by a panametrics 500PR Pulser/Receiver (Panametrics Inc., Massachusetts, US), which generated <20 ns, 250 V negative impulses. A pulse repetition rate of 1 KHz was used to ensure temporal resolution of the ultrasound waveforms. Likewise, this allowed sufficient time for any ultrasound wave reverberations inside the cell to be attenuated to baseline noise levels before subsequent pulses were generated. A 10 MHz wideband transducer (Optel Inc., Wrocław, PL) received the ultrasonic signals, which were digitized using a Handyscope HS3 (TiePie Engineering, Sneek, NL) computer-controlled oscilloscope. Data were sampled at 50 MHz (12 bit) to ensure high temporal resolution in the analysis.

A Plexiglas cell with a 2 cm path length was used as a sample reservoir. To minimize the sample volume required for the analysis, the width of the rectangular reservoir measured 3 mm. The emitting transducer measured 1.6 cm in diameter. To ensure that only ultrasound propagating through the liquid sample was measured, sections of the Plexiglas cell were cut away to create a series of baffles. With these in place, it was verified that no ultrasound signal could be detected with the reservoir empty. Propagation of ultrasound through an interface between two materials can be a source of high signal attenuation due to the poor transmission of ultrasound through air. To maximize the coupling between the ultrasound transducers and the sample cell, a thin layer of petroleum jelly was used. This coupling fluid did not significantly attenuate the signal.

4.5.3 Methods of Analysis

Ultrasonic waveforms were collected from the samples in random concentration order to ensure no correlation with time, instrument changes, or minor temperature fluctuations. All samples were prepared independently and in triplicate. The sensor was added to samples and allowed to incubate for 20 minutes. Data for each sample were then measured continuously for 2 minutes, allowing for the collection of 2500 waveforms, which were then averaged in order to increase the signal to noise ratio. The velocity of ultrasound propagation is highly dependent on temperature. To compensate for phase changes as a result of temperature changes, the data were aligned to the amplitude maxima of the signal. A fast Fourier transform algorithm was then applied to this averaged and aligned data to allow processing in the frequency domain. Variability due to instrumental fluctuations was minimized by total area normalization. Likewise, random noise fluctuations were reduced using a boxcar smoothing function with a 0.2 MHz window.

Each data set was divided into independent calibration and test sets. The calibration set was made up of two replicates of each sample, with the third replicate making up the test set. Frequency spectra in the calibration set were used to develop a multilinear model for concentration of TNF in each sample. Stagewise multilinear regression (SMLR) was used to determine the linear combination of a subset of frequencies to best describe the data in the form

$$Y = b_0 + b_1X_1 + b_2X_2 + \dots + b_nX_n \quad (4.6)$$

where Y is the dependent variable (the concentration of TNF in the sample), $\{X\}$ are independent variables (the magnitude of each frequency in the ultrasound spectrum of a sample), and $\{b\}$ are the weighting coefficients determined. The algorithm computed the regression of the known volume fraction with the intensity at each individual frequency in the spectrum and residual values were then calculated. This process was then repeated iteratively with the subset of the frequency spectrum not yet incorporated into the regression model. The most parsimonious model was selected using an F-test ($\alpha = 0.05$) between calibrations until the addition of any additional parameters would not significantly change the model, this regression model was then used to estimate TNF concentrations in the test data set. Frequency selection in the MLR model is described in Draper and Smith.^{4,20} The SMLR analysis was done in Matlab (The MathWorks Inc., 2006b, Natick, US).

4.6 Results and Discussion

To explore the relationship between the sensor mass and the frequency changes, an antibody-linked dendrimer hydrogel sensor was designed. Due to the precisely controlled synthesis, dendrimeric polymers are highly monodisperse. Sensors were prepared using three dendrimer sizes (generation, G) listed in Table 4.2. The ultrasound frequency spectra of the dendrimer sensors were then measured without any TNF present. Figure 4.4(a) shows the changes in the relative intensity of frequencies, where the mean spectrum has been subtracted. The position of the maximum frequency intensity changes with the dendrimer size. In the $G5$ dendrimer, which has the smallest mass, the peak

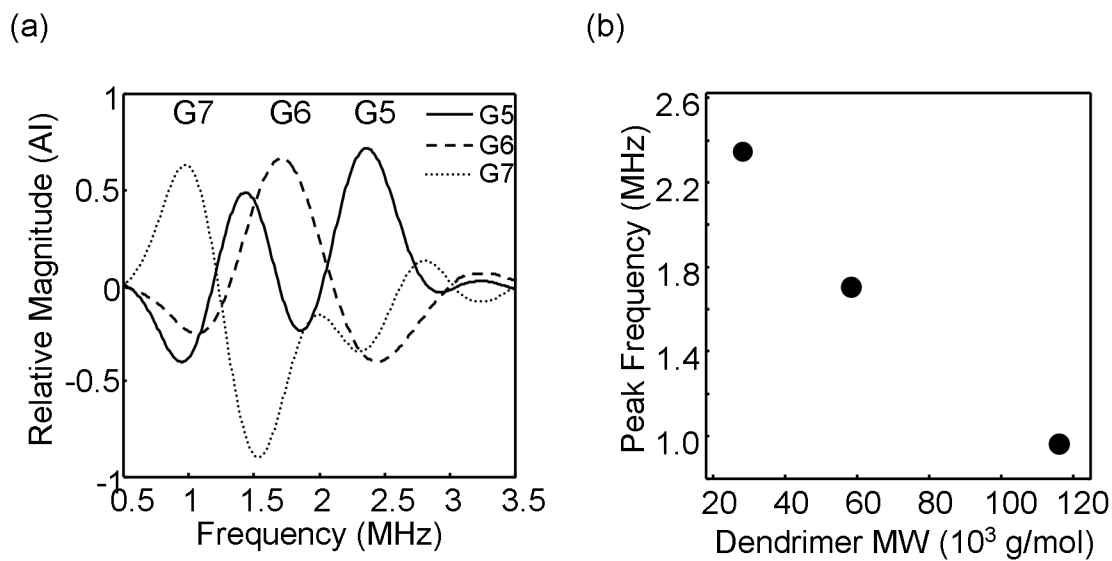


Figure 4.4: Ultrasound frequency changes with increasing dendrimer size (a) Mean centered data showing paired frequency peaks, (b) Frequency position dependent on dendrimer mass.

maximum is centered at 2.35 MHz. In the G6 dendrimer, the maximum is at 1.70 MHz. In the largest dendrimer, G7, the frequency with the highest intensity is 0.97 MHz. As shown in Figure 4.4(b), the position of these frequency peaks follows a monotonic trend with the size of the three dendrimers. This trend would be expected from Equation 4.1, where the resonance frequency is inversely proportional to the mass. This relation would be consistent with the dendrimer and antibody being tethered.

An experiment was designed to determine if the concentrations of TNF could be estimated using dendrimer-based sensors of the three sizes. A series of samples with varying concentration of TNF were prepared independently, in triplicate using the G5 dendrimer. Using the SMLR algorithm, a multilinear regression model was generated using two independently prepared and measured replicates of each TNF concentration. The model was then tested on the third, independent replicate. It was found that using 5 frequencies, the concentration of TNF could be estimated between 77 and 565 pM with an r^2 of 0.98 and a standard error of 57 pM. At lower concentrations, the TNF concentration could not be determined.

Similar analyses were done using the G6 and G7 dendrimer sensors. Independent multilinear regression calibrations were created to estimate the concentration of TNF. Using the G6 dendrimer sensor, an r^2 of 0.93 and a standard error of 55 pM. With the G7 sensor, an r^2 of 0.96 and a standard error of 57 pM could be attained. The concentrations of TNF estimated by the models are plotted against the known values in Figure 4.5(a–c), and the figures of merit are summarized in Table 4.3. Though there is a small bias in the estimation using the G6 sensor, TNF concentration was generally well estimated using all three dendrimer sizes. While the physiological concentrations of TNF are generally

Table 4.3: Figures of merit for the determination of fractional components in binary mixtures.

Dendrimer Generation	r^2	SE (pM)	Range (pM)	Frequencies (MHz)
5	0.98	57	77 – 565	1.81, 0.80, 0.86, 4.29, 2.72
6	0.93	55	77 – 565	0.82, 3.53, 1.33, 1.76, 1.42
7	0.96	60	77 – 565	0.53, 0.59, 1.96, 0.91, 4.41
5/BSA	0.96	56	263 – 922	3.96, 2.25, 2.74, 0.80, 0.92

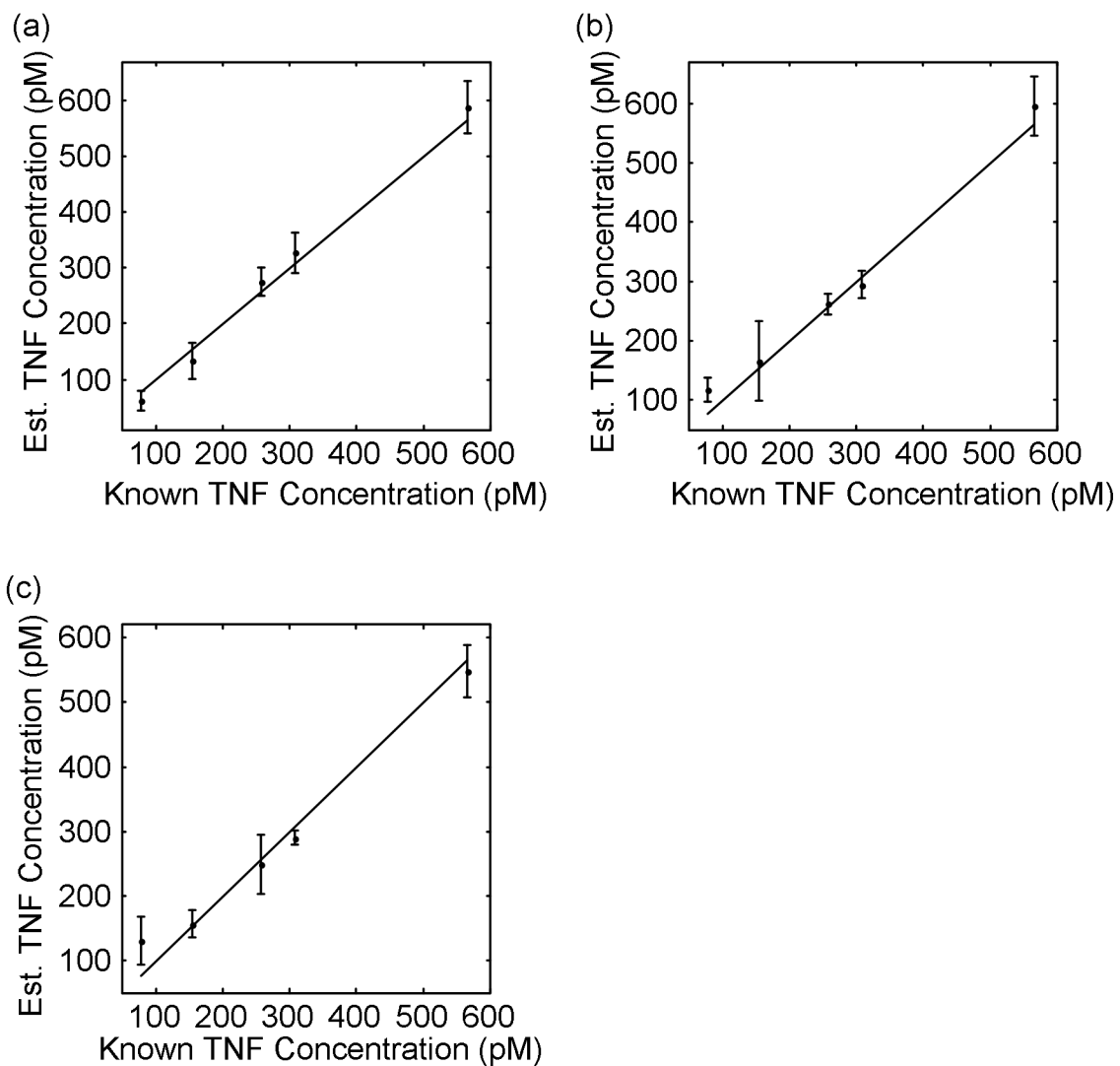


Figure 4.5: Correlation between estimated and known TNF concentrations using dendrimer hydrogel sensor (a) Generation 5, (b) Generation 6, (c) Generation 7.

below 50 pM, infection can elevate levels.^{4.21,4.22} Higher concentrations of TNF are associated with cytotoxicity and death^{4.23-4.25}, making early detection diagnostically important. It was also shown that the resonance frequencies of the dendrimeric sensors are distinct, and different frequencies were used in the multilinear regression models for each dendrimer size. By linking different sized dendrimers to antibodies for separate target antigens, simultaneous determination of multiple analytes may be possible.

The sensitivity of TNF estimation with the dendrimer sensor was also investigated in the presence of BSA to simulate a biological matrix. Albumin is typically found in concentrations between 30 to 50 g/L.^{4.26} This high concentration and relative ubiquity make BSA a likely candidate as an interfering species by nonspecific binding. The high concentration of protein also increases the viscosity of the solution. So, according to Equation 4.5, it would be consistent that the resonance frequency would be shifted, as can be seen in the results. Likewise, an increase in viscosity is also expected to result in a damping of the ultrasound frequencies. These changes were verified by measuring the frequency profile of the G5 sensor in the presence of 30 g/L of BSA. As shown in Figure 4.6(a), the high BSA concentration in these solutions resulted in a broadening of the peaks in the frequency profile. For example, in the peak centered on 1.55 MHz, the full width and half maximum height increases from 0.46 MHz to 0.58 MHz. The maximum frequency of this peak also decreased from 1.56 MHz to 1.54 MHz. These changes indicate that the viscosity of the medium has a significant effect on the ultrasound frequency distribution.

To determine if quantification was possible in the viscous medium, a series of solutions with varying TNF concentrations and 30 g/L of BSA were prepared. Though

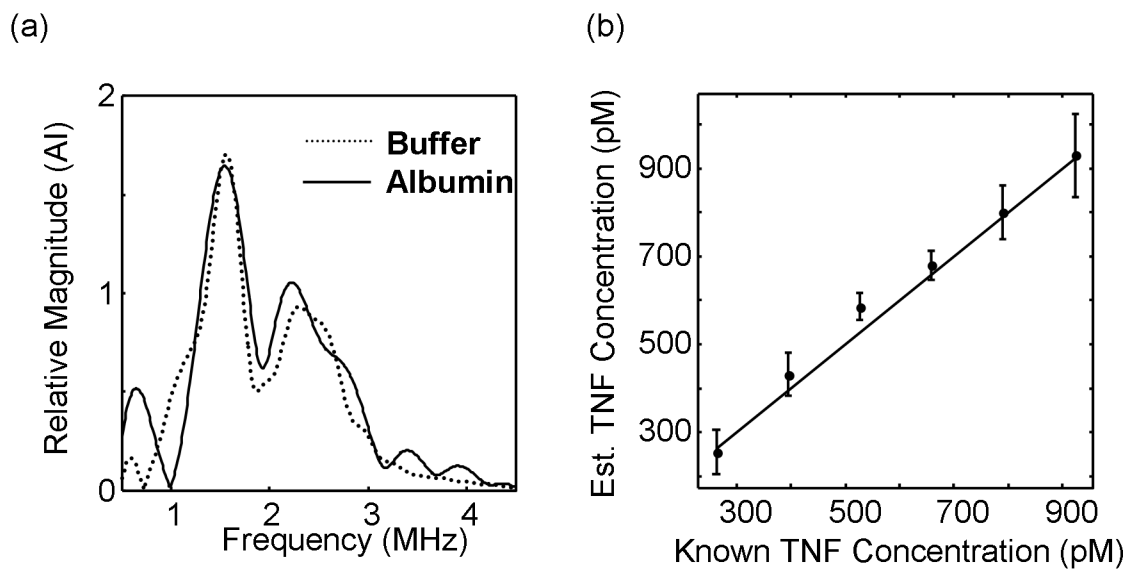


Figure 4.6: Dendrimer sensor performance with BSA. (a) Effect of 30 g/L BSA on the frequency profile of the dendrimer hydrogel (b) Correlation between estimated and known TNF concentrations using dendrimer hydrogel sensor.

the frequency spectra profile was altered by the BSA, it was found that the TNF concentrations could be estimated. However, the quantification was limited to a higher range than in the buffered solutions, which may be the result of the frequency broadening due to viscosity. Samples with TNF concentrations between 263–922 pM could be estimated with an r^2 of 0.96 and a standard error of 56 pM. The concentrations of TNF estimated by the model are plotted against the known values in Figure 4.6(b), and the figures of merit are summarized in Table 4.3. Though there is a slight positive bias in the estimation, concentrations were generally well estimated. This bias may be the result of the damping caused by the highly viscous solution. It is also possible that the resonance frequencies of the dendrimer sensor are partially masked by resonant characteristics of the BSA itself. PAMAM dendrimers are close in size to BSA, which has a diameter of 7 nm.^{4,27} As a result, the resonance characteristics of the BSA may also mask the sensor frequencies, decreasing the sensitivity. However, the direct measurement of the analyte remains appealing for point-of-care analyses, where limiting sample pretreatment is highly advantageous.

4.7 Conclusions

Ultrasonic frequency analysis is a promising technique for the determination of tumor necrosis factor- α using antibody-based, dendrimeric sensors. Using these sensors, quantification of pM concentrations of the TNF was shown using the dendrimer sensors in buffered solutions. Similar sensor performance was also shown in the presence of physiologically relevant concentrations of albumin. Concentrations of TNF which are

indicative of a health concern are small, often below 50 pM.^{4.21,4.22} However, higher concentrations are also sometimes seen and associated cytotoxicity and death.^{4.24,4.25} For examining the lower range, it is likely that the sensitivity of the method could be improved with refinement to the instrumental configuration, for example by controlling the temperature of the system. Likewise, by changing the antibody used in the sensor, the pM detection limit would be suitable for a variety of other important metabolites, including other cytokines.^{4.28}

Three different dendrimer sizes were examined. Each demonstrated a distinctly different ultrasound frequency profile, suggesting that the resonance frequency is highly dependent on the mass of the sensor. Distinct resonance characteristics offer a strong potential for the development of simultaneous, multi-analyte determinations using a combination of sensors with different sizes and using different antibodies, similar to recently developed electronic noses.^{4.29,4.30} The use of ultrasound allows for direct analysis of biological fluids without the need for extensive sample pretreatment that is common in current techniques. This is highly advantageous for the development of point-of-care techniques, which place an emphasis on the immediacy of the results for improving patient treatment. Further, the low instrumentation costs and simple methodology make this technique attractive for routine measurements.

4.8 Acknowledgements

This work was supported in part by the National Science and Engineering Research Council of Canada (NSERC) and the Fonds québécois de la recherche sur la nature et les technologies (FQRNT).

4.9 References

- 4.1. Y. Ishida, T. Kondo, K. Tsuneyama, P. Lu, T. Takayasu, and N. Mukaida, “The pathogenic roles of tumor necrosis factor receptor p55 in acetaminophen-induced liver injury in mice”, *J. Leukocyte Biol.* **75**, 59–67 (2004).
- 4.2. M.A. Cooper and V.T. Singleton, “A survey of the 2001 to 2005 quartz crystal microbalance biosensor literature: applications of acoustic physics to the analysis of biomolecular interactions”, *J. Mol. Recognit.* **20**, 154–184 (2007).
- 4.3. A.C. Mehta, “Sample pretreatment in the trace determination of drugs in biological fluids”, *Talanta* **33**, 67–73 (1986).
- 4.4. R. Panchagnula, A. Sood, N. Sharda, K. Kaur, and C.L. Kaul, “Determination of rifampicin and its main metabolite in plasma and urine in presence of pyrazinamide and isoniazid by HPLC method”, *J. Pharm. Biomed. Anal.* **18**, 1013–1020 (1999).
- 4.5. K.E. Hubbard, P. Schaiquevich, F. Bai, C.H. Fraga, L. Miller, J.C. Panetta, and C.F. Stewart, “Application of a highly specific and sensitive fluorescent HPLC

- method for topotecan lactone in whole blood HPLC method for topotecan lactone in whole blood”, *Biomed. Chromatogr.* **23**, 707–713 (2009).
- 4.6. C.P. Price, and A. St John, J.M. Hicks, “Point-of-Care Testing: What, Why, When, and Where?”, AACC Press, Washington, 2004.
 - 4.7. L.A. Tartagha, D.V. Goeddel, C. Reynolds, I.S. Figari, R.F. Weber, B.M. Fendly, and M.A. Palladino, “Stimulation of human T-cell proliferation by specific activation of the 75-kDa tumor necrosis factor receptor”, *J. Immunol.* **151**, 4637–4641, (1993).
 - 4.8. B. Levine, J. Kalman, L. Mayer, H.M. Fillit, and M. Packer, “Elevated circulating levels of tumor necrosis factor in severe chronic heart failure”, *N. Engl. J. Med.* **323**, 236–241 (1990).
 - 4.9. H. Fillit, W. Ding, L. Buee, J. Kalman, L. Altstiel, B. Lawlor, and G. Wolf-Klein, “Elevated circulating tumor necrosis factor levels in alzheimer's disease”, *Neurosci. Lett.* **129**, 318–320 (1991).
 - 4.10. M.K. Sharief and R. Hentges, “Association between tumor necrosis factor- α and disease progression in patients with multiple sclerosis”, *N. Engl. J. Med.* **325**, 467–472 (1991).
 - 4.11. P. Barath, M.C. Fishbein, J. Cao, J. Berenson, R.H. Helfant, and J.S. Forrester, “Detection and localization of tumor necrosis factor in human atheroma”, *Am. J. Cardiol.* **65**, 297–302 (1990).
 - 4.12. J.R. Dion and D.H. Burns, “Ultrasonic frequency analysis of antibody-linked hydrogel biosensors for rapid point of care testing”, *Talanta* **85**, 1364–1370 (2011).

- 4.13. D. Chatterjee and K. Sarkar, "A Newtonian rheological model for the interface of microbubble contrast agents" *Ultrasound Med. Biol.* **29**, 1749–1757 (2003).
- 4.14. J.T. Burke, "IR spectroscopy or Hooke's law at the molecular level - a joint freshman physics-chemistry experience", *J. Chem. Educ.* **74**, 1213 (1997).
- 4.15. N. de Jong, L. Hoff, T. Skotland, and N. Born, "Absorption and scatter of encapsulated gas filled microspheres: theoretical considerations and some measurements", *Ultrasonics* **30**, 95–103 (1992).
- 4.16. G. Sauerbrey, "Use of quartz oscillators for weighing thin layers and for Microweighing", *Z. Phys.* **155**, 206–222 (1959).
- 4.17. K.K. Kanazawa and J.G. Gordon II, "Frequency of a quartz microbalance in contact with liquid", *Anal. Chem.* **57**, 1770–1771 (1985).
- 4.18. G.C. Dunham, N.H. Benson, D. Petelenqt, and J. Janata, "Dual quartz crystal microbalance", *Anal. Chem.* **67**, 267–272 (1996).
- 4.19. J.D. Lathia, L. Leodore, and M.A. Wheatley, "Polymeric contrast agent with targeting potential", *J. Ultrasonics* **42**, 763–768 (2004).
- 4.20. N. R. Draper and H. Smith, *Applied Regression Analysis* (John Wiley and Sons, New York, 1981) 2nd ed., pp 294–352.
- 4.21. G.E. Grau, T.E. Taylor, M.E. Molyneux, J.J. Wirima, P. Vassalli, M. Hommel, and P.H. Lambert, "Tumor necrosis factor and disease severity in children with falciparum malaria", *N. Engl. J. Med.* **320**, 1586–1591 (1989).
- 4.22. A. Talvani, M.O.C. Rocha, L.S. Barcelos, Y.M. Gomes, A.L. Ribeiro, and M.M. Teixeira, "Elevated concentrations of CCL2 and tumor necrosis factor- α in chagasic cardiomyopathy", *Clin. Infect. Dis.* **38**, 943–950 (2004).

- 4.23. A.P. Lieberman, P.M. Pitha, H.S. Shin, and M.L. Shin, “Production of tumor necrosis factor and other cytokines by astrocytes stimulated with lipopolysaccharide or a neurotropic virus”, *Proc. Natl. Acad. Sci. USA* **86**, 6348–6352 (1989).
- 4.24. T.M. Folks, K.A. Clouse, J. Justement, A. Rabson, E. Duh, J.H. Kehrl, and A.S. Fauci, “Tumor necrosis factor a induces expression of human immunodeficiency virus in a chronically infected T-cell clone”, *Proc. Natl. Acad. Sci. USA* **86**, 2365–2368 (1989).
- 4.25. A. Waage, A. Halstensen, and T. Espevik, “Association between tumour necrosis factor in serum and fatal outcome in patients with meningococcal disease”, *Lancet* **329**, 355–357 (1987).
- 4.26. P.S. Kamath, R.H. Wiesner, M. Malinchoc, W. Kremers, T.M. Therneau, C.L. Kosberg, G. D'Amico, E.R. Dickson, and W.R. Kim, “A model to predict survival in patients with end-stage liver disease”, *Hepatology* **33**, 464–470 (2001).
- 4.27. G. Kong, R.D. Braun, and M.W. Dewhirst, “Hyperthermia enables tumor-specific nanoparticle delivery: effect of particle size”, *Cancer Res.* **60**, 4440–4445 (2000).
- 4.28. A.S. Cho, S.M. Jeon, M.J. Kim, J. Yeo, K.I. Seo, M.S. Choi, and M.K. Lee, “Chlorogenic acid exhibits anti-obesity property and improves lipid metabolism in high-fat diet-induced-obese mice”, *Food Chem. Toxicol.* **48**, 937–943 (2010).
- 4.29. D. James, S.M. Scott, Z. Ali, and W.T. O'Hare, “Chemical sensors for electronic nose systems” *Microchim. Acta.* **149**, 1–17 (2005).
- 4.30. C.D. Natale, R. Paolesse, A. Macagnano, A. Mantini, A. D'Amico, A. Legind, L. Lvova, A. Rudnitskaya, and Y. Vlasov, “Electronic nose and electronic tongue

integration for improved classification of clinical and food samples”, *Sens. Actuators, B.* **64**, 15–21 (2000).

- 4.31. C.L. Jackson, H.D. Chanzy, F.P. Booy, B.J. Drake, D.A. Tomalia, B.J. Bauer, and E.J. Amis, “Visualization of dendrimer molecules by transmission electron microscopy (TEM): staining methods and cryo-TEM of vitrified solutions”, *Macromolecules* **31**, 6259–6265 (1998).

Chapter 5

Determination of Volume Fractions in Multi-Component Mixtures Using Ultrasound Frequency Analysis

5.1 Foreward

Previous chapters have focused on the nonlinear resonance behavior of hydrogel probes. The resonance frequency characteristics of these hydrogel sensors are useful to increase the magnitude of the changes in the ultrasound propagating through the sample. In trying to understand the ultrasound propagation in hydrogels, it was shown that the medium played a significant role in the specific frequency profile distribution. This behavior was seen in Chapters 3 and 4, where biological fluids such as blood and saliva resulted in different ultrasound frequency distributions. In the following chapter, studies are presented that demonstrate ultrasound frequency analysis without the use of hydrogel sensors. Differences in the nonlinear distortion of the ultrasound are used for the quantification of the sample composition.

To quantitatively measure the effects of changing the sample composition, mixtures of water, methanol, and ethanol were prepared. These liquids are all miscible, allowing homogenous solutions to be formed with each component ranging between 0 and 100% of the total volume. Further, these liquids all consist of small molecules that

can form extensive hydrogen bonding networks. The measurement of these mixtures is presented in this chapter.

The goal of this chapter is to examine the effect of changing mixture composition on the frequency distribution of an ultrasound wave. The differences between the three molecules studied in this chapter should lead to different molecular structures in the mixtures. As a result of these different molecular properties, the frequency distribution of ultrasound propagating through the mixtures will vary with composition. Two-component mixtures are first examined to demonstrate that the nonlinear distortion could provide unique quantitative information and advantages over traditional velocity measurements. Mixtures where all three components were varied are also measured, and demonstrate that the ultrasound frequency analysis method allows rapid, non-invasive determination of sample composition.

5.2 Manuscript

Determination of volume fractions in multi-component mixtures using ultrasound frequency Analysis

Authors:

Jonathan R. Dion and David H. Burns

5.3 Abstract

Controlling the composition of mixtures is critical for quality control in a wide variety of applications. There is a need for rapid, on-site measurements to optimize processes in real time. Ultrasound easily penetrates opaque samples and containers, yet currently provides minimal chemical information. We have developed a general approach to determine the volume fraction of a liquid in mixtures with multiple components. Ultrasound waves propagating through a medium undergo distortion processes that are characteristic of the chemical bonding composition. The distortion of the waveform can be measured in the ultrasound frequency profile. An ultrasound pulse-through configuration with matching 5 MHz transducers was used to analyze mixtures of water, methanol, and ethanol. Multilinear regression analysis was used to determine the volume fraction of all components in a series of mixtures. Using this technique, volume fractions were determined simultaneously with correlation coefficients (r^2) greater than 0.98 in two-component mixtures. Determination of volume fractions in three-component

mixtures ranging from 65-100% water also showed correlation coefficients of 0.91 for methanol and 0.94 for ethanol. This technique is attractive for process monitoring due to the short measurement time and the simple methodology that excludes sample pretreatment.

5.4 Introduction

Process control is a crucial step in the manufacture of a wide variety of products including foods, industrial products, and biomedical compounds. A precise balance between any number of constituents is necessary to ensure product quality and consistency.^{5.1,5.2} Due to the sensitivity of many reactions, the immediacy of on-line or at-line measurements is appealing to allow for fast optimization and maintenance.^{5.3} Likewise, on-line monitoring can minimize or completely avoid sample contamination while allowing high sample throughput. The design of technologies for routine and non-invasive analysis is highly desirable.

Ultrasound monitoring for on-line applications is becoming increasingly popular for quality control in food and drink industries.^{5.2,5.4,5.5} Ultrasound technology is an appealing analysis tool because non-destructive measurements can be made rapidly and at low cost. This is an advantage over established analysis methods such as electrochemical, thermal, or chromatographic solutions, which require more extensive sample handling and processing steps. Further, because it is a mechanical wave, ultrasound measurements can be made in highly concentrated or opaque samples that are difficult to measure using optical methods.

Current ultrasonic analyses measure the velocity of the ultrasound wave as it traverses the sample. The propagation velocity is dependent on the viscoelastic properties of the medium, including the specific gravity and the compressibility.^{5,6} Although a velocity measurement can provide quantitative information about one constituent^{5,2}, a single parameter provides insufficient information to make quantitative estimates in multi-component systems with several changing constituents. Several measurements can be made at different temperatures to provide additional parameters for quantitative analysis.^{5,6} However, the need for measurements at multiple temperatures increases both the sampling time and the complexity of the instrument required. This is often not feasible for on-line applications, where rapid turnaround is critical.

Multiple frequency analysis of ultrasound waves has been used to address the limitations of single-parameter measurement. It has been shown that a single ultrasound pulse can generate multiple frequencies from dispersed resonators in a solution.^{5,7,5,8} The frequency response of these resonators is routinely used for contrast enhancement in medical imaging.^{5,9} Recently, resonant gels with specifically-designed molecular recognition sites have been shown to undergo changes in frequency response when binding to target analytes.^{5,10,5,11} This has extended the frequency analysis of contrast agents to allow the determination of analyte concentrations. However, the frequency content of an ultrasound wave is influenced not only by resonating probes, but is also affected by the viscoelastic properties of a medium. Acoustic waves consist of alternating compression and rarefaction phases. However, because of imbalances in the propagation speed of the two phases, the waveform is nonlinearly distorted.^{5,12} Due to the small motion induced by the propagating wave, positive particle velocity (caused by

compression) is slightly faster than the negative velocity (resulting from rarefaction). As a consequence, the positive pressure half of the waveform steepens, while the negative pressure half flattens, transforming a sinusoidal waveform into a sawtooth profile. The change to the waveform is seen as an increase in the magnitude of harmonic frequencies in the frequency domain.^{5.12,5.13} Although the particle velocity is typically smaller than the propagation speed, the nonlinear distortion effect is cumulative.^{5.12,5.14}

The magnitude of the nonlinear distortion in a medium can be described according to the nonlinearity ratio B/A . This value is derived from the state equation of acoustic propagation through a liquid, which relates pressure and density in the medium. This equation can be expressed by a Taylor series expansion as

$$p = p_0 + \left(\frac{\partial p}{\partial \rho} \right)_{\rho=0,s} (\rho - \rho_0) + \left(\frac{\partial^2 p}{\partial \rho^2} \right)_{\rho=0,s} \frac{(\rho - \rho_0)^2}{2!} + \dots \quad (5.1)$$

where p and p_0 are the instantaneous and equilibrium pressures, ρ and ρ_0 are the instantaneous and equilibrium mass densities of the medium, and s is the entropy of the system.^{5.15} With the derivatives taken at $\rho = 0$ and s held constant, this equation can be rewritten as

$$p = p_0 + A \left(\frac{\rho - \rho_0}{\rho_0} \right) + \frac{B}{2!} \left(\frac{\rho - \rho_0}{\rho_0} \right)^2 + \dots \quad (5.2)$$

in which the linear coefficient $A = \rho_0 (\partial p / \partial \rho)_{\rho=0,s} = \rho_0 c_0^2$, where c_0 is the velocity of the ultrasonic wave, and the second order $B = \rho_0^2 (\partial^2 p / \partial \rho^2)_{\rho=0,s}$.^{5.15,5.16} Though nonlinear propagation is also reflected in higher order terms in the Taylor expansion, these are typically neglected.^{5.16} When these higher order terms are ignored, the dimensionless second order elastic ratio

$$\frac{B}{A} = \frac{\rho}{c_0^2} \left(\frac{\partial^2 p}{\partial \rho^2} \right)_{\rho=0,s} \quad (5.3)$$

can be written, which describes the amount of nonlinear waveform distortion caused by the medium through which the acoustic wave propagates.^{5.15} The nonlinear parameter is characteristic of a given medium, relating the distortion processes of a propagating ultrasound wave to the molecular structure of the media. For example, B/A in water is 5.0, while in methanol it is 9.42, and 10.52 in ethanol.^{5.17} Mixtures of two different liquids have B/A values that are not linear combinations of the two pure liquids.^{5.18} This is the result of the solvent-solute interaction of the different components on the macromolecular clusters in the liquid.^{5.19,5.20}

Nonlinear changes in the viscoelastic properties have been associated with the formation of intra-molecular complexes.^{5.21} The ratio of the two liquids determines which fraction is solute, and so the bonds formed between molecules are highly dependent and complex. However, the contribution of molecular vibrations to the magnitude of the changes in the propagating ultrasound is related to the volume fraction of a molecular species.^{5.22} An analysis of ultrasonic frequencies propagating through a medium should therefore allow quantification of the components using a multivariate approach.

In this work, we demonstrate a simple methodology to determine fractional volumes in liquid mixtures based on the frequency analysis of ultrasound. Unlike previous work that has measured the resonance frequencies of dispersive contrast agents, the presented approach investigates the intrinsic frequency distortions caused by the matrix. Molecular interactions in mixtures create distinctive non-linear distortions to a propagating ultrasound wave. A broad range of ultrasonic frequencies were measured simultaneously to examine the relationship between the non-linear distortion caused by

the matrix and the volume fraction of liquids in the mixture. Simultaneous quantification of several components is shown to be possible over a wide range of volume fractions in mixtures with two and three components. Though the specific frequency changes may not be linear, multivariate analysis of the results will allow analytical quantification.

5.5 Materials and Methods

5.5.1 Reagents

Deionized water was purified using a Millipore (Billerica, US) Milli-Q OM-154 water purification system. Anhydrous ethanol and methanol were obtained from Sigma-Aldrich (Oakville, CA).

5.5.2 Ultrasound Apparatus

Ultrasound frequency profiles were measured using a pulse-through transmission configuration, as depicted in Figure 5.1. Two ultrasound transducers were attached to parallel sides of a 1.8 mL aluminum sample reservoir with a 2.2 cm path length. Ultrasound transmission through an interface is highly sensitive. A mismatch between the acoustic impedance on either side of the interface can result in high reflection. Additionally, ultrasound propagation through air is highly limited. To minimize interfacial losses, the transducers were coupled to 60 μm cellulose acetate windows with a thin layer of petroleum jelly. The acetate provided a better intermediate medium

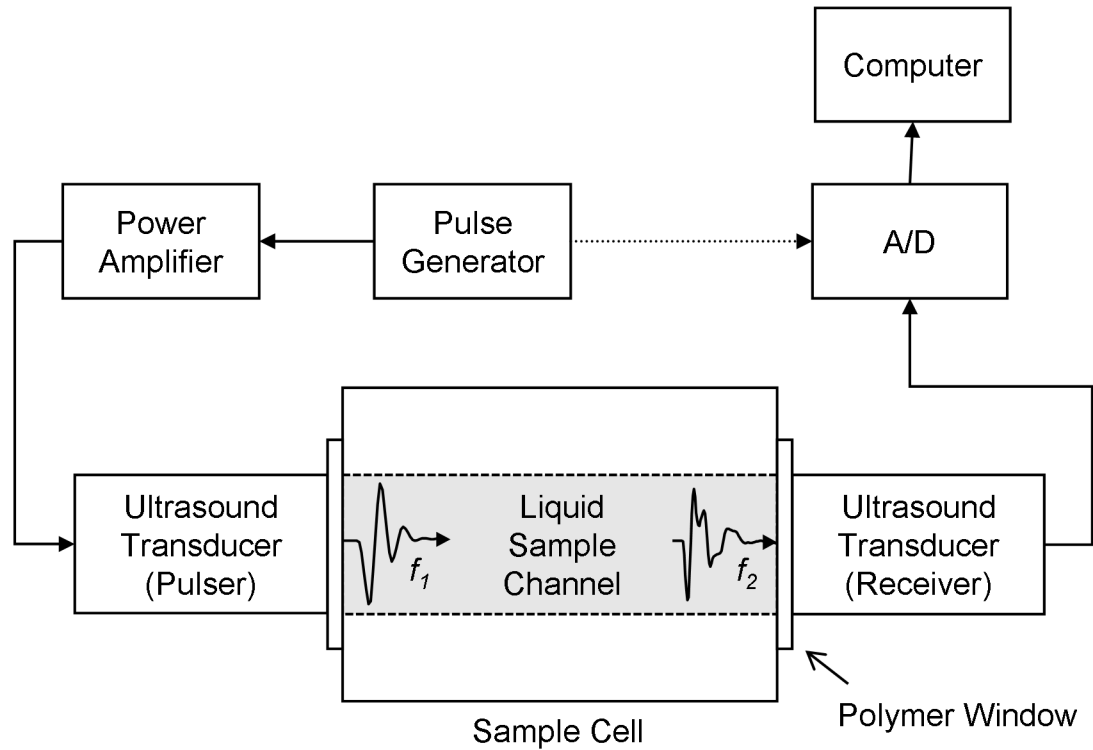


Figure 5.1: Schematic diagram of the ultrasound frequency analyzer. Aluminum sample cell holds the liquid sample in a channel between two ultrasound transducers. One transducer generates a pulse waveform (f_1), which propagates through the media and undergoes specific absorption and nonlinear processes. The second ultrasound transducer records the modified transit waveform (f_2).

between the liquid samples and the transducer than aluminum. The petroleum jelly ensured that no air was trapped between the transducer surface and sample reservoir. The two layers between the sample and transducer did not significantly attenuate the ultrasound wave.

To ensure that no overlapping signals were present due to reverberation in the cell, an ultrasound pulse repetition rate of 1 KHz was used. This frequency allowed sufficient time for the reverberations inside the cell to be attenuated to baseline noise levels before subsequent pulses were generated. Signals received by the second transducer were acquired using a Tietie (Sneek, NL) Handyscope HS3 computer controlled oscilloscope sampling at 50 MHz with a 12 bit dynamic range. The signal to noise ratio was increased by averaging 1500 waveforms for each sample. Total data acquisition time for each sample was 1 minute.

Both the emitting and receiving transducers used were 5.0 MHz (100% bandwidth) General Purpose ultrasonic transducers made by Technisonic (Fairfield, US). The emitting transducer generated an ultrasound pulse and was driven by a 500PR Transmitter/Receiver from Olympus NDT (Waltham, US). This generated a <20 ns, 250 V negative impulse with a 0.002% duty cycle. Though no temperature changes were measured at this power, the reservoir was kept at 21 ± 0.25 °C with a thermoelectric cooler from AMS Technologies. This ensured that any variation in the acoustic properties of the samples due to temperature fluctuations was minimal.

5.5.3 Methods of Analysis.

Analytical processing of ultrasound data consists of three primary steps: phase matching, frequency transformation, and then determination of mixture composition using multilinear regression. The velocity of ultrasonic waves is highly dependent on the propagation medium. Small changes in the fractional composition or in the temperature of the sample change the velocity of the ultrasound wave. In order to compensate for phase changes, each ultrasonic measurement was aligned to the maximum positive signal intensity in the waveform. Data were sampled at 50 MHz so that phase matching of the 5 MHz ultrasound signals could be accomplished with high temporal resolution.

The nonlinear propagation of the ultrasonic wave is dependent on the fractional composition of the samples. The B/A parameter changes nonlinearly as the volume fraction ratios are altered. The specific changes that result from the convolution of the ultrasonic wave due to nonlinear processes can be described as the generation of new components in the frequency domain. By the convolution theorem, a convolution in the time domain can be expressed as a multiplication in the frequency domain, which can be modeled through a series of linear equations. To examine these changes, a fast Fourier transform algorithm was used to determine the modulus frequency spectrum of the ultrasound data. The ultrasound waveform that propagates through the sample cell is partially reflected at interfaces between the window material and the liquid. With a typical velocity of 1480 m/s in water, the pulsed wave train generated by the transducers is relatively short (1.1 μ s) with respect to the propagation time through the cell (15 μ s). As such, the ultrasound reflections are well separated temporally. To reduce high

frequency ringing, only the first ultrasound wave transient was used, and was then zero padded to improve frequency domain interpolation.^{5,23} Frequencies in the spectra between 0.1 and 10 MHz were retained for multilinear analysis. The data were then smoothed using a boxcar average window of 0.08 MHz to reduce noise in the spectra. The frequency spectrum of each waveform was then normalized to the total area to account for potential drifting of the instrumental response.

Ultrasonic frequency spectra were collected in random order to ensure no correlation with time, instrument changes, or minor temperature fluctuations. All samples were prepared independently in triplicate. These measurements were then divided into independent calibration and test sets. The calibration set was made up of two replicates of each sample. The third replicate of each sample was assigned to the test set. The calibration data were used to develop a multilinear model for the fractional composition of each sample. Stagewise multilinear regression (MLR) was used to determine the linear combination of a subset of frequencies to best describe the data in the form

$$Y = b_0 + b_1X_1 + b_2X_2 + \dots + b_nX_n \quad (5.4)$$

where Y is the dependent variable (here the volume fraction of one component), $\{X\}$ are independent variables (the magnitude at a given ultrasound frequency), and $\{b\}$ are the weighting coefficients determined. The algorithm computed the regression of the known volume fraction with the intensity at each individual frequency in the spectrum and residual values were then calculated. This process was then repeated iteratively with the subset of the frequency spectrum not yet incorporated into the regression model. The most parsimonious model was selected using an F-test ($\alpha = 0.05$) between calibrations. This regression model was then used to estimate volume fractions of independent spectra

in the test data set. Effectiveness of each model is tested by calculating the correlation coefficient (r^2) and standard error (SE). Frequency selection in the MLR model is described in Draper and Smith^{5.24} and the routine is presented in Arakaki and Burns.^{5.25} The MLR routine was written in Matlab (The MathWorks Inc., 2008a, Natick, US).

5.6 Results and Discussion

5.6.1 Measurement of Binary Mixtures

Ultrasonic analysis in liquids is not uncommon for sample characterization, yet examining the frequencies carried by ultrasound waves propagating through a sample is not widespread. The magnitude of harmonic frequencies in the ultrasound wave increase due to nonlinear distortion of the wave that is medium-dependent.^{5.13} Likewise, ultrasound waves propagating through a medium are subject to unique frequency-specific absorption and dispersion. The product of these attenuation processes is a change in magnitude of the frequency spectrum. The amount of nonlinear distortion is dependent on the specific medium in which the ultrasonic wave propagates. To investigate the extent of the nonlinear distortion in a series of liquids, ultrasonic frequency profiles of pure water, methanol, and ethanol were measured. As shown in Figure 5.2, characteristic differences are clear between the spectra of water (dashed line) and the two alcohols (solid and dotted lines). Both alcohols show higher intensities than water over a range of frequencies between 1 and 3 MHz. Frequencies above this range (3-9 MHz) show an inverse relationship, as water has a higher magnitude than both alcohols. The relative

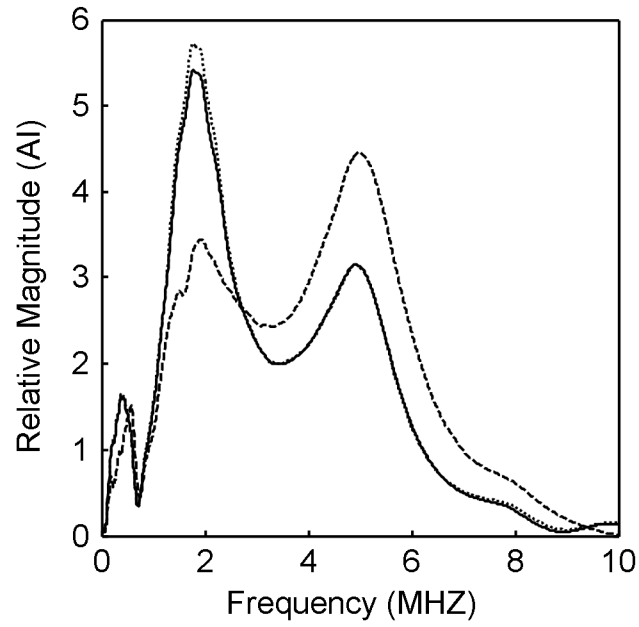


Figure 5.2: Ultrasonic frequency spectra of individual components. Water (dashed line), methanol (solid line), and ethanol (dotted line).

differences between the two alcohols are smaller compared to water. This is expected because the viscoelastic properties of the two alcohols are similar. As a result, the changes to the ultrasound waveform caused by the linear and the nonlinear propagation characteristics in the two alcohols are also comparable. Due to the differences in the frequency distribution of these liquids, multilinear analysis should allow their discrimination.

Methods using the velocity of ultrasound propagation for analytical measurements have been extensively studied. However, estimating the volume fraction in mixtures remains challenging. Figure 5.3 illustrates the velocity of ultrasound through binary mixtures of water and ethanol (+) measured in the aluminum reservoir. Also illustrated is the velocity in binary mixtures of water and methanol (•). This diagram shows that the velocity reaches a maximum when the volume fraction of water approaches 70%. Where the velocity change is non-monotonic, determining the volume fraction of water is not possible using a single measurement. While the thermoelectric controller allows for simple temperature adjustment, measuring the velocity at several temperatures would require several minutes of equilibration. As a result of these limitations, velocity measurements are often not practical and limiting in many on-line applications.

To investigate if the distortions caused by nonlinear propagation of ultrasound can be used to overcome these limitations, an experiment was designed where the fractional composition in mixtures of two components was varied. Two-component mixtures of water and methanol (W/M), water and ethanol (W/E), and methanol and ethanol (M/E) were prepared. The volume fraction of each component was varied between 0% and 100% v/v of the total mixture volume. Ultrasound pulses propagating through binary

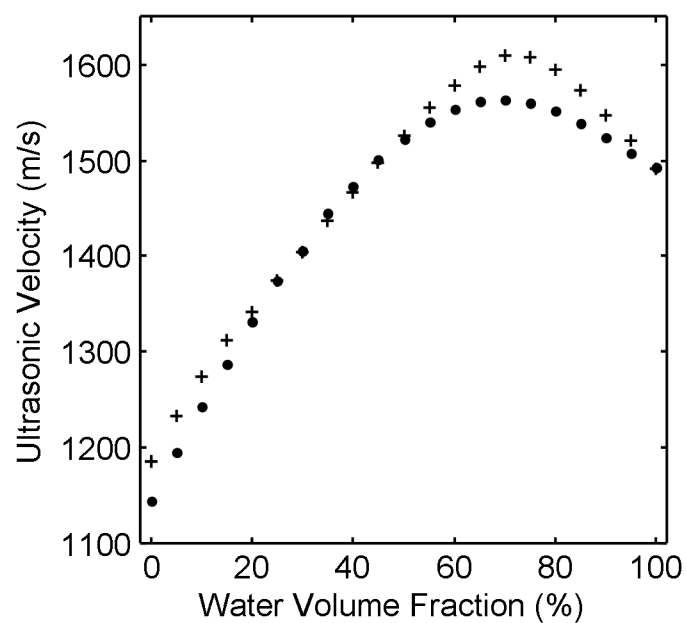


Figure 5.3: Relationship between ultrasound propagation velocity and the volume fraction of water. Mixtures with methanol (•) and mixtures with ethanol (+).

mixtures were recorded and the intensities of the frequency spectrum components were analyzed. Figures 5.4(a and b) show the frequency changes that are seen with changing volume fraction for the W/M and W/E solutions. To enhance the frequency differences measured between samples with different volume fractions, the mean spectral profile was subtracted from spectra at 0, 20, 40, 60, 80, and 100% water volume fractions. For both alcohol mixtures, as the water fraction decreases, frequencies between 1–3 MHz (low range) decrease in magnitude. However, when the water fraction reaches 70%, the trend is reversed and the magnitude in this frequency region begins to increase. This behavior is similar to what is seen in velocity measurements, which is a result of the mixtures having similar viscoelastic properties. Frequencies between 3–9 MHz (high range) increase with increasing water fraction. Unlike the lower frequency range, the magnitude of the ultrasonic frequencies here does not peak at 70% water, but rather increases asymptotically and a frequency shift is seen. This suggests that the velocity of the ultrasound through the sample is more strongly reflected in the lower frequency range. This may partly be explained by the thin acetate boundary between the sample reservoir and ultrasound transducer. A small fraction of the ultrasound magnitude is reflected at the interface, causing a second ultrasonic wave to reverberate through the acetate window before propagating through the cell. As a result, a second wave follows the primary ultrasound wave slightly out of phase. The convolution of the two waveforms results in the appearance of subharmonic frequencies.

The phase offset of the second wave is dependent upon the velocity of the ultrasound through the liquid. As a result, the magnitude of the subharmonic frequencies will also vary based on the velocity of the ultrasound propagation. This was verified by

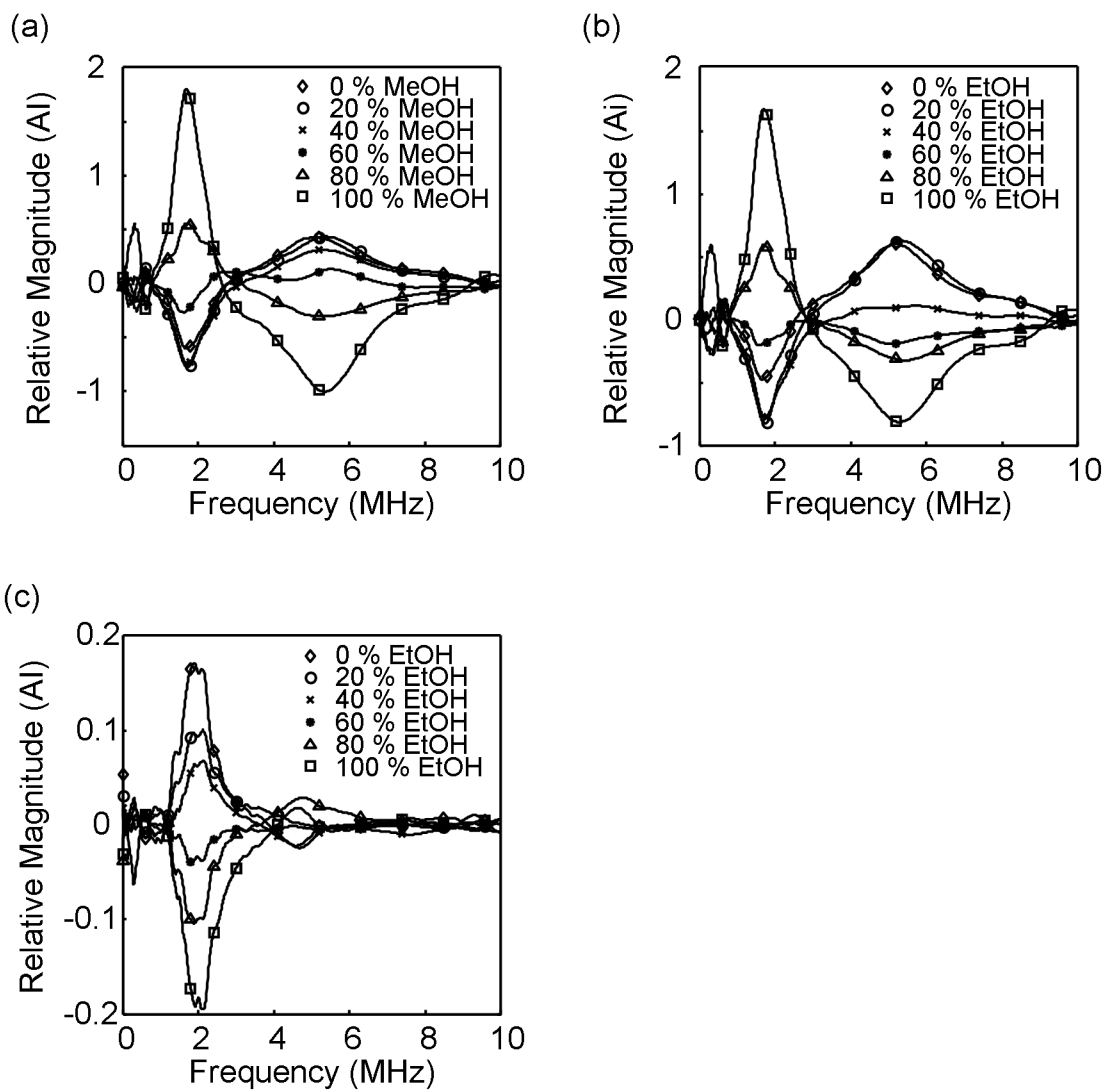


Figure 5.4: Frequency profiles of binary liquid mixtures where the mean spectral profile has been subtracted. (a) 100% methanol to 100% water, (b) 100% ethanol to 100% water, (c) 100% methanol to 100% ethanol.

removing the acetate windows on the sample reservoir. With both the emitting and receiving transducers in direct contact with the solution, the frequency peak between 1 to 3 MHz disappeared. Changes in the magnitude of frequencies above 3 MHz were still seen when different liquids were measured, showing that the linear and nonlinear propagation effects are prominent in this high frequency region. Frequencies within this range are therefore important for quantification. Though the changes are primarily seen in the higher frequency range, retaining the polymer windows on the reservoir is advantageous. The replaceable window material prevents contamination of the ultrasound transducer face, which would change the resonance frequency of the pulses. The convolution of the two waveforms due to the reflection at this window only results in a multiplicative effect on certain frequencies in the Fourier spectrum, which can be accounted for in the multilinear model.

An analysis of the frequency changes in M/E binary mixtures was also done. As Figure 5.4(c) shows, when the mean profile was subtracted from spectra with increasing ethanol concentration, the dominant effect is a frequency exchange in the 1–3 MHz range. As with W/M and W/E binary mixtures, this frequency region is highly correlated with the ultrasound velocity. As the velocity increases (with increasing ethanol content), the magnitude of the ultrasound frequencies in this range decreases. The frequency changes measured as methanol and ethanol volume fractions change are an order of magnitude less intense than those for alcohol and water exchanges. This is attributed to the greater similarity between the viscoelastic properties of the two alcohols compared to water. Although the frequency changes are of lower magnitude, it is possible to determine the volume fraction of the M/E mixtures using the multilinear approach.

Multilinear regression was applied to the frequency data in order to quantify the fractional composition of each mixture. A regression model was generated using a calibration set made up of two thirds of the total data. This model was then used to estimate the composition of mixtures in an independent test set made up of the remaining frequency spectra. The volume fraction of water in W/M and W/E mixtures was estimated. For M/E mixtures, the methanol fraction was estimated. Since there is closure in the system, the volume fraction of the second component is 100 minus the first component, therefore this number is not reported. Multilinear analysis revealed a close correlation between the magnitude of a subset of ultrasonic frequencies and the fractional composition of each mixture. The estimated volume fractions are presented in Figure 5.5 and illustrate that the components in these binary mixtures can be determined over the full range (0 to 100%). The figures of merit for the estimation of volume fraction are shown in Table 5.1. The values for the correlation coefficient for all mixtures is high (≥ 0.98), and the standard errors are relatively low ($\leq 4.2\%$). Results indicate that the nonlinear frequency exchange in the W/M and W/E mixtures does not reduce sensitivity as compared to the M/E samples.

Frequencies used in the multilinear models are primarily associated with the high frequency range (>3 MHz), indicating that the nonlinear propagation effects are primary predictors of the volume fraction. Frequencies from the low range are also chosen for the W/M and M/E mixtures. This suggests that the velocity of the ultrasound through the sample can potentially be a useful variable. For the M/E mixtures, two channels from the lower frequency region were used. This could potentially be attributed to the small difference in the nonlinear parameters describing these two liquids. Because of the

Table 5.1: Figures of merit for the determination of fractional components in binary mixtures.

Mixture	r^2	SEC (%)	SEE (%)	Frequencies (MHz) and {Relative regression weightings}
W/M	0.99	2.4	3.0	6.92{0.3}, 1.90{0.4}, 4.64{1}, 9.30{0.6}
W/E	0.98	3.8	4.2	5.86{-0.6}, 9.44{-0.3}, 3.38{1}, 4.23{-0.6}
M/E	0.98	3.4	3.9	3.23{-0.8}, 9.86{0.8}, 0.77{1}, 0.83{-0.7}

SEC: standard error of calibration; SEE: standard error of estimate

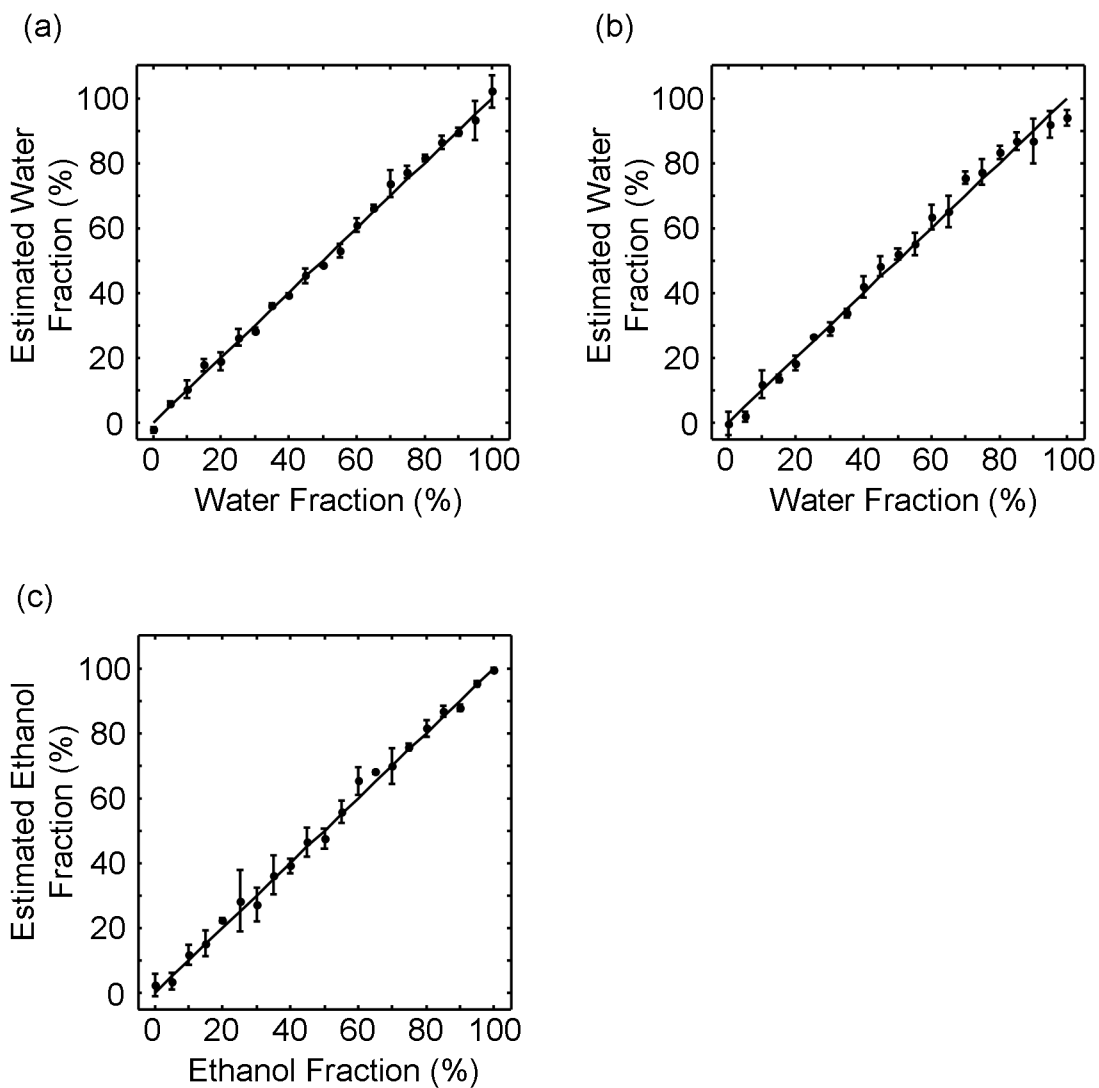


Figure 5.5: Determination of the volume fraction of components in binary liquid mixtures. Known fraction values correlated with the volume fraction estimated by the multilinear model for (a) water in water/methanol mixtures, (b) water in water/ethanol mixtures, and (c) ethanol in ethanol/methanol mixtures.

similarity of the viscoelastic properties, the velocity information is more highly weighted by the model. Similar results are obtained when the multilinear regression algorithm is applied to data only from the 3-9 MHz region. This indicates that while the velocity of the ultrasound can be a useful parameter, the distortions in the ultrasound waveform caused by nonlinear propagation are sufficient for estimation of binary volume fractions.

5.6.2 Measurement of 3-Component Mixtures

Even in ideal conditions and system closure, a single velocity measurement is insufficient to quantify more than two fractions. Vatandas *et al.* have demonstrated the performance of multiple temperature analyses to add another parameter to 3-component mixtures.^{5,6} However, in some cases the velocities of certain volume fractions can overlap, even at different temperatures, and cannot be resolved. Measurements at multiple frequencies could also provide necessary parameters for estimating volume fractions in complex mixtures. To determine if an ultrasound pulse carrying multiple frequencies simultaneously can provide sufficient information for volume fraction determination in multi-component systems, three-component mixtures of water, methanol, and ethanol were prepared. The three liquids were varied between 0% and 100% of the total volume in a series of combinations.

Ultrasonic frequency spectra of the 3-component mixtures show similar characteristics as the 2-component data. With an increase of methanol or ethanol comes a large increase in magnitude of the frequencies 1-3 MHz range. Likewise, the frequencies in the 3-9 MHz range increase asymptotically as the water fraction increases. This is

consistent with the results seen in 2-component mixtures, and suggests that both the velocity and the nonlinear information are reflected in these spectra.

Based on the observed changes in the frequency profile, a multilinear calibration model was developed to estimate the volume fraction of each component. This model was tested on an independent evaluation set to estimate the volume fraction of each liquid. The analysis demonstrated a close correlation between the magnitude of 6 ultrasonic frequencies and the volume fraction of water ($r^2 = 0.98$, SE = 3.8%). Estimates of water percentage in the samples relative to the known values are shown in Figure 5.6(a). This figure illustrates that results are linear over the full range (0-100%) of water fractions, which would not be possible with only a single velocity measurement. Multilinear regression analysis was also used to generate independent models for the methanol and ethanol volume fractions. Results show a lower sensitivity for the two alcohols than for water, as illustrated in Figure 6(b,c). Estimates of methanol volume fractions had higher errors ($r^2 = 0.71$, SE = 16.2%) than those for ethanol volume ($r^2 = 0.85$, SE = 11.5%). The lower correlation between known values and estimates of methanol and ethanol volume fractions suggests that the similar viscoelastic properties of these liquids is limiting.

Nonlinear changes in the velocity with changing concentration have been associated with complex formation between the solvent and solute molecules.^{5,21} Hydrogen bonding is a major contributor to the nonlinear propagation effects and the nonlinear parameter describing the liquid.^{5,26} Methanol and ethanol both form strong hydrogen bonds with water. Due to the amphoteric nature of the three liquids in this study, hydrogen bonds between several different species will be present in the

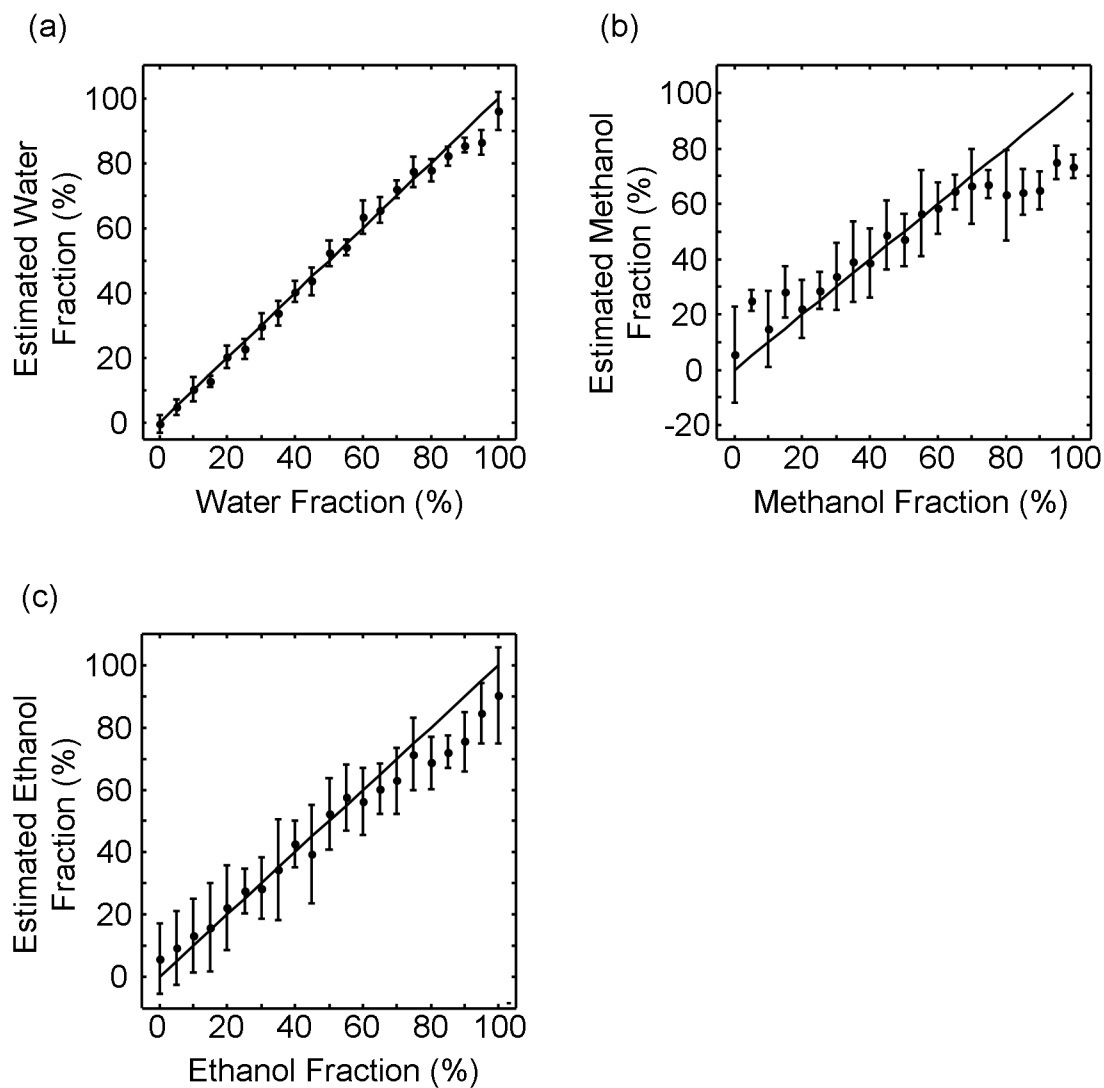


Figure 5.6: Determination of the volume fraction of components in three-component mixtures. Known fraction values correlated with the volume fraction estimated by the multilinear model for (a) water, (b) methanol, and (c) ethanol.

multi-component mixtures. Hydrogen bond lengths (D) vary widely between homodimers and heterodimers. For example, Fileti *et al.* have shown that $D_{\text{H}_2\text{O}-\text{H}_2\text{O}}$ is 2.918Å and $D_{\text{MeOH}-\text{MeOH}}$ is 2.846Å, whereas the heterodimer $D_{\text{H}_2\text{O}-\text{MeOH}}$ has a value of 2.912Å by modelling these systems.^{5.27} Further, if methanol is the electron donor rather than the acceptor in the previous example, $D_{\text{MeOH}-\text{H}_2\text{O}} = 2.844\text{Å}$. The low level bonding structure in a liquid is a determinant of the capability to undergo compression and rarefaction. As a result, the energies in the specific bonds (including the mixture heterodimers) found in the liquid are contributors to the higher order terms of the Taylor expansion for propagation. As the number of components increases, the number of different heterodimers also increases. Homodimers are also present in the mixtures due to incomplete mixing that occurs in water/alcohol systems.^{5.28} As shown in Table 5.2, the homo- and hetero-dimers for the three liquids vary widely.^{5.27} This, coupled with extensive overlap of viscoelastic properties for the alcohols, is likely responsible for the reduced sensitivity and the use of two extra frequencies into the multilinear mixture model.

The greater sensitivity for ethanol than methanol suggests that the mixtures formed between ethanol and water induce larger changes in the frequency spectrum. Though hydrogen bonding dominates the intermolecular bonding in the water lattice, non-polar forces are present in ethanol due to the short carbon chain. Similar forces are present in methanol; however, the role of non-polar forces is expected to be smaller due to the single carbon structure. The contribution of the non-polar forces to viscoelastic properties of the mixtures may be the cause of the lower sensitivity for methanol compared to ethanol.

Table 5.2: Hydrogen bond lengths (Å) in molecular dimers.^{5,27}

	Water	Methanol	Ethanol
Water	2.918	2.844	2.843
Methanol	2.912	2.846	2.888
Ethanol	2.914	2.853	2.850

The apex in the velocity data due to the viscoelastic parameters is also a determinant of nonlinear frequency propagation. Since the velocity measurements show a clear nonlinearity above certain alcohol levels, the range of volume fractions analyzed was narrowed. Frequency profiles from samples with methanol contents of 0–35% were analyzed using the MLR algorithm and tested on an independent evaluation set. Likewise, a range of 0–35% ethanol was also examined. Multilinear analysis over these focused volume ranges demonstrated a significantly better estimation for methanol and ethanol volume fractions. The estimated volume fractions for both methanol and ethanol are shown in Figure 5.7, and illustrate a greater linearity over the focused range. The standard error for the estimation for methanol was decreased almost 4 fold ($r^2 = 0.91$, SE = 3.7%). Ethanol estimates also showed a decrease in error, which was lowered from almost 3 fold ($r^2 = 0.94$, SE = 2.9%). Both liquids required one less calibration frequency (5 total), suggesting that fewer components in the mixtures need to be accounted for over the narrow range. As shown in Table 5.3, frequencies used to estimate methanol and ethanol over this range showed considerable similarity. This is expected due to the close nonlinear parameters for the two liquids. Further, frequencies are used from both the range of frequencies showing nonlinear distortions (>3 MHz) and from the range more strongly correlated with propagation velocity (<3 MHz). This illustrates the importance of the multivariate approach for quantification over a larger range. Many analytical measurements are done over a limited range of concentrations. Reducing the range of the calibration model is demonstrated to improve the sensitivity for these applications. Over large ranges, broad calibrations could give general estimations of sample concentrations, after which it may be possible to a calibration over a limited range to refine the estimate.

Table 5.3: Figures of merit for the determination of fractional volumes in 3-component mixtures.

Component	r^2	SEC (%)	SEE (%)	Frequencies (MHz) and {relative regression weightings}
Methanol	0.91	3.5	3.7	0.90{0.7}, 2.40{-0.4}, 3.52{1}, 5.49{-0.2}, 9.96{0.8}
Ethanol	0.94	2.6	2.9	2.74{-0.7}, 0.83{1}, 3.06{0.5}, 5.80{-0.2}, 2.50{-0.9}

SEC: standard error of calibration; SEE: standard error of estimate

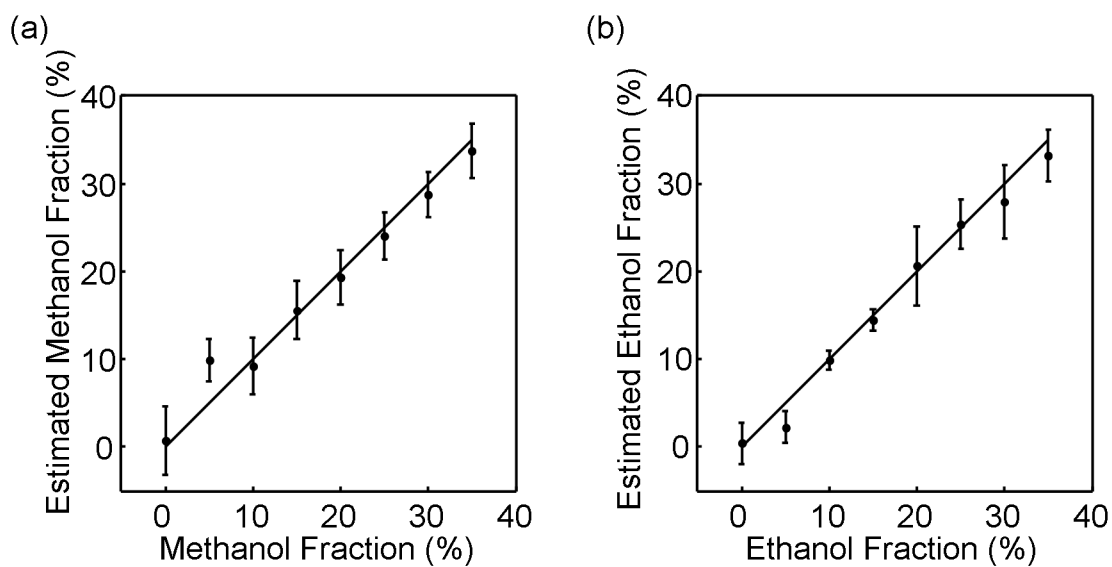


Figure 5.7: Determination of the volume fraction of components in three-component mixtures over a narrow range of volume fractions. Known fraction values correlated with the volume fraction estimated by the multilinear model for (a) methanol, and (b) ethanol.

5.7 Conclusions

Ultrasound frequency spectra of water, methanol, and ethanol mixtures were recorded at varying concentrations. Variations in the volume fraction of each component contributed to differences in the frequency profiles measured. Changes in ultrasonic frequencies can be used to determine the volume fraction of independent components. The results demonstrate that quantification is possible in binary mixtures by measuring a small number of ultrasound frequencies simultaneously. Likewise, determination of the water in three-component mixtures was demonstrated. Methanol and ethanol determination in these mixtures showed larger errors. This was attributed to the overlapping viscoelastic properties of the mixtures at different component ratios. However, narrowing the range of volume fraction in the analysis resulted in a significant improvement in detection limits. Many applications focus on a restricted range of constituents. There is a strong potential to further decrease the error of estimation using iterative regression algorithms, which could potentially increase sensitivity and extend the range of analysis.

There is a significant advantage in using the frequency spectrum of a single pulse approach as we have presented. In previous work using ultrasound for alcohol mixture analysis, multiple velocity measurements at different temperatures were required to estimate volume fractions.^{5,6} While this would be possible for dynamic systems, it is not always practical in many applications. An analysis of the frequency spectrum of a single ultrasound pulse represents substantial savings in time and cost of analysis.

There are two practical concerns that need to be considered for coupling this technique to an industrial process. The first consideration is the physical coupling of the ultrasound transducers to the container or pipeline containing the mixture. The material thickness of the coupling wall affects the lower frequency range of the measurement due to the convolution of reflected ultrasound waves. Therefore, it is important that the regression model is trained on the appropriate container. Likewise, it is important that the wall thickness not change significantly over the course of an analysis, which could be an issue for continuous monitoring of mixtures that are corrosive or that are likely to coat or sediment onto surfaces. For these systems, a dual-beam or separate path reference measurement could be used to correct for changes with time.

The second consideration is the need to account for temperature differences between regression model and the process conditions. Whereas the temperature is unlikely to change over the transmission time of a single ultrasound measurement through a sample, drifting with time could be an issue. Where temperature is expected to change significantly between a reference and determination of a sample, regression models could be made for a series operating temperatures. A simple measure of temperature would then allow the appropriate calibration to be used for sample determination. Likewise, a second reference channel could be used to correct for changes in analysis conditions. If these concerns can be addressed as proposed, this methodology would be well suited for quick and accurate mixture monitoring in industrial and biomedical settings.

5.8 Acknowledgements

This work was supported in part by the National Science and Engineering Research Council of Canada and the Fonds québécois de la recherche sur la nature et les technologies.

5.9 References

- 5.1. J. Salazar, A. Turó, J. A. Chávez, and M.J. García, “Ultrasonic inspection of batters for on-line process monitoring”, *Ultrasonics* **42**, 155–159 (2004).
- 5.2. P. Resa, T. Bolumar, L. Elvira, G. Pérez, and F.M.D. Espinosa, “Monitoring of lactic acid fermentation in culture broth using ultrasonic velocity”, *J. Food Eng.* **78**, 1083–1091 (2007).
- 5.3. J.J. Workman, M. Koch, B. Lavine, and R. Chrisman, “Process analytical chemistry”, *Anal. Chem.* **81**, 4623–4643 (2009).
- 5.4. D.J. McClements, “Ultrasonic characterization of foods and drinks: principles, methods, and applications”, *Crit. Rev. Food. Sci.* **37**, 1–46 (1997).
- 5.5. P. Resa, L. Elvira, and F. Montero de Espinosa, “Concentration control in alcoholic fermentation processes from ultrasonic measurements”, *Food Res. Int.* **37**, 587–594 (2004).
- 5.6. M. Vatandas, A.B. Koc, and C. Koc, “Ultrasonic velocity measurements in ethanol-water and methanol-water mixtures”, *Eur. Food. Res. Technol.* **225**, 525–532 (2007).

- 5.7. L. Hoff, P. C. Sontum, J.M. Hovem, “Oscillations of polymeric microbubbles: effect of the encapsulating shell”, *J. Acoust. Soc. Am.* **107**, 2272–2280 (2000).
- 5.8. A. Kvikliene, R. Jurkonis, M. Ressoner, L. Hoff, T. Jansson, B. Janerot-Sjöberge, A. Lukoševičius, and P. Ask, “Modelling of nonlinear effects and the response of ultrasound contrast micro bubbles: simulation and experiment”, *Ultrasonics*, **42**, 301–307 (2004).
- 5.9. J.M. Correias, L. Bridal, A. Lesavre, A. Méjean, M. Claudon, and O. Hélénon, “Ultrasound contrast agents: properties, principles of action, tolerance, and artifacts”, *Eur. Radiol.* **11**, 1316–1328 (2001).
- 5.10. J.R. Dion and D.H. Burns, “Ultrasonic frequency analysis of antibody-linked hydrogel biosensors for rapid point of care testing”, *Talanta* **85**, 1364–1370 (2011).
- 5.11. D. Troiani, J.R. Dion, and D.H. Burns, “Ultrasonic quantification using smart hydrogel sensors”, *Talanta* **85**, 1371–1375 (2011).
- 5.12. T.G. Muir and E.L. Carstensen, “Prediction of nonlinear acoustic effects at biomedical frequencies and intensities”, *Ultrasound Med. Biol.* **6**, 345–357 (1980).
- 5.13. T. Walsh and M. Torres, “Finite element methods for nonlinear acoustics in fluids”, *J. Comput. Acoust.* **15**, 353–375 (2007).
- 5.14. G. Pinton, F. Coulouvrat, J.L. Gennisson, and M. Tanter, “Nonlinear reflection of shock shear waves in soft elastic media”, *J. Acoust. Soc. Am.* **127**, 683–691 (2010).

- 5.15. R.T. Beyer, "Parameter of Nonlinearity in Fluids", *J. Acoust. Soc. Am.* **32**, 719–721 (1960).
- 5.16. A.B. Coppens, R.T. Beyer, M.B. Seiden, J. Donohue, F. Guepin, R.H. Hodson, and C. Townsend, "Parameter of Nonlinearity in Fluids. II", *J. Acoust. Soc. Am.* **38**, 797–804 (1965).
- 5.17. L. Bjørnø, "Forty years of nonlinear ultrasound", *Ultrasonics* **40**, 11–17 (2000).
- 5.18. K.D. Wallace, C.W. Lloyd, M.R. Holland, and J.G. Miller, "Finite amplitude measurements of the nonlinear parameter B/A for liquid mixtures spanning a range relevant to tissue harmonic mode", *Ultrasound in Med. Biol.* **33**, 620–629 (2007).
- 5.19. C.M. Sehgal, B.R. Porter, and J.F. Greenleaf, "Ultrasonic nonlinear parameters and sound speed of alcohol–water mixtures", *J. Acoust. Soc. Am.* **79**, 566–570 (1986).
- 5.20. N. Prasad, O. Prakash, S. Singh and S. Prakash, "Molecular interaction and other thermodynamic properties in ternary liquid mixtures", *Ultrasonics* **16**, 77–80 (1978).
- 5.21. C.S. Adgaonkar, V.S. Deogaonkar, and P.D. Kadu, "Study of hydrogen-bonded complexes in liquid mixtures from ultrasonic measurements", *Indian J. Pure Appl. Phys.* **15**, 98–100 (1977).
- 5.22. B. Avvaru and A.B. Pandit, "Oscillating bubble concentration and its size distribution using acoustic emission spectra", *Ultrason. Sonochem.* **16**, 105–115 (2009).

- 5.23. D. Donnelle and B. Rust, “The Fast Fourier Transform for Experimentalists, Part I: Concepts”, *Comput. Sci. Eng.* **7**(2), 80–88 (2005).
- 5.24. N. R. Draper and H. Smith, *Applied Regression Analysis* (John Wiley and Sons, New York, 1981) 2nd ed., pp 294–352.
- 5.25. L.S.L. Arakaki and D.H. Burns, “Multispectral Analysis for Quantitative Measurements of Myoglobin Oxygen Fractional Saturation in the Presence of Hemoglobin Interference”, *Appl. Spectrosc.* **46**, 1919–1928 (1992).
- 5.26. Y. Yang and F. Dunn, “Acoustic nonlinearity method for estimating the ratio of bound and free water of biological media”, *Ultrasonics* **31**, 35– 38 (1993).
- 5.27. E.E. Fileti, P. Chaudhuri, and S. Canuto, “Relative strength of hydrogen bond interaction in alcohol-water complexes”, *Chem. Phys. Lett.* **400**, 494–499 (2004).
- 5.28. S. Dixit, J. Crain, W.C.K. Poon, J.L. Finney, and A.K. Soper, “Molecular segregation observed in a concentrated alcohol–water solution”, *Nature* **416**, 829–832 (2002).

Chapter 6

Simultaneous Determination of Alcohol and Carbohydrate Content in Commercial Beverages by Ultrasound Frequency Analysis

6.1 Foreward

In the previous chapter, it was demonstrated the nonlinear distortions induced by propagation through a mixture could be used to determine the fractional composition of that medium. This was an important step towards the implementation of ultrasound as a tool for routine analysis. It was shown that characteristic distortions in the ultrasound frequency spectrum were induced by varying volume ratios in mixtures of water, methanol, and ethanol. In three-component mixtures, it was found that volume fractions could be estimated independently with good accuracy, and that the standard error in could be reduced further by narrowing the range of the analysis.

In this chapter, studies were carried out to determine the applicability of ultrasound frequency analysis for measurement of commercial beverages. Though the previous chapter examined mixtures composed of three liquids, methanol is neither a significant nor desirable component in the food and drink industries. In the beverages studied, the most significant components after water and ethanol are carbohydrates,

which can range up to 0.386 g/mL. Unlike methanol, carbohydrates are larger molecules that are heavily solvated in the water and ethanol mixtures. As a result, carbohydrate molecules are the nucleus of extensive hydrogen bonding structures or shells. The hydration shell that forms around the carbohydrates extends beyond a single layer, influencing the structuring of surrounding solvent molecules. These large hydrogen bonding structures are expected to influence the nonlinear distortion of a propagating ultrasound wave.

The goal of the work presented in this chapter is two-fold. First, the utility of the ultrasound frequency analysis for the quantification of carbohydrates dissolved in water and ethanol mixtures is evaluated. This provides a novel extension of the previous chapter, and forms the fundamental basis for the examination of the more complex beverage samples. The extension of the frequency analysis to the commercial beverages is the second objective, with the aim of improving current measurement techniques.

6.2 Manuscript

Simultaneous Determination of Alcohol and Carbohydrate Content in Commercial Beverages by Ultrasound Frequency Analysis

Authors:

Jonathan R. Dion and David H. Burns

6.3 Abstract

Controlling the composition of commercial beverages is critical for quality control. Rapid on-line measurements allow optimization in real time. We have developed a methodology to monitor the volume fraction of ethanol and the carbohydrate concentrations in liquid mixtures using ultrasound frequency analysis. Characteristic distortion to ultrasound waves propagating through liquids are induced by the specific chemical composition of the mixture. The distortion induced by the hydrogen bonding between water, ethanol, and sucrose can be monitored in the frequency domain using 5 MHz wideband ultrasonic transducers. Multilinear regression was used to quantify both ethanol and sucrose over a wide range of concentrations with correlation coefficients (r^2) greater than 0.98. Calibrations based on prepared solutions were then used to estimate the ethanol volume and carbohydrate concentration in 22 commercial beverages ranging from sodas to distilled alcohols. Results indicate that the ethanol and carbohydrates could be estimated with a 3.18% and 0.032 g/mL error, respectively. Further, by focusing the

analysis over a limited range, the error could be reduced to 0.81% ethanol. This technique demonstrates a strong potential for rapid, *in situ* monitoring of beverage production, which excludes sample extraction and pretreatment.

6.4 Introduction

Quality control is of utmost importance for the manufacture of commercial beverages (“beverages”). Alcoholic beverages are typically mixtures of several different constituents. Two dominant fractions in these beverages are ethanol and carbohydrates. A precise balance between the alcohol and carbohydrate content is required to maintain characteristic product qualities. Monitoring of these two constituents is a key step in optimizing the manufacturing process. Currently, sugars and alcohol are measured using separate methods such as refractometry and densitometry.^{6.1,6.2} The requirement for separate measurements and off-line sample preparation is limiting for routine and high throughput analyses. Techniques such as near infrared spectroscopy offer promise for simultaneous quantification.^{6.2-6.4} However, samples are not always readily analyzed by optical means. For the food and drink industries, where consistency must be balanced with high throughput, rapid, *in situ* analysis techniques would be useful.

In recent years, more attention has been paid to the use of ultrasound for the analysis of sample properties.^{6.1,6.5,6.6} Unlike electromagnetic waves, acoustic waves are carried by oscillations in the material itself. As a result, propagation through opaque liquids or containers is possible. The speed of ultrasound is related to the viscoelastic properties of the medium. By measuring the velocity, it has been shown that

concentrations of alcohols and sugars can be determined over limited ranges.^{6.1,6.7} However, the relationship between sound velocity and chemical composition is not always linear or monotonic. Further, estimating concentrations in multicomponent mixtures is limited as the measured velocity may have a non-unique solution.^{6.8,6.9} Due to the wide array of alcohol and sugar concentrations found in beverages, single ultrasound velocity measurements may provide insufficient information for component quantification.

A frequency analysis of the ultrasound wave provides a promising alternative to address the limitations of single-parameter velocity measurement. The viscoelastic properties of a medium also affect the frequency content of the wave. Small contributions to the velocity of the ultrasound due to particle motion in the medium result in the compressive phases travelling slightly faster than in rarefaction. As a result, the ultrasound takes on a sawtooth characteristic, which can be measured by an increase in harmonic frequency components.^{6.10,6.11} The change in frequency content caused by this nonlinear distortion of the signal can be quantified by the dimensionless ratio

$$\frac{B}{A} = \frac{\rho}{c_0^2} \left(\frac{\partial^2 p}{\partial \rho^2} \right)_{\rho=0,s} \quad (6.1)$$

where ρ is the mass density of the medium, c is the velocity of the ultrasonic wave, p is the pressure, and s is the entropy of the system.^{6.12,6.13} The value of the B/A parameter is related to the viscoelastic properties of a medium with a given composition. For example, the value of B/A in water is 5.0, while in ethanol it is 10.52.^{6.14} As a result, the nonlinear distortion in these two liquids produces characteristically different frequency profiles.^{6.15} In mixtures, the value of the nonlinear parameter is dependent on the ratio of the components.^{6.16} The frequency profiles of mixtures are therefore dependent on the

composition of the matrix, and a multivariate approach should allow the determination of volume ratios in mixtures.

Changes in the viscoelastic properties have been associated with the formation of molecular complexes and hydrogen bonding within a liquid.^{6.17,6.18} While these changes are small, the contribution of molecular vibrations to the ultrasound wave is related to the volume fraction of a species.^{6.15,6.19} Due to the amphoteric nature of water and ethanol, extensive hydrogen bonding between different conformers will be present in multicomponent mixtures.^{6.25} Carbohydrates are larger molecules that must be extensively solvated in water or alcohol mixtures, producing characteristic hydrogen bonding structures or shells around the molecules.^{6.20} The number of solvent molecules in this multiple-layer shell is dependent on the concentration of the specific carbohydrate in the solution.^{6.21,6.22} Likewise, there is also a dependence on the ethanol volume fraction.^{6.23} As a result, changes in the viscoelastic properties are expected with varying carbohydrate concentration.^{6.24} The cumulative molecular interactions result in distinctive ultrasound profiles, where the magnitude of certain frequencies will depend on the concentrations of each component. An analysis of ultrasonic frequencies propagating through a medium would allow quantification of the components using a multivariate approach.

In this work, we demonstrate a simple methodology to simultaneously determine the volume fraction of ethanol and the concentration of the common carbohydrate sucrose in aqueous mixtures by the frequency analysis of ultrasound. Ultrasound frequency profiles were measured to illustrate the quantification of the two constituents over a wide range of concentrations that are found in beverages. Though the specific frequency

changes may not be linear, multivariate analysis of the results allow analytical quantification in both model and commercial mixtures.

6.5 Materials and Methods

6.5.1 Reagents

Calibration using the ultrasound frequency analysis was carried out using model mixtures prepared with distilled water, anhydrous ethanol, and sucrose. Although many types of sugars are common in beverages, sucrose was used due to its important role in human nutrition and solubility in ethanol mixtures.^{6.26} Solutions were mixed for 2 hours to ensure complete dissolution of sucrose. Ethanol and sucrose were obtained from Sigma-Aldrich (Oakville, CA).

The regression calibrations based on the model mixtures were then applied to a series of commercial beverages. These beverages were aliquoted and mixed as in the standard samples. All beverages were purchased from the Société des alcools du Québec. Relevant properties of these beverages are listed in Table 6.1. Beverages such as Coca Cola, which contain carbon dioxide, were degassed by agitation to ensure that the ultrasound would not be scattered by bubbling in the cell.

Table 6.1: Ethanol and carbohydrate content of commercial beverages studied.

Beverage (manufacturer)	Ethanol (% v/v)	Carbohydrates (g/mL)
Diet Coke (<i>The Coca-Cola Company</i>)	0.0	0.000
Gatorade (<i>PepsiCo</i>)	0.0	0.063
Coca Cola (<i>The Coca-Cola Company</i>)	0.0	0.109
Budweiser (<i>AB InBev</i>)	5.0	0.031
Breezer (<i>Bacardi</i>)	5.0	0.098
Rockstar Vodka (<i>Rockstar Inc.</i>)	6.9	0.127
Bleue Dry (<i>AB InBev</i>)	7.1	0.030
Bleue Dry (<i>AB InBev</i>)	8.1	0.030
Bleue Dry (<i>AB InBev</i>)	10.1	0.030
Late autumn Riesling (<i>Inniskillin</i>)	10.5	0.033
Arte Nova White wine (<i>Vins Arista</i>)	11.5	0.026
Arte Nova Red wine (<i>Vins Arista</i>)	11.5	0.026
Sake (<i>Gekkeikan</i>)	15.5	0.049
Muscat de Rivesaltes (<i>André et Bernard Cazes</i>)	15.5	0.117
Tia Maria (<i>Allied Distillers Limited</i>)	20.0	0.338
Blue Curaçao (<i>Marie Brizard</i>)	23.0	0.350
Amaretto (<i>McGuinness Distillers Limited</i>)	23.0	0.386
Triple Sec (<i>La Distillerie Meaghers Ltée</i>)	35.0	0.257
Brandy (<i>Maison Chemineaud Ltée</i>)	40.0	0.000
Troika Vodka (<i>United Distillers Canada Inc.</i>)	40.0	0.000
Goldschlager (<i>Diageo</i>)	40.0	0.202
Grand Marnier (<i>Marnier-Lapostolle SA</i>)	40.0	0.220

6.5.2 Measurement Apparatus

Ultrasound frequency measurements were made using the instrument configuration shown in Figure 6.1. Frequency profiles were measured by a transmission configuration using a pair of piezoelectric ultrasonic transducers with 5.0 MHz center frequencies (100% bandwidth) from Technisonic (Fairfield, US). One transducer was used to generate ultrasonic pulses while the other was used to receive the waveform that propagated through the samples. The two transducers were attached to opposing faces of a 1.8 mL aluminum sample reservoir with a 2.2 cm path length. The reservoir was kept at $21 \pm 0.25^\circ\text{C}$ with a thermoelectric cooler from AMS Technologies. This was done to minimize variations in the acoustic properties of the samples due to temperature changes.

Acoustic matching across interfaces is important to minimize reflective losses.^{6.27} Cellulose acetate (CA) windows were used to better match the impedance of the liquid mixtures examined. A layer of petroleum jelly between the transducer faces and the windows was used to further improve the impedance matching. This ensured that no air bubbles were trapped between the transducers and the CA as this would highly attenuate the signal intensity. The attenuation due to the window material was minimal.

The emitting transducer (ET) was powered by a 500PR Transmitter/Receiver from Olympus NDT (Waltham, US). A <20 ns, 250 V negative impulse was generated with a $<0.01\%$ duty cycle. The low duty cycle did not induce any heating in the sample or reservoir. Due to reflection at the transducer faces, the ultrasound pulses reverberate through the sample reservoir. Pulses were generated at a frequency of 1 kHz, allowing the reverberations to be attenuated to baseline noise levels by the media before the

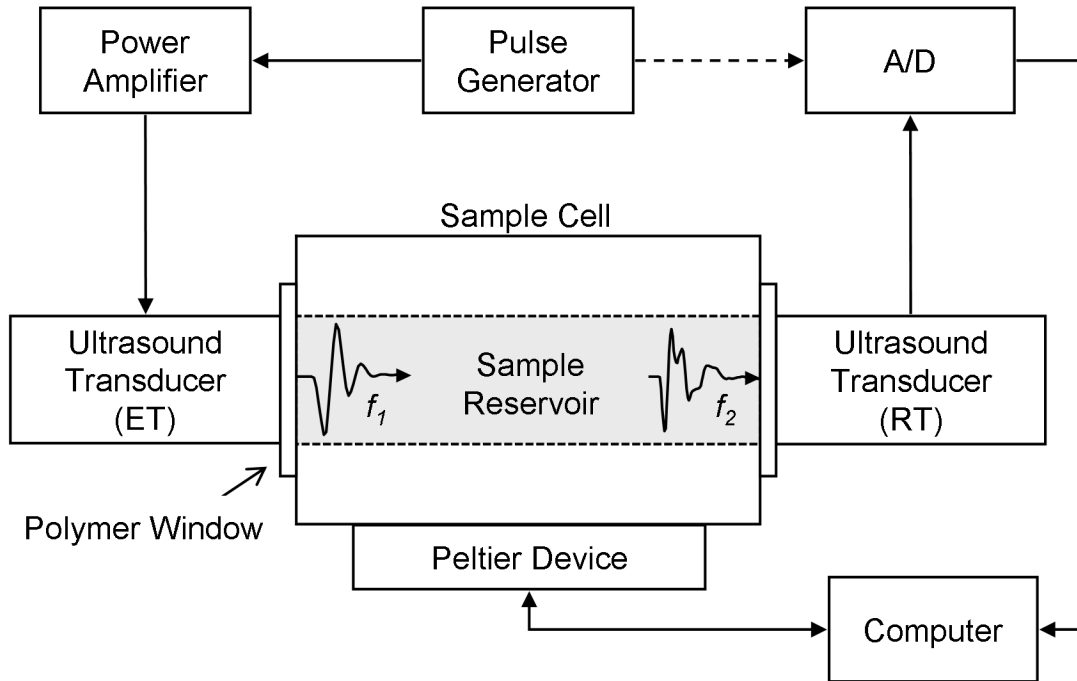


Figure 6.1: Schematic diagram of the instrumentation used for multi-frequency ultrasound measurements. Samples are held in a channel between two ultrasound transducers. The emitting transducer generates a pulse waveform (f_1), which propagates through the media and undergoes specific absorption and nonlinear processes. The receiving ultrasound transducer records the waveform that is modified by the transit (f_2). The temperature in the aluminum sample cell is regulated by a Peltier device.

subsequent pulses were generated. The ultrasound pulse waveform was received by the second transducer (RT). The signal was digitized by a Tiepie (Sneek, NL) Handyscope HS3 computer controlled oscilloscope sampling at 50 MHz with a 12-bit dynamic range. For each sample, 600 waveforms were measured, for a total acquisition time of 30s.

6.5.3 Methods of Analysis

All samples were prepared in triplicate and were measured in random order to minimize any correlation with fluctuations in ambient conditions or instrumental response. Small changes in temperature or other ambient conditions can change the velocity of the ultrasound. To compensate for any potential phase offsets, signals were aligned to the highest positive signal intensity in the ultrasonic waveform. These waveforms were then averaged to increase the signal-to-noise ratio. Although the CA windows and coupling fluid improve impedance matching, a fraction of the waveform was reflected at each interface. As a result, the ultrasound pulse train reverberated in the sample reservoir. However, the pulse duration is low and the length of the ultrasound waveform generated by the transducer was short (1.1 μ s) relative to the path length of the reservoir (15 μ s). As a result, the reverberations were well separated temporally, and only the first pulse transient was retained for further processing.

To examine the frequency content of the signal, a fast Fourier transform was used to decompose the waveform into its component frequency spectrum. Prior to the transform, the waveform was zero padded to improve frequency domain interpolation.^{6.28} Frequencies in the magnitude spectra outside of the 0.5 to 10 MHz frequency window

were excluded from further processing. The data were then smoothed by a 0.1 MHz moving average to reduce the noise in the spectra and the spectra were normalized to the total area to account for potential deviations in the instrumental response over the course of the data acquisition.

For the analysis of model mixtures, data were divided into independent calibration and test data sets. Two of the three replicates for each sample were used to generate a calibration using stagewise multilinear regression (MLR). The linear combination of a subset of frequencies to best describe the data in the form

$$Y = b_0 + b_1X_1 + b_2X_2 + \dots + b_nX_n \quad (6.2)$$

were determined, where Y is the dependent variable (the volume fraction of ethanol or concentration of sucrose), $\{X\}$ are independent variables (the magnitude at a given ultrasound frequency), and $\{b\}$ are the weighting coefficients. The algorithm computed the regression of the dependent variable with the magnitude of each frequency in the ultrasound spectrum. The residual values were then calculated. This was iteratively repeated with the subset of frequencies that were not yet incorporated into the regression model. The most parsimonious model with the fewest frequencies included was selected where an F-test between regression models ($\alpha = 0.05$) showed no significant improvement with additional parameters. This regression equation was then used to estimate the dependent variable in the independent test sample set. These consisted of the independent third replicate of each sample that was not included in the calibration set. The quality of each model was measured by the correlation coefficient (r^2) and standard error (SE). Frequency selection in the MLR model is further described in Draper and

Smith.^{6,29} Separate MLR analyses were performed for the two components of interest, sucrose and ethanol.

For the analysis of beverages, the same MLR procedure was used. The model mixture data were used as the calibration data set. Here, however, all replicates were included in the so that greater variability could be accounted for by the model. As above, the most parsimonious regression models for ethanol and sucrose were selected using an F-test ($\alpha = 0.05$) between calibrations. The concentrations of ethanol and sucrose in the beverages were then estimated using these regression models and the correlation coefficient (r^2) and standard error (SE) are reported. All signal processing and analysis of the ultrasonic data was done in Matlab (2009b, The MathWorks Inc., Natick, US).

6.6 Results and Discussion

6.6.1 Ultrasound Measurements of Two-Component Mixtures

For comparison with the multi-frequency analysis, the velocity of two-component water/ethanol and water/sucrose mixtures was first measured. Changes to the viscoelastic properties of a solution produce measurable changes to the velocity of propagating waves. However, nonlinearities in propagation velocity are limiting in mixtures that contain water, ethanol, and sucrose as major components.^{6,9} To illustrate this, mixtures were prepared with ethanol volume fractions in water ranging between 0 and 40%. As shown in Figure 6.2(a), the initial increase in the measured ultrasound velocity reaches an

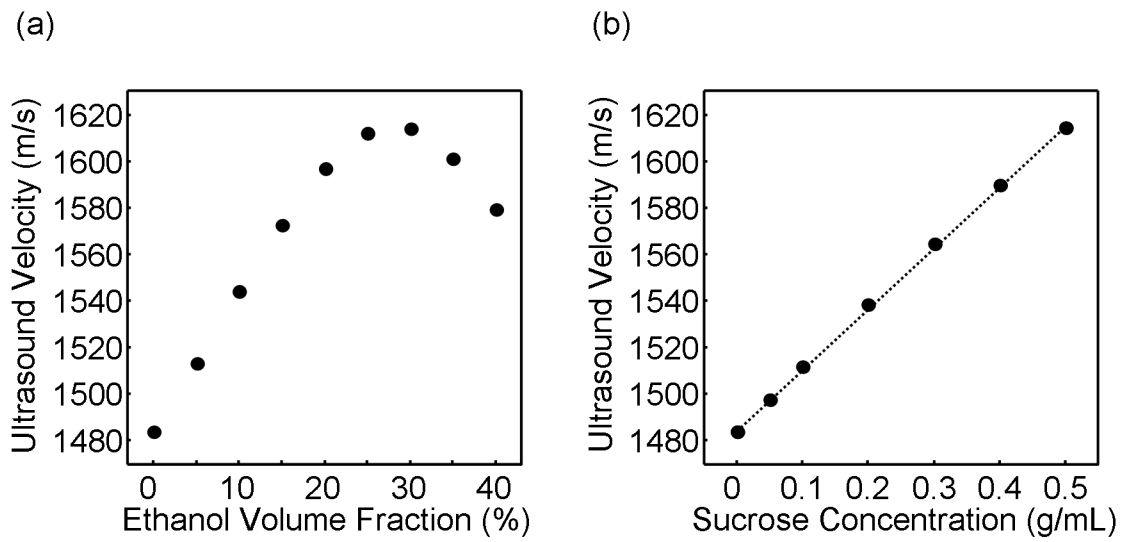


Figure 6.2: Change in ultrasound velocity in water with increasing component levels. (a) ethanol, and (b) sucrose.

inflection point and begins to decrease above approximately 30% ethanol. As the velocity change is non-monotonic, it is not possible to determine the volume fraction of ethanol over the entire range using a single measurement of velocity. In contrast, the relationship between sucrose content and ultrasound velocity is monotonic over a wide concentration range. As shown in Figure 6.2(b), as sucrose concentration increases from 0 to 0.5 g/mL, ultrasonic velocity also increases. However, despite the absence of an inflection point, the velocity change is not linear, as shown by the deviation from the linear trace between the low and high concentrations. These examples demonstrate that the velocity of ultrasound propagation can be useful for component determination over limited ranges in systems with closure. However, nonlinearities over wide ranges and non-monotonic behavior limit applicability to wider concentration ranges. Likewise, as the velocity in both systems spans a similar range. As a result, mixtures in which both components vary would result in overlapping velocities at certain mixture ratios.

To address these limitations in nonlinear systems, multiple-measurement approaches have been taken, such as measuring the velocity at several temperatures.^{6,8} However, the need to precisely ramp the temperature of the system increases the cost, complexity, and time of the analysis. Likewise, this is not desirable for *in situ* analysis. It has also been shown that a frequency analysis of ultrasound waves can allow quantification in non-monotonic systems such as alcohols.^{6,15} To demonstrate the applicability of this methodology to the components in beverages, a series of water/ethanol and water/sucrose mixtures were prepared. The changes in the measured frequency spectra for these mixtures were examined to illustrate the effect of viscoelastic changes on the nonlinear propagation.

As shown in Figure 6.3(a), when ethanol is added to water, there is a change in the frequency profile. To better illustrate the changes in the frequency domain, the mean spectral profile was subtracted from the spectra. These mean-centered frequency profiles for water/ethanol mixtures are shown in Figure 6.3(b). As ethanol increases from 0 to 40%, changes in the spectrum can be divided into two major regions. First, the magnitudes of frequencies below 3 MHz change in a manner similar to the velocity fluctuation. With increasing ethanol, the magnitude in this lower frequency range initially decreases. There is a minimum at approximately 25% ethanol, after which the magnitude begins to increase. As in the velocity measurements, the rate of change in the ultrasound signal is nonlinear with increasing ethanol. Different behavior is seen in frequencies above 4 MHz. In this range, both magnitude changes and frequency shifts are present. The magnitude of the ultrasound frequencies increase with rising ethanol content until an inflection at 25%, after which a decrease is measured. The frequency envelope in this range also shifts monotonically to lower frequencies as the concentration of ethanol increases. These changes in the frequency profile should allow quantification of ethanol volume fractions in mixtures.

Water/sucrose mixtures were also prepared to demonstrate the frequency changes in this system. Concentrations of 0 to 0.5 g/mL were prepared, representing a range which is common in beverages. As shown in Figure 6.3(c), the effect of increasing the concentration of sucrose is an exchange in magnitude between the high and low frequency range. Figure 6.3(d) shows the mean-centered frequency profiles of the the water/sucrose samples, illustrating the exchange in frequencies. However, at the maximum concentration, different behavior is seen as the frequencies above 5 MHz begin

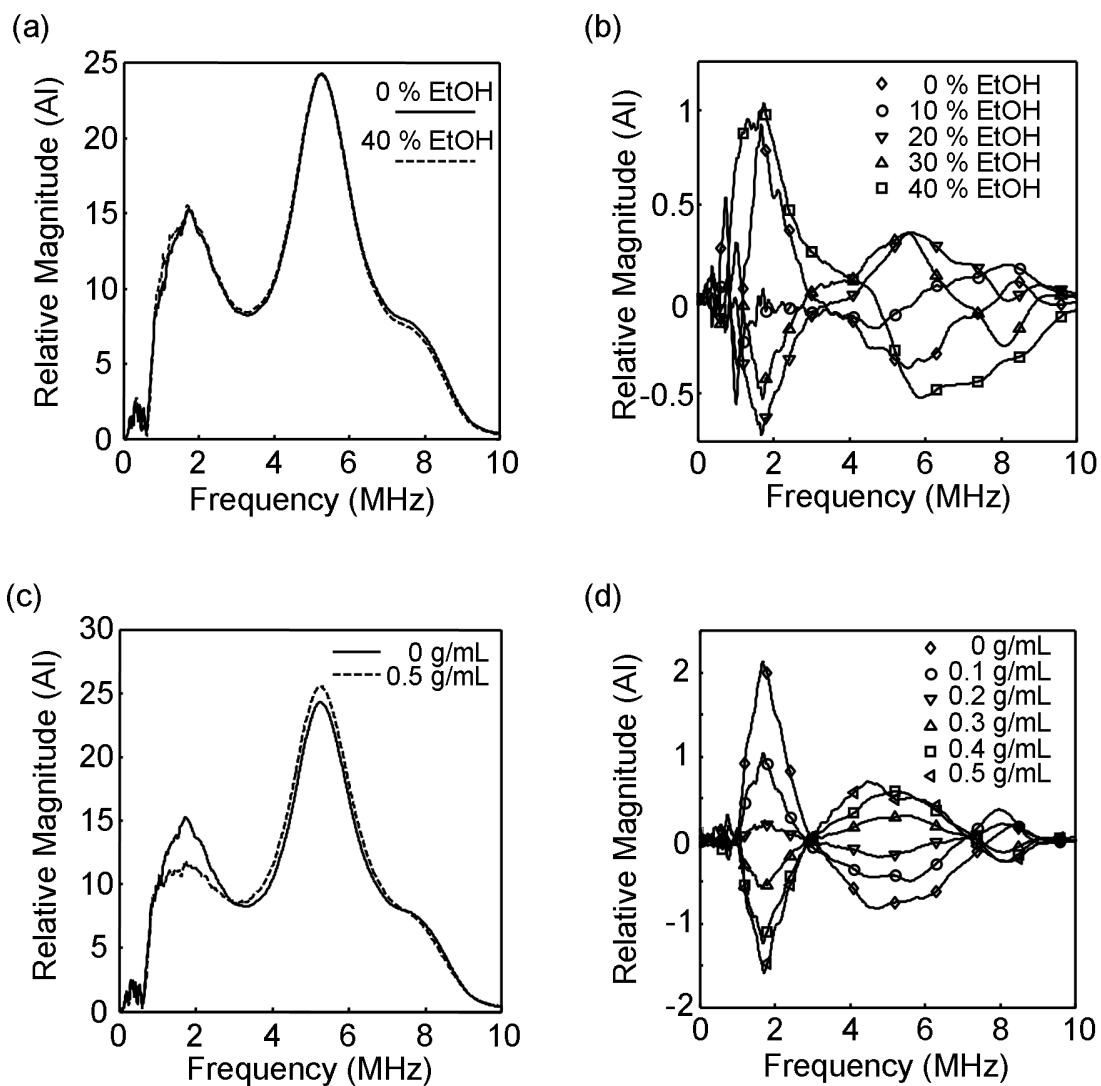


Figure 6.3: Frequency profiles of binary liquid mixtures showing changes with (a) ethanol volume fraction, (b) ethanol volume fraction where the mean spectral profile has been subtracted, (c) sucrose concentration, and (d) sucrose concentration where the mean spectral profile has been subtracted.

to decrease. As with ethanol, the characteristic changes in the frequency domain are expected to allow multivariate determination of sucrose concentrations in mixtures.

A multilinear regression analysis was done to determine if the magnitude of the frequencies in the ultrasound spectrum could be used to estimate the composition of a mixture. The frequency spectra were first divided into two data sets. A calibration set composed of two replicates at each concentration was used to generate a regression. This regression was then used to estimate the sample concentrations in the test set, which was made up of an independent replicate of each concentration. For water/ethanol mixtures, multilinear analysis revealed a close correlation between the magnitude of a subset of the ultrasound frequencies and the volume fraction of ethanol. Using two ultrasonic frequencies, ethanol volumes could be estimated with an r^2 greater than 0.99 and a standard error of 0.95%. Figure 6.4(a) illustrates the estimates of ethanol volume fractions relative to the known values. This shows that the results are linear over the entire range examined, which is not the case when using a single velocity measurement. The volume fractions were estimated using frequencies from both the low frequency range (1.06 MHz) and the high frequency range (3.29 MHz). This suggests that both velocity of propagation and the nonlinear propagation distortions are useful for estimating the mixture composition. As this is a two-component mixture with system closure, the second component (water) can be determined by subtraction with the same error.

The multilinear regression algorithm was also used to estimate concentrations of sucrose in water ranging between 0 and 0.5 g/mL. A close correlation was found between

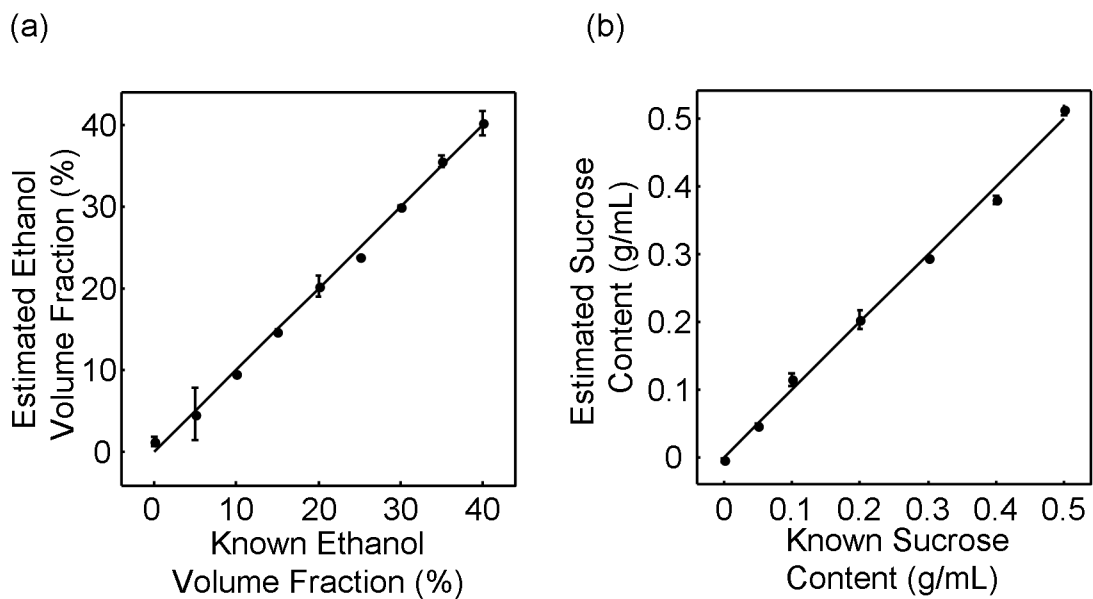


Figure 6.4: Determination of components in binary liquid mixtures. Known concentration values correlated with the values estimated by multilinear regression for (a) ethanol in water/ethanol mixtures, (b) sucrose in water/sucrose mixtures.

the magnitude of a single ultrasound frequency and the concentration of sucrose, which could be estimated with an r^2 greater than 0.99 and a standard error of 0.004 g/mL. These data are illustrated in Figure 6.4(b). The determination of sucrose required one parameter from the low frequency range (1.39 MHz). As with the water/ethanol mixtures, this indicates that the region of the frequency spectrum showing partial correlation with the velocity is useful for component determination. To determine if the correlation was due to the velocity bias in this range, a separate calibration was made using only frequencies above 3 MHz. Similar sensitivity could be obtained by focusing on this range, suggesting that the velocity only adds an offset in the low frequency. The use of fewer frequencies relative to the water/ethanol system is attributed to the monotonic change of the physical properties in water/sucrose mixtures.

It is important to note that the configuration of the instrument influences the measured frequency spectrum. Transmission of ultrasound through a thin window creates a secondary wave due to partial reflection at the interface. This secondary waveform is slightly out of phase with the primary wave. The convolution of the two waveforms produces subharmonic frequencies that are dependent on the ultrasound velocity.^{6.15} This may account for correlation between the velocity and the magnitude of the frequencies in the <3 MHz region. To again verify that the velocity is not the only parameter being measured, the transducers were placed in direct contact with the liquid and frequency profiles for a series of mixtures were measured. Changes in the frequency distribution were seen using this configuration. The magnitudes of frequencies in the 1-3 MHz region decreased by approximately 50%. This was accompanied by a similar increase in magnitude of the higher range surrounding the fundamental frequency. Variations in the

frequency distribution with mixture composition and comparable sensitivities for both ethanol and sucrose estimation were still observed. Therefore, the coupling between the liquid sample and the transducers only affects the relative frequency distribution and not quantification.

Although the thin windows are responsible for the convolution in the data, contact between the ultrasound transducers and the mixtures is not always practical. For routine analyses, contamination or degradation of the transducer surface would change the frequency profile of the ultrasound pulse and reduce the sensitivity. Additionally, it would be preferable to monitor the composition of beverages inside a process container or in a bottled product rather than extracting a sample. In analyzing data where the transducers are not in direct contact with the solution, the frequency spectra are modified in a characteristic manner, which can be examined using multivariate methods.

6.6.2 Ultrasound Measurement of Three-Component Mixtures

Even in ideal conditions and with system closure, a single velocity measurement is insufficient to quantify more than two components. Velocity measurements can be enhanced by repeated measurement over varying temperatures^{6,8} or supplemented with secondary techniques such as density measurement.^{6,9} Over large ranges, however, the overlap in the measured velocities remains limiting. Further, multiple measurements are time consuming, and in many practical applications changing the conditions the reaction vessel is not possible. To address these concerns, an experiment was designed to determine whether the frequency analyses could simultaneously determine the

concentrations of ethanol and sucrose in water. Mixtures were prepared with ethanol volume fractions between 0 and 40% and sucrose concentrations between 0 and 0.5 g/mL in a series of combinations.

The ultrasound frequency profiles of the three component mixtures show similar characteristic changes as seen in the two-component data. Changes occur in the two primary regions: the 1-3 MHz range and the 3-9 MHz range. The intensities of the ultrasound frequencies in the 1-3 MHz region change in a manner similar to the propagation velocity in the mixture. In the higher frequency range, nonlinear changes with varying mixture composition are more pronounced, including shifts in peak maxima and changes in the rate of signal magnitude variation with composition. A multilinear regression analysis was done to determine if the concentrations of ethanol and sucrose could be simultaneously determined in three-component mixtures based on the observed changes in the spectra. Samples were divided into independent calibration and test sets. The calibration set was used to develop a multilinear regression model. This regression was then used to estimate the property of interest in the test data set. As shown in Figure 6.5(a), estimates of ethanol volume fractions relative to the known values are linear over the entire range examined. The volume fractions could be estimated with an r^2 of 0.98 and a SE of 2.07% ethanol using four frequencies as shown in Table 6.2. As with the two-component ethanol determination, both the 1-3 and 3-9 MHz regions in the frequency spectrum were used by the MLR regression model. The small increase in estimation error was attributed to the added viscoelastic changes caused by the varying sucrose concentrations. Despite the increase in error, this analysis showed that the volume fraction of ethanol in water could be estimated in the presence of varying

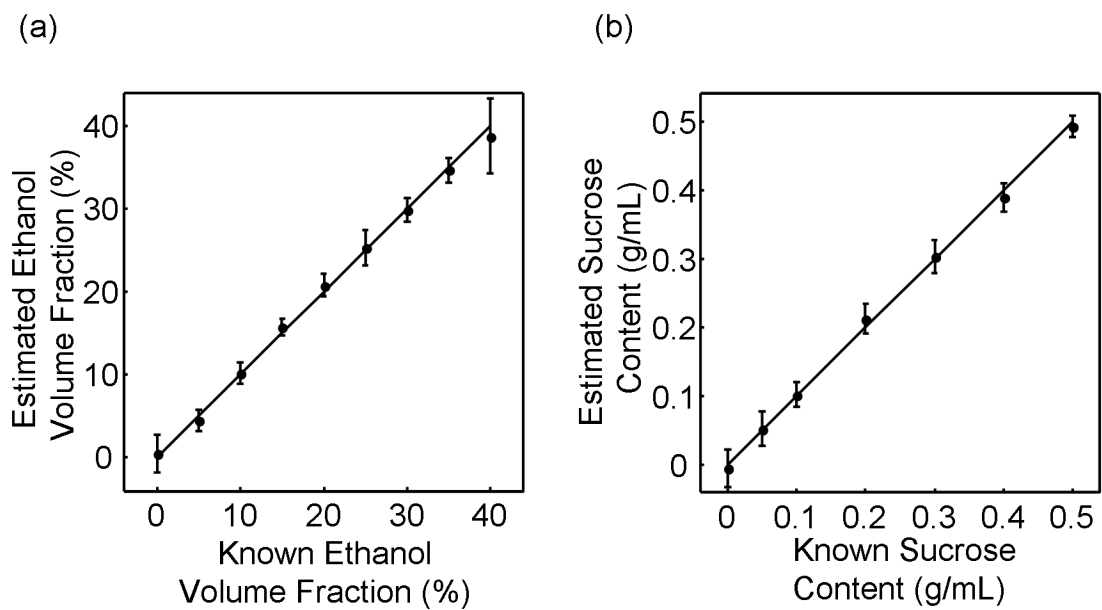


Figure 6.5: Determination of components in three-component mixtures of water/ethanol/sucrose. Known concentration values correlated with the values estimated by the multilinear regression for (a) ethanol, (b) sucrose.

sucrose concentrations.

A separate multilinear regression model was made to estimate the concentration of sucrose in the mixtures. It was found that the magnitude of two ultrasound frequencies was well correlated with the concentration of sucrose. As shown in Table 6.2, the volume fraction of ethanol could be estimated with an r^2 of 0.98 and a SE of 0.027 g/mL. The two frequencies used for this determination were 4.18 MHz and 7.63 MHz. Unlike the two-component mixtures of water/sucrose, the higher frequency range was shown to be of greater predictive value. As with the determination of ethanol, the viscoelastic properties of the media are also affected by the presence of other species in the solution, resulting in a small increase in estimation error. However, as with ethanol, this analysis demonstrates that estimation of sucrose content over a wide range is possible using ultrasound frequency analysis.

Sucrose-solvent complexes and hydrogen bonding between water and ethanol were shown above to influence the nonlinear distortion of the ultrasound wave. In three-component mixtures, the viscoelastic properties of the solution will depend on both of these factors. The interrelationship between these parameters is likely the cause of the reduced sensitivity as compared to the 2-component mixture determination. However, with the incorporation of additional frequencies in the multilinear model, ethanol and sucrose concentrations are both well estimated. Both components can be measured simultaneously rather than using separate methods. Further, the non-invasive ultrasound methodology removes the need for extensive sample preparation. As a result, this methodology would provide substantial savings in time and cost of analysis.

Table 6.2: Figures of merit for the determination of fractional components in three-component mixtures.

Component	r^2	SE	Model Frequencies
Ethanol	0.98	2.07%	1.09, 5.62, 1.72, 2.01
Sucrose	0.98	0.027 g/mL	4.18, 7.63

6.6.3 Ultrasound Measurement of Commercial Beverages

To determine the applicability of the ultrasound frequency analysis to commercial product testing, samples of 22 beverages were examined. These ranged from 0 to 0.386 g/mL of carbohydrates and had volume fractions of ethanol between 0 and 40%. The beverages were used without any pre-treatment, meaning that a wide variety of other chemical constituents were also present. Ultrasonic frequency spectra of these beverages were measured and the sucrose and ethanol concentrations were then estimated using multilinear regressions trained on the model water/ethanol/sucrose model mixtures. The ethanol content of the beverages was estimated using frequencies determined by MLR analysis of the model solutions. With four frequencies, the volume fractions of ethanol were estimated with an r^2 of 0.95 and a standard error of 3.18% ethanol. The frequencies incorporated into this model are found in Table 6.3. As in the three-component model system, the velocity information in the low frequency (1–3 MHz) region was found to be important. Likewise, frequencies above 3 MHz were also used for ethanol estimation, demonstrating the value of the nonlinearities that have been associated with the viscoelastic changes. The mean estimated values for the ethanol volume fractions of the calibration data (circles) and beverages (squares) are plotted against the known values in Figure 6.6(a). Although there is higher error in estimating certain beverages, the volume fraction estimates were generally well correlated to the model system trend. It is likely that the beverages with larger prediction errors contained other constituents that have a significant impact on the viscoelastic properties. Although sucrose was used to generate the model solutions making up the calibration set, different

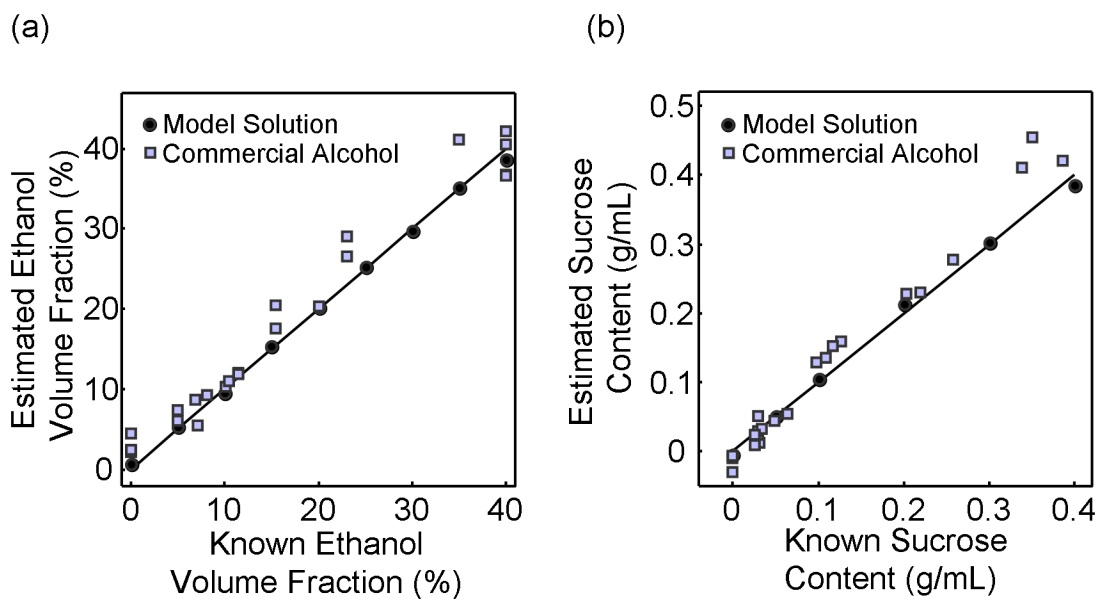


Figure 6.6: Determination of components in commercial beverages. Known concentration values correlated with the values estimated by the multilinear regression for (a) ethanol, (b) sucrose.

Table 6.3: Figures of merit for the determination of fractional components in beverages.

Component	r^2	SE	Model Frequencies
Ethanol	0.95	3.18%	2.76, 1.13, 6.94, 1.07
Sucrose	0.98	0.032 g/mL	1.33, 7.57, 4.04

carbohydrates present in certain beverages may have been less well approximated by these solutions.

Separate estimation of sucrose in the beverages also showed a close correlation between carbohydrate concentration and a subset of frequencies. Sucrose concentration in the beverages was estimated with an r^2 of 0.97 and a SE of 0.032 g/mL using the frequencies found in Table 6.3. The similarity between these frequencies and those used for the two and three-component model mixtures suggests that the frequencies associated with the nonlinear distortion caused by sucrose in the solution are minimally affected by the presence of other components in the beverage matrices. Figure 6.6(b) shows the mean estimated values for the calibration solutions (circles) and beverage estimates (squares) plotted against the known values. This illustrates that the concentration estimates are well correlated to the model system trend. The varying carbohydrate composition may account for the larger estimation errors in beverages with carbohydrate concentrations above 0.3 g/mL. In contrast, the error of this model when estimating the carbohydrate content of the 4 beer samples was found to be only 0.017 g/mL. This factor of 2 improvements by isolating to just the one matrix suggests that the regression model is better calibrated for the carbohydrates found in this beverage class. These results indicate that a regression trained on model mixtures with the appropriate carbohydrates found in a given beverage should improve the sensitivity of the method further.

The beverages examined also contain several other components in varying concentrations. These include different sugars such as glucose, fructose, and polysaccharides, as well as caffeine, proteins, and salts. These compounds would be expected to also induce characteristic nonlinear distortions in the propagating ultrasound

wave that would be different than those of ethanol and sucrose. Additionally, while the compressibility of small molecules can be considered to be negligible, it may be significant in larger polymers.^{6,23} To reduce offsets resulting from other components, more specific multilinear regression models could be made by using model solutions that better mimic the beverage being investigated.

Component estimation in the beverages can also be improved by narrowing the range of samples analyzed. As a demonstration, a subset of the beverages with a maximum ethanol volume fraction of 15% and a maximum sucrose concentration of 0.3 g/mL were examined. A new, independent multilinear regression analysis was carried out using model solutions that were likewise limited to these concentration ranges. This analysis revealed that an improved estimation was possible, showing errors in ethanol volume of only 0.81%. Figure 6.7(a) illustrates that the linearity was also improved and showed minimal bias. As shown in Table 6.4, the MLR model incorporated frequencies in similar ranges to those in the above models (1.74 MHz and 6.97 MHz). This suggests that these frequencies show a strong correlation with ethanol content at low volume fractions independent of other matrix components. The incorporation of additional frequencies is then likely due to the variety of other beverage constituents.

The estimation of ethanol content in beverages with higher volume fractions can also be improved. An independent regression model was generated using model solutions containing 20-40% ethanol. In this case, the error in the ethanol estimation was reduced to 1.64% with the frequencies listed in Table 6.4. The frequencies determined by this multilinear regression differed from those used for the model solutions or the full range

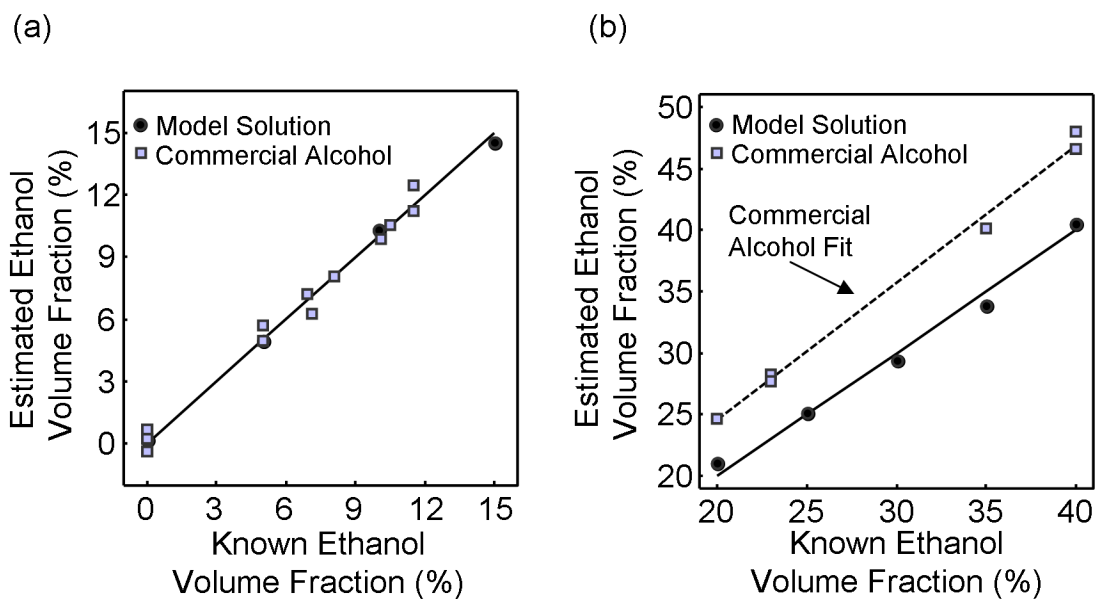


Figure 6.7: Determination of components in commercial beverages over narrow concentration ranges. Known concentration values correlated with the values estimated by the multilinear regression for (a) 0 to 15% ethanol, (b) 20 to 40% ethanol.

Table 6.4: Figures of merit for the determination of fractional components in beverages over targeted ranges.

Component	r^2	SE (%)	Model Frequencies
Ethanol, 0-15%	0.95	0.81	1.74, 6.97, 2.18, 4.84, 3.07
Ethanol, 20-40%	0.97	1.64	5.57, 4.70, 5.64, 4.69

beverage analysis. However, two frequencies (4.70 MHz and 4.69 MHz) were similar to ones used in the analysis of 0–15% ethanol beverages. This may indicate that certain frequencies are more correlated with ethanol when the number of other constituents in the complex beverage matrices is reduced. As shown in Figure 6.7(b), however, there is an offset in the ethanol estimation in these distilled beverages. This may be due to common components that these beverages share. By using one of the beverages as a control point, this offset can be subtracted, greatly reducing the error. Although adding more parameters to the multilinear model could account for bias, using model solutions that better mimic the beverages being studied would allow for more robust estimation and reduce overfitting. Likewise, by examining beverages over more targeted ranges, the error would be expected to decrease further.

Although the estimation error is somewhat higher when measuring a wide range of concentrations, many commercial analyses are performed over a narrow range of concentrations. For routine analysis, broad calibrations could provide initial estimates of sample properties that would then be refined using separate multilinear models calibrated to appropriate matrices. This would improve the sensitivity of the method, while having little impact on the analysis time. The overall sensitivity of the ultrasonic ethanol estimation is comparable to the <0.20% errors expected using current reference methods.^{6.30} Though invasive carbohydrate measurements can be made with an error of <0.002 g/mL,^{6.31} using a targeted carbohydrate mixture may provide improve the sensitivity of the ultrasound technique to similar levels. While reference methods can potentially provide more sensitive detection of ethanol and carbohydrates, the immediacy of the measurement using the ultrasound frequency analysis is a key advantage. Likewise,

the low cost and lack of sample pre-treatment are advantageous over current measurement techniques for routine analysis.

6.7 Conclusions

This work has demonstrated that frequency analysis of ultrasound can provide quantitative information about the composition of mixtures containing water, ethanol, and sucrose. Nonlinear distortions of the frequency spectrum arise due to inter-molecular complex formation. Using a multilinear approach it was shown that these complexes could be probed to determine the concentrations of sucrose and ethanol simultaneously using different subsets of frequencies. The analysis was further extended to look at a selection of 22 commercial beverages ranging from non-alcoholic sodas to distilled alcohols. By measuring the frequency components, the volume fraction of ethanol was determined over a range of 0 to 40% by volume. Likewise, the carbohydrate contents ranging between 0 and 0.386 g/mL in these beverages could be approximated using a multilinear model.

This methodology demonstrates a distinct advantage over conventional analyses used for quality control in food and drink production. Although highly sensitive, conventional methods measure ethanol and carbohydrate content separately. Further, these techniques typically require sample extraction and preparation prior to analysis. Other ultrasound approaches have been suggested to address these issues using multiple measurements at different temperatures,^{6,8} however, this is not always practical. The

methodology outlined in this work could be used to quickly measure multiple components *in situ*, which would provide substantial savings in time and cost of analysis.

There are practical concerns which must be addressed to allow use of this methodology for routine food and drink analysis. Although measurement of the ultrasound frequencies is rapid, the initial development of the calibration model is critical and more complex. The viscoelastic properties of the solution are temperature dependent. It is therefore important that the temperature at which the measurements are made be kept constant. As the temperature is typically well controlled during manufacturing of commercial beverages, it should not prove difficult to regulate to less than ± 0.25 °C as was done in this study. If the conditions cannot be controlled, separate regression models could also be made at different temperatures. A simple measurement of temperature would then allow the appropriate calibration model to be used for rapid sample analysis.

As discussed in previous sections, the low frequency range of the ultrasound spectrum is also sensitive to waveform reflections at the coupling interfaces. It is therefore important that the regression model is trained on the appropriate container. In case of any changes to the container caused by corrosion or coating by the beverage, a second reference measurement across a separate path could be used to correct for changes over time. In combination with a temperature measurement, this would allow continuous monitoring of beverages, facilitating process optimization and quality control. For industries such as the food and drink production where consistency must be maintained, the methodology outlined would be a useful tool if these practical concerns could be addressed as indicated.

6.8 Acknowledgements

This work was supported in part by the National Science and Engineering Research Council of Canada and the Fonds québécois de la recherche sur la nature et les technologies.

6.9 References

- 6.1. M. Van Sint Jan, M. Guarini, A. Guesalaga, J. Ricardo Pérez-Correa, and Y. Vargas, “Ultrasound based measurements of sugar and ethanol concentrations in hydroalcoholic solutions”, *Food Control* **19**(1), 31–35 (2008).
- 6.2. D.W. Lachenmeier, “Rapid quality control of spirit drinks and beer using multivariate data analysis of Fourier transform infrared spectra”, *Food Chem.* **101**, 825–832 (2007).
- 6.3. S. Castritius, A. Kron, T. Schäfer, M. Rädle, and D. Harms, “Determination of Alcohol and Extract Concentration in Beer Samples Using a Combined Method of Near-Infrared (NIR) Spectroscopy and Refractometry”, *J. Agric. Food Chem.* **58**, 12634–12641 (2010).
- 6.4. D.W. Lachenmeier, R. Godelmann, M. Steiner, B. Ansay, J. Weigel, and G. Krieg, “Rapid and mobile determination of alcoholic strength in wine, beer and spirits using a flow-through infrared sensor”, *Chem. Cent. J.* **4**, 5 (2010).

- 6.5. P. Resa, L. Elvira, and F. Montero de Espinosa, "Concentration control in alcoholic fermentation processes from ultrasonic measurements", *Food Res. Int.* **37**, 587–594 (2004).
- 6.6. D.J. McClements, "Ultrasonic characterization of foods and drinks: principles, methods, and applications", *Crit. Rev. Food. Sci.* **37**, 1–46 (1997).
- 6.7. N.I. Contreras, P. Fairly, D.J. McClements, and M.J.W. Povey, "Analysis of the sugar content of fruit juices and drinks using ultrasonic velocity measurements", *Int. J. Food Sci. Technol.* **27**, 515–529 (1992).
- 6.8. M. Vatandas, A.B. Koc, and C. Koc, "Ultrasonic velocity measurements in ethanol-water and methanol-water mixtures", *Eur. Food. Res. Technol.* **225**, 525–532 (2007).
- 6.9. P. Resa, L. Elvira, F. Montero de Espinosa, and Y. Gómez-Ullate, "Ultrasonic velocity in water–ethanol–sucrose mixtures during alcoholic fermentation", *Ultrasonics* **43**, 247–252 (2005).
- 6.10. T.G. Muir and E.L. Carstensen, "Prediction of nonlinear acoustic effects at biomedical frequencies and intensities", *Ultrasound Med. Biol.* **6**, 345–357 (1980).
- 6.11. T. Walsh and M. Torres, "Finite element methods for nonlinear acoustics in fluids", *J. Comput. Acoust.* **15**, 353–375 (2007).
- 6.12. R.T. Beyer, "Parameter of Nonlinearity in Fluids", *J. Acoust. Soc. Am.* **32**, 719–721 (1960).

- 6.13. A.B. Coppens, R.T. Beyer, M.B. Seiden, J. Donohue, F. Guepin, R.H. Hodson, and C. Townsend, "Parameter of Nonlinearity in Fluids. II", *J. Acoust. Soc. Am.* **38**, 797–804 (1965).
- 6.14. L. Bjørnø, "Forty years of nonlinear ultrasound", *Ultrasonics* **40**, 11–17 (2000).
- 6.15. J.R. Dion and D.H. Burns, "Determination of volume fractions in multicomponent mixtures using ultrasound frequency analysis", *Appl. Spectrosc.* **65**, 648–656 (2011).
- 6.16. C.M. Sehgal, B.R. Porter, and J.F. Greenleaf, "Ultrasonic nonlinear parameters and sound speed of alcohol–water mixtures", *J. Acoust. Soc. Am.* **79**, 566–570 (1986).
- 6.17. C.S. Adgaonkar, V.S. Deogaonkar, and P.D. Kadu, "Study of hydrogen-bonded complexes in liquid mixtures from ultrasonic measurements", *Indian J. Pure Appl. Phys.* **15**, 98–100 (1977).
- 6.18. Y. Yang and F. Dunn, "Acoustic non-linearity method for estimating the ratio of bound to free water of biological media", *Ultrasonics* **31**, 35–38 (1993).
- 6.19. B. Avvaru and A.B. Pandit, "Oscillating bubble concentration and its size distribution using acoustic emission spectra", *Ultrason. Sonochem.* **16**, 105–115 (2009).
- 6.20. J.A. Te, M.L. Tan, and T. Ichiye, "Solvation of Glucose, Trehalose, and Sucrose by the Soft Sticky Dipole-Quadrupole-Octupole Water Model", *Chem. Phys. Lett.* **491**, 218–223 (2010).
- 6.21. A.T. Allen, R.M. Wood, and M.P. McDonald, "Molecular association in the sucrose-water system", *Sugar Technol. Rev.* **2**, 165–180 (1974).

- 6.22. M. Heyden, E. Bründermann, U. Heugen, G. Niehues, D.M. Leitner, and M. Havenith, “Long-Range Influence of Carbohydrates on the Solvation Dynamics of Water Answers from Terahertz Absorption Measurements and Molecular Modeling Simulations” *J. Am. Chem. Soc.* **130**, 5773–5779 (2008).
- 6.23. H. Shiio, T. Ogawa, H. Yoshihashi, “Measurement of the Amount of Bound Water by Ultrasonic Interferometer”, *J. Am. Chem. Soc.* **77**, 4980–4982 (1995).
- 6.24. W.K. Law, L.A. Frizzell, F. Dunn, “Ultrasonic determination of the nonlinearity parameter B/A for biological media”, *J. Acoust. Soc. Am* **69**, 1210–1212 (1981).
- 6.25. E.E. Fileti, P. Chaudhuri, and S. Canuto, “Relative strength of hydrogen bond interaction in alcohol-water complexes”, *Chem. Phys. Lett.* **400**, 494–499 (2004).
- 6.26. W.C. Winder, D.J. Aulik, and A.C. Rice, “An Ultrasonic Method for Direct and Simultaneous Determination of Alcohol and Extract Content of Wines”, *Am. Soc. Enol. Viticult.* **21**(1), 1–11 (1970).
- 6.27. D. Laux, G. Lévêque, and V. Cereser Camara, “Ultrasonic properties of water/sorbitol solutions”, *Ultrasonics* **49**, 159–161 (2009).
- 6.28. D. Donnelle and B. Rust, “The Fast Fourier Transform for Experimentalists, Part I: Concepts”, *Comput. Sci. Eng.* **7**(2), 80–88 (2005).
- 6.29. N. R. Draper and H. Smith, *Applied Regression Analysis* (John Wiley and Sons, New York, 1981) 2nd ed., pp 294–352.
- 6.30. D.W. Lachenmeier, P.A. Burri, T. Fauser, W. Frank, and S.G. Walch, “Rapid determination of alcoholic strength of egg liqueur using steam distillation and oscillation-type densimetry with peristaltic pumping”, *Anal. Chim. Acta* **537**, 377–384 (2005).

- 6.31. M.T. Yang, L.P. Milligan, and G.W. Mathison, “Improved sugar separation by high-performance liquid chromatography using porous microparticle carbohydrate columns”, *J. Chromatogr.* **209**, 316–322 (1981).

Chapter 7

Conclusions and Future Work

7.1 Conclusions

The work presented in this dissertation has demonstrated the application of ultrasound for the determination of analytes in liquids. It was found that using an ultrasound transmission methodology allowed rapid and accurate measurements of both hydrogel sensors and solution composition. This practical method is applicable for routine measurements, such as monitoring process quality or medical point-of-care diagnostics. For a particular application, a target analyte could be determined either by harmonic frequency components generated from hydrogel sensor oscillation, or by the nonlinear distortion of the waveform propagating through the medium.

Multilinear regression analysis was found to be useful for the development of calibration models based on the ultrasound frequency data. These calibrations were designed to create predictive models relating the analyte concentration to the measured ultrasound frequency distributions. The analytes tested make up two groups. The first group consists of analytes present at <10 mM concentrations. This group included theophylline, acetaminophen, and tumor necrosis factor- α , and were measured using hydrogel sensors. The second group of analytes examined included methanol, ethanol,

and sucrose, which made up greater fractions of the total sample masses. For these analytes, no hydrogel sensor was used, but the nonlinear distortion in the ultrasound waveform was measured.

We have demonstrated that the mechanical properties of hydrogel sensors can be modulated by binding with an analyte. Using dynamic light scattering, both the molecularly imprinted and antibody-linked cellulose hydrogels were shown to increase in size with binding. It was then shown that these induced mechanical changes caused changes in the measured ultrasound frequencies. This was attributed to a change in the fundamental resonance frequency of the hydrogel sensors. This behavior was also confirmed using temperature-induced changes in the hydrogels. Continuous changes in the frequency profiles could be measured, with a steeper change when the hydrogels would undergo phase transition. Using known models, the fundamental resonance frequencies of the hydrogels are expected to be higher than the range measured. However, nonlinear oscillation is known to produce sub-harmonic frequency components. Therefore, changes in the frequency profiles measured are attributed to the resonating sensor sub-harmonics, and could be correlated to the hydrogel state.

Molecular imprinting of cellulose hydrogels was used to make hydrogel sensors with target-specific binding sites. One such sensor, targeted for the molecule theophylline, showed a change in resonance characteristics with binding. Changes in the ultrasound frequency profiles were correlated with concentrations of theophylline between 0.2 and 6.1 mM using a 1 wt% hydrogel solution. By decreasing the concentration of the hydrogel sensor tenfold, theophylline levels between 10 and 50 μM could also be determined. Though the relationship between the concentration of the

sensor and the sensitivity is likely nonlinear, this indicated that the signal-to-noise ratio is improved by more closely matching the concentration of the sensor with the targeted analyte.

Antibody-linked hydrogel sensors were also designed. Concentrations of acetaminophen between 3.5 and 20.8 nM were determined by measuring the ultrasound frequency profiles of these sensors. Likewise, antibody-linked sensors were used to determine concentrations of tumor necrosis factor- α . For this significantly larger analyte, the changes in the ultrasound frequencies could be used to estimate concentrations between 77 and 922 pM. The results using these antibody-linked sensors illustrated two factors that can increase the sensitivity of the ultrasound method. First, the higher binding strength and selectivity of the antibody increased the sensitivity of the measurement. Second, raising the mass of the analyte relative to that of the sensor was also an important factor in increasing the sensitivity of the method.

The hydrogel sensors could also be used in a variety of different biological media. It was also shown that the resonance frequency components of the hydrogel sensors were not affected significantly by the media. Although changes in the characteristic ultrasound frequency profiles were noted with changing media, these did not affect the analyte quantification. The frequencies used for multilinear regression analyses were clustered in certain regions, indicating that the resonance frequencies of the hydrogel sensors could be measured somewhat independently from distortions caused by the medium. It was also shown that by using dendrimeric hydrogel sensors of different sizes, the resonance frequency components of the sensors shift in a characteristic manner. As the resonance

frequencies can be determined in somewhat independently of the medium, using multiple sensors of different sizes to quantify several analytes simultaneously should be possible.

The effect of the medium on the ultrasound frequency profile was also separately investigated using simple liquid mixtures. It was shown that when ultrasound propagated through mixtures, the nonlinear distortion depended on the specific ratio between components. By measuring the ultrasound frequency profiles of a series of water, methanol, and ethanol mixtures, the volume fraction of each component could be determined. In general, the volume fractions of mixtures were best estimated over narrow volume ranges rather than over all possible volume fractions. The error in methanol and ethanol volumes were $>10\%$, but by examining samples with volumes between 0 and 35%, the estimation error was reduced to $<4\%$. This result indicates that calibrations over a wide range can be used to generate estimates which can then be refined using focused regression models.

This methodology was then employed for the practical application of simultaneously determining multiple components in commercial beverages. This analysis extended the investigation of mixtures to carbohydrate components dissolved in liquids. Using the multilinear regression approach, quantification of carbohydrates and ethanol in beverages was possible with a good accuracy. Though commercial beverages contain a wide variety of other constituents, water, ethanol, and sucrose solutions provided a usable calibration model for the simultaneous determination of both components. For improved quantification, hierarchical calibration could also be used. With this approach, a decrease in the error of ethanol estimation from 3.18% to 0.81% was shown.

Overall, the ultrasound frequency analysis approach for the quantification of analytes in liquids was demonstrated to allow sensitive and selective determination of several analytes. The methodology shows significant advantages over established techniques due to the mechanical nature of the ultrasound wave. One of the current trends in analytical instrumentation development is miniaturization and portability. Be it for point-of-care or for on-line quality control, rapid and accurate measurements provide significant savings in time and cost. In biomedical diagnostics, this can improve patient outcomes and save lives, and in commercial settings can prevent product fouling and optimize processes.

7.2 Future Work

Based on the success of the frequency domain analysis developed in this dissertation, there are several new research directions for this work. These can be divided into three primary categories: instrumentation, resonance frequency sensors, and nonlinear distortion in bulk media. Methods are proposed below for both improving upon the current configuration, as well as a selection of applications that would benefit from using this ultrasound frequency analysis technique.

7.2.1 Instrumentation

The measurements made throughout this thesis have required careful design and elaborate calibration procedures. With improvements to the instrument configuration, the

robustness of the system, as well as the ease of use could easily be improved. The development of portable instrumentation is a major driving force in current analytical instrument development. Integration of individual instrument components into a single, durable, and temperature controlled enclosure would increase the stability of the measurements. Likewise, this would allow measurements on site, which is the final step towards a point-of-care device.

It was suggested in Chapter 3 that the hydrogel sensors likely resonate at higher frequencies than those measured. Although monitoring sub-harmonic frequencies was useful for accurate analyte estimation, the magnitude of the changes cause by analyte binding would be greater when measuring closer to the fundamental resonance frequencies of the sensors. While this thesis has focused on ultrasound transducers that are sensitive between 1-10 MHz, higher frequency transducers are available, which could be used to increase the sensitivity. It is important to note that the tradeoff for increased sensitivity will be a decrease in penetration depth. However, the penetration depths of several centimeters using 1-10 MHz would likely not be necessary in many low volume applications.

7.2.2 Resonance frequency Sensors

The work presented in this thesis outlines a general platform for the development of hydrogel sensors. The molecular recognition elements, imprinting and antibody linking, are designed to be modular approaches. To expand the analyses, molecularly imprinted hydrogels could be synthesized using a different template molecule. The

process has been used widely in the literature over the past decade to produce molecularly imprinted materials for a variety of targets including ions, small molecules, proteins, and viruses.^{7.1} In the case of proteins and viruses, it is expected that the changes induced by binding to the large molecules would increase the sensitivity due to the larger change in relative mass.

The implementation of other binding schemes could be also examined. The use of nucleic acid aptamers has been growing steadily for analyte recognition and binding of small molecules and proteins.^{7.2} The aptamer molecules can be conveniently tailored to bind with a desired analyte by *in vitro* selection, and can show binding constants on par with antibodies.^{7.3} Once the sequence is known, they can be produced quickly and inexpensively. Aptamers could be linked to hydrogels, similar to the antibodies in Chapters 3 and 4, creating sensors for a wide variety of molecules such as antibiotics or water contaminants. Further, the low cost would be beneficial for routine analyses, such as screening for drugs of abuse in emergency departments.

Ultrasound sensors based on other binding molecules that are produced *in vivo* could also be designed. As with antibodies, the highly selective molecular recognition in proteins that target molecules should allow the sensor to have a high specificity. One example is the Vitamin D binding protein (VDBP), which was examined during the course of undergraduate student Andrew Dafoe's Honours research under my co-supervision. It was shown that the VDBP could be linked to a cellulose gel and detected using ultrasound. The use of the VDBP allowed sensitive measurements of the vitamin D precursor 25-Hydroxycholecalciferol to be made, as shown in Figure 7.1. Concentrations between 9 nM and 54 nM could be determined using a subset of

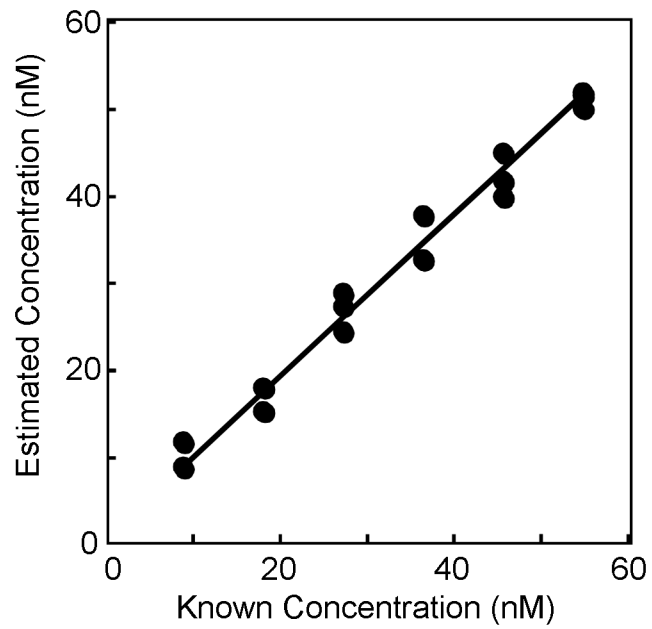


Figure 7.1: Determination of vitamin D3 using a binding protein-linked sensor.

ultrasound frequencies, with an r^2 of 0.99 and a standard error of 1.9 nM. This result is comparable to current reference techniques, while providing significant advantages due to the rapid and simple measurement technique.^{7,4} Mr. Dafoe is currently continuing this Vitamin D research as part of his Ph.D.

Results presented in this thesis also suggest that simultaneous determination of multiple sensors should be possible. Hydrogel sensors with distinctly different resonance frequencies should be resolvable in the frequency domain, allowing multiple different analytes to be measured simultaneously. Development of multi-sensor “cocktails” could be used, similar to “electronic noses” consisting of quartz crystal microbalance arrays. This multiple-resonator approach would be advantageous for simultaneous determination of several analytes, for example in analyzing environmental water contamination. The critical research for this work would be the development of sensors with resonance frequencies that could be distinguished rapidly. Care would have to be taken to ensure that cross-reactivity did not occur, as this would reduce the accuracy of the method.

7.2.3 Nonlinear Distortion in Bulk Media

As the nonlinear distortion of the ultrasound waveform is a cumulative process, measurements in larger volumes would increase the changes seen with varying sample composition. This could improve understanding of the underlying mechanisms resulting in the characteristic frequency profiles of mixtures. Likewise, while two and three-component systems were investigated, mixtures with a large number of constituents could be examined. In real liquids, whether beverages, reaction vessels, or biological

fluids, the actual number of components will generally be much higher. It would be important to understand and characterize what effect this will have on the nonlinear distortion of the ultrasound. The ultrasound propagation has also not been examined in mixtures of either non-polar or aprotic liquids. While hydrogen bonding is the major contributor to the molecular structure in the samples in this thesis, the behavior of non-polar liquids such as hexane, benzene, or chloroform would provide important information about the interaction of the ultrasound with the bonding structures in these media. This information could offer insight into the frequency changes expected when looking at other systems.

As an illustration of how this could be used in other systems, preliminary research on water contamination was done using the nonlinear ultrasound method. Water samples were prepared with a variety of contaminants including glycerin, potassium phosphate, sodium nitrate, sodium sulfate, soil, and urine. Significant differences were seen in the ultrasound frequency profiles. As shown in Figure 7.2, it was possible to differentiate between these different adulterants using a principal component approach. It was also demonstrated that the concentrations of these species in water could be determined, as shown in Figure 7.3. These data provide groundwork for environmental water analysis, which is an important field for not only conservation, but also in the analysis of well water and in water purification. With further research, this methodology could allow rapid determination of other contaminants such as steroids, heavy metals, and oils. The nonlinear distortions could also be used in conjunction with hydrogel sensors to determine concentrations of low-abundance contaminants.

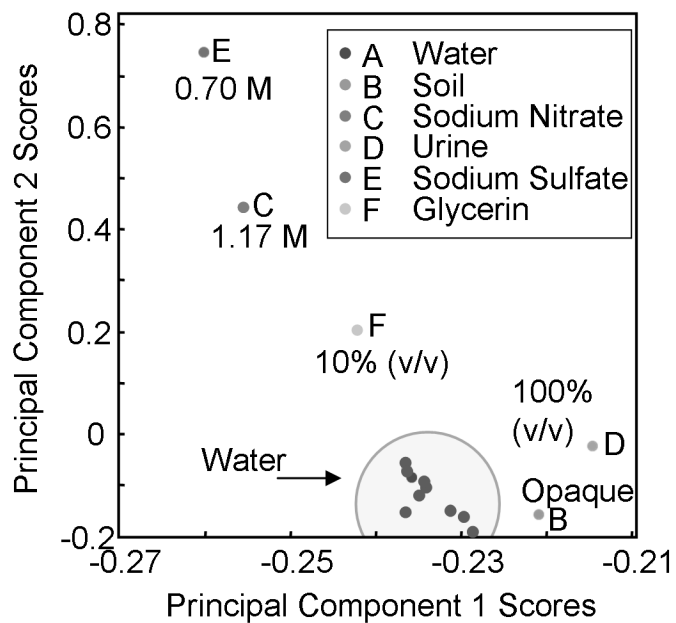


Figure 7.2: Determination of water contaminants.

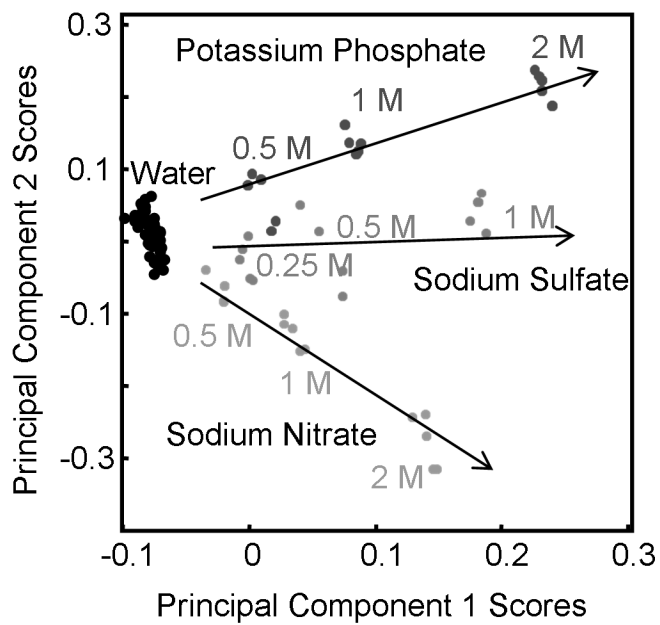


Figure 7.3: Effect of increasing concentrations of water contaminants.

7.3 References

- 7.1. M.E. Byrne and V. Salián, “Molecular imprinting within hydrogels II: Progress and analysis of the field” *International Journal of Pharmaceutics* **364** (2008) 188–212 (2008).
- 7.2. P.S. Lau and Y. Li, “Functional nucleic acids as molecular recognition elements for small organic and biological molecules”, *Curr. Org. Chem.* **15**, 557–575 (2011).
- 7.3. E.N. Brody, M.C. Willis, J.D. Smith, S. Jayasena, D. Zichi, and L. Gold, “The use of aptamers in large arrays for molecular diagnostics”, *Mol. Diagn.* **4**, 381–388 (1999).
- 7.4. J.E. Zerwekh, “The measurement of vitamin d: analytical aspects”, *Ann. Clin. Biochem.* **41**, 272–281 (2004).

Appendix A

Ultrasonic Quantification using Smart Hydrogel Sensors

Authors: David Troïani, Jonathan R. Dion, David H. Burns

A.1 Abstract

Analyte quantification in samples with extensive matrix effects can be challenging using conventional analytical techniques. Ultrasound has been shown to easily penetrate samples that can be difficult to measure optically or electrochemically, though it provides little chemical information. Recent ultrasound contrast agents provide highly localized contrast within a sample based on concentration. We have developed a general approach for creating smart biosensors based on molecularly imprinted hydrogel polymers that recognize and bind a target analyte, changing ultrasonic properties with analyte concentration. Multilinear analyte calibration in hydrogel solutions provided quantification of the chosen analyte, theophylline, from 8.4 μM to 6.1 mM with a high degree of linearity (correlation coefficient exceeding 0.99). Simultaneous quantification of both theophylline and of an interfering species, caffeine, was also carried out, providing an avenue for simultaneous analyte analysis with one smart biosensor that can be dispersed and remotely detected.

A.2 Introduction

A.2.1 Background

Detection and quantification of analytes in biomedical applications is typically done by optical spectroscopies or electrochemical techniques. However, many samples containing multiple analytes with overlapping chemical signatures often require chromatographic separation or extensive sample pre-cleaning.^{A.1–A.3} We have developed a general system for creating smart biosensors based on molecularly imprinted hydrogel polymers. The biosensor exhibits a characteristic ultrasound frequency profile that is dependent on the stiffness and size of the polymer. Target recognition and binding cause changes to these physical parameters, and changes to the ultrasonic frequency profile are measured. We have applied this technique to the analytical determination of theophylline, a therapeutic agent for respiratory diseases. Therapeutic concentrations of theophylline are typically in the 55 to 110 μM range.^{A.4} Caffeine, a structurally similar molecule, was also investigated by this method as a competitive agent. Using this technique, a high degree of linearity for individual and simultaneous quantification of both chemical species is demonstrated.

Hydroxypropyl cellulose (HPC) and N-isopropylacrylamide (NIPA) hydrogels undergo a reversible, volume phase transition between swollen and condensed states in solution. In the swollen state, hydrogel solutions are clear, owing to a large and diffuse structure. The condensed state is characterized by an increase in turbidity as the hydrogel microspheres contract, becoming stiffer and expelling water from the structure. As a

result of these physical changes, ultrasonic properties of hydrogels are highly dependent on the phase of the gel. Hydrogel phase transitions can be prompted by external forces such as fluctuations in ionic strength, temperature, or hydrostatic pressure.^{A.5,A.6} When the temperature of the hydrogel solution is elevated past the critical threshold temperature (T_c), a broad change to the ultrasound spectrum will be seen. Figure A.1 shows the ultrasound frequency profiles of the HPC and NIPA hydrogels. The mean of the spectra has been subtracted to more clearly illustrate the changes in the frequency power spectrum when the hydrogels undergo a temperature-induced phase transition. It can be seen that frequency exchanges occur over the entire spectrum, including both in-phase and out-of-phase changes.

To promote analyte specificity in the hydrogel biosensors, molecularly-selective binding sites can be created by allowing self-assembly of the hydrogel monomers and analyte prior to polymerization.^{A.7,A.8} Upon docking of the analyte into an imprinted pocket, the hydrogel will undergo a change in physical properties and in ultrasonic response. Molecular sensitivity of the binding sites is dependent on the affinity of imprinted hydrogels for an analyte. This affinity for the template is based on hydrogen bonding between the polymer network and the template molecule, as well as steric factors due to the shape of the molecularly imprinted pocket. By adjusting the specific chemistries of the hydrogels, both low and high affinity biosensors can be created. With high molecular weight HPC, affinity towards the analyte is based on large, loose hydrogen bonding pockets once crosslinking is complete.^{A.9} In contrast, high affinity binding is achieved in NIPA hydrogels that are copolymerized with methacrylic acid (MAA), which forms strong hydrogen bonds with the template.^{A.10} Molecularly imprinted

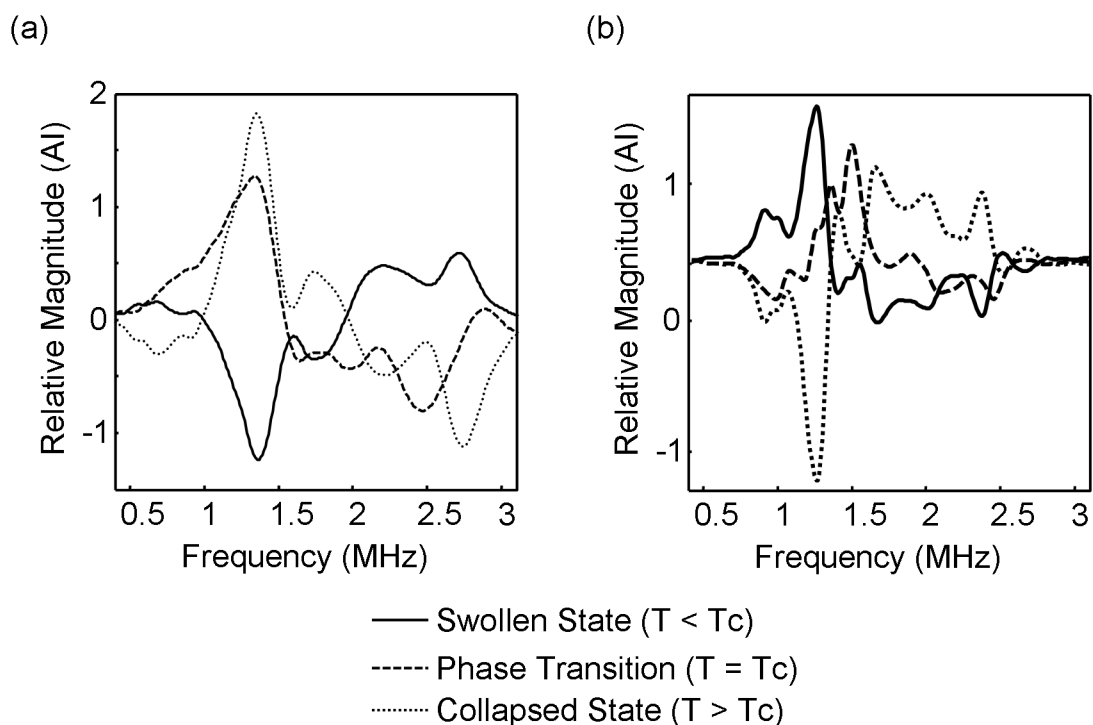


Figure A.1: Frequency profiles of NIPA and HPC hydrogels undergoing phase transition as a result of increasing temperature. Mean ultrasound spectral profile has been subtracted to emphasize the changes before ($T < T_c$) (solid line), during ($T = T_c$) (dashed line), and after ($T > T_c$) phase transition relative to critical threshold temperature T_c .

NIPA hydrogels have been shown to exhibit turbidity changes with sub-mM concentrations of theophylline.^{A.11}

We present a unique method for analyte quantification using imprinted hydrogels in concert with ultrasonic detection. Molecularly imprinting hydrogels with analyte template can provide high degrees of analyte specificity. Non-invasive ultrasonic detection of hydrogels provides potential for rapid, efficient detection of analytes based on contrast enhanced backscatter at select frequencies.

A.2.2 Principle

A conceptual model can be developed to illustrate the changes to the ultrasonic frequency profile of hydrogel polymers when an analyte binds to the molecularly imprinted pockets. Considering hydrogels to be deformable microspheres in solution with given diameter and modulus, changes in hydrogel microsphere physical properties at equilibrium can alter ultrasonic profile. Each microsphere resonates at a given frequency when perturbed by ultrasound pressure waves. Resonance frequency shifts occur as a result of altering the size and stiffness of the microsphere. Physical properties of molecularly imprinted hydrogels change with docking of an analyte. In particular, hydrogel microspheres have been shown to both increase in stiffness and decrease in size as analyte molecules occupy the binding sites.^{A.12,A.13} With ultrasonic compression and rarefaction, polymer beads oscillate isotropically at specific resonance frequencies dependent on these physical properties.^{A.14} A model, while not ideal for network hydrogel beads in solution, approximates behavior in ultrasonic fields by assuming hydrogels to be

gas-filled microspheres with a thin polymer shell. This thin shell approximation is straightforward to model. Though exact comparisons would not be expected from the shell model for spherical hydrogel networks, the model illustrates relative trends of the resonance frequency with changing hydrogel physical properties. Hydrogel resonance frequency for thin-shelled microspheres in solution can be derived from the resonance frequency of gas-filled contrast agent microbubbles as

$$f_0 = \frac{1}{2\pi a_e} \sqrt{\frac{1}{\rho_L} \left(3kp_0 + 12G_s \frac{d_{se}}{a_e} \right)}, \quad (\text{A.1})$$

where a_e is the equilibrium radius of the microbubble, ρ_L is the density of the surrounding liquid, k is the polytropic exponent of the gas, p_0 is atmospheric pressure, G_s is the shell shear modulus, and d_{se} is the shell thickness.^{A.15} Bulk modulus of an adiabatic gas, K_g , can be written as,

$$K_g = kp_0, \quad (\text{A.2})$$

while the bulk modulus of a polymeric microbubble, K_p , receives additional contributions from the outer shell,

$$K_p = K_g + 4G_s \frac{d_{se}}{a_e}. \quad (\text{A.3})$$

For a deformable hydrogel microbubble with thin shell and no interior gas, the bulk modulus contribution from adiabatic gas can be negated ($K_g = 0$), and using Equation A.3, Equation A.1 can be rewritten as,

$$f_0 = \frac{1}{2\pi a_e} \sqrt{\frac{3K_p}{\rho_L}}, \quad (\text{A.4})$$

which resembles the Minnaert equation for microbubbles. As the modulus (or stiffness) increases, the resonance frequency of the hydrogel would increase. In contrast, an increase in hydrogel radius would result in the hydrogel resonance frequency decreasing.

An imprinted hydrogel will have a specific resonance frequency based on the size and stiffness. When the template molecule binds to the molecularly imprinted pocket, both the size and stiffness of the gel are expected to change, leading to a more complicated relationship of the resonance frequency. Though a structurally similar molecule with lower affinity may also interact with the molecularly imprinted pocket, the decreased hydrogen bonding would result in different physical changes through the hydrogel network. In a hydrogel with multiple pockets, the relationship between the modulus and radius leads to specific frequency profiles for hydrogels dependent on both the concentration and affinity of the hydrogel analytes bound. In addition, nonlinear propagation of pulsed ultrasound in aqueous samples at high acoustic pressures broadens the frequency content.^{A.16} Therefore, multiple resonance frequencies could be probed with one ultrasonic pulse. The concentration of analyte absorbed into the hydrogel pockets was estimated based on measurements of multiple frequencies within the ultrasound pulse propagating through the sample cell.

A.3 Materials and Methods

A.3.1 Synthesis of Theophylline Imprinted HPC Polymer

Low affinity molecularly imprinted HPC was prepared by 0.5 g of HPC powder (100000 MW) and 0.1 g of theophylline to 49.4 g of dH₂O and stirring for 3 days to form a homogeneous 1 wt% solution of HPC. Forty μ L of divinylsulfone (DVS) and sodium chloride to a concentration of 1 mM were added.^{A.17} After 3 hours of stirring, 5 drops of 1 M sodium hydroxide were added to the solution to raise the pH to 12. The cross-linking reaction was allowed to continue for 5 hours. The cross-linked polymers were then dialyzed against dH₂O for 3 days to remove the theophylline and any free DVS. The extraction of theophylline was confirmed spectroscopically at 271 nm. All chemicals were purchased from Sigma-Aldrich (Oakville, CA). The mean HPC hydrogel diameter was determined to be 105 nm (0.39 PDI and batch-to-batch variability of 20%) by dynamic light scattering using a Brookhaven Instruments ZetaPALS particle size analyzer.

A.3.2 Synthesis of Theophylline Imprinted NIPA Polymer

High affinity molecularly imprinted NIPA was prepared by adding 1.0 g of NIPA monomer, 0.08 g of N,N'-methylene-bis-acrylamide (MBA), 0.08 g methacrylic acid, and 0.18 g theophylline to 99 mL of distilled water (dH₂O) to form a homogeneous 1 wt% NIPA solution with stirring over 4 hours to ensure complete dissolution.^{A.18}

Oxygen in the solution was purged with nitrogen gas during this time. Following this, 15 mg of ammonium persulfate to initiate the polymerization and 60 μL of tetramethylethylenediamine as an accelerator. The solution was left to polymerize for 4 hours with gentle stirring. Once the imprinted hydrogel was formed, the theophylline was removed by successive methylene chloride extractions. The extraction of theophylline was confirmed spectroscopically at 271 nm. The mean NIPA hydrogel diameter was determined to be 396 nm (0.39 PDI and batch-to-batch variability of 5%) by dynamic light scattering using a Brookhaven Instruments ZetaPALS particle size analyzer.

A.3.3 Hydrogel Solutions

HPC and NIPA hydrogels were used to estimate theophylline concentrations based on the ultrasonic response. Solutions containing 1% imprinted hydrogel by weight in water were made and increasing amounts of analyte were added to each solution. In the low affinity-binding imprinting HPC, concentrations of theophylline ranged between 0.2 to 6.1 mM. In order to reflect the higher affinity binding in NIPA, concentrations of theophylline ranged between 8.4 to 167 μM theophylline.

To assess the selectivity of the molecularly imprinted hydrogels, caffeine was used as an interfering species while calibrating for theophylline, due to the chemical structures differing by one methyl group. Matrices of 25 HPC and 30 NIPA 1% by weight solutions were prepared, wherein the concentrations of both theophylline and caffeine were varied. For NIPA, concentrations of caffeine ranged from 4.1 to 21 μM

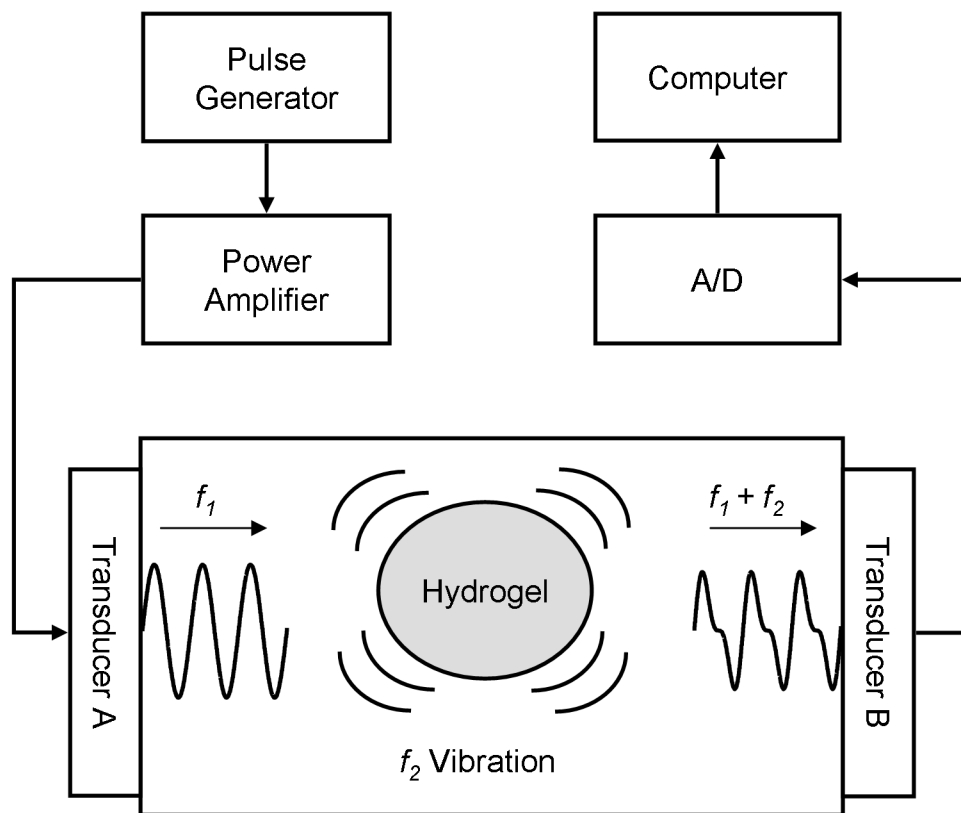


Figure A.2: Schematic for ultrasound data acquisition. A pulse generator and power amplifier are used to drive an ultrasound transducer. Transducer A generates pulses at frequency f_1 , which travel through the sample cell and interact with the hydrogel sensors. Transducer B on the parallel end of the sample cell records the ultrasound pulse that includes frequency f_2 cause by the resonating polymer. A computer controlled oscilloscope digitized the signal for further analysis.

over six solutions and concentrations of theophylline spanned 8.4 to 24 μM over five solutions per caffeine concentration. Likewise, for HPC, the caffeine and theophylline concentrations ranged from 0 to 9.1 mM and 0.2 to 6.1 mM, respectively.

A.3.4 Instrumentation

Ultrasound transducers for sending and receiving pulses were affixed to the sample reservoir as shown in Figure A.2. The sample cells used were a 1.8 cm Plexiglas cuvette for the HPC solutions and a 3.8 cm aluminum cell for the NIPA solutions. A 1.9 MHz narrow-band transducer (Advanced Technology Labs Inc., Pennsylvania, US) generated ultrasound pulses and a 10 MHz wideband transducer (Optel Inc., Wrocław, PL) received the ultrasonic signal. A Panametrics 500PR Pulser/Receiver (Panametrics Inc., Massachusetts, US) as the pulse generator for the transducers. The Panametrics 500PR generated 10 ns 250 V negative impulses to drive the 1.9 MHz narrow-band transducer. A SDS 200 oscilloscope (SoftDSP Co., Seoul, KR) sampling at 12.5 MHz using 9 bit A/D conversion, and Handyscope HS3 (TiePie Engineering, Sneek, NL) sampling at 50 MHz using 12 bit A/D conversion, collected the ultrasonic data from the 10 MHz wideband transducer for the NIPA and HPC, respectively.

A.3.5 Data Processing

Ultrasound waves propagating through the sample cell were measured by the receiving transducer and digitized by the computer controlled oscilloscope. Data for each

sample were acquired over 3 minutes, for a total number of 4000 waveforms. These waveforms were averaged to increase the signal to noise ratio. A fast Fourier transform algorithm was then applied to the averaged data to allow processing in the frequency domain. Variability due to instrumental and temperature changes was minimized by total area normalization, and random noise fluctuations were removed using a boxcar smoothing function. Frequency spectra were divided into independent calibration and test sets. The test set consisted of a series of samples with varying theophylline levels at one caffeine concentration that was not found in the calibration data set.

Stagewise multilinear regression (SMLR) was used to estimate the concentration of theophylline based on the magnitude of the ultrasound frequencies measured for a given sample. The algorithm determined the regression of the magnitude at each frequency with the analyte concentrations in the calibration set in order to determine the highest correlation. The residual values are then calculated and the process is repeated iteratively with the subset of frequencies not yet included in the model. Based on the linear combination of this subset of ultrasonic frequency intensities, the data are described in the form

$$Y = b_0 + b_1X_1 + b_2X_2 + \dots + b_nX_n \quad (\text{A.5})$$

where Y is the dependent variable, $\{X\}$ are independent variables, and $\{b\}$ are weighting coefficients. This multilinear model was subsequently used to estimate the concentration of the analyte in the independent test set samples. To avoid overfitting of data by the model, parsimony was determined by F-test ($\alpha = 0.05$) between the standard errors of each model so that the addition of additional parameters would not significantly impact

the SMLR model and estimation.^{A.19} All data analysis was done in Matlab (The MathWorks Inc., 2008a, Massachusetts, U.S.).

A.4 Results and Discussion

To examine the relationship of the ultrasound signal with analyte binding in the hydrogels, we have quantified the target analyte sensitivity in a matrix free of interfering species. In both HPC and NIPA hydrogels, the concentration of theophylline was estimated with three frequencies in the derived model. In the low affinity binding HPC, concentrations of theophylline were determined in the millimolar range. A standard error of estimate (SEE) of 0.1 mM with a correlation coefficient (r^2) exceeding 0.99 was obtained in the 0.1 to 6.1 mM range. With theophylline binding, the mean particle size of the HPC hydrogel increased by 14%. The higher affinity binding of NIPA permitted using a micromolar theophylline concentration range, with a SEE of 2.6 μ M and an r^2 exceeding 0.99 in the 8.4 to 167 μ M range. Unlike the HPC sensor, binding to theophylline resulted in a 16% decrease in overall sensor diameter. The decrease in size suggests that the stronger hydrogen bonding between NIPA and theophylline results in a tighter induced fit in the molecularly imprinted binding pocket. The greater structural changes would cause larger changes to the resonance frequency of the NIPA hydrogel, increasing the sensitivity.

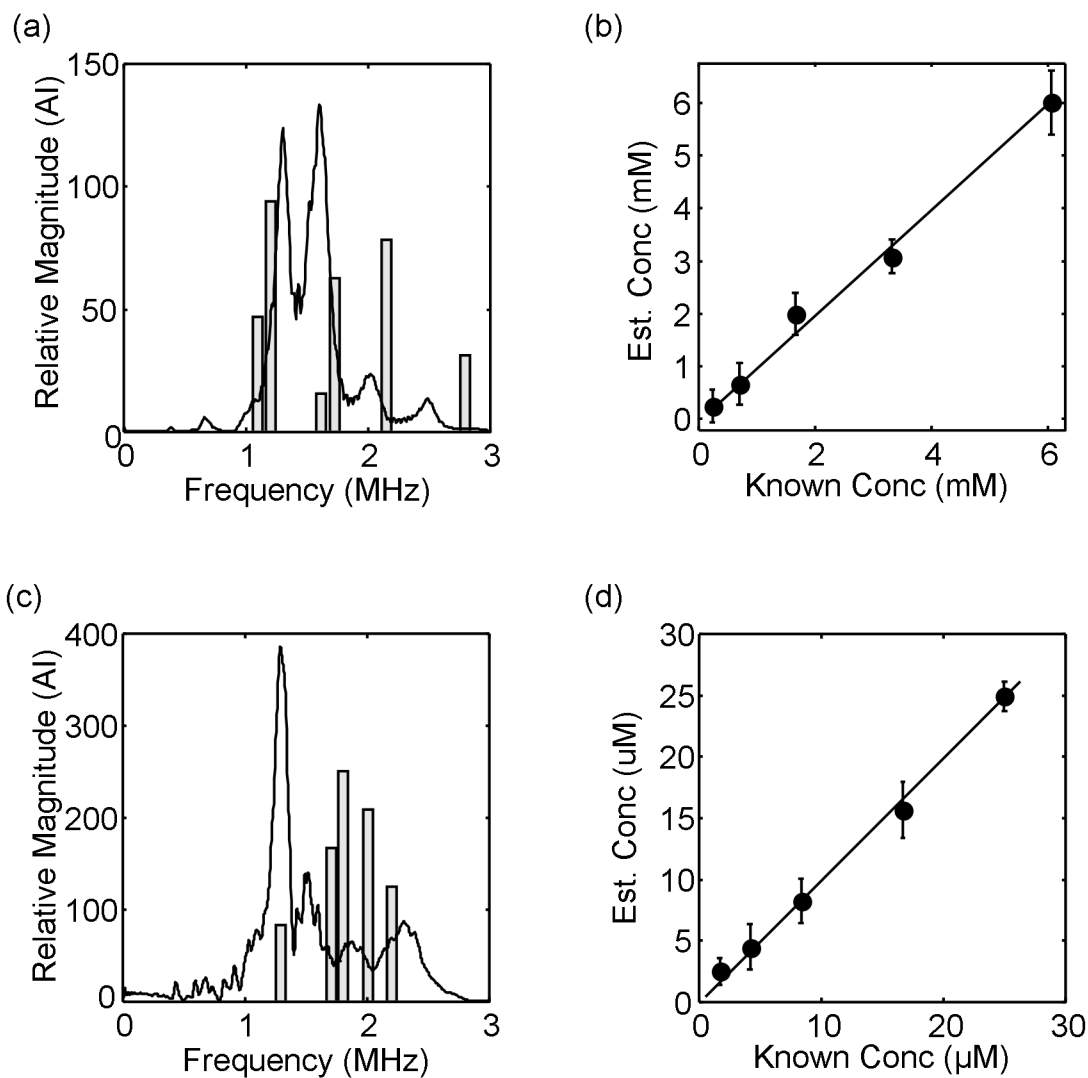


Figure A.3: Theophylline quantification results in presence of caffeine. a) ultrasonic frequencies selected to determine analyte concentrations in HPC, b) estimates of theophylline concentrations with HPC sensors using a multilinear model plotted against known values, c) ultrasonic frequencies selected to determine analyte concentrations in NIPA, d) estimates of theophylline concentrations with NIPA sensors using a multilinear model plotted against known values.

An interfering species was used in order to assess the specificity of the molecularly imprinted hydrogels. A commonly used pair of chemicals to determine sensitivity and specificity of imprinted hydrogels is theophylline and caffeine, which are molecularly-similar xanthine derivatives.^{A.11,A.20} Presence of an additional N-methyl group on caffeine decreases hydrogen bonding potential and increases steric hindrance for molecularly imprinted binding sites resulting in a lower binding constant. Solutions were prepared in which theophylline and caffeine of comparable concentrations were independently varied. Caffeine concentrations ranged from 0 to 9.1 mM in HPC and from 0 to 21.0 μ M in NIPA. Likewise, concentrations of theophylline were ranged from 0.2 to 6.1 mM and from 8.4 to 24.0 μ M for HPC and NIPA, respectively.

To estimate the concentration of theophylline independently of caffeine, separate calibration models using SMLR were created for HPC and NIPA sensors. Models were tested on an independent evaluation set consisting of one concentration of caffeine excluded from the calibration data. For low affinity HPC, the use of six frequencies, 1.2, 2.2, 1.7, 1.1, 2.8, and 1.6 MHz, was determined to be the most parsimonious for the quantification of theophylline and resulted in a SEE of 0.6 mM with a corresponding r^2 of 0.95. Figure A.3(a) illustrates the typical frequency spectrum of HPC hydrogels, as well as the frequencies used by the multilinear model for theophylline estimation. The concentrations of theophylline estimated by the SMLR model are plotted against the known values in Figure A.3(b), showing linearity of the full range with minimal bias. The most parsimonious estimation of theophylline in high affinity NIPA hydrogels was obtained with five frequencies, 1.8, 2.0, 1.7, 2.2, and 1.3 MHz. A SEE of 1.5 μ M with a corresponding r^2 of 0.98 was obtained. Figure A.3(c) illustrates the typical frequency

spectrum of NIPA hydrogels, as well as the frequencies used for theophylline estimation. The concentrations of theophylline estimated by the SMLR model are plotted against the known values in Figure A.3(d), showing linearity of the full range with minimal bias. The difference in selected frequencies and correlation coefficients for multilinear quantification in both hydrogels can be partly explained by the different analyte binding strengths and levels of interferent competition. Two nearly identical molecules competing for the same localized hydrogen bonding sites can alter with the hydrogel resonance frequencies. The low affinity HPC hydrogel required an additional frequency component to quantify theophylline with caffeine due to the greater impact an interferent has on a less specific analyte binding environment. Results show that calibration was possible for both hydrogels independent of caffeine interference with an overall linear quantification spanning the micromolar to millimolar range.

To determine if simultaneous analyte quantification was possible using the ultrasound signal, concentration of caffeine in the above theophylline/caffeine mixtures was estimated. Chemical similarity between the two xanthines allows both of the compounds to access the binding sites, albeit with separate binding constants. The decreased interaction between caffeine and the molecularly imprinted pocket as compared to theophylline should induce distinctly different physical changes in the hydrogel. As with theophylline, sensitivity of HPC to caffeine was lower than in NIPA, and for this analyte, proved to be too low for quantification ($r^2 < 0.6$). The mean particle size increased by 23% with caffeine binding, compared to 14% with theophylline. It is possible this greater increase in particle size decreased the resonance frequency of the

HPC hydrogels so that the bandwidth of the ultrasonic transducers was not optimal for the determination of caffeine-bound sensors.

Simultaneous caffeine quantification was possible with the NIPA sensor using five frequencies resulting in a SEE of 3.3 μM and an r^2 of 0.87. The mean particle size for caffeine binding with NIPA showed only a 5% decrease, as compared to the 16% decrease with the theophylline molecule. This suggests that while the hydrogen bonding may still have formed strong associations, the presence of the additional methyl group likely resulted in a steric strain on the pocket, preventing certain conformational changes that result when the template molecule occupies the pocket. Lower correlation coefficients were expected when quantifying caffeine in this scenario, as the hydrogels were molecularly imprinted with a theophylline template which is structurally different than caffeine. Results are consistent with the proposed model and provide a mechanism for simultaneous quantification of multiple analytes with one hydrogel sensor. With tuning of the imprinted hydrogel using different binding mechanisms such as, hydrophobicity and π stacking, high sensitivity and specificity should be possible for several analytes.

A.5 Conclusions

We have successfully quantified theophylline in solutions ranging between 8.4 μM and 6.1 mM using two molecularly imprinted hydrogels. This allows physiological monitoring of theophylline within the therapeutic range (55 μM to 110 μM), as well as higher concentrations which are toxic.^{A.4} The model for contrast agent resonance

frequency suggests that the change in the ultrasonic signal with increased analyte concentration is likely due to changes in hydrogel physical properties, notably modulus and radius. Furthermore, it was also shown that this molecular quantification is possible in a matrix containing an interfering species with a nearly identical chemical structure. Measurement of multiple frequencies allowed quantification of an imprinted analyte in a matrix containing an interfering analyte with a nearly identical chemical structure. Molecular imprinting of NIPA hydrogels provides a greater analyte selectivity, which is attributed to the presence of the MAA binding group. Likewise, increased specificity due to stronger binding results in a hydrogel more adaptable to analyte molecules and analogous species. These findings are strongly indicative that the molecular imprinting process provided the selectivity required to implement a detection system using ultrasound. It is also possible to quantify the interfering species by looking at different frequencies of the ultrasonic response. This opens up several possibilities for simultaneous detection of multiple compounds with a single templated molecularly imprinted hydrogel. Overall, ultrasonically detected smart hydrogel biosensors appear very promising for a variety of environmental, industrial and clinical applications.

A.6 Acknowledgements

This work was supported in part by the National Science and Engineering Research Council of Canada and by the Fonds Québécois de la Recherche sur la Nature et les Technologies.

A.7 References

- A.1. A. Ojha and A. Pargal, “Determination of nicorandil concentrations in human plasma using liquid chromatography”, *J. Pharm. Biomed. Anal.* **21**, 175–178 (1999).
- A.2. R. Panchagnula, A. Sood, N. Sharda, K. Kaur, and C.L. Kaul, “Determination of rifampicin and its main metabolite in plasma and urine in presence of pyrazinamide and isoniazid by HPLC method”, *J. Pharm. Biomed. Anal.* **18**, 1013–1020 (1999).
- A.3. I. Calleja, M.J. Blanco-Prieto, N. Ruz, M.J. Renedo, and M.C. Dios-Viéitez, “High-performance liquid-chromatographic determination of rifampicin in plasma and tissues”, *J. Chromatogr. A.* **1031**, 289–294 (2004).
- A.4. P.J. Barnes, “Theophylline: New Perspectives for an Old Drug”, *Am. J. Resp. Crit. Care.* **167**, 813–818 (2003).
- A.5. E. Kato, “Volume-phase transition of N-isopropylacrylamide gels induced by hydrostatic pressure”, *J. Chem. Phys.* **106**, 3792–3797 (1997).
- A.6. T. Oya, T. Enoki, A.Y. Grosberg, S. Masamune, T. Sakiyama, T. Takeoka, K. Tanaka, G. Wang, T. Yilmaz, M.S. Feld, R. Dasari, and T. Tanaka, “Reversible molecular adsorption based on multiple-point interaction by shrinkable gels”, *Science* **286**, 1543–1545 (1999).
- A.7. K. Mosbach and O. Ramström, “The Emerging Technique of Molecular Imprinting and Its Future Impact on Biotechnology”, *Nat. Biotechnol.* **14**, 163–170 (1996).

- A.8. M.E. Byrne and V. Salián, “Molecular imprinting within hydrogels II: Progress and analysis of the field”, *Int. J. Pharm.* **364**, 188–212 (2008).
- A.9. R.S. Gill, M. Marquez, and G. Larsen, “Molecular imprinting of a cellulose/silica composite with caffeine and its characterization”, *Micropor. Mesopor. Mat.* **85**, 129–135 (2005).
- A.10. G. Vlatakis, L.I. Anderson, R. Muller, and K. Mosbach, “Drug assay using antibody mimics made by molecular imprinting”, *Nature* **361**, 645–647 (1993).
- A.11. W. Fan and W.R. Seitz, “Swelling theophylline selective microparticles for sensing applications”, *Analyst* **132**, 1103–1106 (2007).
- A.12. R. Nossal, “A Novel Dynamic Light-Scattering Method to Determine the Modulus of Gels”, *Rubber Chem. Technol.* **16**, 255–260 (1988).
- A.13. W.R. Seitz, M.T.V. Rooney, E.W. Miele, H. Wang, N. Kaval, L. Zhang, S. Doherty, S. Milde, and J. Lenda, “Derivatized, swellable polymer microspheres for chemical transduction”, *Anal. Chim. Acta* **400**, 55–64 (1999).
- A.14. A. Strybulevych, V. Leroy, M.G. Scanlon, and J.H. Page, “Characterizing a model food gel containing bubbles and solid inclusions using ultrasound”, *Soft Matter* **3**, 1388–1394 (2007).
- A.15. L. Hoff, P. C. Sontum, J.M. Hovem, “Oscillations of polymeric microbubbles: effect of the encapsulating shell”, *J. Acoust. Soc. Am.* **107**, 2272–2280 (2000).
- A.16. A. Kvikliene, R. Jurkonis, M. Rössner, L. Hoff, T. Jansson, B. Janerot-Sjöberg, A. Lukoševičius, and P. Ask, “Modelling of nonlinear effects and the response of ultrasound contrast micro bubbles: simulation and experiment”, *Ultrasonics* **42**, 301–307 (2004).

- A.17. U. Anbergen and W. Oppermann, "Elasticity and swelling behaviour of chemically crosslinked cellulose ethers in aqueous systems", *Polymer* **31**, 1854–1858 (1990).
- A.18. M.E. Byrne, K. Park, and N.A. Peppas, "Molecular imprinting within hydrogels", *Adv. Drug Deliv. Rev.* **54**, 149–161 (2002).
- A.19. N. R. Draper and H. Smith, *Applied Regression Analysis* (John Wiley and Sons, New York, 1981) 2nd ed., pp 294–352.
- A.20. S.R. Carter and S. Rimmer, "Molecular Recognition of Caffeine by Shell Molecular Imprinted Core–Shell Polymer Particles in Aqueous Media", *Adv. Mater.* **14**, 667–670 (2002).

You have to try... You have to care...